NirA is an alternative nitrite reductase from *Pseudomonas aeruginosa* with potential as an anti-virulence target.

Samuel Jacob Fenn

Thesis submitted to the University of Nottingham for the degree of Doctor of Philosophy

November 2021

Unless otherwise stated, the work presented in this thesis is my own. No part has been submitted for another degree at the University of Nottingham or any other institute of higher learning.

Samuel Jacob Fenn

November 2021

Abstract

Pseudomonas aeruginosa is capable of causing a wide-range of diseases due to production of an extensive arsenal of virulence factors. This opportunistic pathogen is capable of causing both acute and chronic infection, with treatment complicated due to its intrinsic resistance and tolerance of antibiotics. With the antibacterial pipeline drying up, anti-virulence therapy has become an attractive alternative strategy to the traditional use of antibiotics to treat *P. aeruginosa* infections. The work presented in this thesis builds upon the successful 'integrated whole-genome screening for *Pseudomonas aeruginosa* virulence genes using multiple disease models', performed in our lab as part of the NABATIVI project to combat anti-virulence target identification.

In this previous study, Tn5 mutant was identified to be inserted into the hypothetical protein PA4130, causing attenuation in pyocyanin production; swarming motility; *Drosophila melanogaster*; *Caenorhabditis elegans*; and A549 human epithelial cell culture. The work from this screen was validated through generation of in-frame PA4130 deletion mutants in multiple phylogenetically distinct clinical strains of *P. aeruginosa*, demonstrating that the observed reductions in pyocyanin and swarming motility were conserved. Subsequent re-screening of PAO1-L ΔPA4130 through invertebrate infection models and tissue culture confirmed the phenotypes observed in a PA4130::Tn5 mutant, and further screening in acute murine lung models revealing an 80% increase in survival as compared to the isogenic wild-type strain. Sequence analysis of PA4130 revealed resemblance to nitrite or sulphite reductase hemoprotein sub-units with successful over-expression and purification reliant on siroheme synthase co-overexpression. Structural characterisation of PA4130 by crystallography failed, however, methyl viologen oxidation assays with purified PA4130 demonstrated that this enzyme is an ammonium-forming nitrite reductase operating in a ferredoxin-dependent manner. PA4130 was subsequently renamed NirA to fit with current nomenclature.

With *P. aeruginosa* encoding a second siroheme-dependent assimilatory nitrite reductase in NirB, functional redundancy and overlap was explored between NirA and NirB. When grown with nitrate or nitrite as a single nitrogen source

under aerobic conditions, *nirB* mutants were unable to grow, whilst deletion in *nirA* had no effect, suggesting NirA is not an assimilatory nitrite reductase. However, under micro-aerobic conditions, deletion of *nirA* resulted in attenuated growth. Previous work demonstrated that *nirA* is upregulated by cyanogenesis and functions alongside CioAB and the PA4129-34 gene cluster in protection from cyanide intoxication. Cyanide is normally a potent inhibitor of heme-containing enzymes; therefore it was hypothesized that NirA encodes a cyanide resistant nitrite reductase that supports the function of NirB under increasing cyanide concentrations. Functional assays revealed NirA demonstrates significant nitrite reductase activity at 600μm cyanide, with the *E. coli* sulphite-reductase homologue CysI completely inhibited by 50μm.

With high levels of bacterial or host-derived cyanide and nitrite/nitrate found during infection, we propose a model by which NirA is essential for detoxification of nitrite due to NirB/NirS inactivation by cyanide. Whilst further work is required to confirm this assessment in conjunction with NirS, potential inhibition of NirA could sensitise *P. aeruginosa* to cyanide or nitrite self-intoxication. This work supports the increasingly recognised role of reduced oxygenation and nitrate metabolism during *P. aeruginosa* infection.

Acknowledgements

At times over the last 2 years I never believed I would get to this point. Having worked in an academic lab prior to my PhD, I believed myself uniquely positioned to handle the challenges that would be thrown my way. However, negotiating a PhD in the midst of a global pandemic has been a challenge no-one could envisage or prepare for. Given everything else that people faced and lost during this time, delaying submission of this work by a year is of little concern. I found myself in an extremely privileged position and would like to extend my thanks to The Wellcome Trust and the University of Nottingham for the funding extensions which allowed me to complete my work during a time of great uncertainty.

The importance of a supervisor cannot be overestimated. For his invaluable supervision, I would like to thank Professor Miguel Camará. Miguel's encouragement, support and seemingly boundless enthusiasm throughout this process have been nothing short of extraordinary. His passion for science is infectious, and something I aspire to maintain throughout my career. I would also like to praise Professor Jonas Emsley, for his efforts in the early stages of my project, and the eternally busy Dr. Jean Dubérn for essentially becoming my 3rd supervisor. Jean's willingness to make time for all my supervision meetings, offer technical advice and discuss potential avenues of exploration are greatly appreciated. Special thanks to all members, past and present, of the C-floor microbiology labs. A PhD can feel like a solitary venture at times. The comradery, mutual moans and drinks we have shared over the years have made this process far more fun. I hope we get to share many more in the future!

My eternal love and thanks go to my Parents, Grandparents and Sisters who have supported me unconditionally in my academic pursuits. Words cannot express how thankful I am for your sacrifice and the platform in life you provided me with. Especially my Mum who actually forced me to go to University in the first place. Without her, I would never have found this career I truly love. A huge thanks to all my friends, especially those that are no longer with us. Your support, usually veiled with insults about me being a tax dodger, is appreciated beyond anything I can convey. Last, but by no means least, my partner Aislinn. I often joke that I completed this PhD in spite of you, nothing could be further from the truth. Whilst I am grateful for many things from my PhD, the thing I am most grateful for is that it brought me back to Nottingham so I could meet you.

Whilst they will never read this work, I dedicate this thesis to my Family, Aislinn and Danny.

Contents

Chapter 1 – Introduction……1
1.1 The global antimicrobial crisis and *Pseudomonas aeruginosa*.....2
1.2 Antimicrobial tolerance and resistance in *P. aeruginosa*……4
1.2.1 Antimicrobial tolerance……....4
1.2.2 Antimicrobial resistance……7
1.3 Development of novel antimicrobials……12
1.3.1 Phage therapy……..13
1.3.2 Bacterial vaccination……14
1.3.3 Anti-virulence therapeutics……14
1.5 Aims and objectives……25

Chapter 2 – Materials and Methods.....27
2.1 Bacterial strains……28
2.2 Plasmids……29
2.3 Oligonucleotides……..30
2.4 Chemical reagents……..31
2.5 Growth media and bacterial storage……31
2.5.1 Lysogenic broth……32
2.5.2 Artificial sputum media and modifications……32
2.5.3 MOPS-minimal media……..32
2.5.4 *Pseudomonas* isolation agar……...32
2.5.5 Terrific Broth……..32
2.5.6 Bacterial strain storage……33
2.5.7 Monitoring bacterial growth……33
2.6 DNA manipulations……..33
2.6.1 Genomic DNA isolation……33
2.6.2 Plasmid DNA preparation……33
2.6.3 Polymerase chain reaction……33
2.6.4 DNA agarose gel electrophoresis……34
2.6.5 DNA gel extraction……35
2.6.6 Restriction enzyme digest……35
2.6.7 DNA ligation……..35
2.6.8 DNA sequencing and analysis……35
2.7 Transformation and conjugation……35

2.7.1 Preparation of chemically competent *E. coli*……35
2.7.2 Chemical transformation of *E. coli*……36
2.7.3 Preparation of electro-competent *P. aeruginosa*……36
2.7.4 Conjugal transfer of plasmid DNA to *P. aeruginosa*……36
2.7.5 Gene deletion in *P. aeruginosa*……..37
2.8 Plasmid and strain construction……38
2.8.1 Construction of in-frame deletion mutants……38
2.8.2 Construction of protein and enzyme overexpression vectors……39
2.8.3 Construction of LacZ translational reporter vectors……40
2.9 In vitro virulence factor production assessment……..41
2.9.1 Pyocyanin……..41
2.9.2 Pyoverdine……41
2.9.3 Universal protease activity……..42
2.9.4 LasB elastase activity……..42
2.9.5 Abiotic bacterial attachment……42
2.9.6 Colony biofilm model……43
2.10 *In vivo* virulence and tissue culture models……44
2.10.1 *Drosophila melanogaster*……44
2.11.2 *Caenorhabditis elegans*……..44
2.10.3 A549 lung epithelial tissue culture……44
2.10.4 Murine infection models……45
2.11 Protein expression and purification……...46
2.11.1 SDS-polyacrylamide gel electrophoresis……..46
2.11.2 Tricine-polyacrylamide gel electrophoresis……47
2.11.3 Screening heterologous protein codon usage……47
2.11.4 Protein induction and solubility trials……47
2.11.5 Preparative-scale protein overexpression and sample preparation……...48
2.11.6 Immobilised metal ion affinity chromatography……..50
2.11.7 Anionic exchange chromatography……50
2.11.8 Size-exclusion chromatography……51
2.11.9 Mass spectrometry for protein identification……51
2.11.10 PA4130/NirA crystallography trials……51
2.12 Enzymatic characterisation assays……..52
2.12.1 UV-visible spectrum spectroscopy……..52
2.12.2 Methyl-viologen oxidation assays……..52
2.12.3 Nitrite reduction assay: detection of nitrite and ammonium…….53

2.12.4 Ferredoxin-linked nitrite reduction assays…….....53
2.12.5 Potassium cyanide inhibition…….....53
2.13 Micro-aerobic growth and translational reporter assays……54
2.13.1 Micro-aerobic culturing of *P. aeruginosa*…….....54
2.13.2 Nitrate and nitrite shock assays…….....54
2.13.3 Fluorescence based detection of LacZ production…….....54

Chapter 3 – Identification of a potential novel anti-virulence target PA4130.....56
3.1 Introduction.....57
3.1.1 Identification of novel *P. aeruginosa* virulence factors.....57
3.1.2 Host-specific nature of *P. aeruginosa* virulence.....59
3.2 Aims of this chapter.....63
3.3 Results.....65
3.3.1 Effect of PA4130 deletion on *P. aeruginosa* virulence factor production.....67
3.3.2 Effect of PA4129 deletion on *P. aeruginosa* virulence factor production.....77
3.3.3 PA4130 virulence phenotypes are phylogenetically conserved.....79
3.3.4 PA4130 contributes to virulence in phylogenetically diverse *in vivo* models.....92
3.4 Conclusions.....97

Chapter 4 – Overexpression and purification of PA4130.....98
4.1 Introduction.....99
4.2 Aims of this chapter.....100
4.3 Results.....100
4.3.1 Purification of PA4130 – method development.....100
4.3.2 Spectral properties of PA4130.....119
4.3.3 Attempted structural determination of PA4130.....124
4.4 Conclusions.....129

Chapter 5 – Functional characterisation of PA4130.....131
5.1 Introduction.....132
5.1.1 Nitrite or sulphite reductase metabolic pathways.....132

5.1.2 Nitrite or sulphite electron donor utilisation....134
5.2 Aims of this chapter....135
5.3 Results....136
5.3.1 PA4130 is an ammonium-forming nitrite reductase....136
5.3.2 NirA utilises 2Fe-2S ferredoxins as electron donors....142
5.4 Conclusions....149

Chapter 6 – Interplay between the ammonium-forming nitrite reductases and cyanogenesis....150
6.1 Introduction....151
6.1.1 Loss of nitrate reduction attenuates *P. aeruginosa* virulence....151
6.1.2 *P. aeruginosa* nitrite reductases are differentially regulated....152
6.2 Aims of this chapter....158
6.3 Results....158
6.3.1 NirA is not an assimilatory nitrite reductases....158
6.3.2 Impact of oxygenation on NirA function....166
6.4 Conclusions....174

Chapter 7 – Discussion....176
7.1 Does NirA represent a viable anti-virulence target....177
7.1.1 Is in vitro virulence factor production dependent on nitrate....177
7.1.2 Failure to determine the structure of NirA....179
7.1.3 Impact of NirA on growth and biofilm formation under micro-aerobic conditions....180
7.2 Hypothetical role of NirA in P. aeruginosa virulence....181
7.2.1 Reduced oxygenation and nitrate availability....181
7.2.2 Impact of cyanide on *P. aeruginosa* respiration....185
7.2.3 Cyanide, host-derived nitrate and NirA....187
7.3 Future perspectives....189

References....191

Abbreviations

AHL	*N*-acylhomoserine lactone
AMR	Antimicrobial resistance
bp	Basepair
C12-AHL	3-oxo-dodecanoyl homoserine lactone
C4-AHL	Butanoyl-homoserine lactone
CF	Cystic fibrosis
CFU	Colony forming units
dH2O	Deionised water
DNA	Deoxyribonucleic acid
EDTA	Ethylenediaminetetraacetic acid
g	Grams
g/L	Grams per litre
h	Hours
HCl	Hydrochloric acid
HHQ	2-heptyl-4-quinolone
IPTG	Isopropyl-1-thio-(-*D*-galactopyranoside)
Kb	Kilobase
kDa	Kilodalton
LB	Lysogeny Broth
M	Molar concentration
M-ASM	Modified artificial sputum media
MDR	Multiply drug resistant
mg	Milligrams
mins	Minutes
ml	Millilitres
mM	Millimolar concentration
ng	Nanograms
NO	Nitric oxide
OC	Degrees celsius
PIA	Pseudomonas isolation agar
PQS	Pseudomonas quinolone signal; 2-heptyl-3- hydroxy-4-

	quinolone
QS	Quorum sensing
s	Seconds
SD	Standard deviation
SDS	Sodium-dodecyl sulphate
SDS-PAGE	Sodium-dodecyl sulphate polyacrylamide gel electrophoresis
TAE	Tris-acetate-EDTA buffer
TB	Terrific broth
TBS	Tris-buffered saline
UV	Ultraviolet
V	Volts
v/v	Volume per volume
w/v	Weight per volume
xg	Times gravity centrifugal force
µg	Micrograms
µl	Microlitres
µm	Micromolar concentration

Chapter 1

Introduction

1.1 The global antimicrobial crisis and *Pseudomonas aeruginosa*

Bacteria are capable of surviving across a diverse range of environmental conditions, adapting to almost every ecological niche known to man. This success has led to extreme competition for resources between bacterial and fungal species occupying similar environments. To overcome and gain a monopoly over the often-limited carbon and nitrogen sources, microbial warfare is employed to kill or inhibit competing organisms. Humans have adapted some of these natural products for medical use, with the discovery of antibiotics and subsequent large-scale production of these antimicrobial compounds revolutionising medicine.

Antimicrobial resistance in not a new phenomenon. Prior to the use of antibiotics in general medicine it was known that bacteria could evolve to become resistant to these drugs. Penicillin G resistance was detected in 1940 before the release of this drug in 1943 (1). Widespread resistance to Penicillin G was found to be present in the bacterial population by the 1950's, limiting the effectiveness of this drug (2). Following this, humans own form of warfare with infectious bacteria began, with the discovery and development of new antibiotics pursued to keep ahead of the ever-expanding arsenal of resistance mechanisms and subsequent spread. This trend continued throughout the 'golden era' of antibiotic discovery, resulting in a wide range of antibiotics with various mechanisms of action being discovered. However, upon introduction into the clinic resistance soon emerged. In part, this was due to overzealous use of antibiotics in both clinical and agricultural practices, posing a wider selection pressure for the development of these antimicrobial resistant pathogens by forcing genetic bottlenecks (3).

In 2016 the Review on Antimicrobial Resistance, led by the economist Jim O'Neill, published the startling figure that an estimated loss of 100 trillion dollars could occur due to the emergence and spread of antimicrobial resistant infections by 2050. Currently around 700,000 deaths a year are attributed to antimicrobial resistance (AMR) infections, making AMR one of the biggest 'emerging' threats in modern-healthcare (4). With the 'golden age' of antimicrobial discovery in the past, and the limited number of new

antimicrobials currently in development, discovery of unique antimicrobials and novel therapies has never been of a higher priority.

Pseudomonas aeruginosa is a Gram negative, motile, rod-shaped bacterium capable of surviving in diverse environments. The ability of *P. aeruginosa* to colonise multiple environments is underpinned by its large genome size and extensive regulatory network, with 8.4-9.4% of ORF's encoding genes involved in regulation (5). This enables adaptation to diverse environments with modulation of metabolic and adaptation/protection genes ensuring survival. One of these environments is the human body, with *P. aeruginosa* causing 10-15% of nosocomial infections, placing a significant burden on healthcare world-wide (6). Underpinned by its metabolic versatility and plethora of virulence factors, *P. aeruginosa* can cause a diverse range of diseases enabling colonisation and infection at various body sites. For example, in 16.6% of ventilator associated pneumonia; 14% of wound; 14.1% of urinary and 8.2% of bloodstream infections, *P. aeruginosa* was found to be the main causative organism (7). *P. aeruginosa* can also attach and form biofilms on catheters, implants and respiratory equipment, often leading to establishment of chronic infections which are difficult to eradicate with standard antimicrobial therapy. These infections primarily occur in patients who are immunocompromised, such as those with cystic fibrosis, cancer, AIDS and diabetes (8).

P. aeruginosa is a member of the ESKAPE group of pathogens, differentiated according to their clinical relevance and ability to evolve multiple drug resistance (MDR) (9). Worryingly, strains of *P. aeruginosa* are now emerging which are considered pan-resistant, rendering current antimicrobial therapies ineffective (10-12). As of 2019, there were over 20000 infection cases by this organism of which 17% of the causing isolates were classified as carbapenem-resistant (13). As a result, the World Health Organisation (WHO) have listed carbapenem-resistant *P. aeruginosa* (CRPA) as 'priority 1' where there is critical need for the development of new antimicrobials with novel mechanisms of action (14). Development of new antibiotics with activity against CRPA or extended-spectrum beta-lactamase (ESBL) resistant *P. aeruginosa* has slowed, with only 2 currently in phase 3 trials as of March 2021. Both treatments rely on the use of new beta-lactamase inhibitors, combined with beta-lactam (cephalosporin) treatment (15). Neither of these satisfy the WHO directive of developing new drugs with a novel mechanism of action for use against CRPA.

With beta-lactamase variants already demonstrated to evolve resistance to beta-lactamase inhibitors, it seems likely that these new *P. aeruginosa* treatments will only be effective for a limited amount of time. This demonstrates the urgent need for the discovery of new antimicrobial compounds with a novel mechanism of action against *P. aeruginosa*.

1.2 Antimicrobial tolerance and resistance in *Pseudomonas aeruginosa*

1.2.1 Antimicrobial tolerance or adaptive resistance

Antimicrobial tolerance or adaptive 'resistance' is the process by which transient changes in gene expression or metabolic activity facilitates higher levels of antimicrobial tolerance in the absence of a dedicated resistance mechanism. This phenomenon was discovered as often treatment of chronic *P. aeruginosa* infections displaying no defined antimicrobial resistance mechanisms fails, with exacerbations re-occurring following treatment. Cells which are tolerant do not replicate in the presence of antimicrobial challenge, however they are also not killed. This distinguishes tolerance from active resistance, which enables bacteria to continue replication in the presence of antimicrobial challenge. The primary mechanisms by which this tolerance arises in *P. aeruginosa* is through production of a biofilm or the persister cell phenotype. Both phenotypes are interlinked and contribute to the tolerance exhibited by *P. aeruginosa*.

1.2.1.1 Biofilms and antimicrobial tolerance

One such behaviour resulting from transient changes in gene expression in *P. aeruginosa* is biofilm formation. The definition of what constitutes a biofilm is the subject of much debate. In the context of this thesis it is defined as an aggregate of micro-organisms encased by self-produced extracellular polymeric substances. This lifestyle is commonly divided into 5 stages, attachment, cell to cell adhesion, proliferation, maturation and dispersal. However, this view has recently been challenged as only specific to laboratory conditions whereas the *in vivo* dynamics are more complex. Bacterial life

predominantly exists as these communities, with the planktonic culture predominantly used throughout research seen as an intermediate phase in this lifestyle, facilitating spread of the bacterial population (16).

One of the key processes governing this transition from a planktonic to biofilm lifestyle is the universal signalling molecule c-di-GMP. Increased synthesis of c-di-GMP induces production of biofilm matrix components such as Psl, Pel and alginate, whilst decreased c-di-GMP downregulates production of these exopolysaccharides and induces dispersal of the biofilm. Production of c-di-GMP is mediated by diguanlyate cyclases (DGCs) whilst phosphodiesterases (PDEs) degrade this molecule. *P. aeruginosa* encodes over 40 DGCs and PDEs with many containing regulatory activation domains, requiring signal input before producing of degrading c-di-GMP. This c-di-GMP signalling network intersects with multiple 2-component regulators (GacSA, BfiRS and HsbAD), orphan histidine kinases (PA1611, LadS, SagS and ErcS), sigma factors (HsbA and FlgM), response regulators (RsmAN, FliA, FleQ, WspR) and small non-coding RNAs (RsmYZW). This forms an extremely complex regulatory network, with the processes governing this transition from a planktonic to biofilm lifestyle being the subject of several excellent reviews (17-19).

The *P. aeruginosa* biofilm is strain specific, consisting of exopolysaccharides and extracellular protein, lipids and extracellular DNA (eDNA) creating a complex architecture around bacterial cells (20). This protects the encased cell population from the immune system with components of the innate immune system, such as polymorphnuclear leukocytes (PMN's), unable to overcome the physical barrier imposed by the presence of the biofilm (21). Some antibiotics are also not able to penetrate the biofilm, primarily due to interactions with the extracellular matrix. This effect has been extensively studied with the positively charged tobramycin, sequestered by the negativity charged phosphate sugar backbone of eDNA in the biofilm (22, 23). Similar impedance mechanisms have also been described for aminoglycosides, beta-lactams and cationic antimicrobial peptides (16, 24, 25). Recalcitrant *P. aeruginosa* infections are linked with the presence of biofilms *in vivo*. This is primarily due to this antimicrobial tolerant phenotype, conferring up a 1000-fold increase in tolerance over their planktonic counterparts, enabling survival during multiple rounds of antimicrobial challenge (26, 27).

Part of this antimicrobial tolerance is imparted by the 3-dimensional structure of biofilms or bacterial aggregates. The physicochemical properties of these structures lead to establishment of multiple gradients, with resources such as metal ions, oxygen or nutrients depleted at the centre of biofilm-like structures (28-30). These gradients result in heterogeneous regions of bacterial gene expression, contributing to activation of antimicrobial tolerance and resistance mechanisms. For example, oxygen and nutrient limitation across a biofilm induces *P. aeruginosa* to enter a metabolically inert state, reducing the effectiveness of many antimicrobials which require active cell division to exert their bacteriostatic or bactericidal effect. These metabolically inactive bacteria are known as persister cells (PC's) (29, 31).

1.2.1.2 Persister cells and antimicrobial tolerance.

Physical impedance of entry by biofilm components is not enough to explain the array of antimicrobials *P. aeruginosa* can tolerate. Many non-polar antimicrobials are able to penetrate the biofilm effectively, yet *P. aeruginosa* still persists both *in vitro* and *in vivo* (32). The metabolically inert cells occur at a higher frequency in the depths of biofilms conferring extensive tolerance to antimicrobials which require active division to exert their effect (31). PCs are not unique to biofilms, with a sub-population present in stationary phase planktonic cultures (33). This transition is likely due to a similar mechanism seen in biofilms, where nutrient and oxygen become limiting because of the biological demand exerted by high cell density cultures (31, 34, 35). Nutrient and oxygen deprivation are not the only driving force behind PC formation, with various forms of environmental stimuli linked to emergence of this phenotype, including oxidative stress, antibiotic treatment and DNA damage (34, 35). Whilst biofilm formation does play a key role in the recalcitrance of *P. aeruginosa* infections, the driving force is PC formation. In the presence of antimicrobials, metabolically active cells in the biofilm are killed whereas PC cells are dormant and survive. Once treatment has ended, these cells can transition to a metabolically active state and proliferate, resulting in exacerbations of *P. aeruginosa* infection. Biofilm formation is hypothesized to be the mechanism by which high level PC's form *in vivo*, enabling survival from multiple rounds of antimicrobial therapy whilst the biofilm provides protection

from the host immune system (33, 35). This is linked to the emergence of active resistance mechanisms since continual exposure to multiple antimicrobials over a long-duration invariably leads to the development of MDR *P. aeruginosa*.

1.2.2 Antimicrobial resistance in P. aeruginosa

P. aeruginosa encodes a wide range of intrinsic resistance mechanisms, which can evolve to confer higher level or an extended spectrum of resistance, complicating treatment of even non-MDR *P. aeruginosa* infections. In addition to this innate resistance, the ability to acquire new resistance genes from various sources, makes *P. aeruginosa* extremely difficult to combat with standard antimicrobials.

1.2.2.1 Intrinsic resistance

Intrinsic resistance refers to the ability of an organism to diminish the effectiveness of an antimicrobial through use of inherent structural or functional mechanisms. *P. aeruginosa* possesses an extensive arsenal of intrinsic resistance mechanisms, which can be classified into 3 main categories: reduced outer membrane potential; efflux of target molecules; and modification of antimicrobials.

In Gram-negatives, the outer membrane consists of a phospholipid bilayer, permeated with protein structures termed porins. These structures form channels through the outer membrane enabling transfer of molecules in both directions. *P. aeruginosa* encodes 11 of these porins with the major non-specific porin being monomeric OprF (36). The action of OprF is linked to the lower membrane potential exhibited by *P. aeruginosa*. Porins of this family allow the uptake of ions and saccharides but have a narrow channel and low affinity for antimicrobials when compared to the major trimeric porins of *E. coli* OmpF and OmpC. As a result of this difference, it has been reported that *P. aeruginosa* has up to a 100-fold lower permeability compared to *E. coli*, slowing the uptake of many hydrophilic antibiotics (37, 38). This intrinsic resistance mechanism is very powerful, increasing resistance against many families of

antibiotics including Aminoglycosides, Quinolones, β-lactams and Polymyxins (32, 36).

Porins can also form part of a larger machinery termed efflux pumps enabling active removal of antimicrobial compounds before they can compromise the site of action. Gram negatives rely on RND-type transporters with antimicrobial efflux capability typically adopting a tripartite configuration with MFP-RND-Outer Membrane Protein (MFP-RND-OMP) components (39). *P. aeruginosa* has been shown to express up to 12 efflux pumps however, only 4 are reported to be clinically relevant in regards to antimicrobial resistance, MexAB-OprM, MexXY-OprM, MexEF-OprN and MexCD-OprJ (40) (Figure 1.1 I). These pumps are able to remove a wide range of molecules, with various structures, and often have overlapping substrate profiles. Efflux pumps are not specific for antimicrobials, but also have the ability to remove various molecules from the cytosol, including quorum sensing (QS) molecules (Figure 1.1 I). If not controlled, these efflux mechanisms could hinder QS-dependant adaptation to the host environment altering virulence (41-43). Therefore *P. aeruginosa* utilises multiple regulators with different inputs to manage expression, ensuring efflux is only upregulated under conditions of antimicrobial stress or when certain virulence factor production is no longer advantageous, such as during chronic infection.

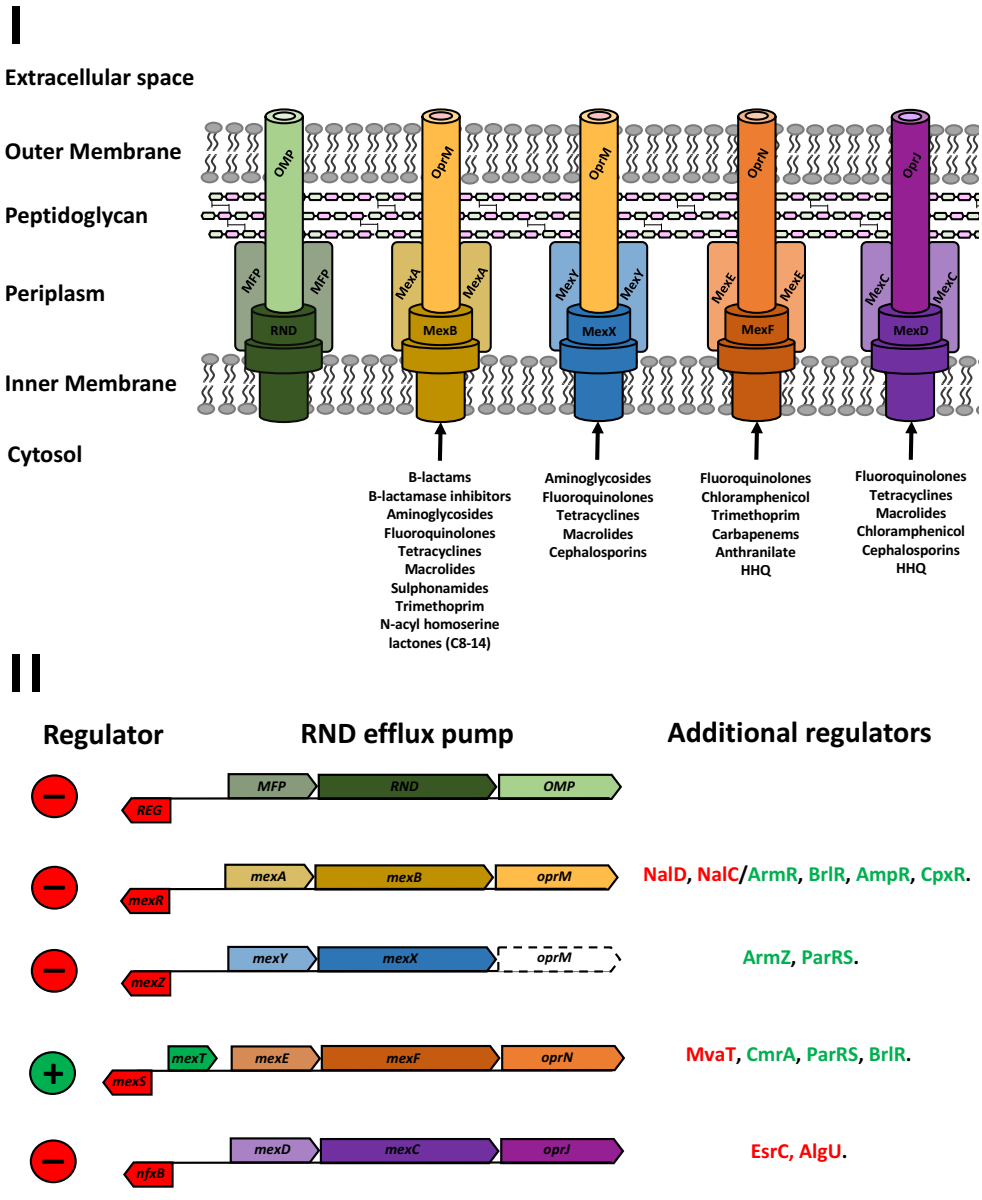

Figure 1.1 – Structural and genetic diagram of efflux pumps relevant to clinical antimicrobial resistance in *P. aeruginosa.* I) Structure of the prototypical RND efflux pump and pumps contributing to antimicrobial resistance in *P. aeruginosa*. The prototypical RND efflux pump consists of MFP-RND-OMP components with *P. aeruginosa* forming MexAB-OprM, MexXY-OprM, MexEF-OprN and MexCD-OprJ utilised to efflux antimicrobials and other compounds including quorum sensing signals. II) Genetic organisation and regulation of *P. aeruginosa* efflux pumps. The prototypical RND-type efflux pump operon consists of *MFP-RND-OMP* genes with a putative negative regulator upstream of the *MFP* gene denoted in red. Primary regulatory control mediated by MexR, MexZ, MexS/T and NfxB for *mexAB-oprM*, *mexYZ*, *mexEF-oprN* and *mexCD-oprJ* respectively. *P. aeruginosa* efflux pumps exhibit genetic and regulatory diversity in the mexXY and mexEF-oprN operon. In the case of mexXY, no putative OMP is encoded, instead complexing with OprM. Whilst the *mexEF-oprN* also contains the transcriptional activator protein *mexT* indicated in green, which is negatively regulated by *mexS.*

P. aeruginosa also possesses a number of antimicrobial modifying enzymes, inactivating harmful compounds before they can exert an anti-bacterial effect, including beta-lactamases and aminoglycoside transferases. For example, conserved amongst Gram negatives and *P. aeruginosa* is the chromosomally encoded *ampC,* a type C β-lactamase (44). This enzyme hydrolyses the β-lactam ring, via an active site serine, preventing inhibition of DD-transpeptidases involved with peptidoglycan cross-linking during cell wall synthesis. *P. aeruginosa* AmpC has been shown to target cephalosporins and its expression is induced upon detection of cephalosporin damage to the bacterial cell wall (45).

1.2.2.2 Acquired resistance

Supplementing the intrinsic antimicrobial resistance mechanisms commonly genome encoded, *P. aeruginosa* can acquire new genetic AMR determinants or adapt current resistance mechanisms. *P. aeruginosa* is able to quickly mutate and adapt, altering antimicrobial targets or regulators to prevent antimicrobial binding or enable overexpression of currently genome encoded resistance mechanisms. Furthermore, *P. aeruginosa* can also modulate its genetic content to enable foreign DNA to be assimilated, such as further antimicrobial resistance genes.

1.2.2.2.1 Regulatory re-wiring and resistance

Of special concern in *P. aeruginosa* is the regulatory re-wiring of efflux pumps, facilitating resistance to multiple unrelated antimicrobial compounds simultaneously. Mutation in key regulators can lead to hyper-expression of multiple efflux pumps with this phenomenon commonly displayed in clinical *P. aeruginosa* isolates. These mutations take a number of appearances with everything from a non-synonymous base pair substitution to frame-shifting responsible for overexpression. MexAB-OprM efflux has a very broad substrate range and is often overexpressed in mutant strains, resulting in basal resistance to multiple antimicrobials (Figure 1.1 I). Common mutations in the negative regulators of MexAB-OprM expression, *mexR*, *nalC* and *nalD*, lead to disinhibition and thus constitutive expression of the efflux pump (46-48). This

effect is not limited to the MexAB-OprM system, with concomitant upregulation of 2 or 3 efflux pumps observed in the clinic (49, 50). Mutation in *mexZ* results in constitutive activation of MexXY expression; modification in the *nfxB* reading frame causes disinhibition of the *mexCD-oprJ* operon; whilst activation of *mexT* or repression of *mexS* produces MexEF-OprN over-producing strains (Figure 1.1 II) (51-53). Overexpression of multiple pumps enables a broader range of antimicrobials to be removed offering a simplistic way for *P. aeruginosa* to adapt to new challenges.

1.2.2.2.2 Acquisition of resistance

Many bacteria possess the ability to take up and assimilate foreign DNA. This process is known as horizontal gene transfer, and has played a significant role in shaping the genomic landscape of bacteria as we know it (54). Three main mechanisms of horizontal gene transfer exist, conjugation, transformation and transduction. Antimicrobial resistance genes can be disseminated by specific DNA elements with plasmids, transposons, integrons and prophages transferred via 1 of the 3 mechanisms (54). The ESKAPE pathogens are particularly adept at this process, with horizontal gene transfer underpinning the extensive levels of resistance seen in these pathogens.

An important vehicle of antimicrobial resistance gene transfer are integrons. These elements contain an integrase gene; promoter and a site-specific recombination site enabling capture of mobile genetic elements and production of a composite ORF known as a cassette (55). This enables linkage and expression of multiple resistance genes from a single genetic element. *P. aeruginosa* integrons have been identified carrying resistance mechanisms to β-lactams, aminoglycosides, chloramphenicol, tetracycline, sulphonamides, macrolides, chloramphenicol, carbapenems, antiseptics and disinfectants (55, 56). This has important implications clinically as use of a single antimicrobial could inadvertently select for multiple resistances in a process known as co-selection. Despite integrons being considered mobile elements, they do not encode the machinery required for transfer. This does not account for the dissemination of antimicrobial resistance seen in bacteria. Intercellular and interspecies transfer of resistance genes are primarily mediated through phage transduction; natural transformation and conjugative plasmid transfer (57).

One of the key drivers of antimicrobial resistance in Enterobacteriacea is the presence and dissemination of plasmids encoding multiple antimicrobial resistance genes. Plasmids are extra-chromosomal DNA which possess their own replication machinery to ensure maintenance from generation to generation. Some of these plasmids encode machinery responsible for conjugative transfer, forming a type VI-like pili, through which a plasmid can transfer horizontally cell to cell (57). However, the role plasmids play in dissemination of MDR in *P. aeruginosa* is not well understood with most studies focussing on other members of Enterobacteriacea. It stands to reason that plasmids play a similar role in *P. aeruginosa* antimicrobial resistance dissemination and the evidence is beginning to mount. Around 30-40% of MDR *P. aeruginosa* harbour one or more plasmids, whilst a recently identified group of megaplasmids codes for numerous resistance genes with β-lactam, aminoglycoside, sulfanomides, tetracycline, macrolides and phenicols; alongside an efflux pump (MexCD-OprJ) being identified in clinical strains of *P. aeruginosa* (57, 58). This extensive range of resistance determinants are associated with multiple integrons and transposons. Normally only capable of intracellular transfer, mobilization onto a plasmid enables the antimicrobial resistance genes accumulated on integrons and transposons to be disseminated both vertically and horizontally. This process can be both intra and inter-species enabling *P. aeruginosa* to derive antimicrobial resistance genes from a wide variety of sources and adapt accordingly.

1.3 Development of novel antimicrobials

The wide range of mechanisms, and mobile nature of antimicrobial resistance demonstrates a critical problem with our current approach to tackling bacterial infections. Initial success with antibiotic development led to reduced investigation into alternative therapies such as phage treatment or vaccination. However, this reliance on antibiotics as a ‘fix all’ treatment has now rendered a large amount of these compounds useless. The AMR problem is multi-faceted, therefore a range of alternatives are required to enable effective treatment. Development of novel antibiotics is critical to success in the fight against AMR, but the development of alternative treatments is essential in extending the

lifecycle of these essential compounds. As a result, research into alterative antimicrobial therapies has taken an important place in the ongoing battle against antimicrobial resistance (4). Summarised below are a few alternative therapies being explored to bypass AMR.

1.3.1 Phage therapy

Bacteriophage are viruses which specifically target bacteria, entering the bacterial cytoplasm and taking over cellular machinery to synthesize new bacteriophages. This eventually results in bacterial lysis, with the progeny capable of infecting more bacteria, continuously repeating the cycle until no prey remains (59). In light of the antimicrobial resistance problem, research utilising bacteriophage medicinally has renewed. The interaction between phage and bacteria is highly specific and phages can be identified to target most bacterial species, irrespective of MDR (60). In Eastern Europe phage therapy has long been utilised to treat bacterial infections however, in Western countries the approved use of phages is limited to treatment of food products with ListShield, EcoShield and SalmoFresh used to eradicate *Listeria monocyogenes*, *E. coli* and *Salmonella sp.* respectively (61). Medicinal phage-based therapies are now in clinical trials to treat many of the ESKAPE pathogens, including *P. aeruginosa*. These are largely limited to topical applications with products such as Phagoburn applied directly to burn wounds and soft-tissue infections respectively (62). Phage cocktails have also been used to target CF pathogens, including *P. aeruginosa*, with either direct delivery into the lung or though nebulisation and inhalation of phage. This is still the subject of ongoing research, with use of such phage cocktails the result of compassionate use as opposed to clinical trials (63-65). Much like antibiotics, resistance may become a problem, with clinically important pathogens such as *Salmonella* and *Clostridium difficile* demonstrating extensive phage resistance or evolving resistance post-treatment (66, 67).

1.3.2 Bacterial vaccination

Vaccination is one of the most successful tools utilised to combat harmful infections, priming the immune system to deal with future infections. Bacterial vaccines were primarily used to target lethal childhood infections. With simplistic preparative techniques, live-attenuated or killed whole cell vaccines were developed to combat a variety of diseases, such as cholera, tuberculosis and typhoid fever (68). As with phage therapy, research into bacterial vaccination was reduced due to reliance on antibiotics as a remedy for all. With most bacterial infections manifesting in the elderly population, it was presumed that bacterial vaccination would have limited application with natural immune senescence limiting the response generated in the at-risk population (69). Recent advances in adjuvant development have demonstrated improved responses in the important 65+ category. With the newly developed RZV and Heplilav-B vaccines against Herpes-zolster and Hepatitis B demonstrating 91-92% efficacy, it was shown that the elderly immune system can still be primed, given the correct stimulation (70). Whether these new adjuvants can be adapted to bacterial vaccination has yet to be determined however, focus should be on targeting ESKAPE pathogen infections in this key age bracket, with 40% of all antimicrobials being prescribed to the 65+ age category (71). Previous attempts to combat *P. aeruginosa* via surface exposed immunogenic structures and proteins such as LPS and flagellar have largely failed due to a combination of toxicity and antigenic drift. These attempts are summarised nicely in a review by Priebe and Goldberg (72). More recent research has focused on identification of new vaccine targets, with promising data now emerging through use of whole genome and proteomics approaches, to identify surface exposed vaccine targets which are conserved in the population (73, 74). Whilst a promising avenue of research worthy of further investigation, the release of a vaccine for *P. aeruginosa* remains years away from significantly contributing to the current AMR problem.

1.3.3 Anti-virulence therapeutics

The focus with current antimicrobials is to eradicate an infection through inhibition of bacterial growth pathways. This places a large selection pressure

on the causative organism, forcing the bacteria to adapt or perish. Anti-virulence therapeutics take an alternative approach, by limiting the capacity of the causative organism to adapt, colonise and cause disease. Pathogenic bacteria produce an arsenal of structures and biomolecules, collectively termed virulence factors, which facilitate the establishment of bacterial infections. Virulence factors have numerous roles in disease establishment and progression, for example they may: cause local host cellular damage; subvert the host immune system; and allow the organism to successfully outcompete the host microbial population. By inhibiting specific aspects of virulence which are indispensable to the success of the pathogen, adaptation to the host environment and disease progression will be impeded, providing valuable time for the host immune system to clear these pathogens (Figure 1.1).

Multiple approaches have been researched when implementing an anti-virulence strategy. These approaches can mechanistically be defined as:

1) Direct virulence factor neutralisation.
2) Inhibition of virulence factor assembly and secretion.
3) Interference with virulence factor regulation.

1.3.3.1 Virulence factor neutralisation

Direct interference with virulence factor function has been explored as a viable anti-virulence approach since the 19th century, with the development of an antiserum to combat diptheria toxin (75). Technological limitation and the discovery of antibiotics soon after, prevented wide-scale use. Advances in technology and enhanced understanding of virulence factors and their interactions with the immune system paved the way for development of multiple anti-virulence therapeutics based on toxin neutralisation. Immunoglobulin based therapies have been developed to inhibit botulinum neurotoxin (*Clostridium botulinum*): lethal toxin and oedema toxin (*Bacillus anthracis*) and LdtAB (*Clostridium difficile*) (76-78). This approach is now being explored in ESKAPE pathogens, with small molecule inhibitors of alpha-hemolysin (*Staphylococcus aureus*) (79); shiga toxins Stx1 and 2 (*E. coli*) (80, 81). Direct toxin neutralisation approaches for *P. aeruginosa* have recently been explored, with single-chain antibodies developed targeting Exotoxin A and the elastase

LasB (Figure 1.2) (82-84). However, research in this area is at early stages with work only characterised *in vitro*.

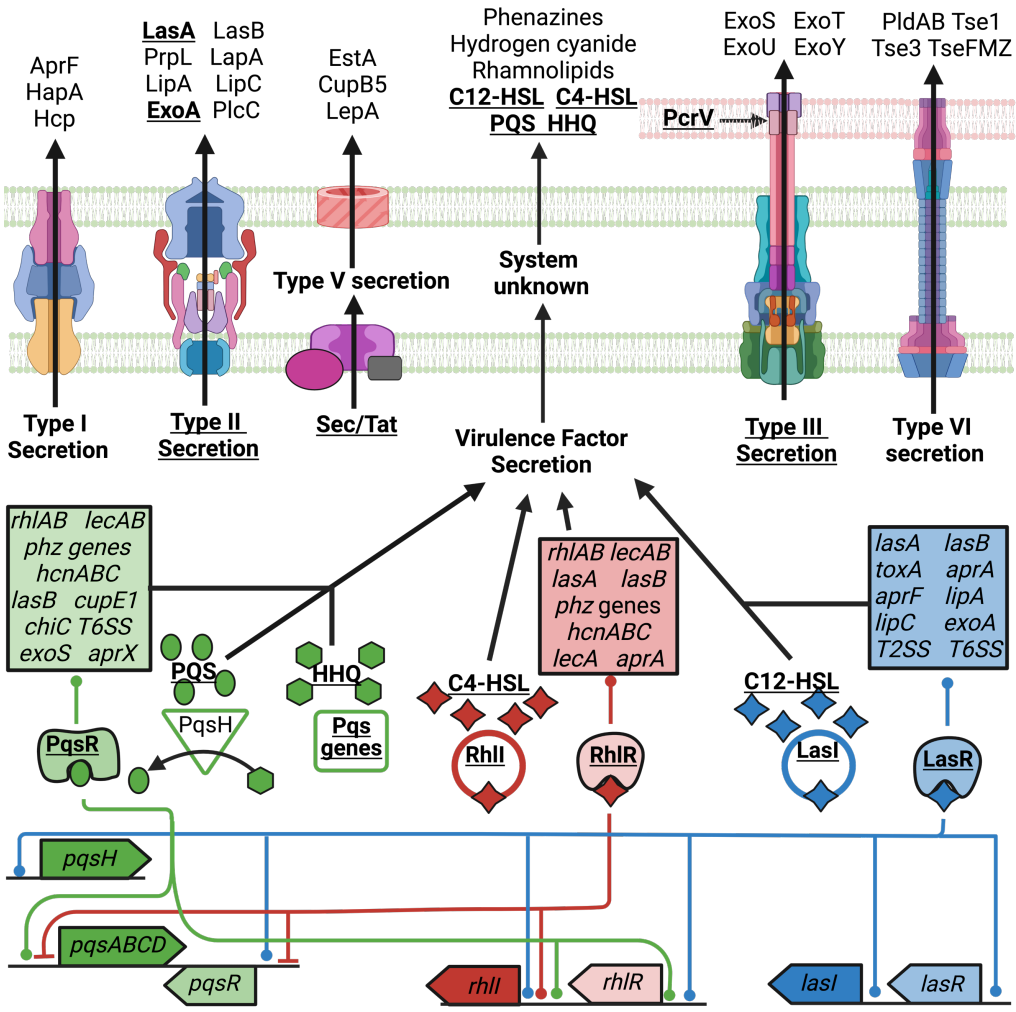

Figure 1.2 – Diagram depicting regulation, production and secretion of virulence factors important for *P. aeruginosa* pathogensis. Under laboratory conditions LasR is the master regulator of QS, upregulating auto-inducer biosynthesis of the *rhl* and *pqs* systems. RhlR negatively regulates *pqsABCD* and *pqsR* whilst PqsR positively regulates *rhlI* and *rhlR* transcription. These interconnected systems control transcription of numerous virulence factors and have distinct but overlapping regulons. The secretion systems of *P. aeruginosa* are responsible for delivering these effectors into extracellular space (Type I, II and V); directly into a eukaryotic cell (Type III); or into competing microbial organisms (Type VI). Anti-virulence therapeutics can be designed to inhibit various aspects of virulence factor production including, regulation, secretion or effector binding. Those components indicated in **bold and underlined** are the subject of inhibitory studies using an anti-virulence strategies. More details on these strategies can be found in tables 1.1 and 1.2.

1.3.3.2 Targeting virulence factor secretion and assembly

With virulence in *P. aeruginosa* being a multi-faceted process involving multiple toxins, proteases and biostructures, inhibition of a single virulence factor would likely be insufficient for widespread use as a universal treatment strategy. Bacterial secretion systems are an attractive therapeutic target as these specialised structures are surface exposed and responsible for delivery of multiple virulence factors to the site of action (Figure 1.2). As a result, inhibition of these systems will theoretically inhibit multiple processes required for virulence. *P. aeruginosa* uses a variety of secretion systems to deliver virulence associated proteins into the local environment (Type I, II and V), or directly into a target host cell of competing organism (Type III and VI) (85). All of these systems are responsible for secreting multiple virulence associated proteins or enzymes involved with adhesion, biofilm formation, protease, lipase and exotoxin secretion (Figure 1.2).

The extensively characterised needle-like Type III secretion system (T3SS) has been the prime target of inhibition. Multiple clinically relevant MDR Gram-negative pathogens such as *E. coli*, *Shigella sp., Salmonella sp., Vibrio sp., Burkholderia sp., Yersinia sp.* and *Pseudomonas sp*. all utilise T3SS systems to deliver multiple effector proteins (86). As a result, any inhibitors developed would be specific to these pathogens and provide treatment options to MDR variants of these organisms. The T3SS of *P. aeruginosa* has only 4 known effector proteins, exotoxins ExoS, ExoT, ExoU and ExoY however, these effectors target a broad-range of eukaryotic cells (87). Inhibition attempts have primarily focussed on disruption of T3SS assembly or function, preventing translocation of effectors to the target cell. Numerous T3SS inhibitors have been identified targeting the essential ATPase, needle or translocon assembly and effector secretion. However, *in vivo* efficacy data is scarce and the number of these therapies in clinical trials is low (88). The only potential therapies to make clinical trials are therapeutic antibodies targeting the T3SS translocation protein PcrV (KB001), and a novel bivalent antibody (MEDI3902) targeting both PcrV and the Psl exopolysaccharide (89, 90). KB001 phase II clinical trials were abandoned as the antibody failed to meet efficacy endpoints, whilst MED3902 is currently in phase II clinical trials although this was delayed due to the impact of the SARS-COV2 pandemic (91, 92). An increased focus on translational research into the clinic by both academic and pharmaceutical research groups

is required to screen the effectiveness of these potential therapies as alternatives to antimicrobial treatment. Details of further secretion inhibition attempts in *P. aeruginosa* can be found in table 1.1.

Secretion Inhibitors	Inhibitor type	Inhibitory activity	Mechanism of action	Virulence factors	In vivo attenuation?	Ref
KB001	Antibody	Anti-T3SS	Inhibits T3SS assembly	Antibody that binds and inactivates T3SS tip protein PcrV.	Chronic murine lung model	(89, 91)
MEDI3902	Antibody	Anti-T3SS Anti-biofilm	Inhibits T3SS assembly and host cell attachment	Bivalent antibody targetting PcrV and Psl exopolysaccharide	Murine pneumonia, burn and sepsis models	(92)
Tanshinones	Small-molecule	Anti-T3SS	Inhibits PscF needle biogenesis	T3SS components PscEFG	No	(93)
C5631	Small-molecule	Anti-T3SS	Interrupts T3SS regulation	ExcA, AraC-type positive transcriptional regulator of T3SS assembly Reduced exotoxin release and toxicity in Chinese hamster ovary cell culture	No data	(94)
MBX2359	Small-molecule	Anti-T3SS	Inhibts PscF needle biogenesis	T3SS structural components PscEFG Reduced ExoTSU release	Murine abscess model	(95)
R101SPM	Small-molecule-	Anti-T3SS Anti-QS?	Blocks spermidine and spermine dependent regulation	ExcA, AraC-type positive transcriptional regulation of T3SS assembly Decreased expression of *rhlI* and *pqsA* Reduced virulence in A549 epithelial cell line	Intraperitoneal murine lung model	(96)
Mab4e4	Antibody-spermidine conjugate	Anti-T3SS	Blocks spermidine and spermine uptake dependent regulation of T3SS	Reduced exotoxin release Reduced toxicity in A549 epithelial cell line	Acute murine lung infection	(97)
INP0341	Small-molecule	Anti-T3SS	Interferes with T3SS regulation	Reduced exotoxin production and release Reduced virulence in THP-1 monocyte and A549 epithelial cell lines	No data	(98)
INP1750 (hydroxyquinoline)	Small-molecule	Anti-T3SS	Inhibits ATPase of T3SS	Reduced exotoxin release and swimming motility Reduced virulence in THP-1 monocyte and A549 epithelial cell lines	No data	(98)
TAT-1 and TAT-2	Small-molecule	Anti-Tat	Not defines	Reduced pyoverdine production	No data	(99)
T2S-1	Small molecule	Anti-T2SS	Not defined	Reduced elastase production	No data	(99)
77790677 and 7801810	Small molecule	Anti-T2SS	Not defined	Reduced LasB and PlpH/C secretion	No data	(100)

Table 1.1 – Anti-virulence strategies targeting secretion in *P. aeruginosa*.

1.3.3.3 Targeting virulence factor regulation

Bacterial communication systems are key to successful establishment of a bacterial infection. Coordinated expression of virulence factors is required to enable colonisation, immune system subversion, interspecies competition and persistence at the site of infection. Quorum-sensing (QS) is one of the most widely distributed communication systems amongst pathogenic bacteria, synchronising expression of multiple virulence associated proteins upon accumulation of a threshold concentration of specific auto-inducer signal. The auto-inducer signal is secreted into the local environment and diffuses into the cytoplasm of bacteria in close proximity. These signals are subsequently bound by cognate receptors, triggering alterations in gene expression associated with upregulation in virulence factors (Figure 1.2) (101).

P. aeruginosa utilises three distinct QS signalling systems, LasRI, RhlRI and PqsABCDEHR. LasI and RhlI synthesize *N*-3-oxododecanoylhomoserine lactone (C12-AHL) and *N*-butanoylhomoserine lactone (C4-AHL) respectively, whilst PqsR recognises 2-heptyl-3-hydroxy-4(1*H*)-quinolone or the Pseudomonas Quinolone Signal (PQS) and the precursor molecule 2-heptyl-4(1*H*)-quinolone (HHQ) as auto-inducer signals (Figure 1.2) (102). The QS systems of *P. aeruginosa* controls multiple virulence factor expression directly or indirectly, with overlapping but distinct regulons. These QS systems also regulate each other, fine-tuning expression of virulence associated genes depending on the environment and stage of infection (Figure 1.2) (102). This could prove advantageous from an anti-virulence development perspective, with knockdown of a single QS system triggering dysregulation in the remaining systems. As a result of this property, development of anti-virulence compounds specific to *P. aeruginosa* QS systems is a highly active area of research. Targeting of these bacterial communication systems can be separated into three main mechanisms:

1. Inhibition of auto-inducer biosynthesis.
2. Interference with auto-inducer detection.
3. Inactivation of the auto-inducer signal.

Targeting each of these aspects of QS has advantages and caveats. Inhibition of auto-inducer biosynthesis has largely been explored with small-molecule

inhibition, focussing on structural analogs of the auto-inducer signal or precursors. For example, multiple small-molecule inhibitors have been designed to target the first enzyme in the PQS biosynthesis pathway, the anthranilyl-CoA ligase PqsA. Inhibitors of this system are structural mimetics, such as anthranilyl-MAS, methyl-anthranilate and halogenated-anthranilate (103). These molecules bind to PqsA and occlude access of the PQS precursor anthranilate. Acyl homoserine lactone (AHL) analogues have also been explored as inhibitors of the AHL synthases LasI and RhI through increasing the length of the acyl carbon chain or use of 3'-sulfide containing AHL-like molecules (104-106). Similarly, inhibition of auto-inducer detection has been ligand based with quinazolinone and meta-bromo-thiolactone structurally similar to PQS and AHL respectively (107, 108). Targeting auto-inducer signal synthases and detection in this way would be advantageous from an inhibitor development perspective, as humans do not produce these enzyme and regulators, minimising off-target effects in the host. However, the intracellular location of these enzymes could prove problematic, with inhibitors required to cross both membranes and are potentially susceptible to resistance development through efflux upregulation (109). Non-ligand based inhibitors of QS could partially alleviate this problem of efflux, with multiple non-competitive inhibitors developed to inhibit auto-inducer detection.

Direct inactivation of the auto-inducer signals circumvents the problem of cellular localisation, due to the secreted nature of the signal molecule. This simplifies access by anti-QS inhibitors, although the highly specific nature of these QS signals may limit interspecies use. Inhibitors of this nature are termed quorum-quenching (QQ), with many enzymes inactivating autoinducer molecules occurring in nature as a microbial warfare strategy. Enzymes which inactivate the auto-inducers of *P. aeruginosa* have been identified and purified from diverse bacterial species, suggesting this is a widespread mechanism of interspecies competition (109, 110). The first anti-Pseudomonas QQ enzymes identified were the AHL-lactonases with AiiA reported by Dong and colleagues in 2000 (111). These enzymes are capable of hydrolysing the homoserine-lactone ring of the *rhl* and *las* AHL auto-inducers, with heterologous expression of AiiA in *P. aeruginosa* demonstrated to reduce accumulation of both C12-AHL and C4-AHL. This has since expanded with multiple enzymes identified to have QQ activity from diverse bacterial species (110). The AHL-acylases destroy the amide-bond between the lactone ring and acyl tail; AHL-

oxidoreductases modify the oxidation state of the acyl-chain reducing affinity to the cognate receptor; and dioxygenases from *Mycobacterium absessus* (AqdC1 and AqdC2) target alkyl-quinolone molecules such as PQS (110, 112). Engineered versions of these enzymes have been tested for effectiveness in animal infections models with the SsoPox-W2631 and AiiM lactonases demonstrated to reduce lung damage and mortality in an acute murine lung infection model (113, 114). Table 1.2 summarises the anti-QS approaches taken above alongside numerous more attempts taken to inhibit virulence. This list is far from exhaustive with anti-QS based virulence inhibition an extremely active area of research in *P. aeruginosa*.

Secretion Inhibitors	Inhibitor type	Inhibitory activity	Mechanism of action	Virulence factors	In vivo attenuation?	Ref
2-(methylsulfonyl)-4-(1H-tetrazol-1-yl)pyrimidine	Small-molecule	Anti-QS Anti-Biofilm	Dual PqsD and PqsR structural analogues	Reduced pyocyanin, pyoverdine and biofilm production	*G. mellonella*	(115)
TZD-C8	Small molecule	Anti-QS Anti-Biofilm	LasR or RhlR antagonist	Reduced biofilm formation Reduced swarming motility	No data	(116)
Meta-bromo-thiolactone	Small molecule	Anti-QS Anti-Biofilm	RhlR antagonist	Reduced biofilm formations Downregulation of *rhlAB* and *phz* genes Reduced virulence in A549 epithelilal cell line	*C. elegans*	(107)
Zingerone	Small molecule	Anti-QS Anti-biofilm	Undefined inhibitor of AHL signal detection	Reduced biofilm, pyocyanin, hemolysin, elastase and rhamnolipid production.	No data	(117)
AHL-nitric oxide hybrids	Small molecule	Anti-QS	LasR antagonist + NO releasing group	Reduced pyocyanin and elastase production	No data	(118)
Parthenolide	Small molecule	Anti-QS Anti-Biofilm	Undefined AHL signal synthase or receptor inhibitor	Reduced pyocyanin, protease and biofilm production	No data	(119)
N-(4-{fluroanilno}-butanoyl-L-homoserine lactone	Small molecule	Anti-QS Anti-Biofilm	AHL analogues	Reduced biofilm production	No data	(120)
Pyrone analogs	Small molecule	Anti-QS Anti-Biofilm	LasR antagonists	Downregulation of *lasA, lasB, rhlAB, phzC1* and *phzE1*. Reduced biofim production	No data	(121)
Pyridoxal lactohydrazone	Small molecule	Anti-QS Anti-biofilm	LasR antagonist	Reduced biofilm, alginate and pyocyanin. Reduced swarming and twitching.	No data	(122)
Fluoro-substituted Isothiocyanates	Small molecule	Anti-QS	LasR antagonist	Reduced pyocyanin production and swarming motility Reduced virulence in ex-vivo human skin burn model	*C. elegans*	(123)
Zeaxanthin	Small molecule	Anti-QS Anti-biofilm	LasR and RhlR anatagonist	Reduced biofilm formation Downregulated *rhlA* and *lasB*	No data	(124)

Phenyllactic acid	Small molecule	Anti-QS Anti-biofilm	RhlR and PqsR antagonist	Reduced pyocyanin, protease, rhamnolipid and hemolysin production Reduced swarming motility and biofilm formation	Mendaka fish	(125)
Metformin	Small molecule	Anti-QS Anti-biofilm	LasR and RhlR antagonist	Reduced biofilm, pyocyanin, protease, hemolysin and elastase production Reduced swimming and twitching motility	No data	(126)
Glyceryl trinitrate	Small molecule	Anti-QS Anti-Biofilm	LasR and RhlR antagonists	Reduced biofilm, pyocyanin and protease production	No data	(127)
4-amino-quinolone-based compounds	Small molecule	Anti-QS Anti-biofilm	PqsR antagonists	Reduced biofilm and pyocyanin production	No data	(128)
Quinazolinone based compounds	Small molecule	Anti-QS Anti-biofilm	PqsR antagonist	Reduced biofilm and pyocyanin production	No data	(108)
Courmarin	Small molecule	Anti-QS Anti-biofilm	Unknown	Reduced c-di-GMP, biofilm, protease, pyocyanin and T3SS production. Downregulated *lasI, rhlI, rhlR, pqsB, pqsC* and *pqsH*.	*Lucila sericata*	(129)
Clofoctol	Small molecule	Anti-QS Anti-biofilm	PqsR antagonist	Reduced pyocyanin, swarming and biofilm production	*G. mellonella*	(130)
Anthranilyl-MAS Methyl-anthranilate Halogenated-anthranilates	Small molecule	Anti-QS	PqsA antagonists	Reduced HHQ and PQS production.	No data	(103)
SsoPox-W2361	Enzyme	Anti-QS Anti-biofilm	AHL-lactonase	Reduced pyocyanin, elastase and protease production	Acute murine lung model	(113)
AqdC1, AqdC2 and QsdA	Enzyme	Anti-QS	HHQ and PQS dioxygenase	Reduced pyocyanin, pyoverdine and rhamnolipid production	*C. elegans*	(131)
AiiM	Enzyme	Anti-QS	AHL-lactonase	Reduced pyocyanin, protease, pyoverdine and elastase production	Acute murine lung model	(114)

Table 1.2 – Anti-virulence strategies targeting quorum-sensing in *P. aeruginosa.*

1.3.3.4 Anti-biofilm therapeutics

The anti-virulence strategies and compounds discussed above are primarily targeted towards acute *P. aeruginosa* infection, inhibiting production of virulence factors associated with this lifestyle. *In vivo*, *P. aeruginosa* forms aggregates and biofilms characterised by extensive exopolysaccharide and eDNA production. As discussed in section 1.2.1, bacteria in this aggregated and biofilm state are more tolerant to antimicrobial treatment and can potentially reoccur once treatment is withdrawn. As a result, anti-virulence therapeutic development is also being explored to combat bacterial biofilm

formation. With regards to *P. aeruginosa*, the hope would be to use anti-biofilm compounds to trigger dispersal or reduce the tolerance of these communities, re-sensitising the bacteria to antimicrobial or acute anti-virulence treatment. In theory, this combination would allow full eradication, combatting both acute and chronic infection.

Due to the highly conserved use of c-di-GMP as a universal signal for the transition to a biofilm lifestyle, development of small molecule inhibitors that can either activate phosphodiesterases (PDEs) or inhibit diguanylate cyclases (DGCs) may trigger biofilm dispersal. The structure of these enzymes can be highly variable, often found fused to regulatory or effector domains. This allows PDEs and DGCs to control the transition from planktonic to sessile and vice versa (132). Despite these differences, generating molecules which selectively interact with PDEs or DGC's is extremely challenging as both strongly bind c-di-GMP. Adding to this complexity is the fact that some PDEs and DGCs do not manipulate c-di-GMP concentrations, instead regulating other aspects of metabolism and virulence factor production (133). Extensive functional and structural characterisation of target PDEs and DGCs is first required to ensure the desired outcome. Despite this difficulty, progress has been made in identifying PDE activators and DGC inhibitors. For example, nitric oxide (NO) has been identified to induce biofilm dispersal in *P. aeruginosa*. This molecule is produced as a reactive nitrogen species (RNS) by polymorphnuclear leukocytes (PMNs) in response to bacterial infection, with NO acting as a potent respiratory inhibitor (21, 134). Low levels of NO have also been shown to stimulate PDE activity, enhancing degradation of c-di-GMP and triggering biofilm dispersal, giving NO two modes of antimicrobial activity (135). *In silico* screening for molecules that competitively inhibited the *P. aeruginosa* DGC WspR identified four candidates (LP1062, LP3134, LP3145 and LP4010). These small-molecules were shown to prevent biofilm formation and induce dispersal in *P. aeruginosa*, re-sensitising the biofilms to antimicrobial treatment (136). Other attempts at inhibiting establishment of biofilm and mature biofilms have looked to interfere with the physical components of the biofilm, such as exopolysaccharide, eDNA, fimbrae, rhamnolipids and extracellular proteins. DNAse has been used to promote biofilm removal without killing *Camplylobacter jejuni* (137). Single-chain variant fragment antibodies have been designed to target the exopolysaccharide Psl, mediating

opsonophagocytic killing and inhibiting *P. aeruginosa* attachment to lung epithelial cells (138).

As highlighted in table 1.2, there is a clear link between biofilm formation and the QS network in *P. aeruginosa*. The majority of the inhibitors targeted towards the *las*, *rhl* or *pqs* systems demonstrate anti-biofilm characteristics, although the molecular mechanisms underpinning this link are complex and only just beginning to be understood. In part, the requirement of QS for biofilm formations is due to QS positively regulating production of virulence factors supporting biofilm maturation. For example, pyocyanin and phenazines function is not limited to their cytotoxicity. These redox active molecules aid respiration in biofilms, shuttling electrons to regions where electron acceptors such as oxygen and nitrate are limited (139, 140). Further to this, phenazines can cause H_2O_2 production, resulting in lysis of competing organisms in mixed biofilm populations and eDNA release (141). Release of eDNA is also governed by QS directly with PQS, regulating membrane vesicles release containing eDNA PQS and triggering kin lysis in a small population of the biofilm through prophage induction (142, 143). Conversely, QS can trigger biofilm dispersal. Rhamnolipids, controlled by the AHL signalling systems, are important for mature biofilm formation by maintaining the intracellular channels responsible for nutrient and oxygen delivery. However, production of rhamnolipids also triggers *P. aeruginosa* release in mature biofilms, lowering surface tension to trigger dispersal events (144, 145). This counterintuitive relationship can also be shown in production of the Pel exopolysaccharide. LasI and RhlI auto-inducer production has been demonstrated to transcriptionally activate the *pel* genes, whilst LasR triggers upregulation of the PDE TpbB, reducing c-di-GMP and downregulating Pel production (146, 147). With nutritional cues such as carbon and nitrogen source metabolism; biofilm model; stage of biofilm development; and genetic background influencing biofilm development, these regulatory mechanisms may be context specific and thus, the anti-biofilm properties of many of these anti-QS compounds may also be context specific (148). Careful screening of these anti-QS and biofilm compounds must first be performed with multiple biofilm models, medias and preferentially *in vivo* before confirming true inhibition of biofilm development.

1.5 Aims and objectives

Whilst a large number of anti-virulence and anti-biofilm compounds have been identified, none have yet made it into the clinic (Table 1.1). This type of work is still in its infancy, and these difficulties are in part due to the characteristics required of these compounds. The majority of antibiotics function by inhibiting bacterial growth pathways. This simplifies screening of potential antibiotics as the impact on growth can be easily observed using high throughput technologies. As a result, potential antibiotics are identified before the mechanism of action is uncovered.

Candidate anti-virulence compounds are more difficult to identify as they demonstrate no attenuation in growth with these drugs not targeting microbial growth pathways. This complicates identification of anti-virulence drugs since assays based on bio-reporters, *in vitro* virulence factor production or *in vivo* virulence attenuation need to be used to identify effects. These methods are more laborious and do not lend themselves to high-throughput assays, resulting in an inability to define success when screening compound libraries for virulence inhibitors. As a result of these caveats in virulence inhibitor identification, focus is placed on identifying virulence targets and understanding the function of these proteins and enzymes prior to inhibitor development. From this, specific *in vitro* or *in situ* assays can be developed based on the function of the target, enabling high-throughput screening of inhibitor candidates. As a result, alternative virulence targets need to be identified to eventually allow an arsenal of anti-virulence compounds to be developed, combatting *P. aeruginosa* in different phases of infection at multiple host sites.

The work in this thesis aims to functionally and structurally characterise a potential anti-virulence target identified using the transposon mutagenesis platform designed by Dubern and colleagues (149). The transposon mutant PAJD21 was identified as attenuated for pyocyanin production and swarming motility, with survival in *C. elegans* and *D. melanogaster* also compromised when compared to the PAO1-L wildtype strain. At the outset, the primary aims were as follows:

1) Validate the role of PA4130 in virulence and virulence factor production using in-frame deletion mutants and genetic complementation.

2) Determine the structure and function of a novel target with a view to developing a high-throughput assay and identifying virulence inhibitors.

3) Elucidate the mechanism of regulation and how the novel virulence factor contributes to *P. aeruginosa* virulence.

Chapter 2

Materials and Methods

2.1 Bacterial strains

All strains used in this study are listed in Table 2.1.

Strains	Description	Origin
P. aeruginosa **strains**		
PAO1-L	PAO1 Lausanne collection wild type	(150, 151)
PAJD21	Strain PAO1-L with Tn5 insertion in PA4130 Gm^R in PAO1-L	This study
PASF06	In-frame marker-less deletion of PA4129 in PAO1-L	This study
PAJD25	In frame marker-less deletion of PA4130/*nirA* in PAO1-L	This study
PAJD25 CTX4130	PAJD25 with pCTX4130 integrated at the *attB* site.	This study
PASF10	In-frame marker-less deletion of *nirB.*	This study
PASF11	In frame marker-less deletion of PA4130 and *nirB* in PAO1-L	This study
PAO6344	In frame marker-less deletion of *hcnB* in PAO1-L	Collection of Prof. Haas
PA7 Bo599	Clinical PA7 strain	(152)
PA7 Bo599 ΔPA4130	In-frame marker-less deletion of PA4130 orthologue	This study
PA14 AUS471	Clinical PA14 strain	(152)
PA14 AUS471 ΔPA4130	In-frame marker-less deletion of PA4130 orthologue	This study
LESB58 PA-W39	Clinical LESB58 strain isolated from wound.	(152)
LESB58 PA-W39 ΔPA4130	In-frame marker-less deletion of PA4130 orthologue	This study
PAO1-L SJF10	PAO1-L wild-type with a *PnirA-lacZ* translational reporter chromosomally integrated.	This study
PAO1-L SJF11	PAO1-L wild-type with a *PhcnA-lacZ* translational reporter chromosomally integrated.	This study
PAO1-L SJF12	PAO1-L wild-type with a *PnirB-lacZ* translational reporter chromosomally integrated.	This study
E. coli **strains**		
NEB5-alpha	F−,φ80d*lacZ*ΔM15,Δ(*lacZYA-argF*)U169,*deoR*,*recA1*, *endA1*, *hsdR17*(rk−,mk+), *phoA*, *supE44*, λ−, thi1, *gyrA96*, *relA1*	New England Biolabs
S17.1 λpir	pro, res^- *hsdR17* (rK^- mK^+) $recA^-$ with an integrated RP4-2-Tc::Mu-Km::Tn7, Tp^r *λpir*	(153)
BL21 (DE3)	F– *ompT gal dcm lon hsdSB*(rB–mB–) λ(DE3 [*lacI* lacUV5-T7p07 *ind1 sam7 nin5*]) [*malB*+]K-12(λS)	(154)
NiCo21 (DE3)	F– *ompT gal dcm lon hsdSB*(rB–mB–) λ(DE3 [*lacI* lacUV5-T7p07 *ind1 sam7 nin5*]) [*malB*+]K-12(λS) *glmS6ala slyD-CBD arnA-CBD*	(155)
MG1655	E. coli ST10 wild-type laboratory reference strain	Lab collection

Table 2.1 – Summary of bacterial strains used and created over the course of this thesis.

2.2 Plasmids

All plasmids used in this study are listed in Table 2.2.

Plasmid	Description	Origin
pME3087	Suicide vector, ColE1 replicon, Tc^R	(156)
pME4129	pME3087 based vector with upstream and downstream regions of PA4129 spliced together for marker-less deletion generation.	This study
pME4130	pME3087 based vector with upstream and downstream regions of PA4130 spliced together for double-crossover generation	This study
pME*nirB*	pME3087 based vector with upstream and downstream regions of *nirB* spliced together for marker-less deletion generation.	This study
mini-CTX-1	*aatB P. aeruginosa* integrative vector, Tc^R	(157)
pCTX4130	Integrative PA4130 complementation vector under control of the native promoter (+498bp), Tc^R	This study
pSK67	pTOPO type vector for protein overexpression under control of a T7 promoter and IPTG inducible. Amp^R	Lab stock
pCold1	Protein overexpression vector under dual control of T7 and *cspA* promoter, enabling expression at low temperature in the presence of IPTG.	Takara
pCold-GST	pCold1 overexpression vector with Glutathione S-transferase inserted downstream of hexa-histidyl tag to enhance solubility of downstream products.	Takara
pCDF-DUET1	DUET vector containing 2 T7 promoters under the control of LacI. Enables co-expression of up to 4 target proteins. Sp^R	Novagen
pUC118-Tn7-Gm-lacZ	Tn7-based integration vector for transcriptional or translational LacZ reporter generation. Gm^R	(158)
pSTNK	Tn7-helper vector containing temperature sensitive origin of replication with transposase for Tn7-based vectors. Km^R.	(159)
pSJF01	pSK67 based vector with N-terminal hexa-histidyl tagged PA4130 inserted at the EcoR1 and SacI restriction sites for overexpression	This study
pSJF02	pCold1 based vector with N-terminal hexa-histidyl tagged PA4130 inserted at EcoR1 and SacI restriction sites for overexpression	This study
pSJF03	pCold-GST based vector with N-terminal hexa-histidyl tagged GST-PA4130 fusion protein inserted at EcoR1 and SacI restriction sites for overexpression.	This study
pSJF04	pCDF-DUET1 based vectors with *cysG* derived from E. coli BL21 (DE3) inserted into MCS2 using BglII and XhoI	This study
pSJF05	pSK67 based vector with N-terminal hexa-histidyl tagged *fdx1* derived from PAO1-L Inserted at EcoRI and SacI for overexpression	This study
pSJF06	pSK67 based vector with N-terminal hexa-histidyl tagged *fdx2* derived from PAO1-L. Inserted at EcoRI and SacI for overexpression	This study
pSJF07	pSK67 based vector with N-terminal hexa-histidyl tagged *fdxA* derived from PAO1-L. Inserted at EcoRI and SacI for overexpression	This study
pSJF08	pSK67 based vector with N-terminal hexa-histidyl tagged *napF* derived from PAO1-L. Inserted at EcoRI and SacI for overexpression	This study
pSJF09	pSK67 based vector with N-terminal hexa-histidyl tagged *hcnA* derived from PAO1-L. Inserted at EcoRI and SacI for overexpression	This study
pSJF10	pUC118- Tn7-Gm-*lacZ* vector with *nirA* promoter fragment spanning +6 to -499bp relative to the transcriptional start site. Inserted using NsiI and KpnI restriction sites.	This study
pSJF11	pUC118-Tn7-Gm-*lacZ* based vector with *hcnA* promoter fragment spanning +6 to -500bp relative to the transcriptional start site. Inserted using NsiI and KpnI restriction sites.	This study
pSJF12	pUC118-Tn7-Gm-*lacZ* based vector with *nirB* promoter fragment spanning +6 to -490bp relative to the transcriptional start site. Inserted using NsiI and KpnI restriction sites.	This study
pSJF13	pSK67 based vector with N-terminal hexa-histidyl tagged CysI, derived from *E. coli* MG1655. Inserted with SacI and EcoR1 restriction sites.	This study

Table 2.2 – Summary of plasmids used and created over the course of thesis.

2.3 Oligonucleotides

All oligonucleotide primers were synthesized by Sigma (UK). Where necessary, restriction sites or hexa-histidyl tags were added to the 5' region of the primers to aid cloning and downstream protein purification. Primer sequences can be found in Table 2.3.

Oligos	Sequence	Mods
4129F1	5'-ATAGAATTCTGTGGCGCGAGGCCTGCG-3'	EcoRI
4129R1	5'-CTAGCGTCGGCGGAACAGGTTGTTCATGCCGGTTCC-3'	N/A
4129F2	5'-GGCATGAACAACCTGTTCCGCCGACGCTAGGCATAC-3'	N/A
4129R2	5'-TATGGATCCGCTGGAACAGCGTGGCGGAG-3'	BamHI
4130F1	5'-ATATCTAGATCATTTTTCGTAGGCCCATC-3'	XbaI
4130R1	5'-TCATGCCGGTTCCTCGTACTGGTACATCGCAAAGCC-3'	N/A
4130F2	5'-GCGATGTACCAGTACGAGGAACCGGCATGAACAACC-3'	N/A
4130R2	5'-ATAAAGCTTTCCTCGACGTTCTTGTCCTC-3'	HindIII
4130CTXF	5'-ATAAAGCTTGGGCCGTTCACCGCCGAC-3'	HindIII
4130CTXR	5'-TATGGATCCTCATGCCGGTTCCTCCATCCTG-3'	BamHI
NirBF1	5'-ATAGAATTCGCTGCGCCTGCTGGATTTCGG-3'	EcoRI
NirBR1	5'-GCAAGGGATTCAGACGTTCTTCTTCATGCGGAGTAGCTCCTG-3'	N/A
NirBF2	5'-CTACTCCGCATGAACAAGAACGTCTGAATCCCTTGCCCGGGC-3'	N/A
NirBR2	5'-TATAAGCTTCGCCAGCTTGTTGAAGGCGTAGTAG-3'	HindIII
NTH4130F	5'-TTAGAATTCATG**CATCACCATCACCATCAC**TACCAGTACGATGAATACG-3'	EcoRI 6XHis
NTH4130R	5'-TTACTCGAGTCATGCCGGTTCCTCCATCCT-3'	SacI
Hfdx1F1	5'-ATAGAATTCATG**CATCACCATCACCATCAC**CTGAAAATCACTGACGATTG-3'	EcoRI
Hfdx1R1	5'-TATGAGCTCTCAGGCCTTGCCGGTGATC-3'	SacI
Hfdx2F1	5'-ATAGAATTCATG**CATCACCATCACCATCAC**CCGCAGATCGTGATTCTGCC-3'	EcoR1
Hfdx2R1	5'-TATGAGCTCTCAGTGGCCTTCCGACACCTG-3'	SacI
HfdxAF1	5'-ATACCATGGATG**CACCATCACCATCACCAT**ACCTTCGTCGTCACCGAC-3'	NcoI
HfdxAR1	5'-TATCTCGAGTGGCGTATCAGCGCTCCAG-3'	XhoI
HnapFF1	5'-ATAGAATTCATG**CATCACCATCACCATCAC**AGCAGTCGCCGAGAGCTGTTC-3'	EcoR1
HnapFR1	5'-TATGAGCTCTCAGGCATGTCGTGGAGACTC-3'	SacI
HhcnAF1	5'-ATAGAATTCATG**CATCACCACCATCACCAT**CTTCTTGAACGTCAACACG-3'	EcoR1
HhcnAR1	5'-TATGAGCTCTCATGGCCGTTCCTCCTGGTC-3'	SacI
Co30-F1	5'TTATTAGAGCTCTACCAGTACGATGAATACG-3'	XhoI
Co30-R1	5' TTATTGCTCGAGTCATGCCGGTTCCTCCATCCT-3'	SacI
M2cysGF1	5'-ATACCATGGGTGGATCATTTGCCTATATTTTGC-3'	NcoI
M2cysGR1	5'-TATGGATCCTTAATGGTTGGAGAACCAGTTCAG-3'	XhoI
NTHcysIF1	5'-ATAGAATTCATG**CATCACCATCACCATCAC**AGCGAAAAACATCCAGGGCC-3'	
NTHcysIR1	5'-TATGGTACCTTAATCCCACAAATCACGCGCC	KpnI
PnirAF1	5'-ATAATGCATGGCCGTTCACCGCCGACG-3'	NsiI
PnirAR1	5'-TATGGTACCCGCAAAGCCCTCATCGACAG-3'	KpnI
PnirBF1	5'-ATAATGCATGCCTGGATCGACGACCTGCTG-3'	NsiI
PnirBR1	5'TATGGTACCGCGGAGTAGCTCCTGCATAAG-3'	KpnI
PhcnAF1	5'-ATAATGCATCGCTGGCCAACATCGCGACC-3'	NsiI
PhcnAR1	5'-TATGGTACCTGCCCTTTCATCCGTGAGAGAGA-3'	KpnI

Table 2.3 – Summary of oligonucleotides and modifications used over the course of thesis. Restriction sites indicated with underline and hexahistidyl-tags displayed in **bold**.

2.4 Chemical reagents

Reagents were purchased from Sigma (UK) unless otherwise stated.

2.4.1 Antibiotics and IPTG

Antibiotics were prepared according to manufacturer's instructions and stored at -20^{O}C, with the exception of gentamycin which was stored at 4-8^{O}C. Stock solutions and working concentrations used for both *Escherichia coli* and *Pseudomonas aeruginosa* can be found in Table 2.4.

		Working concentration (μg/ml)	
Antibiotic	**Stock concentration (mg/ml)**	***E. coli***	***P. aeruginosa***
Tetracycline	50	12.5	125-150
Nalidixic acid	15	15	15
Carbenicillin	100	100	400
Gentamycin	20	10	20
Kanamycin	50	25	350

Table 2.4 – Antibiotic stock concentration and working concentration used throughout this thesis.

2.5 Growth media and bacterial storage

Bacterial strains were routinely cultured at 37^{O}C with aeration at 200rpm in orbital-shaker incubator using the media described below. All media was prepared with dH_2O and where appropriate, were solidified with 1.5% (w/v) Technical Agar No. 3 (Oxoid). All medias were prepared using deionized water. Where appropriate, media was sterilised at 121^{O}C for 20 minutes using 15 pounds per square inch (psi). Media and components not suitable for autoclave were sterilised with bench-top filtering systems (Corning).

2.5.1 Lysogenic Broth

The methods of Sambrook and Russell (2001) were used to prepare Lysogenic broth (LB), consisting of 10 g/L tryptone, 5 g/l yeast extract, 10 g/l NaCl and sterilised by autoclave.

2.5.2 Artificial Sputum Media and modifications

Artificial sputum media was prepared as previously published with potassium nitrate added to a final concentration of 0.5mM (160). Magnesium sulphate and potassium nitrate were substituted for hydrogen sulphide and ammonium chloride for nitrate and sulphate metabolism experiments

2.5.3 MOPS minimal media

MOPS minimal media was prepared according to the instructions of LaBauve and Wargo (161). Sodium succinate was used as a carbon source at a final concentration of 20mM. Ammonium chloride, potassium nitrite and potassium nitrate were added at 10mM, as a source of nitrogen for growth.

2.5.4 **Pseudomonas** *isolation agar*

Pseudomonas isolation agar (Sigma) was prepared according to manufacturer's instructions. Glycerol was added to the dissolved powder at 10g/L.

2.5.5 Terrific Broth

Terrific broth (TB) was prepared according to Cold Spring Harbour Protocols (2015). TB solution **A** consisted of 24 g yeast extract, 12 g tryptone, 4 g glycerol dissolved in 900ml of deionised water and autoclaved. TB solution **B** consisted of 23g/l KH_2PO_4 and 164g/l of K_2HPO_4 and filter sterilised. To 900ml of solution **A**, 100ml of solution **B** was added prior to bacterial culturing.

2.5.6 Bacterial strain storage

Bacterial strains were grown for 16h in 5ml of LB at 37^{O}C. Cells were centrifuged at 8000G for 5 mins, supernatant removed and cells re-suspended in 5ml of fresh LB. A 600ul aliquot of this cell suspension was added and mixed

with 800ul of sterile 80% glycerol and flash-frozen using liquid nitrogen. Vials were stored at -80^{O}C and served as stocks for future culturing.

2.5.7 Monitoring of bacterial growth

Where appropriate, bacterial growth was monitored at OD_{600nm} using a Jenway 6315 UV-Vis spectrophotometer. All measurements were normalised to blank media.

2.6 DNA manipulations

Specific plasmid and mutant constructions are detailed in section **2.4**. Below are the standard methods used to purify, handle and manipulate DNA.

2.6.1 Genomic DNA isolation

Chromosomal DNA was isolated from 1.5ml of an overnight culture using a GenElute bacterial genomic DNA kit (Sigma) according to manufacturer's instructions.

2.6.2 Plasmid DNA preparation

Plasmids were isolated using a GenElute plasmid DNA kit (Sigma) following manufacturer's instructions.

2.6.3 Polymerase chain reaction (PCR)

For new construct synthesis, DNA amplification was performed with Phusion High-Fidelity Master Mix with GC buffer (New England Biolabs). Each reaction contained: 25µl of Phusion Master Mix; 50ng of template DNA; 2.5ul of forward and reverse primer (10um); 1.5µl DMSO; and dH2O to a total volume of 50µl. For identification of successful constructs using colony PCR, GoTaq Green Master Mix (Promega) was used for DNA amplification. Each reaction contained: 12.5µl of GoTaq Master Mix; 0.5µl of forward and reverse primer (10um); 0.75µl of DMSO; dH2O to a total volume of 25µl; and a small amount

of bacterial colony inoculated with a sterile pipette tip or cocktail stick. Amplification for both Phusion and GoTaq were performed in a Biometra Professional gradient thermocycler using the cycling conditions indicated in table 2.5.

Cycle	Phusion		GoTaq	
	Temp (^{O}C)	Time (mins)	Temp (^{O}C)	Time (mins)
Initial denaturation	98	10	95	20
Denaturation X32	98	0.5	95	0.5
Annealing X32	42-72	0.5	55	0.5
DNA extension X32	68/72	0.5 per kb	68	1 per kb
Final extension	68/72	5-10	68	5-10
Storage	4	∞	4	∞

Table 2.5 – PCR cycle conditions used for DNA amplification with Go Taq and Phusion 2X Master Mix. Extension with Taq was performed at 68^{O}C and Phusion 72^{O}C.

2.6.4 DNA agarose gel electrophoresis

DNA fragments and plasmids were routinely analysed using 1-1.5% agarose gels with 1µl per 10ml of SYBR Safe added to enable product visualisation. Gels were prepared according to standard techniques (162). DNA fragment and plasmid lengths were compared to a Quick-Load 1kb plus DNA ladder (New England Biolabs). Gels were run in 1XTAE buffer (40 mM Tris-acetate, pH 8.0; 1 mM EDTA) using a BIORAD electrophoresis cell set at 100V for 40-50 minutes. Fragments were then visualised and imaged using a BIORAD Gel Doc XR+.

2.6.5 DNA Gel extraction

DNA required for cloning or sequencing was excised from agarose gels with a sterile scalpel. Following this a Monarch gel extraction kit (New England Biolabs) was used to purify DNA according to manufacturer's instructions.

2.6.6 Restriction enzyme digest

All restriction enzymes used were purchased from New England Biolabs. Reactions consisted of: 1µg of DNA product; 5µl of 5XCutSmart buffer; 1µl of restriction enzyme; and dH2O to 50µl. Samples were incubated at 37^{O}C for 3h and enzymes heat inactivated at 80^{O}C for 20 minutes where appropriate. Plasmids required for cloning were also incubated with alkaline phosphatase (New England Biolabs) according to manufacturer's instructions.

2.6.7 DNA ligation

DNA and plasmid products for ligation were first quantified using a ND-1000 NanoDrop (Thermo scientific). Ligations were performed using T4 DNA ligase (New England Biolabs) with a 3:1 or 5:1 insert to plasmid ratio in a total reaction volume of 20µl. Reactions were performed at 16^{O}C for 18h.

2.6.8 DNA sequencing and analysis

DNA sequencing was performed using Source Biosciences Sanger sequencing service. Sequences obtained were compared to the PAO1 reference sequence available at pseudomonas.com (163) using EMBOSS Pairwise Sequence Alignment (164).

2.7 Transformation and conjugation

2.7.1 Preparation of chemically competent **E. coli**

A single *E. coli* colony was picked and inoculated into 10ml of LB at 37^{O}C for 14-18h. On the same day Buffer **A** (0.05M $CaCl_2$) and Buffer **B** (0.1M $CaCl_2$ 15% glycerol) were prepared, autoclaved and place on ice overnight. *E. coli* cultures were diluted 1:100 in the desired volume of preheated LB and cultured at 37^{O}C on an orbital-shaking platform at 200rpm (name). Once an OD_{600nm} of 0.4-0.6 was reached, cells were harvested at 6000G for 10 minutes in a pre-chilled centrifuge (4^{O}C), and stored on ice for 10 minutes. Cells were re-suspended in Buffer **A** to 1/5 the volume of the original culture. *E. coli* was again harvested at 6000G for 10 minutes, re-suspended in Buffer **A** at 1/25 of the original culture volume, and this process repeated with a final resuspension

at 1/50 of the original culture volume. Cells were incubated on ice for 16h, pelleted at 6000G for 10 minutes and re-suspended in 1/100 of the original culture volume of Buffer **B**. Competent cells were stored at 50-100µl aliquots, frozen in liquid nitrogen and stored at -80^{O}C for future use.

2.7.2 Chemical transformation of E. coli

950µl of LB in a 2ml Eppendorf tube was placed in a 37^{O}C incubator 30mins before beginning of procedure. 50-100ng of purified vector or ligation preparation were added to chemically competent *E. coli* and stored on ice for 5mins. The cell-plasmid mixture was then incubated in a 42^{O}C water bath for 30s and placed back on ice for 5 minutes. Cells were then re-suspended in the pre-warmed LB and incubated at 37^{O}C for 1h before being recovered on LB agar with relevant selection.

2.7.3 Preparation of electro-competent and transformation of **P. aeruginosa**

Electro-competent *P. aeruginosa* were prepared according to the method of Choi and colleagues (165). To this suspension, 50-100ng of vector was added and electroporated with a Bio-Rad mini-pulsar set to Bacteria programme Ec2. Electroporated *P. aeruginosa* was re-suspended in 900µl of LB, incubated at 37^{O}C for 2h, before being recovered on LB agar with relevant selection.

2.7.4 Conjugal transfer of plasmid DNA to **P. aeruginosa**

Plasmids were mobilised into *P. aeruginosa* by conjugation using *E. coli* S17-1 *λ-pir*. Both the recipient and donor strain were grown in 5ml LB for 16-18h. The recipient *P. aeruginosa* was cultured at 42^{O}C whilst the donor *E. coli* was grown at 37^{O}C. Overnight cultures were washed in 5ml fresh LB and harvested at 6000xg for 10 minutes and then re-suspended in 100µl LB. Recipient and donor strains were then mixed at a 1:1 ratio, spotted onto freshly prepared LB agar and incubated at 30^{O}C for 6-8h. The use of 30^{O}C for incubation was to minimise *P. aeruginosa* virulence factor production and prevent *E. coli* killing. Cells were recovered from the plate, washed in 1ml of LB and then plated on PIA with relevant selection for 24-48h at 37^{O}C.

2.7.5 Gene deletion in P. aeruginosa

Vector pME3087 was selected for gene-deletion studies in this thesis as it contains a ColE1 origin of replication. This means the vector can replicate in E. coli for manipulation, put not in *P. aeruginosa*, making it suitable as suicide vector (166). Following pME3087 conjugation into *P. aeruginosa*, exconjugants were selected for on *Pseudomonas* isolation agar supplemented with 200ug/ml tetracycline. Double-recombinants were then selected for using carbenicillin enrichment. This protocol works on the premise that carbenicillin only targets actively growing cells undergoing peptidoglycan synthesis. Addition of the bacteriostatic antibiotic Tc will allow resistant colonies to continue replication (exconjugants), whilst double-recombinants which are Tc sensitive will cease growth. Subsequent addition of carbenicillin will selectively target the rapidly dividing exconjugants, enriching the Tc sensitive double-recombinant population.

Briefly, exconjugants were grown in 5ml of LB at 37^{O}C overnight in the absence of selection, allowing double recombination events to take place. The following day overnight cultures were washed and 30µl used to re-seed 3ml of fresh LB. Cultures were grown at 37^{O}C for 2h, spiked with 20µg/ml of tetracycline, followed by a further 1h incubation. Carbenicillin was then added at a concentration of 2mg/ml and the culture re-incubated for 4-6 hours. Live cells were pelleted at 4000xg for 10 minutes, washed in 5ml of LB twice, and plated on LB agar using a 10-fold dilution series to 10^{-7}. Following overnight incubation at 37^{O}C, colonies were screened for sensitivity to tetracycline. Sensitive colonies were subjected to colony PCR and sequencing for confirmation of gene deletion.

2.8 Plasmid and strain construction

2.8.1 Construction of in-frame deletion mutants

All strains, plasmids and oligonucleotides used for generation of new strains are listed in tables 2.1-3.

2.8.1.1 PA4130 mutant construction and complementation

To construct an in-frame deletion in PA4130, two DNA fragments 427 bp upstream and 433 bp downstream from PA4130 were generated and fused by overlap extension PCR using PAO1-L genomic DNA as a template. The upstream 427-bp fragment was amplified with primers PA4130F1 which carries an XbaI restriction site and PA4130R1 containing the first 12 nucleotides of PA4130 with an overhanging end containing the last 15 nucleotides of the PA4130 ORF; the downstream 433-bp fragment was amplified with PA4130F2 containing the last 15 nucleotides of PA4130 with an overhanging end containing the first 12 nucleotides and PA4130R2 containing a HindIII restriction site. To perform the overlap extension PCR, a secondary PCR was performed with the 427-bp and 433-bp fragments serving as the templates and primers PA4130F1/PA4130R2. The final PCR product was cloned using the XbaI/HindIII restriction sites into the vector pME3087, resulting in the suicide plasmid pME4130. This vector was then transformed into *E. coli* S17-1 *λ-pir,* and conjugated into PAO1-L, PA7 Bo599, PA14 AUS471 and LESB58 PA-W39 using the procedure outlined in **2.3.4**. Allelic exchange for generation of in-frame PA4130 deletion mutants was carried out according to the procedure outlined in **2.3.5**.

2.8.1.2 PA4129 mutant construction

The suicide plasmid used to generate the PA4129 mutant was constructed as described for pME4130 (above), using primer pairs PA4129F1/PA4129R1 and PA4129F2/PA4129R2 to generate a 519bp upstream and 525bp downstream PCR product respectively. Overlap extension of these 2 fragments was performed with primer pairs PA4129F1/PA4129R2 to generate the final PCR product containing a deletion in PA4129. This fragment was cloned into pME3087 using restriction sites EcoRI and BamHI, forming suicide plasmid pME4129. This vector was mobilised into PAO1-L by conjugation, with allelic exchange carried out according to the procedure outlined in **2.3.5**.

2.8.1.3 nirB *mutant construction*

The suicide plasmid used to generate nirB mutants was constructed as described for pME4130 and pME4129 (above), using primer pairs

nirBF1/nirBR1 and nirBF2/nirBR2 to generate a 744bp upstream and 791bp downstream PCR product respectively. Overlap extension of these 2 fragments was performed with primer pairs nirBF1/nirBR2 to generate the final PCR product containing a deletion in PA4129. This fragment was cloned into pME3087 using restriction sites EcoRI and HindIII, forming suicide plasmid pME*nirB*. This vector was mobilised into PAO1-L and PAJD25 by conjugation, with allelic exchange carried out according to the procedure outlined in **2.3.5**.

2.8.2 Construction of protein and enzyme over-expression vectors

2.8.2.1 PA4130/NirA overexpression vectors

Vectors pSK67, pCold1 and pCold-GST were selected for attempted PA4130 purification. The PA4130 ORF was amplified from PAO1-L genomic DNA using primer pairs NT4130F1/NT4130R1 and Co30F1/Co30R1. Primer pair NT4130F1/R1 were modified with an N-terminal hexahistidyl tag and EcoRI/SacI restriction site. Whilst vectors pCold and pCold-GST already contain a hexahistidyl tag therefore, primer pair Co30F1/R1 were modified with restriction sites SacI/EcoRI only. The modified PA4130 fragments was cloned into vector pSK67, pCold1 and pCold-GST using the EcoRI/SacI (pSK67) or SacI/EcoRI (pCold vectors) restriction sites as appropriate, resulting in plasmids pSJF01 (pSK67::6XH-PA4130), pSJF02 (pCold1::PA4130) and pSJF03 (pCold-GST::PA4130) respectively.

2.8.2.2 CysG overexpression vector

The *cysG* ORF was amplified from *E. coli* BL21 (DE3) using primer pair CDFcysGF1/CDFcysGR1, modified with BglII/XhoI restriction sites. The generated PCR product was then cloned into vector pCDF-DUET1 at the second multiple cloning site BglII and XhoI, forming vector PSJF04. This vector was selected as the origin of replication was compatible with previously constructed PA4130 overexpression vectors.

2.8.2.3 Ferredoxin overexpression vectors

The *fdx1*, *fdx2*, *fdxA*, *napF* and *hcnA* ORFs were PCR amplified from PAO1-L with primer pairs Hfdx1F1/R1, Hdfdx2F1/R1, HfdxAF1/R1, HnapFF1/R1 and

HhcnAF1/R1. All forward primers were modified with N-terminal hexahistidyl tags with details of restriction site insertions detailed in **table 2.3**. The generated PCR products were then cloned into pSK67 with the relevant restriction sites forming vectors pSJF05 (pSK67::6XH-*fdx1*), pSJF06 (pSK67::6XH-*fdx2*), pSJF07 (pSK67::6XH-*fdxA*), pSJF08 (pSK67::6XH-*napF*) and pSJF09 (pSK67::6XH-*hcnA*).

2.8.2.4 CysI overexpression vector

The *cysI* ORF was amplified from *E. coli* MG1655 using primer pair NTHcysIF1/NTHcysIR1, modified with an N-terminal hexahistidyl tag and EcoRI/SacI restriction sites. The generated PCR product was then cloned into vector pSK67 with EcoRI and SacI, forming vector pSJF13 (pSK67::6XH-*cysI*).

2.8.3 Construction of pUC118-Tn7-Gm-LacZ translational reporters

To construct PA4130/*nirA*, *hcnA* and *nirB* LacZ translational reporter fusions the promoter regions of each gene were amplified using primer pairs PnirAF1/R1, PhcnAF1/R1 and PnirBF1/R1, with all primers modified with NsiI/KpnI restriction sites. The PA4130/*nirA* promoter fragment spanned +6 to -499bp; *hcnA* fragment +6 to -500bp; and *nirB* fragment +6 to -490bp relative to the translational start site. The resulting PCR products were cloned in-frame with the *lacZ* gene of pUC118-Tn7-Gm-lacZ via the engineered NsiI/KpnI restriction sites, forming vectors pSJF10 (pUC118-Tn7-Gm-P*nirA*-lacZ), pSJF11(pUC118-Tn7-Gm-P*hcnA*-lacZ and pSJF12 (pUC118-Tn7-Gm-P*nirB*-lacZ) respectively. Vector pUC118-Tn7-Gm-lacZ does not encode the transposase required to mediate integration onto the *P. aeruginosa* chromosome. Constructs were integrated onto the *P. aeruginosa* chromosome according to the protocols of Créplin and colleagues (159), through use of the temperature sensitive Tn7 transposase containing vector pSTNK.

2.9 *In vitro* virulence factor production assays

2.9.1 Pyocyanin

Pyocyanin production was quantified using the method of Essar and colleagues (167). Briefly, overnight *P. aeruginosa* cultures were standardised to an OD_{600nm} of 1.0. This was then diluted 1:100 into 15ml of the relevant media and grown in 150ml flasks at 37^{o}C with shaking at 200rpm. 5ml of bacterial samples were taken at the desired time points (8 or 20h), whole cells pelleted, and supernatant filtered with a 0.2µm filter. Samples were then mixed with 3ml of chloroform, with the resulting blue coloured chloroform layer transferred to a separate tube and mixed with 1ml of 0.2M HCl. Following vigorous vortexing, the samples were centrifuged and the pink HCl layer removed. Absorption of the extracted sample was read at 520nm using a spectrophotometer (brand) and concentration determined using the extinction coefficient of pyocyanin at 4310 M^{-1} cm^{-1}. The results were background corrected using PAO1-L *phzA1-G1 phzA2-G2* since this strain is unable to synthesize any phenazine based compounds.

2.9.2 Pyoverdine

Pyoverdine secretions were qualitatively assessed through pyoverdine specific absorbance at 405nm. Overnight *P. aeruginosa* cultures were standardised to an OD600nm of 1.0, and diluted 1:100 into 15ml of iron-depleted M-ASM in 150ml flasks. Cultures were grown at 37^{o}C with shaking at 200rpm. At the desired time-point, three 1ml samples were extracted, whole cells pelleted, and supernatant filtered with a 0.22µm filter. Absorbance of the pyoverdine containing sample were then read at 405nm with a spectrophotometer and the value divided by the OD_{600nm} of the original culture to give pyoverdine produced per unit cell density.

2.9.3 Universal protease activity

Universal protease production was assessed using a skimmed milk agar-plate method based loosely on the methods of Sokol *et al* (168). Skimmed milk was filter sterilised and added to cooled LB or M-ASM agar at a concentration of 13% (v/v). 20ml of the skimmed milk containing agar was then poured into petri dishes and allowed to solidify. Overnight *P. aeruginosa* cultures were then diluted to an OD_{600nm} of 1.0, and 10µl of this solution spotted onto skimmed milk plates. Once dry, plates were incubated inverted at 37^{o}C for 16h and imaged using a Nikon digital camera (D3500 DSLR) Images were then imported into

ImageJ, and the area of skimmed milk clearance corresponding to protease activity measured. Measurements were normalised to the relevant wild-type strains to infer biological effect.

2.9.4 LasB elastase activity

P. aeruginosa cultures were grown overnight and OD600nm normalised to 1.0. This was then diluted 1:100 into 15ml of the relevant media and grown in 150ml flasks at 37^{o}C with shaking at 200rpm. At the desired time-point (4, 8, 16 and 24h), 1ml of culture was extracted, whole cells pelleted and supernatant filter sterilised with a 0.22µm filter. 100µl of the filtered supernatant was then added to 900ul of a 20mg/ml solution of elastin congo red in ECR buffer (100mM Tris, 1mM $CaCl_2$, pH 7.5) and incubated at 37^{o}C for 4h at 200rpm. Following incubation samples were centrifuged at 16000xg for 5 minutes and supernatant transferred to black flat-bottomed 96-well plates (Grenier) and absorbance measured at 495nm using a microplate reader (Tecan Spark).

2.9.5 Abiotic bacterial attachment

Abiotic attachment of *P. aeruginosa* strains were assessed using flat-bottomed, polystyrene, tissue-culture treated 48-well plates. *P. aeruginosa* strains were cultured overnight and normalised to an OD_{600nm} of 1.0. 10ul of this suspension was added to the appropriate well, containing 600ul of the relevant liquid media supplemented with 1 or 10mM KNO_3 as needed. Plates were then sealed with a gas permeable membrane (4titude) and placed in a small box containing a body of water to increase humidity and prevent media evaporation. These samples were incubated at 37^{o}C statically. After 20h the plates were taken out and the gas permeable membrane removed, with the OD_{600nm} read using a multiwall reader (Tecan Spark). Media was removed and washed with 700µl of sterile PBS at room temperature. 700µl of 0.1% of crystal violet solution was then added to each well and stained at room temperature for 15 minutes with agitation at 50rpm. Crystal violet was then aspirated and wells washed carefully with 700ul of PBS to avoid contact with the well-edges. Bound crystal violet was then solubilised with a solution of 30% (v/v) acetic acid and the absorbance measured at 570nm using a multiwall plate reader (Tecan Spark). This value was then divided by the original OD_{600nm} to give the amount of crystal violet per unit cell density.

2.9.6 Colony biofilm model

LB agar was used a base for colony biofilm formation and supplemented with KNO_3 as required, with viable count used to evaluate colony biofilm formation. Agar was dispensed into polystyrene, tissue culture treated, 6-well plates with a UV-sterilised filter disc of pore size 0.22µm (Millipore) placed at the centre of each well once the agar set. *P. aeruginosa* overnight cultures were washed with fresh LB and diluted to an OD600nm of 1.0, with 10ul of this sample used to inoculate at the centre of each filter disc. Samples were then incubated at 37^{o}C for 24h under the relevant atmospheric conditions. Following growth, filter discs were lifted from the agar pad and placed in 5ml sterile PBS containing in 7ml bijouxs. Colony biofilms were disrupted in an ultrasonic water-bath (name) for 15 minutes, followed by mechanical pipetting to distribute the bacteria uniformly in PBS. Cells were then pelleted and enumerated using a variation of Miles-Misra for viable count. Briefly, a 10-step 10-fold serial dilution was performed in sterile PBS with 20µl of bacterial suspension spotted onto PIA using 3 biological replicates with 3 technical replicates each. Once dry, plates were incubated inverted at 30^{o}C for 20-22h and discrete colonies counted only when in the range of 2-20. Technical replicates were averaged to determine colony forming unit (CFU) value for each biological replicate. CFUs per ml then calculated with the following equation:

Number of colonies per dilution x 50 x dilution factor.

2.10 *In vivo* virulence models and tissue culture

2.10.1 Drosophila melanogaster

Fruitfly killing assays were conducted as described by Apidianakis and Rahme (169) with minor modifications. 15 flies were used per replicate as opposed to 10 and incubated at 26^{O}C after infection. For each trial, triplicate sets of flies were used with experiments performed in duplicate. If more than 5 flies died due to injuries caused by inoculation with *P. aeruginosa*, the experiment was abandoned and repeated. Surviving flies were enumerated at 18, 20, 22 and 24h post infection.

2.10.2 Caenorhabditis elegans

Nematode slow-killing assays were performed as previously described by Loré and colleagues (170). Surviving worms were counted at 24, 48 and 72h with survival rates determined from 3 independent replicates totalling ~90 worms.

2.10.3 A549 tissue culture

2.10.3.1 P. aeruginosa cytotoxicity

Cytotoxicity of *P. aeruginosa* culture supernatant was assessed using the procedure of Ulrich and colleagues (171). Overnight *P. aeruginosa* cultures were diluted to an OD_{600nm} of 0.05 and grown to an OD of 1.0 corresponding to $8x10^8$ cells. Culture supernatants were extracted and incubated with A549 alveolar basal epithelial cells for 1h at 37^{o}C. A549 survival and death was then assessed using the Syto13/propidium iodide viability test according to manufacturer's instructions (Molecular probes). Results were normalised to $8x10^8$ as expressed as a ratio of wild-type *P. aeruginosa* cytotoxicity.

2.10.3.2 P. aeruginosa invasion

Invasion was determined using a Polymyxin B protection assay as performed by Bianconi *et a*l (172) with minor modifications. A549 alveolar basal epithelial cells were cultured as a monolayer using previously described methods (173). Briefly*, P. aeruginosa* strains were grown overnight in LB. The following day fresh LB was inoculated from the overnight at an OD_{600nm} of 0.05 and grown to mid-exponential phase (OD600nm of 0.5-0.6 corresponding to 10^6 cells). *P. aeruginosa* preparations were used to infect an A549 monolayer at a multiplicity of infection of 100:1. Infection was allowed to proceed for 2h and subsequently washed with sterile PBS and treated with 100µg/ml of polymyxin B for 2h. A549 cells were then washed with PBS, lysed with H2O and plated on PIA at 30^{O}C overnight. Surviving bacteria were normalised to the original inoculum of 10^6 cells and results of mutants displayed a ratio compared to the wild-type strain.

2.10.3.3 IL-8 induction

IL-8 levels were determined using the procedure described by Bianconi and colleagues (172). Supernatants from the procedure described above served as samples for an IL-8 ELISA kit (Biosource Europe). Values were normalised to the original inoculum of 10^6 cells and results expressed as a ratio compared to wild-type strain IL-8 production.

2.10.4 Murine infection models

2.10.4.1 Acute murine lung infection

C57BL/6NCrlBR male mice (8-10 weeks of age) were purchased from Charles River Laboratories, Italy. In the acute murine lung infection model, *P. aeruginosa* strains were grown for 3h in tryptic soy broth (TSB). Bacteria were then harvested, washed twice with sterile PBS and re-suspended in sterile PBS to the desired dose for infection of $5x10^6$ CFUs/mouse. Mice were anaesthetized and the trachea directly visualised by a ventral midline incision, exposed and intubated with a sterile, flexible 22-gr cannula attached to a 1 ml syringe accordingly to established procedures (170). A 60µl inoculum of $5x10^6$ CFUs was implanted into the lung via cannula. Following infection, mice were monitored twice a day for four days. Mice that lost >20% body weight and presented signs of severe clinical disease were sacrificed by CO_2 administration before termination of the experiment.

2.10.4.2 Agar-bead murine lung infection

C57BL/6 male mice (6-10 weeks of age) were purchased from Charles-River Laboratories, Germany. The agar bead mouse model was performed according to established procedures (174). Fresh cultures were prepared in 5 ml TSB and incubated for 3h. Bacterial cells were harvested and embedded in agar beads according to Bragonzi and colleagues (175). Five to ten mice were used for experiments and intratracheally infected with $4.6x10^6$ CFUs. Following infection, mice were monitored twice a day for 2 days. Mice that lost >20% body weight and presented signs of sever clinical disease were sacrificed by injection of 2ml 20% pentobarbital. For quantitative bacteriology, lung, liver and spleen were excised aseptically and homogenized using the homogenizer DIAX 900 (Heidolph GmbH, Schwabach, Germany). Bacterial numbers in the

organs were determined by 10-fold serial dilutions of the homogenates, spotted onto blood plates after incubation at 37°C for 18 h.

2.10.4.3 Ethics statement

Acute murine infection studies were conducted according to protocols approved by the San Raffaele Scientific Institute (Milan, Italy) Institutional Animal Care and Use Committee (IACUC) and adhered strictly to the Italian Ministry of Health guidelines for the use and care of experimental animals. Agar-bead infection studies were conducted according to protocols approved by Institute of Medical Microbiology and Hygiene (Tübingen, Germany) and adhered strictly to guidelines set by German Ministry of Health and Animal Welfare Institute (Baden-Württemberg).

2.11 Protein expression and purification

2.11.1 SDS-polyacrylamide gel electrophoresis (SDS-PAGE)

To analyse protein expression and purification samples SDS-PAGE was performed according to Laemmeli and colleagues (176). Agarose resolving gel concentrations varied depending on the size of the protein, with gels formulated following the protocols outlined in table 2.6.

	Acrylamide concentration (%)					
Reagent	**7**	**9**	**12**	**15**	**18**	**5**
1.5M Tris.HCl pH8.8	2.5ml	2.5ml	2.5ml	2.5ml	2.5ml	n/a
0.5M Tris.HCl pH6.8	n/a	n/a	n/a	n/a	n/a	0.62ml
dH20	5.1ml	4.4ml	3.4ml	2.4ml	1.4ml	2.5ml
30% Acrylamide	2.3ml	3ml	4ml	5ml	6ml	0.83ml
10% SDS (w/v)	100µl	100µl	100µl	100µl	100µl	50µl
20% APS (w/v)	50µl	50µl	50µl	50µl	50µl	50µl
TEMED	15µl	15µl	15µl	15µl	15µl	5µl

Table 2.6 – Standard recipes for formulation of SDS-PAGE gels per 2 small gels. Resolving gels with variable acrylamide concentrations contain 1.5M Tris-HCl whilst the stacking gel contains 5% acrylamide only with 0.5M Tris-HCl

2.11.2 Tricine-polyacrylamide gel electrophoresis

To analyse protein expression and purification samples Tricine-SDS-PAGE (Tri-PAGE) was performed according to (177). Pre-cast gels were purchased from Invitrogen at an acrylamide concentration of 16%, with samples run at 120V for between 90-120 minutes.

2.11.3 Screening heterologous protein codon usage

PA4130 codon usage was compared to *E. coli* BL21 (DE3) using the graphical codon usage analyser tool (178). Codons with a relative codon adaptiveness above 0.4 were considered common; 0.2-0.4 less common; and below 0.2 as rare. Results were displayed with GraphPad prism version 9.

2.11.4 Protein induction and solubility trials

For screening PA4130 induction and solubility, temperature and induction strength were varied to optimise soluble expression. Expression was screened with varying 20,25 and 30^{O}C with IPTG induction at 0.1, 0.3 and 0.5mM. Small-scale cultures were prepared in 100ml conical flasks with 20ml of Terrific broth per condition. Cultures were grown at 37^{O}C to an OD_{600nm} of 0.6-0.8, transferred to the relevant screening temperature for 30mins, then induced with either 0.1,0.3 or 0.5mM IPTG. Induction and solubility samples for each condition were collected at 4 and 18h. For routine analysis of IPTG induced pellets on SDS-PAGE or Tri-PAGE gels, 200µl of *E. coli* overexpressing the desired protein was pelleted, and re-suspended in 100µl of 2XSDS-sample buffer (100 mM Tris-HCL pH 6.8, 200 mM DTT, 4% SDS (w/v) ,0.2 % (w/v) Bromophenol blue and 12% glycerol (v/v)) Samples were boiled at 98^{O}C for 10mins and loaded into gels whilst warm to minimise increases in viscosity. To analyse sample solubility during trials, 5ml of each culture was pelleted and re-suspended in 1ml of of Tris-Buffered Saline (TBS) (pH 7.5). Small-scale samples were then lysed with BugBuster (Millipore), centrifuged at 15000G for 10 minutes, and lysate retained as the soluble fraction. Remaining cell pellet/debris protein contents were then solubilised in TBS with 8M Urea for 30mins at room temperature, centrifuged at 15000G for 10 minutes, and the supernatant retained as the insoluble fraction. Soluble and insoluble fractions were then mixed with 1XSDS-sample buffer 50 mM Tris-HCL pH 6.8, 100 mM

DTT, 2% SDS (w/v) ,0.1 % (w/v) Bromophenol blue and 6% glycerol (v/v)) at a ratio of 1:1 and a total of 2-5ul of this sample analysed by SDS or Tricine-PAGE.

2.11.5 Preparative-scale protein overexpression and sonication

2.11.5.1 PA4130 and CysI overexpression

Competent *E. coli* strains NiCo21 and Suf++ were co-transformed with vector pSJF04 (*cysG*) and either pSJF01 (PA4130) or pSJF13 (*cysI*). Single colonies were grown in LB overnight with carbenicillin and spectinomycin, and inoculated at a 1/100 ratio in TB, and grown to an OD_{600nm} of 0.6-0.8. Cultures were then transferred to 20^{O}C incubator for 30-40mins and induced with 0.3mM IPTG. PA4130 and CysI overexpression samples were supplemented with 0.1M $FeSO_4.6H_20$ to ensure iron is not limiting successful siroheme biogenesis due to enhanced siroheme synthase expression (CysG). Following 16-18h incubation, overexpression pellets were harvested at 3000xg for 20 minutes, washed in Tris-Buffered Saline (TBS) (pH 8), frozen in liquid nitrogen and stored at -80^{O}C.

2.11.5.2 Fdx1, Fdx2, FdxA and NapF overexpression

Competent *E. coli* Suf++ was transformed with vectors pSJF05 (*fdx1*), pSJF06 (*fdx2*), pSJF07 (*fdxA*) or pSJF08 (*napF*). Single colonies were grown overnight with carbenicillin as selection, inoculated at a 1/100 ratio in TB, and grown to an OD of 0.6-0.8 at 37^{O}C. Cultures were then transferred to a 28^{O}C incubator for 30-40mins and induced with 0.5mM IPTG. Ferredoxin overexpression samples were supplemented with 0.1M $FeSO_4.6H_20$ to ensure iron availability does not limit iron-sulphur cluster biogenesis. Following a 4-5h incubation, cells were harvested at 3000xg for 20 minutes, washed in TBS, frozen in liquid nitrogen and stored at -80^{O}C.

2.11.5.3 HcnA overexpression

HcnA overexpression was performed using the methods described for the other ferredoxins with 1 modification. Washing of HcnA-overexpressing pellets was performed in TBS at pH 7.4. The isoelectric point of 6XH-HcnA is predicted to

be 8.04, therefore a higher pH buffer was used for all washing and downstream purification steps to prevent precipitation.

2.11.5.4 Overexpression lysate preparation

Frozen *E. coli* over-expression pellets were defrosted in water for 10-20 minutes. PA4130, CysI, Fdx1, Fdx2 and FdxA were re-suspended in ice-cold sonication buffer **A** consisting of 50mM Tris, 150mM NaCl, 10mM imidazole, 1% glycerol at pH 8.0. HcnA sample pellets were re-suspended in ice-cold sonication buffer **B** consisting of 50mM Tris, 150mM NaCl, 10mM imidazole, 0.5mM EDTA and 1% glycerol at pH 7.4. Prior to sonication, EDTA-Free cOmplete ULTRA protease inhibitor cocktail (Sigma) was added according to manufacturer's instruction. Sonication was performed with a Qsonica Sonicator Q700 (Fisher scientific) for 8 minutes following a 15s ON/OFF programme to allow heat dissipation. Samples were then centrifuged at 12-15000xg and the lysates filtered through a 0.22µm pore diameter.

2.11.6 Immobilised metal ion affinity chromatography (IMAC)

All purifications described below were performed with a 5ml Hi-Trap chelating column (GE healthcare) loaded with 0.05M $NiCl_2$ according to manufacturer's instructions. Prior to sample loading, columns were washed with 5 column volumes (CV) of DH20 with a P-1 peristaltic pump (GE healthcare) at a flow rate of 2ml/min. Using the same flow rate, columns were then equilibrated with 5-10CV of IMAC buffer B, followed by 5CV of IMAC buffer A. Buffers used were protein specific and detailed in the below in table 2.7**.** Overexpression lysates containing the protein of interest were applied to the column as a flow rate of 1ml/min to maximise his-tag binding. Samples were then washed with 5CV of IMAC buffer A, followed sequentially by 5CV of Buffer A with 40mM Imidazole.

For on-bench purifications using a peristaltic pump, a further wash step was implemented with 0.06-0.08M imidazole. Samples were then eluted with a step-wise gradient using 0.1, 0.2 and 0.4M imidazole with 2-4 CV obtained at each concentration. For purifications using fast protein liquid chromatography (FPLC) an AKTA prime plus (GE healthcare) system was used. Samples were eluted with a linear imidazole gradient using IMAC buffer A and B across

100CV. Protein elution was tracked through UV absorbance at 280nm with elutions and analysed by SDS or Tri-PAGE.

Protein or enzyme	IMAC buffer A	IMAC buffer B
PA4130 and CysI	0.05M Tris.HCl, 0.5M NaCl, 0.02M imidazole, 5% glycerol (v/v) at pH 8.0.	0.05M Tris.HCl, 0.5M NaCl, 0.5M imidazole, 5% glycerol (v/v) at pH 8.0.
Fdx1, Fdx2, FdxA and NapF	0.05M Tris.HCl, 0.25M NaCl, 0.01M imidazole, 5% glycerol (v/v) at pH 8.0.	0.05M Tris.HCl, 0.25M NaCl, 0.4M imidazole, 5% glycerol (v/v) at pH 8.0.
HcnA	0.05M Tris.HCl, 0.25M NaCl, 0.01M imidazole, 5% glycerol (v/v) at pH 7.4.	0.05M Tris.HCl, 0.25M NaCl, 0.4M imidazole, 5% glycerol (v/v) at pH 7.4.

Table 2.7 – Details of IMAC buffers used for purification of all proteins and enzymes in this thesis.

2.11.7 Anionic exchange chromatography

Anionic exchange chromatography (AEC) was carried out using a HiTrap Q-sepharose fast flow column (GE healthcare). Prior to PA4130 column loading samples were desalted using a PD-10 (GE healthcare) column into AEC buffer A (0.05M Tris.HCl, 0.02M NaCl, 1% glycerol at pH 8.0) according to manufacturer's instructions. Equilibration and sample application was performed with a peristaltic pump. Before loading, equilibration was performed with 10CV of AEC buffer B (0.05M Tris.HCl, 1M NaCl, 1% glycerol at pH 8.0), followed by 10CV of AEC buffer A. Samples were then applied to the column at a flow rate of 0.5ml/min, followed by washing with 5CV of AEC buffer A at 2ml/min. PA4130 was then eluted with an AKTA prime plus using a linear 0.02-1M NaCl gradient with AEC buffers A and B. Protein elution was tracked through UV absorbance at 280nm with peaks analysed by SDS or Tri-PAGE.

2.11.8 Size-exclusion chromatography

Size exclusion chromatography of PA4130/NirA (SEC) was carried out using a Superdex S200-pg 16/600 gel filtration column (GE healthcare), connected to an AKTA prime plus. Prior to sample preparation, the column was equilibrated with 1.5CV of dH20 followed by 1.5CV of SEC-buffer (0.025M Tris.HCl, 0.15M NaCl, pH 7.5) at a flow-rate of 0.5ml/min. PA4130/NirA samples were then concentrated to 5ml using Vivaspin centrifugal filter unit (Cytiva) with an

exclusion limit of <30kDa, and injected onto column through use of a 5ml capacity loop. Samples were resolved based on hydrodynamic focussing under flow at 0.8ml/min. Protein elution was tracked through UV absorbance at 280nm with peaks analysed by SDS-PAGE.

2.11.9 Mass spectrometry for protein identification

Identification of protein and contaminants was performed through The University of York Protein ID service. SDS-PAGE gel bands were excised and sent to this service. Samples were then de-stained; digested with trypsin; and the resulting peptides identified by MALDI-MS using a Bruker ultraflex III MALDI-TOF/TOF.

2.11.10 PA4130/NirA crystallography trials

PA4130/NirA samples purified by SEC were initially spin concentrated to 10mg/ml. Prior to crystal trials, optimisation of protein concentration required was performed using the Pre-Crystallisation Test (Hampton research) according to manufacturer's instructions. Following protein concentration optimisation, PA4130/NirA samples were diluted to 1, 2, 3 and 4 mg/ml in SEC-buffer and subjected to high-throughput 96-well format crystallography screening. The High-throughput screens used were Index (Hampton), Morpheus (Molecular dimensions), Midas (Molecular dimensions), Structure 1&2 (Molecular dimensions), PEGs (Molecular dimensions) and JCSG Plus (Molecular dimesions). Crystallisation trials were set up using sitting-drop vapor-diffusion, with each reservoir of a 96-well crystallisation plate (Hampton) inoculated with 100µl of trial condition. Automation of sample preparation was achieved with a Mosquito crystallization robot (SPT Labtech) dispensing 300nl of PA4130/NirA and 300nl of reservoir solution as a sitting-drop. Plates were then sealed and incubated across a range of temperatures from 4^{O}C-25^{O}C. Trials were monitored for crystal growth every 3-5 days for up to 1 year.

2.12 Enzymatic characterisation assays

2.12.1 UV-visible spectrum spectroscopy

The UV-visible spectra of PA4130, CysI, Fdx1, Fdx2, FdxA and HcnA were recorded using a Jenway 6315 UV-Vis Spectrophotometer. Samples were normalised to a buffer only blank and readings were obtained between 300-800nm in 1nm intervals.

2.12.2 Methyl-viologen oxidation assays

The PA4130 protein was tested for nitrite/sulfite reductase activity using the artificial electron donor methyl viologen (MV); the MV reduction reaction in the presence of sodium dithionite produces a blue coloration. The assay was adapted using the methods of Schnell and colleagues (179). Briefly, the assay mixture contained 0.05M Tris-HCl, 0.5mM MV, 1-5mM of Na_2SO_3 or KNO_2, 2µm of PA4130 and 0.015M of sodium dithionite. Assays were performed under anaerobic conditions in a Coy vinyl anaerobic tent with loss of MV blue colouration tracked every 5s at 605nm using a Jenway 6315 UV-Vis Spectrophotometer. The 0.05M Tris-HCl buffer solution was incubate in the anaerobic tent for 16-18 hours to pre-reduce dissolved oxygen and used to create stocks of all required solutions. Reactions were initiated upon addition of sodium dithionite.

2.12.3 Nitrite reduction assay: detection of nitrite and ammonium

Nitrite reduction assays were performed as above however only 1mM of KNO_2 was used as an electron acceptor. Remaining nitrite was detected using the Griess Reagent System (Promega) according to manufacturer's instructions. Reactions were diluted 10-fold in 0.05M Tris-HCl to bring the concentration of KNO_2 into the linear range of this assay.

Production of ammonium was monitored using the fluorogenic Ammonia Assay Kit (Abcam) according to manufacturer's instructions.

2.12.4 Ferredoxin-linked nitrite reduction assays

Ferrodoxin nitrite reductase assays were performed as described in **2.8.2** with minor modifications. MV was replaced with 60uM of each ferredoxin and reactions were performed under aerobic conditions, as re-oxidation of MV was no longer a concern. With the redox state of the purified ferredoxins not

determined, reactions were initiated upon addition of nitrite to prevent premature reduction and allow sodium dithionite mediated reduction of ferredoxins.

2.12.5 Potassium cyanide inhibition assays

Cyanide inhibition assays were performed for NirA and CysI as described in 2.8.2. The NirA reaction used 5mM KNO_3 as an electron acceptor with *E. coli* CysI using 5mM Na_2SO_4. KCN was added to reactions at concentrations of 25, 50, 100, 200, 300, 400, 600, 800 and 1000µm as needed. Reactions were initiated with sodium dithionite, and monitored spectrophotometrically at 605nm using a Tecan spark instrument fitted with a gas control module set to 0% oxygen.

2.13 Micro-aerobic growth and translational reporter assays

2.13.1 Micro-aerobic culturing of P. aeruginosa

For experiments performed under reduced oxygenation, *P. aeruginosa* was routinely cultured in a MACS-500 micro-aerobic cabinet (Don-Whitely scientific) with a gas mix at a ratio of 88:5:5:2, N_2:CO_2:O_2:H2 at 37^{O}C. Media used in these experiments were placed in the cabinet for 16-18 hours to pre-reduce dissolved oxygen. Where appropriate, cultures were shaken with a small orbital-shaker (Stuart) set to 250rpm to encourage gas exchange between the atmosphere and media.

2.13.2 Nitrate and nitrite shock assays

To assess the effect of nitrate and nitrite exposure at mid-exponential phase, *P. aeruginosa* was grown in MOPS-succinate-NH_4Cl minimal media as described in section **2.1.3**. After 4 hours of incubation, cultures were pelleted, washed in MOPS-minimal media without a carbon or nitrogen source, and re-suspended in the same media with either 10mM KNO_3 or KNO_2. Samples were taken immediately post transfer, then every 1-2h, with *P. aeruginosa* viability

assessed using the modified Miles-Misra viable count method described in section **2.5.6**.

2.12.3 Fluorescence based detection of LacZ production

P. aeruginosa strains harbouring LacZ translational reporters were cultured under the desired conditions. A 500µl sample was then taken, centrifuged at 6000xg for 10mins, supernatant removed and pellet frozen at -80^{O}C for processing the following day. Access of the substrate (indicated below) to the intracellular LacZ was achieved through use of a permealization solution containing 0.1M Na_2HPO_4, 0.02M KCl, 2mM $MgSO_4$, 0.8mg/ml hexadecyltrimethylammonium bromide (CTAB), 0.4mg/ml sodium deoxycholate and 5.4ul/ml β-mercaptoethanol. Cells were defrosted on ice for 20 mins before resuspension in 100µl of permealisation solution. Samples were then incubated at 37^{O}C for 20 minutes and 10µl of whole cell extract used per sample for downstream detection. LacZ quantification was performed with the FluoReporter lacZ/Galactosidase Quantitation Kit (Invitrogen). This method relies upon the β-Galactosidase substrate 3-carboxyumbelliferyl β-D-galactopyranoside. Hydrolysis of this substrate produces blue-fluorescent 7-hydroxycoumarin-3-carboxlic acid which was detected in a 96-well format on Tecan Spark at 460nm.

Chapter 3

Identification of a potential novel anti-virulence target PA4130.

3.1 Introduction

With the growing threat of antimicrobial resistance, therapies with a novel mode of action are urgently required for the treatment of MDR *P. aeruginosa* (14). Anti-virulence strategies are proposed to be a suitable alternative, with the primary aim of disarming the pathogen to combat symptoms and prevent adaptation to Ithe host environment (149, 180, 181). *P. aeruginosa* encodes an extensive arsenal of virulence factors, many of which remain unidentified. The PAO1 genome contains 5570 known ORFs. Only 22% have been functionally characterised with over 2000 ORFs without functional annotation. This genetic dark matter may yield numerous highly specific targets for therapeutic development.

3.1.1 Identification of novel P. aeruginosa *virulence factors*

Over the years, great strides have been taken in the identification of *P. aeruginosa* virulence factors to gain a better understanding of the mechanisms employed to cause disease in human. Classical genetics has been the bedrock of these discoveries, with single gene mutation followed by phenotypic characterisation using both *in vitro* and *in vivo* assays. However, this research process is cumbersome and lengthy. With the high number of ORFs in *P. aeruginosa* PAO1, high-throughput screening methods were developed through generation of transposon mutant libraries and use of *in vivo* infection models to discern the contribution to virulence. Multiple studies of this nature have now been performed using a wide range of phylogenetically diverse virulence models as a surrogate for human virulence. Kim and colleagues generated a library of 4018 random transposon mutants in PA14-UCBPP and screened the effect on virulence in *D. melanogaster*, leading to the identification of 8 virulence factors essential for infection in this model (182). Feinbaum and colleagues generated a transposon library of 5850 non-redundant mutants corresponding to 80% of the PA14-UCBPP genome, screening the impact of mutation in *C. elegans*, successfully identifying 170 new virulence associated genes (183). Whilst Potvin and colleagues generated 7968 signature-tagged transposon mutants and screened the impact on chronic murine lung infection followed by *D. melanogaster*, identifying 36 mutants attenuated for virulence in both models, with other groups

subsequently adopting this methodology to further screen virulence factors required during chronic infection (172, 184, 185). Studies of this nature have limitations in 3 key areas:

1) Size of the transposon mutant library screened
2) Use of a single *P. aeruginosa* strain.
3) Number of disease models used.

The use of a limited number of mutants and strains can be attributed to bottlenecks in workflow, with labour intensive disease models and *in vitro* assays required to screen virulence attenuation. Potvin and colleagues calculated that 55760 signature tagged transposon mutants would be required to achieve full coverage of the genome, a significant undertaking for a single strain (184). Therefore, using transposon mutagenesis-based virulence screens on multiple phylogenetically distinct *P. aeruginosa* strains would prove challenging. The limited number of disease models can also be attributed to the labour and time intensive nature of the work. However, seminal work in the field justified this use of single models as a surrogate for human *P. aeruginosa* infection. Comparison of infection mechanisms in the plant *Arabidopsis thaliana* and mice revealed that *P. aeruginosa* uses a shared subset of virulence genes to cause disease (186). These conserved virulence mechanisms theoretically enable the use of a single infection model to dissect *P. aeruginosa* virulence, with various studies utilising the nematode *Caenorhabditis elegans* (187), fruit-fly *Drosphila melanogaster* (169), silkworm *Bombyx mori* (188), larvae *Galleria melonella* (189), Zebrafish embryos (190), *ex vivo* organ (191), and multiple murine burn and lung infection models (174, 192-195). Whilst these studies have contributed a wealth of knowledge concerning *P. aeruginosa* virulence, the use of such a diverse array of models complicates the identification of virulence factors relevant to human infection. Each of these models operate at drastically different temperatures and have distinct immune systems, altering the *P. aeruginosa* disease process. For example, *G. melonella* virulence is elastase mediated whilst the fast-killing *C. elegans* model is dependent on HCN production (196, 197). Whilst a subset of these virulence factors are conserved, the differences in pathogenesis between models makes it likely that a large subset of the novel virulence factors identified using single disease model screens are host specific.

3.1.2 Host-specific nature of P. aeruginosa *virulence*

Combatting disease model bias is key to identifying *P. aeruginosa* virulence targets relevant to human infection. In an effort to combat this problem the NABATIVI (Novel Approaches to Bacterial Target Identification, Validation and Inhibition) project combined whole-genome transposon mutagenesis with screening in multiple *in vitro* and *in vivo* models (Figure 3.1) (149). In total, A 57560 transposon mutant library was produced in PAO1-L representing around 95% of the genome. This is in agreement with the 55760 mutants hypothesized to be required by Potvin and colleagues to saturate the PAO1 genome (184). Complete coverage could not be achieved due to the presence of essential genes required for housekeeping functions such as cellular division. The *in vitro* aspect of this initial screen selected pyocyanin, protease and swarming motility as behaviours associated with *in vivo* virulence. This was designed to select Tn5 mutants attenuated in multiple virulence factor production, acting as a genetic filter prior to *in vivo* model screening to reduce the unnecessary use of animal disease models. Mutants attenuated in 2/3 of these behaviours were subsequently passed through a cascade of virulence models including *C. elegans*, *D. melanogaster*, tissue cytotoxicity, IL-8 production, invasion and murine lung infection models (Figure 3.1). This approach revealed the host-specific nature of *P. aeruginosa* infection with only limited cross-over in virulence requirement between multiple models (149). Furthermore, virulence attenuation in invertebrate models did not necessarily translate across to murine models, highlighting the importance of a multi-model approach in identifying *P. aeruginosa* virulence determinants with a mammalian model as the final validation step (149). Based on this discovery, the NABATIVI genetic screen only considered mutants attenuated across all models as potential virulence targets. Attenuation across distinct models implies that the mechanisms responsible for the Tn5 mutant attenuation are conserved. This would suggest that any targets identified in this way are more likely to be relevant to human infection and not model specific, enabling a more targeted approach for the development of anti-virulence inhibitors.

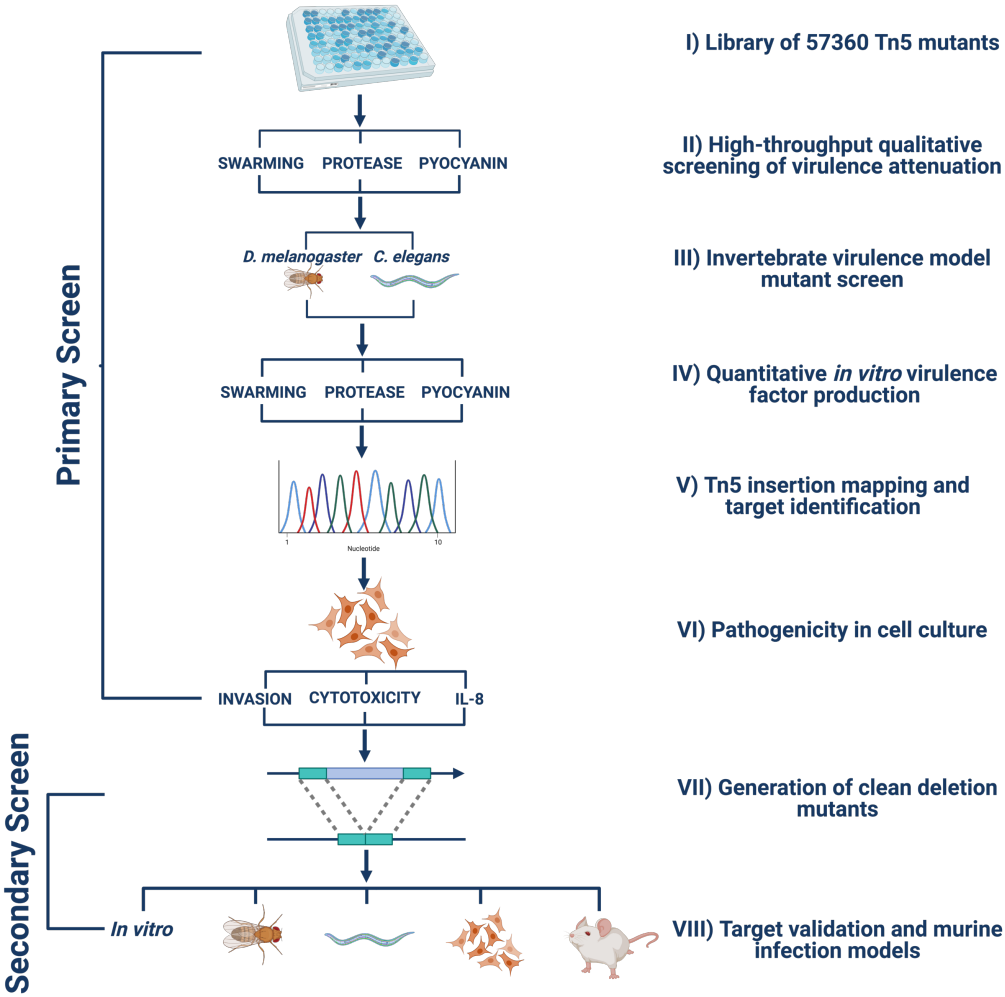

Figure 3.1 – Diagram of integrated whole genome transposon mutagenesis screen combined with multiple *in vitro* and *in vivo* models conducted for *P. aeruginosa*. Genetic screen conducted in PAO1-L as part of the NABATIVI project for novel anti-virulence target identification. Figure adapted from (149).

Using the whole-genome transposon mutagenesis platform described in (149), it was uncovered that a Tn5 insertion into the lab wild-type strain PAO1-L ORF PA4130 resulted in reduction in pyocyanin and swarming motility (Figure 3.2 and Table 3.1). Subsequent screening across invertebrate and tissue culture disease models revealed a conserved attenuation in virulence (Table 3.1). The exact role PA4130 plays was unknown, with the hypothetical protein exhibiting low-level amino acid homology with nitrite and sulphite reductase hemo-protein subunits. These enzymes catalyse the 6-electron reduction of nitrite or sulphite to ammonium or sulphide respectively (Figure 3.3) (198). Whilst these reductases have the capacity to reduce both nitrite and sulphite, there is a pronounced preference for one of these electron acceptors. This preference is

impossible to probe via sequence analysis and requires manual assertion via enzymatic and biological assessment (179).

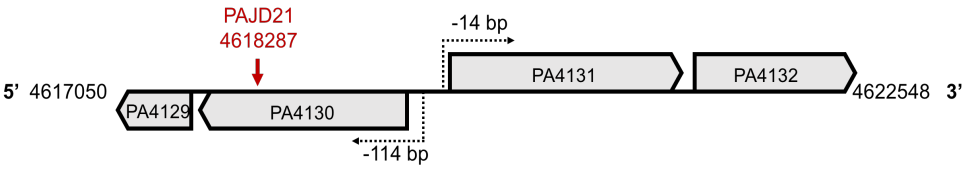

Figure 3.2 – Diagram of Tn5 insertion location for strain PAJD21, as determined by DNA sequencing. This revealed that PA4130 is in an operon with the hypothetical protein PA4129.

NABATIVI SCREEN SUMMARY	
Virulence Assay	PAJD21
Pyocyanin	
Protease	
Swarming	
D. melanogaster	
C. elegans	
A549 cytotoxicity	
A549 invasion	
A549 IL-8 production	
Acute murine lung	
Agar-bead murine lung	

Table 3.1 – Summary of PAJD21 phenotypes observed during NABATIVI genetic screen. RED-Attenuated, NAVY- not affected and GREY not assessed.

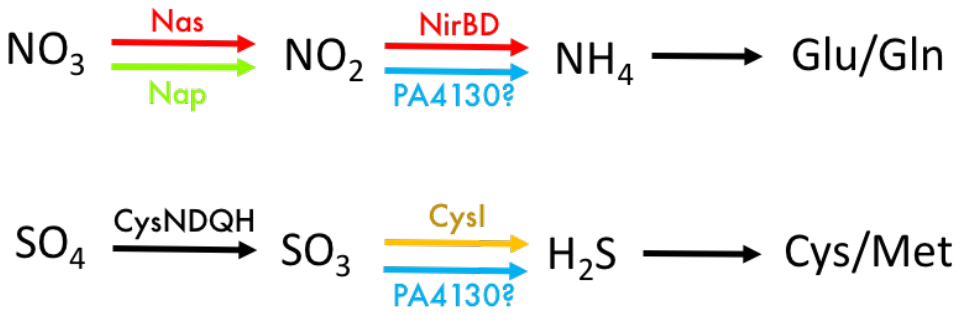

Figure 3.3 – Diagram depicting the reduction of nitrate and sulphate *in P. aeruginosa*. PA4130 resembles nitrite/sulphite reductases, likely catalysing the 6-electron reduction of nitrite and sulphite to ammonium and hydrogen sulphide respectively.

PA4130 has been demonstrated to be upregulated in the presence of hydrogen cyanide (HCN) and is reliant on the upstream regulator MpaR (199, 200). HCN is an important virulence factor of *P. aeruginosa* demonstrated to contribute to virulence in *C. elegans* (197)*, D. melanogaster (201)* with detection of cyanide associated with poor outcomes in CF and non-CF bronchiectasis patients (202, 203). The exact role cyanide plays is unknown, although it has been suggested to be important for both outcompeting the local microbiota and promoting local cellular damage during infection. Cyanide acts as a potent inhibitor of aerobic respiration through binding of cytochrome c oxidase heme a_3-CuB centres, the last enzyme in the respiratory electron transport chain (204). PA4130 is induced alongside the PA4129-34 gene cluster (Table 3.2), which has been shown to operate alongside the cyanide-resistant terminal oxidase chain CioAB in protecting *P. aeruginosa* from the toxic effects of HCN (199). The mechanism by which PA4129-34 protects from HCN is unknown. It is hypothesized that PA4133-34 (*ccoN4Q4*) forms a cyanide-resistant *cbb*$_3$-type terminal oxidase chain, enabling aerobic respiration in the presence of cyanide under oxygen limiting conditions (205). PA4133 or CcoN4 has also been demonstrated to facilitate redox balancing under low oxygen tension through reduction of phenazines, facilitating survival in a colony biofilm model (140). The potential role PA4130 plays in both of these mechanisms has largely been overlooked due to a lack of functional characterisation.

ORF	Gene name	Function	Fold change
PA4129	Hypothetical	DUF934-domain containing protein	+24.98
PA4130	Hypothetical	Nitrite or sulphite reductase.	+42.99
PA4131	Hypothetical	Membrane iron-sulphur protein resembling CcoG2 cytochrome c oxidase accessory protein.	+51.41
PA4132	*mpaR*	MvrF mediated PQS and anthranilate regulator.	+22.28
PA4133	*ccoN4*	Cytochrome C oxidase catalytic sub-unit	+110.26
PA4134	*ccoQ4*	Cytochrome C oxidase accessory sub-unit	+31.10

Table 3.2 – Function of PA4129-34 genes upregulated in response to cyanogenesis. Adapted from (199).

Prior to functional and structural characterisation, PA4130 must be confirmed as a virulence target. PA4130 is in a 2-gene operon with PA4129 (Figure 3.2). Therefore, it should be confirmed that disruption of PA4130 is responsible for the virulence phenotypes observed and not due to a polar effect over PA4129 expression as a consequence of the Tn5 insertion. These screens are experimentally demanding with such target validations usually performed retrospectively. This is a major drawback in the screening methodology, with a high volume of follow-up work required to confirm virulence targets. Another aspect noted by Dubern and colleagues (149) is the use of only a single *P. aeruginosa* strain (PAO1-L). It has been demonstrated that the virulence factor requirement of *P. aeruginosa* varies depending on the genetic background of the strain (206). Whilst use of multiple-models limits identification of host-specific virulence determinants, the use of a single strain may lead to the identification of strain specific virulence determinants.

3.2 Aims of this chapter

The work presented in this thesis builds upon the successful screening methodology utilised by Dubern *et al* (2). This chapter focuses upon validating the results obtained for PAJD21 (Table 3.1), whilst simultaneously addressing caveats of the screening methodology used. Hence, to confirm PA4130 as a viable therapeutic target and further our mechanistic understanding, the aims of this chapter are:

1. Confirm whether previously observed phenotypes are specific to PA4129 or PA4130 using a combination of marker-less in frame deletion mutants and genetic restoration (complementation).

2. Determine whether the role of PA4130 is phylogenetically conserved.

3. Further characterise the impact of PA4130 mutation on basic and virulence associated functions of *P. aeruginosa*.

3.3 Results

3.3.1 Effect of PA4130 deletion on P. aeruginosa virulence factor production.

P. aeruginosa produces an extensive arsenal of virulence factors responsible for host colonisation and damage. During the transposon screen pyocyanin, protease and swarming motility were selected as initial virulence phenotypes due to their close association with disease. The PAJD21 Tn5 mutant exhibited defects in pyocyanin production and swarming motility whilst protease secretion was unaffected. Initial assessments set out to demonstrate that these phenotypes are specific to PA4130, and not due to a polar effect on the downstream PA4129. To confirm this, 3 strategies were employed.

I. Construct and confirm that an in-frame PA4130 deletion mutant displays similar phenotypes to PAJD21

II. Complement PA4130 function with genetic restoration

III. Construct an in-frame deletion mutant of PA4129 and screen for phenotypic overlap with PA4130 mutants.

3.3.1.1 Construction of PAJD25 and PAJD25 CTX4130*

It has previously been demonstrated that PAJD21 (PA4130::Tn5), is attenuated in multiple *in vivo* models. Whilst transposon mutagenesis is a good tool for high-throughput screening of potential virulence targets, insertion of such a large section of DNA (5.8kb) can cause pleiotropic knockdown of genes both up and downstream. To confirm that the phenotypes exhibited by PAJD21, a PA4130 in-frame deletion was constructed in PAO1-L.

To construct an in-frame deletion mutant in PA4130, the 427bp upstream and 433bp downstream nucleotides of PA4130 were amplified and fused by overlap extension PCR. The upstream fragment was amplified with primers PA4130F1 modified with an XbaI restriction site, and PA4130R1 containing the first 12

nucleotides of PA4130 and an overhanging end containing the last 15 nucleotides of the PA4130 ORF. The downstream 433bp fragment was amplified with PA4130F2 containing the last 15 nucleotides of PA4130 with an overhanging end containing the first 12 nucleotides and PA4130R2 containing a HindIII restriction site (Table 2.3). These 2 fragments were linearized using the engineered homologous overlap regions and served as a template for overlap PCR with PA4130F1/PA4130R2 (Figure 3.4) The final PCR product was cloned using the XbaI/HindIII restriction sites into the pME3087 vector, forming suicide-plasmid pME4130. This vector was mobilised into PAO1-L with conjugation, and an in-frame deletion mutant generated by allelic exchange forming strain PAJD25 (PAO1-L ΔPA4130) (Figure 3.4).

Deletion of PA4130 was functionally restored in PAJD25 through reintroduction of PA4130, under control of its native promoter, at a distal *attB* genomic site. A 2172 nucleotide fragment containing the PA4130 ORF and +498bp of the translation start site, using primers 4130CTXF1 and 4130CTXR1 (Table 2.3). The PCR product was cloned into pMINI-CTX-1 using the HindIII/BamHI restriction sites engineered onto 4130CTXF1 and4130CTXR1, forming vector pCTX4130. This vector was then mobilised into PAJD25 with conjugation, forming strain PAJD25 CTX4130. The promoter region selected for amplification mimics a previously successful pPA4130-*lacZ* transcriptional fusion synthesized by Frangipani and colleagues (199). Chromosomal complementation of PA4130 ensures that only a single copy of the gene is present, whilst control through the native promoter attempts to replicate wild-type transcriptional levels. This minimises copy-number and transcriptional expression defects often observed in vector or artificial induction complementation strategies, more accurately portraying wild-type protein copy number.

**The PA4130 mutant was generated prior to my arrival on this project. This was performed by Dr. Jean Frederic-Dubern and the strain subsequently named PAJD25 in acknowledgement of this.*

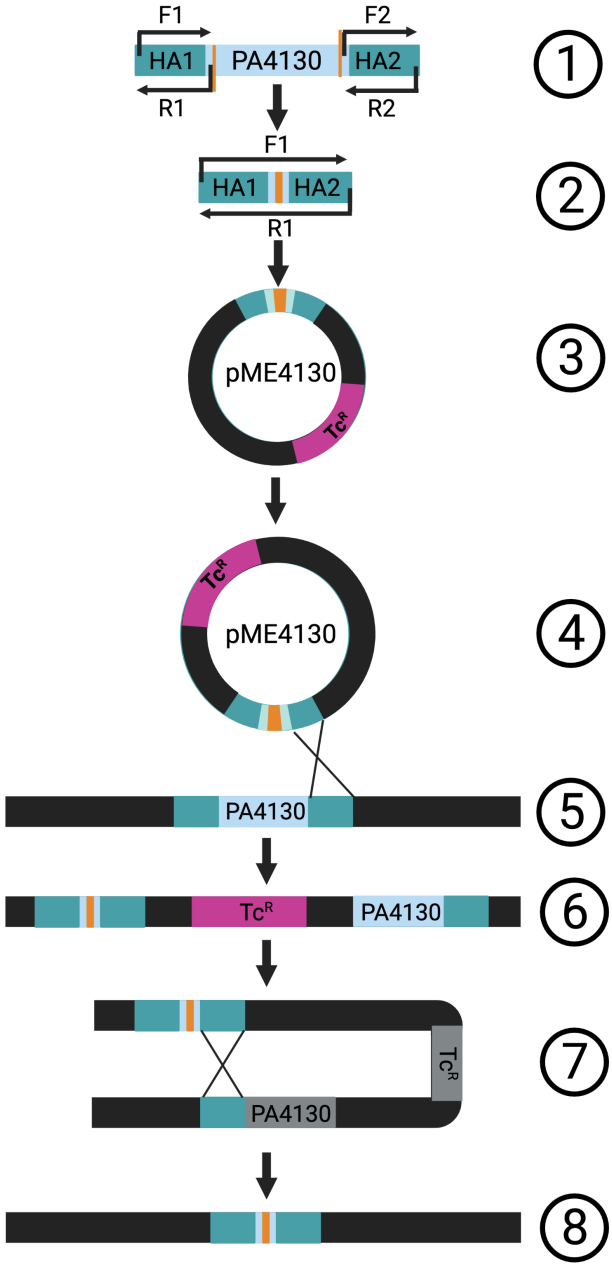

Figure 3.4 – Schematic detailing construction of a marker-less PA4130 deletion mutant in PAO1-L. 1) The 427bp upstream and 433bp downstream nucleotides are amplified by PCR forming homology arms (HA) 1 and 2. **2)** Primers R1 and F2 are designed with homologous regions to allow HA1 and HA2 to anneal. Overlap PCR is then performed on these annealed fragments using the F1 and R2 primers, producing a single nucleotide fragment with PA4130 excised. **3)** The generated fragment and vector pME3087 are then digested with XbaI/HindIII restriction enzymes, and ligated together with T4 DNA ligase (Promega), forming pME4130. **4-6)** Vector $_{p}$ME4130 is then mobilised into PAO1-L by conjugation using the procedure outlined in **2.7.4**, and single cross-over events requiring one homology arm are resolved by plating conjugants on tetracycline. **7)** Spontaneous secondary recombination events occur by culturing conjugants in the absence of the tetracycline marker. Enrichment of double recombinants was performed as described in **2.7.5**. **8)** Double recombinants can revert to wild-type or allow deletion of PA4130. Successful removal of PA4130 from the genome of PAO1-L was confirmed with PCR and sanger sequencing.

3.3.1.2 Effect of PA4130 deletion on secreted virulence factor production

To confirm the pyocyanin phenotype is attributable to interruption of PA4130, pyocyanin production by PAO1-L, PAJD21, PAJD25 and PAJD25 CTX4130 was quantified in both, LB and M-ASM. For LB both PAJD21 and PAJD25 demonstrate a 2 and 2.3-fold reduction in pyocyanin production respectively. However, at 20h PAJD21 and PAJD25 pyocyanin production is indistinguishable from wild-type PAO1-L (Figure 3.5 I). This reduction in pyocyanin is more prominent in M-ASM, with reduced levels observed at both 8 and 20h (Figure 3.5 II). Complementation of PAJD25 with pCTX4130 restores the pyocyanin phenotypes observed in both LB and M-ASM (Figure 3.5 I-II). Protease production remains unaffected in PAJD25 (Table 3.3).

Whilst pyocyanin and protease production are important in *P. aeruginosa* virulence, a number of other secreted virulence factors are also closely associated with disease manifestation including, but not limited to, elastase and pyoverdine production. Elastase production was unaffected in both PAJD21 and PAJD25 (Table 3.3). However, pyoverdine production was reduced by 2-fold at 20h in M-ASM as assessed using pyoverdine specific absorbance at 405nm. This phenotype was only partially complemented with PAJD25 CTX4130 still showing reduced pyoverdine levels relative to the wild-type PAO1-L (Figure 3.5 III).

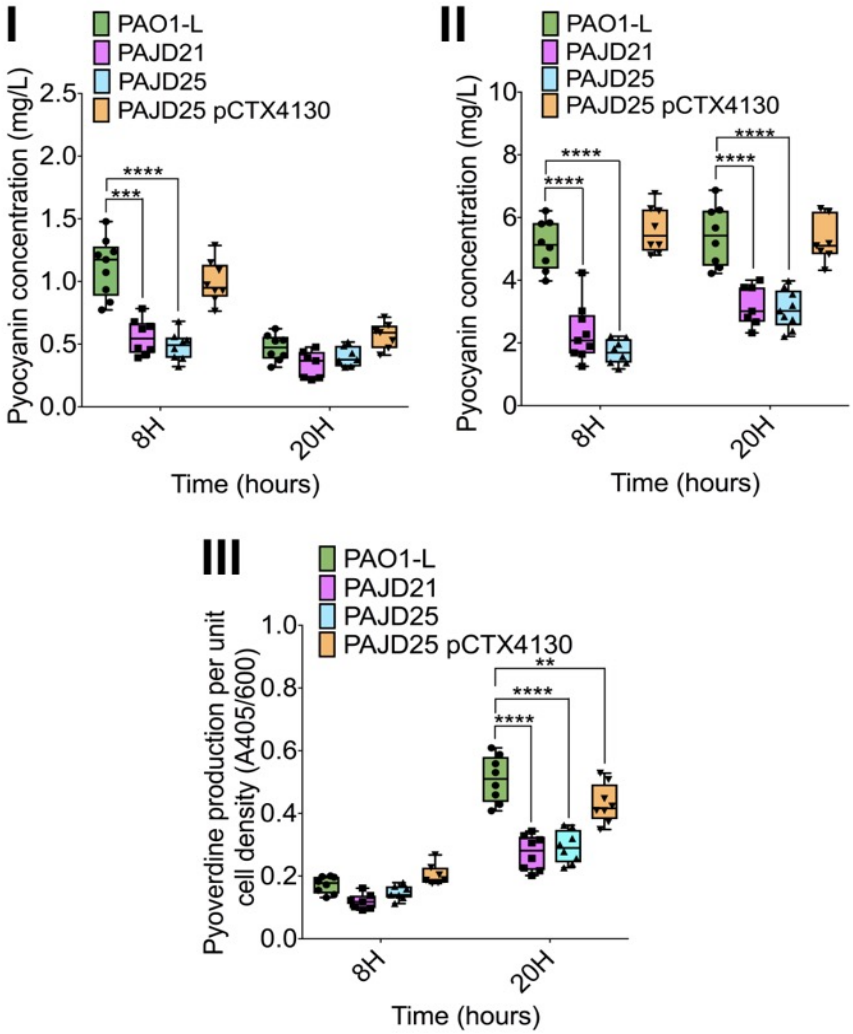

Figure 3.5 – Pyocyanin and pyoverdine secretion determined in culture supernatants from PAO1-L, PAJD21, PAJD25 and PAJD25 pCTX4130. (**I**) Quantification of pyocyanin produced in LB at 8 and 20 h; (**II**) pyocyanin produced in M-ASM at 8 and 20 h; and (**III**) pyoverdine specific absorbance at 405nm normalised to cell density at 8 and 20 h. Data collated from 2 independent experiments with at least 4 replicates. **P <0.0021, ***P <0.0021, ****P <0.0001, Dunnett's multiple comparisons test.

3.3.1.3 Impact of a PA4130 mutation on motility

Swarming motility was found to be impaired in PAJD21 during the initial transposon screen. To confirm the swarming phenotype is consistent between PAJD21 and PAJD25, this assay was repeated. Swarming motility is reduced in both PAJD21 and PAJD25 with complementation restoring wild-type swarming capacity (Figure 3.6). Swimming and twitching motility were not previously assessed in PAJD21 with swarming motility selected due to its frequent association with virulence factor production and suitability for high

throughput screening. Both swimming and twitching motility behaviours were unaffected in PAJD21 and PAJD25 with the impact of PA4130 on motility seemingly specific to swarming motility (Table 3.3).

The similar phenotypes exhibited by PAJD21 and PAJD25 in pyocyanin, pyoverdine and swarming motility combined with genetic restoration of function suggest that PA4130 is solely responsible for the impact on the different virulence traits affected in the previous screening. This validated PA4130 as a potential anti-virulence target and justified further investigations to characterise the effect of PA4130 mutation and better understand, I) the role PA4130 plays during the disease process and II) whether PA4130 is a virulence-target worth pursuing for therapeutic development.

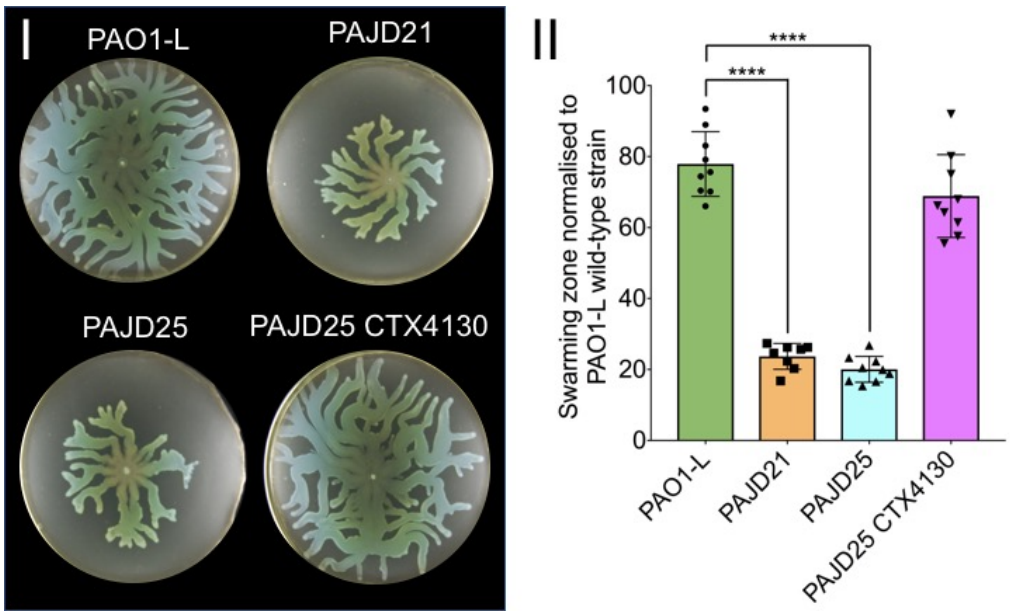

Figure 3.6 – **Swarming motility of PAO1-L and PA4130 mutants determined on 0.5% agar. I)** Representative images from swarming assays; **II)** Swarming zone calculated as percentage plate coverage and normalised to PAO1-L wild-type strain. Percent surface coverage was calculated using ImageJ analysis software. Data collated from 2 independent experiments with at least 5 replicates. ****P <0.0001 Dunnett's multiple comparisons test.

	Strains			
Assay	**PAO1-L**	**PAJD21**	**PAJD25**	**PAJD25 CTX4130**
Protease	100±8.1	94.7±10.2	110.2±11.3	92±13.1
Elastase	100±7.1	90.3±12.6	108±10.1	91.3±8.4
Swimming	100±6	93.1±10.4	95.2±7.7	92.2±5
Twitching	100±11.2	92±14.9	87.1±16.2	90.1±15

Table 3.3 – Data summary of virulence and motility phenotypes not affected by PA4130 interruption. Values normalised as a percentage of PAO1-L wild-type results. Elastase and protease assays collated from 3 independent experiments with 3 replicates. Swimming and twitching motility collated from 2 independent experiments with at least 4 replicates.

3.3.1.4 Does mutation of PA4130 impact P. aeruginosa growth

One key characteristic of anti-virulence targets is that their inhibition should not impair microbial growth in a manner similar to antibiotics. To ensure the impact on virulence traits observed in PAJD21 and PAJD25 was not due to growth defects, growth kinetics were assessed in LB and M-ASM. Since PA4130 has been shown to be regulated by cyanogenesis which is maximally produced at 5% oxygen (207, 208), growth was assessed under both aerobic and micro-aerobic conditions. No significant effect on growth is observed due to interruption of PA4130 under aerobic conditions in both LB and M-ASM (Figure 3.7 I-II). Under micro-aerobic conditions, PAJD21 and PAJD25 growth was also unaffected in LB however, it was noted that the PA4130 mutants consistently exhibit a larger drop in optical density during stationary phase in M-ASM (Figure 3.7 III-IV).

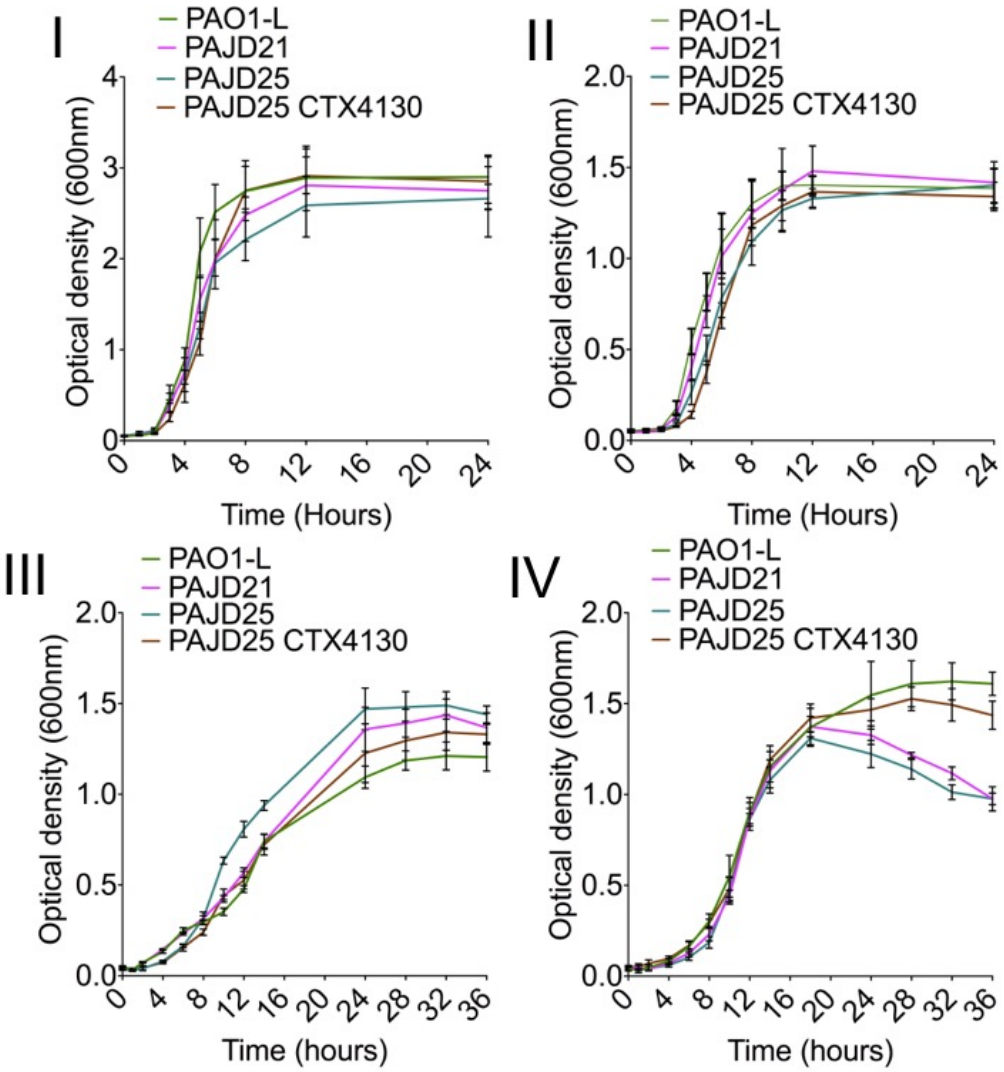

Figure 3.7 – Growth kinetics of PAO1-L, PAJD25, PAJD25 and PAJD25 CTX4130 in LB and M-ASM under aerobic or micro-aerobic (5% O2) conditions. (**I**) Aerobic in LB; (**II**) Aerobic in M-ASM; (**III**) Micro-aerobic in LB; and (**IV**) Micro-aerobic in M-ASM.

Since the amino acid sequence of PA4130 appears to be homologous to nitrite or sulphite reductase hemo-protein sub-units, it was hypothesized that the decrease in OD could be due to an impaired micro-aerobic nitrate or sulphate reduction pathway. Therefore, to determine if these nutrients play a role, sulphate and nitrate sources were removed from M-ASM and substituted with sulphide and ammonium respectively, bypassing both respective pathways (Figure 3.2).

Growth was reassessed in M-ASM under micro-aerobic conditions. When sulphate was substituted with sulphide, no change was observed, with PAJD21 and PAJD25 OD falling upon entry into stationary phase (Figure 3.8 I). When subjected to growth in M-ASM, substituting nitrate for NH_4Cl, the drop in optical density for strains PAJD21 and PAJD25 during stationary phase was no longer seen (Figure 3.8 II). This indicates that PA4130 mutants are nitrate responsive, providing evidence that PA4130 participates in nitrate metabolism. Although no effect on growth was seen in M-ASM when sulphate is present, a role for PA4130 in sulphate metabolism cannot be ruled out as it is present in extremely low concentrations in M-ASM (35-40um). Mucin can also serve as a reservoir of sulphate for *P. aeruginosa*, making control of this nutrient very difficult as removal of mucin would alter the physicochemical properties of this medium. Functional assessment of PA4130 is required to confirm whether PA4130 belongs to the nitrate or sulphate reduction pathway.

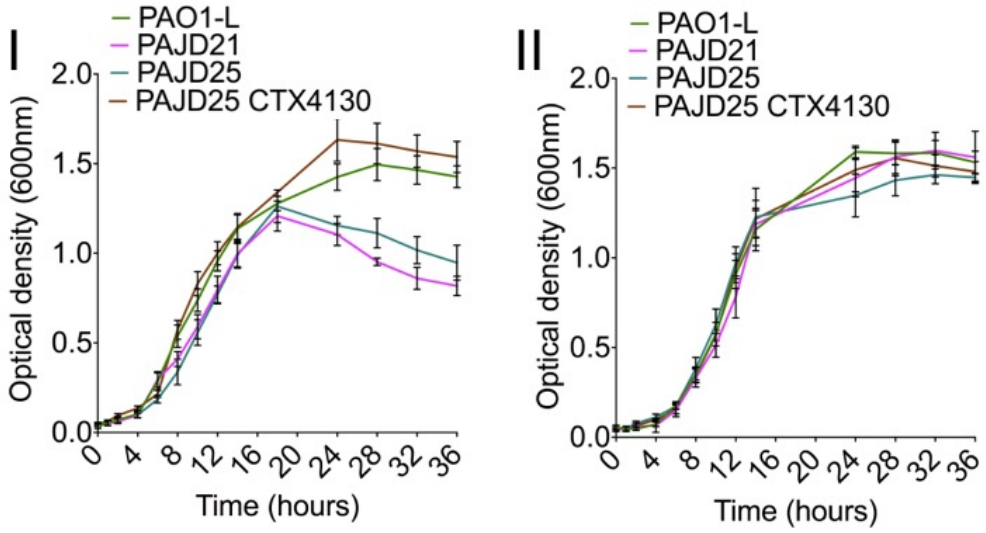

Figure 3.8 – Growth of PA4130 mutant strains in M-ASM with and without nitrate or sulphate under micro-aerobic conditions in M-ASM. I) M-ASM with inorganic sulphate replaced by sulphide **II)** M-ASM supplemented with 1mM NH_4Cl in place of KNO_3. Growth curves not displayed in log^{10} to more easily display subtle phenotype.

3.3.1.5 Attachment and biofilm formation on abiotic surfaces

Previous characterisation of PAJD21 and PAJD25 failed to determine the effect of PA4130 deletion on biofilm formation. Swarming motility and biofilm formation often exhibit an inverse relationship with reduced swarming associated with increased biofilm formation and vice versa. Therefore, we hypothesised that PA4130-dependant attenuation of swarming would result in a hyper-biofilm phenotype. In order to determine the impact of PA4130 on cellular attachment and biofilm formation both multi-well plate attachment and colony biofilm attachment assays were performed under aerobic and micro-aerobic conditions.

3.3.1.5.1 Role of PA4130 in abiotic attachment

Attachment was assessed for PAO1-L, PAJD21, PAJD25 and PAJD25 CTX4130 in 48-multiwell plates for 2 days with either LB or MOPS-succinate-minimal media, followed by staining with 0.1% crystal violet. Attempts to use M-ASM to assess attachment failed, with *P. aeruginosa* preferring to form floating biofilm-like structures. Given the nitrate responsive nature of the PA4130 mutant strains, attachment assays were also performed in the presence of supplemented NH_4Cl, KNO_2 and KNO_3 at 10mM.

Under aerobic conditions, no difference in PAJD21 and PAJD25 attachment was seen in both LB and MOPS-succinate minimal media when grown without KNO_2 and KNO_3. However, in LB and MOPS-succinate minimal media containing KNO_2 and KNO_3, attachment was increased (Figure 3.9 I-II). Since PA4130 is upregulated by HCN, we sought to mimic conditions where HCN is maximally produced by repeating these assays under micro-aerobic conditions. In LB and LB with NH_4Cl, an increase in abiotic attachment was observed in the absence of nitrite or nitrate at 5% O_2 (Figure 3.9 III). This same nitrite and nitrate independent increase was not observed in MOPS-succinate minimal media supplemented with casamino acids or NH_4Cl as an N source (Figure 3.9 IV). Under these low oxygen tensions, the presence of KNO_2 or KNO_3 further enhanced attachment of PA4130 mutants, with complementation only partially restoring this phenotype (Figure 3.9 III-IV).

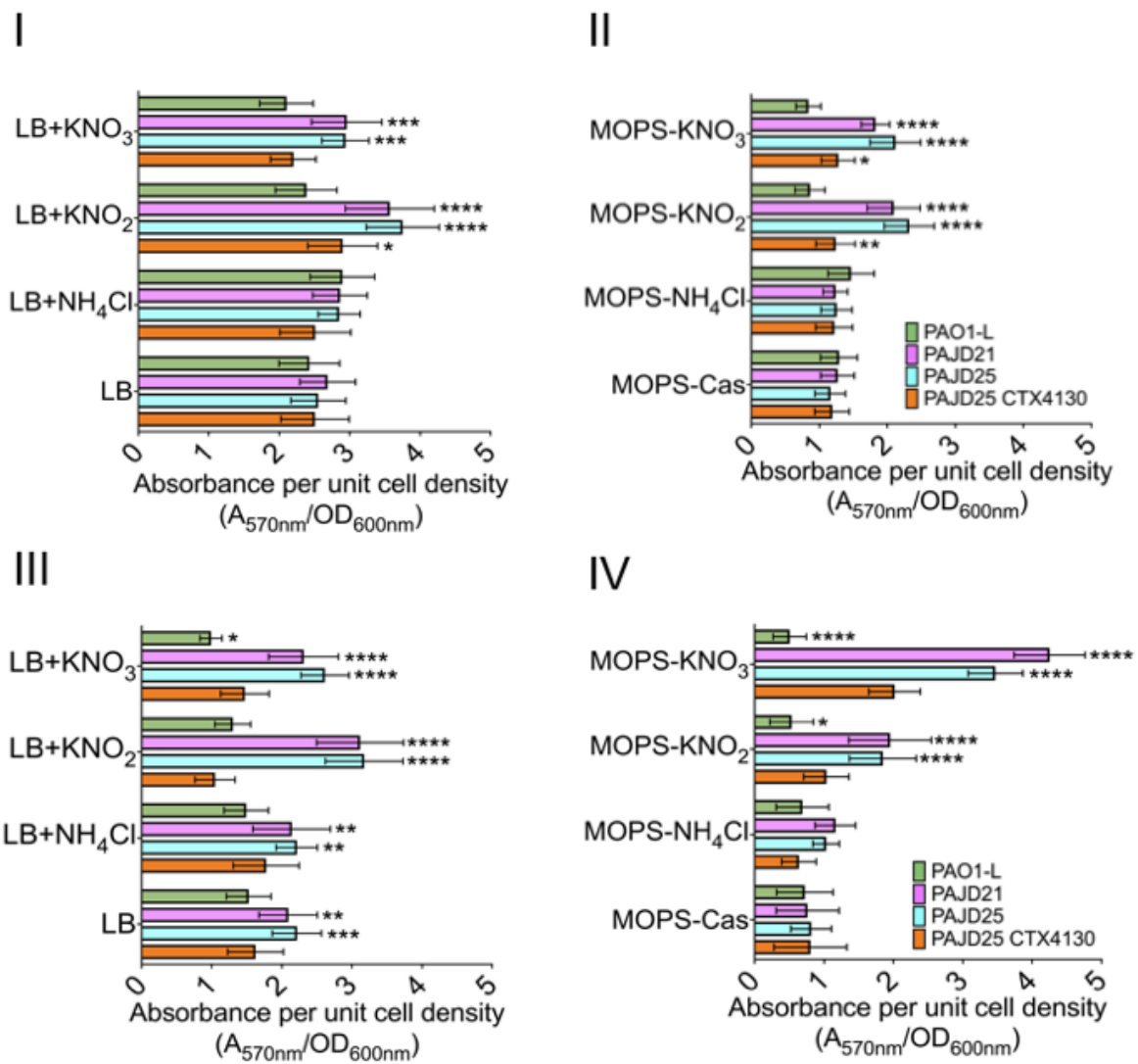

Figure 3.9 – **Assessment of bacterial attachment to 48-well polypropylene plates in LB and MOPS-succinate minimal media supplemented with 10mM NH_4Cl, KNO_2, KNO_3. I)** LB with additional nitrogen sources under aerobic conditions. **II)** MOPS-succinate minimal media with single nitrogen sources under aerobic conditions. **III)** LB with additional nitrogen sources under micro-aerobic conditions. **IV)** MOPS-succinate minimal media with single nitrogen sources under micro-aerobic conditions. Data collated from 2 independent experiments with 5-6 replicates and compared to isogenic wild-type strain. *P <0.0332, **P <0.0021, ***P <0.0002, ****P <0.0001, Dunnett's multiple comparisons test

3.3.1.5.2 Impact of PA4130 on colony biofilm formation

Whilst increased attachment of PA4130 interrupted strain is not a desirable trait, it is not necessarily indicative of a hyper-biofilm phenotype. Attempts to establish biofilms on abiotic surfaces gave mixed results with no consistent pattern emerging. PAO1-L is renowned as a poor biofilm former in comparison to other *P. aeruginosa* strains, producing 1/3 of the biomass of a PA14 biofilm (128). This meant PAO1-L biofilm formation on abiotic surfaces cannot be reliably assessed, especially when varying oxygen concentrations. Instead, a colony biofilm model was used as an easy experimental procedure to assess biofilm formation under aerobic and micro-aerobic conditions. This model is advantageous when exploring the effect of oxygenation as it is agar-plate based with oxygen obtained from air at the colony interface. Liquid medium based assays are likely anaerobic by the end of the experiment due to the biological oxygen demand exerted by a high density bacterial culture.

No statistically significant difference was exhibited by colony biofilms established on LB under aerobic or micro-aerobic conditions (Figure 3.10). Colony biofilms were then established in the presence of 0.1mM, 1mM and 10mM KNO_3 with these concentrations selected as it has been reported that the cystic fibrosis lung can contain between 0.072-1mM nitrate (209). As the concentration of nitrate increased, wild-type PAO1-L exhibited a slight increment in CFU's (Figure 3.10). This may be due to nitrate supporting anaerobic growth or persistence at the bottom of the colony biofilm due to formation of an oxygen gradient through the colony biofilm (210). At 0.1mM nitrate, no effect on PAJD21 and PAJD25 was observed under aerobic conditions, however under micro-aerobic conditions PAJD21 and PAJD25 showed a 1.5-log reduction in CFUs when compared to PAO1-L (Figure 3.10). This effect was further enhanced at 1mM and 10mM nitrate, with PA4130 interrupted strains demonstrating a reduction in CFUs under both aerobic and micro-aerobic conditions (Figure 3.10). The reduction in CFUs was partially

complemented by pCTX4130, although PAJD25 CTX4130 consistently showed reduced CFUs compared to PAO1-L.

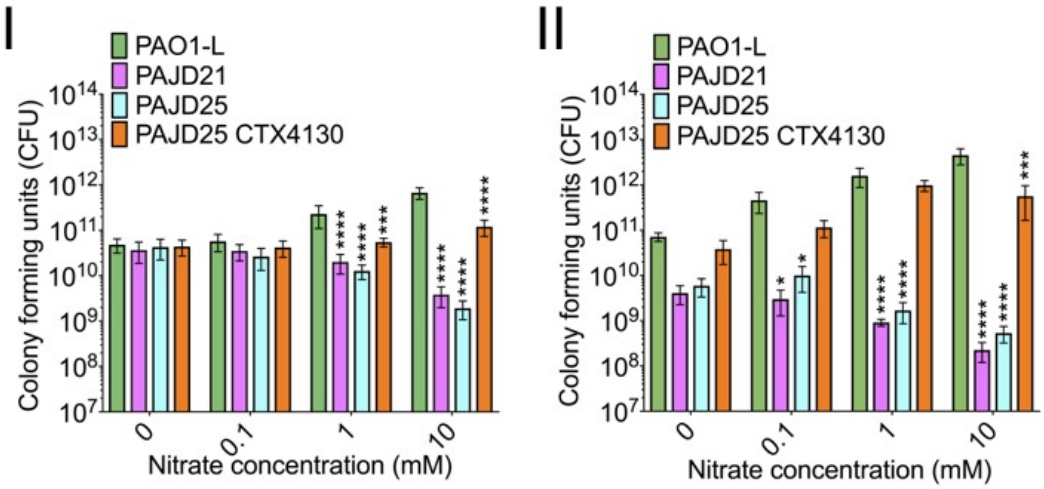

Figure 3.10 – Quantification of bacterial growth on LB using a colony biofilm model. Performed under aerobic (I) and micro-aerobic (II) conditions with increasing concentrations of nitrate. Data collated from 3 independent experiments with at least 3 biological replicates. *P <0.0332, ***P <0.0002, ****P <0.0001, Bonferroni's multiple comparisons test.

3.3.2 Effect of PA4129 deletion on P. aeruginosa *virulence factor production.*

PA4129 is a DUF934-domain containing hypothetical protein found in an operon with PA4130 (Figure 3.2). The molecular function these proteins play is not yet unknown. However, PA4129 homologues have been identified as accessory proteins required for sulphate assimilation in *Pseudomonas*, *Marinobacter adehaerans* and *Cupriavidus basilensis* (211). *P. aeruginosa* encodes a PA4129 homologue designated PA1837. This gene is the 2nd in an operon with the PA4130 homologue CysI, a confirmed sulphite reductase. PA4130 and CysI share 70.3% nucleotide sequence similarity whilst PA4129 and PA1837 display 63.6% similarity, raising the possibility that these 2 homologues arose in *P. aeruginosa* through gene-duplication. This could imply that PA4129 also functions alongside PA4130 in either nitrate or sulphate metabolism. If this is the case, it is expected that a PA4129 mutant would show similar virulence phenotypes to PAJD21 and PAJD25. To probe this relationship, an in-frame PA4129 mutant was generated and screened for overlapping phenotypes caused by deletion of PA4130.

3.3.2.1 Construction of PA4129 deletion mutant

A PA4129 mutant was constructed in a manner similar to PAJD25. Two PCR products were generated upstream and downstream of PA4129 using primer pairs PA4129F1/PA4129R1 and PA4129F2/PA4129R2. These fragments were then joined and overlap PCR performed using PA4129F1/PA4129R2. The final PCR product, containing a deletion in PA4129, was cloned into PME3087 using the EcoRI/BamHI restrictions sites added onto PA4129F1 and PA4129R1 respectively forming pME4129. Vector pME4129 harbouring the PA4129 DNA deletion, was used to construct an in-frame PA4129 deletion mutant in PAO1-L using allelic exchange, forming strain PASF06. Successful double recombination events were confirmed with PCR and DNA sequence analysis.

3.3.2.2 Role of PA4129 in secreted virulence factor production

Secreted virulence factors that were identified as attenuated in PAJD21 and PAJD25 were limited to pyocyanin and pyoverdine. Strain PASF06 was tested in conjunction with the isogenic wild-type PAO1-L and PAJD25 to look for overlapping secreted virulence factor attenuation. As expected protease and elastase production were unaffected in both PASF06 and PAJD25 (Table 3.4). Production of pyoverdine in M-ASM and pyocyanin in both LB and M-ASM were unaffected in a PA4129 deletion background (Table 3.4) suggesting that the virulence attenuation observed in PA4130 is not due to a downstream polar effect.

3.3.2.3 Impact of PA4129 deletion on P. aeruginosa motility

To establish if a mutation in PA4129 has an impact on motility, swarming, swimming and twitching motility were assessed using PAO1-L, PASF06 and PAJD25. As seen previously, swimming and twitching motility were unaffected in PAJD25 with PASF06 also demonstrating no reductions in motility. Swarming motility was not impacted by deletion of PA4129, whilst PAJD25 demonstrated the same reduction as seen previously (Table 3.4).

The lack of phenotypic overlap between PA4130 and PA4129 deletion mutants suggests that PA4129 is not required in a similar manner to PA1837, with the role of PA4130 in secreted virulence factor production functionally independent of PA4129. This further confirms that the virulence phenotypes observed in both PAJD21 and PAJD25 are specific to PA4130 and not due to a polar effect on PA4129. Due to the lack of phenotypic conservation between the PA4129 and PA4130 deletion mutants, the function of PA4129 was not explored further in this project.

	Strains		
Assay	**PAO1-L**	**PAJD25**	**PASF06**
Pyocyanin	100±8.6	48±7.2	88±10.5
Pyoverdine	100±5.8	67±9.8	94±11.4
Protease	100±8.4	90±9.3	93±5.3
Elastase	100±6.4	108±5.8	91±7.4
Swarming	100±12.2	20±4.8	106±7.2
Swimming	100±7.2	88±10.2	96±8.8
Twitching	100±14.7	92±11.3	89±14.1

Table 3.4 – Table summarising in vitro virulence factor production and motility exhibited by PASF06 in comparison to wild type PAO1-L and PAJD25. Figures are expressed as a percentage of PAO1-L however, statistical analysis were performed on raw data.

3.3.3 PA4130 virulence phenotypes are phylogenetically conserved.

P. aeruginosa is a phylogenetically diverse organism with virulence shown to be dependent on a plethora of pathogenicity related-genes that interact in various different ways *in vivo* (206). This means that virulence attenuation exhibited by a particular mutation in a single strain is not necessarily predictive of virulence in other *P. aeruginosa* strains carrying the same mutation. To combat this problem, potential virulence targets should be screened in multiple genetic backgrounds to ensure conservation of virulence phenotypes.

3.3.3.1 Phylogenetic conservation of PA4130 orthologues in P. aeruginosa.

The conservation of PA4130 in different genomes was initially studied using BLAST against the NCBI taxonomic database (taxID:287). A 90% sequence similarity cut-off was used as *P. aeruginosa* encodes the PA4130 homologue CysI. PA4130 and CysI share 71% nucleotide and 62.1% amino-acid sequence similarity in strain PAO1, therefore the use of a high cut-off ensures CysI orthologues are not mistaken for PA4130. BLAST revealed that PA4130 is highly conserved, with 363/367 (98.9%) of screened *P. aeruginosa* genomes encoding a PA4130 orthologue (data not shown).

3.3.3.2 Construction of PA4130 mutants in clinical P. aeruginosa strains.

Clinical strain isolates from different sublines were selected to best represent the phylogenetic diversity of *P. aeruginosa*. This was based on the observations of Moore and colleagues (212), with PA7 Bo599, PA14 AUS471, LESB58 PA-W39 and PAK W-11 selected for genetic manipulations. Vector pME4130 harbouring the PA4130 DNA deletion, was used to construct an in-frame deletion mutant in the gene designations indicated in Table 3.5. For simplicity, these designations are collectively referred to as PA4130 orthologues in the remainder of this thesis. Successful deletion was confirmed in PA7 Bo599, PA14 AUS471 and LESB58 PA-W39 by PCR and DNA sequencing. Attempts with PAK PA-W11 were not successful with double recombinants reverting to wild-type.

Strain	Description	PA4130 orthologue designation	Source
PA7 Bo599	Burn wound clinical isolate	IPC867_RS21670	(152)
PA14 AUS471	Ear infection clinical isolate	IPC282_RS26830	(36)
LESB58 PA-W39	Soft-tissue wound clinical isolate	IPC1298_RS25615	Lab stock
PAK PA-W11	Cystic fibrosis clinical isolate	Y880_RS18905	(152)

Table 3.5 – Details of *P. aeruginosa* clinical strains and PA4130 orthologue designations.

3.3.3.3 Effect of PA4130 orthologue deletion on secreted virulence factor production

Screening of secreted virulence factor production in PAO1-L demonstrated that mutation of PA4130 reduced pyocyanin and pyoverdine secretion. To see if the effect of a PA4130 orthologue mutation is conserved across different strains, pyocyanin and pyoverdine production was screened using the newly generated PA4130 orthologue mutants in PA7 Bo599, PA14 AUS471 and LESB58 PA-W39. Pyocyanin production was reduced in all PA4130 orthologue mutant strains grown in LB and M-ASM (Figure 3.11 I-II) but this was not the case for pyoverdine production in all strains when grown in M-ASM. PA7 Bo599 and LESB58 PA-W39 PA4130 orthologue mutants displayed slightly elevated pyoverdine production, whilst PA14 AUS471 showed attenuation, as reported in PAO1-L (Figure 3.11 III). The reasons for this difference remain unclear however, pyoverdine production is a complex trait with various different forms of pyoverdine and multiple regulators influencing the expression of the pyoverdine biosynthetic genes (213-215). Both elastase and protease production were unaffected in the PA4130 clinical isolates orthologue mutants, consistent with the impact of this mutation in PAO1-L phenotypes (Table 3.6).

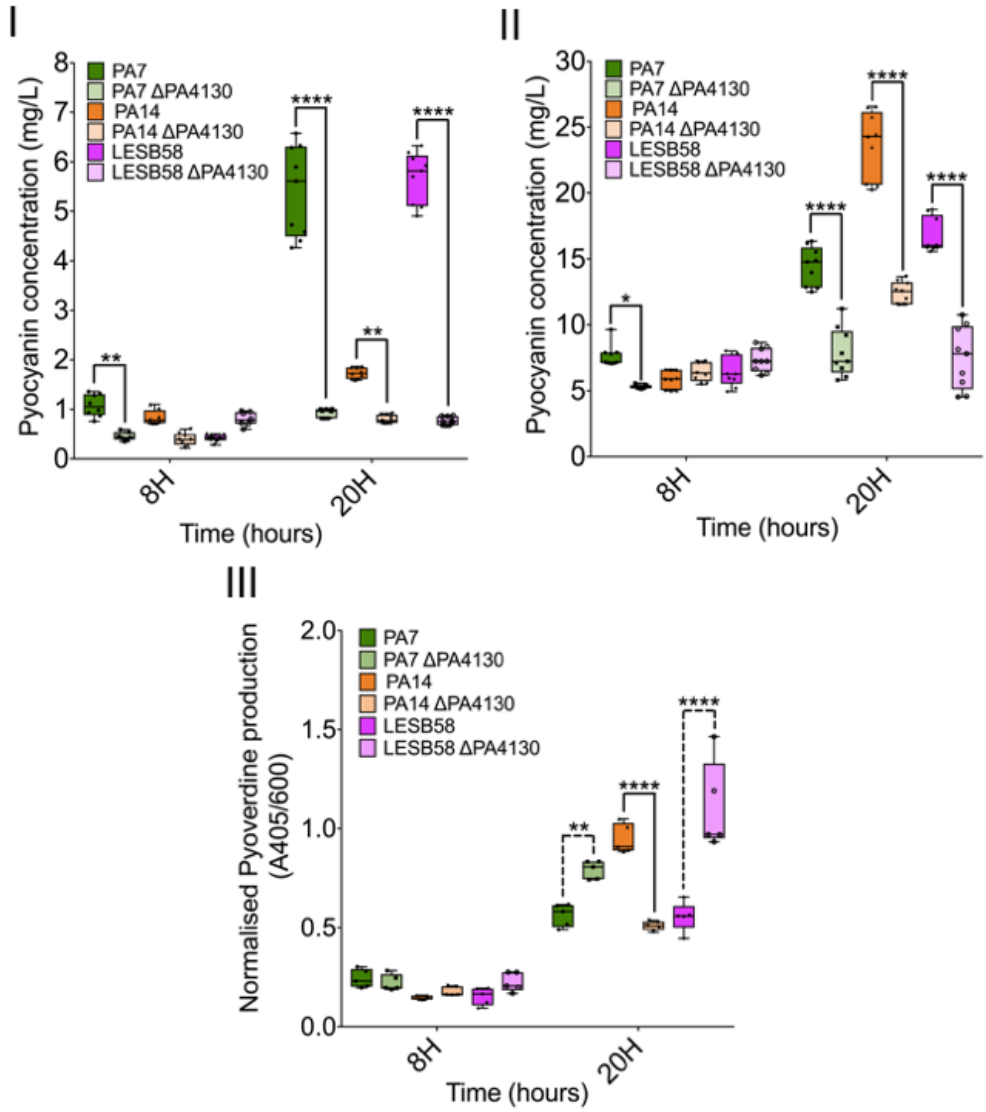

Figure 3.11 - Pyocyanin and pyoverdine secretion determined in culture supernatants from PA7, PA14, LESB58 and PA4130 orthologue mutants. (**I**) Quantification of pyocyanin produced in LB at 8 and 20 h; (**II**) pyocyanin produced in M-ASM at 8 and 20 h; and (**III**) pyoverdine specific absorbance at 405nm normalised to cell density at 8 and 20 h. Data collated from 2 independent experiments with at least 4 replicates. **P <0.0021, ***P <0.0021, ****P <0.0001, Dunnett's multiple comparisons test.

	Strains					
Assay	**PA7**	**PA7 ΔRS21670**	**PA14**	**PA14 ΔRS26830**	**LESB58**	**LESB58 ΔRS25615**
Pyocyanin (LB)	100±16.9	17.2±9.2	100±6.3	53.9±10.1	100+9.2	13.58±10.9
Pyocyanin (ASM)	100±10.2	54.7±20.4	100±11.8	52.7±6.6	100±7.9	44.9±22.3
Pyoverdine	100±10.1	141±5.1	100±7.8	53.7±4.5	100±13.5	199±20.3
Protease	100±11.4	110±12.9	100±13.6	89.7±9.1	100±6.7	111.1±14.9
Elastase	100±12.9	94±8.2	100±7.8	103±9.4	100±8.8	92±13.4

Table 3.6 - Table summarising remaining *in vitro* virulence factor production exhibited by PA7 Bo599, PA14 AUS471 and LESB58 PA-W39 strains deleted for PA4130. Orthologues. Figures are expressed as a percentage of relative wild-type strains with standard deviation however, statistical analysis were performed on raw data. All results are collated from 2 independent experiments with at least 3 biological replicates.

3.3.3.4 Impact of PA4130 orthologue deletion on motility

In line with the negative impact on swarming of a PA4130 mutation in PAO1-L, the mutation of this gene in the clinical isolates resulted in similar results (Figure 3.12 I and III). In contrast, whilst the PAO1-L mutant had no impairment on swimming or twitching motility, deletion of PA4130 in PA7, PA14 and LESB58 resulted in attenuated motility, although the pattern was not consistent in all strains. Swimming motility was unaffected in PA4130 mutants in PA7 and PA14, whilst the one in LESB58 showed a 2-fold reduction in surface coverage (Figure 3.12 I-II). Interestingly, twitching motility exhibited the inverse phenotype to swimming in these mutants, with a 28 and 48% reduction in the ones in PA7 and PA14, whilst twitching was unaffected in the LESB58 mutant (Figure 3.12 I-IV).

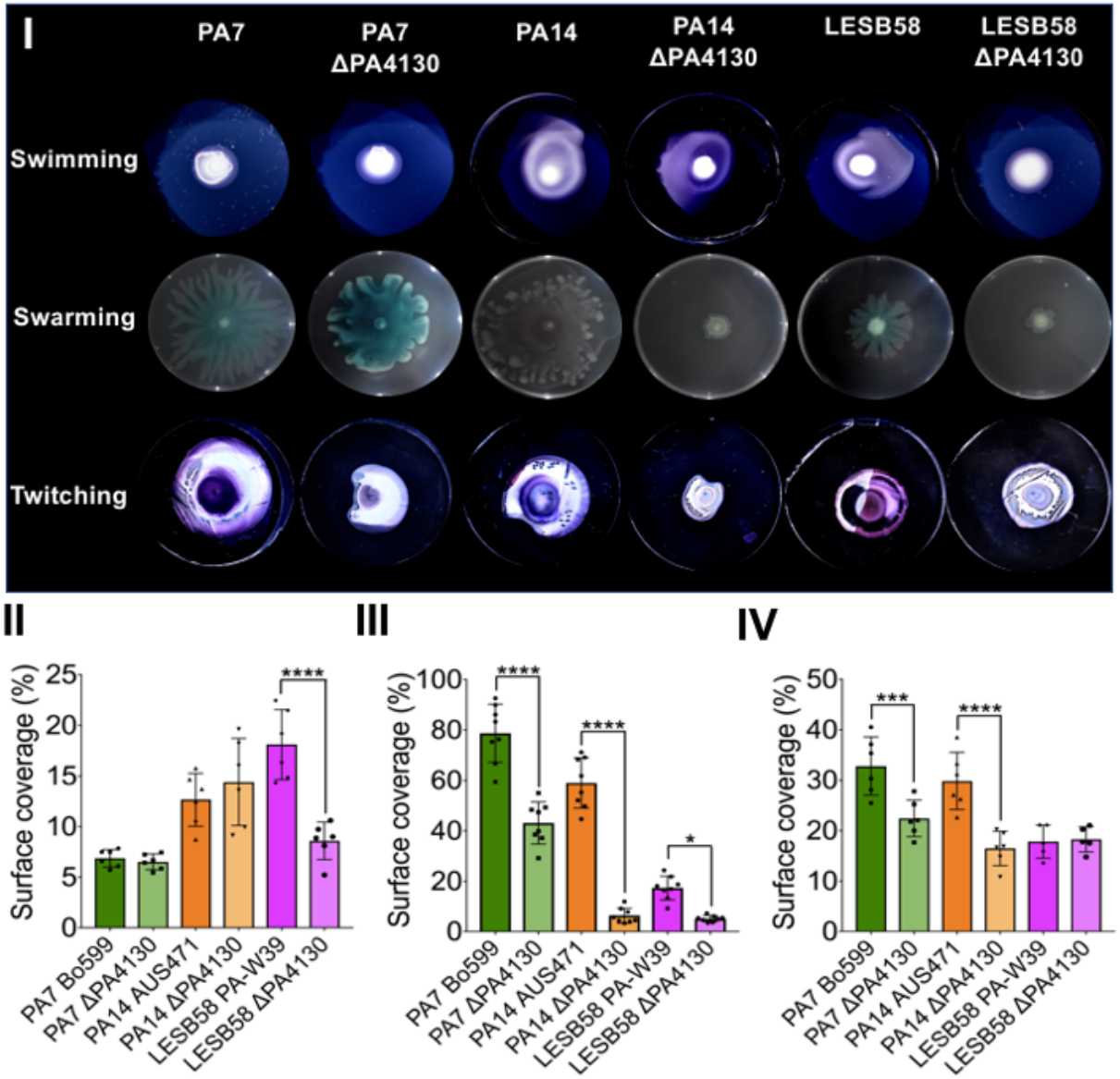

Figure 3.12 – Specialised motility of *P. aeruginosa* clinical strains compared to PA4130 orthologue mutants. (**I**) Representative swimming, swarming and twitching motility images. (**II**) Swimming, (**III**) swarming and (**IV**) twitching motility measurements calculated as percent surface coverage. Data collated from 2 independent experiments with 3-5 biological replicates. Data analysed by comparing PA4130 mutants to its respective wild-type strain. **P <0.0021, ***P <0.0021, ****P <0.0001, One-way ANOVA, Sidak's multiple comparisons test.

3.3.3.5 The effect of nitrate on PA4130 mutant viability is conserved

Deletion of PA4130 in PAO1-L resulted in a nitrate-dependent reduction in optical density upon entry into stationary phase. These assays were repeated for the PA4130 orthologue mutants, with the impact on growth assessed in LB and M-ASM under aerobic and micro-aerobic conditions. As observed previously, no significant effect can be seen aerobically in any of the mutants in LB and M-ASM. Under micro-aerobic conditions, the same OD reduction can be observed in stationary phase for the PA7 Bo599 and PA14 AUS471 PA4130 orthologue mutants when compared to their respective wild-type strains (Figure 3.13). When subjected to growth in M-ASM devoid of nitrate, no loss in OD during stationary phase is observed for all PA4130 orthologue mutants (Figure 3.14). This same pattern was not observed in the LESB58 PA-W39, with a PA4130 orthologue demonstrating wild-type growth (Figure 3.13 and 3.14). Whilst LESB58 did not appear to show a nitrate-responsive phenotype, the similar phenotypes exhibited by PA4130 orthologue mutants in PAO1-L, PA7 and PA14 provide strong evidence that PA4130 participates in the nitrate reduction pathway. This conserved function demonstrates that the role of PA4130 is phylogenetically conserved.

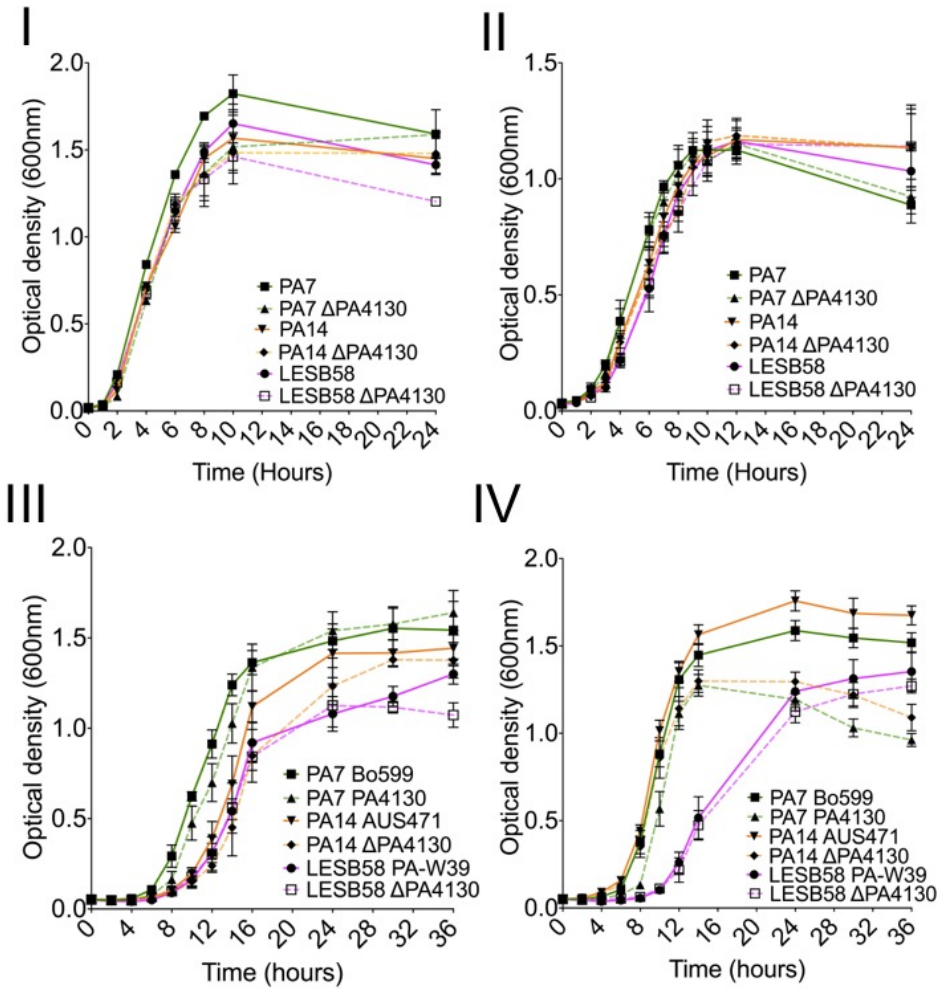

Figure 3.13 - Growth kinetics of PA4130 orthologue mutants compared to wild-type clinical strains in LB and M-ASM under aerobic or micro-aerobic (5% O_2) conditions. I) Aerobic in LB; **II)** Aerobic in M-ASM; **III)** Micro-aerobic in LB; and **IV)** Micro-aerobic in M-ASM. Assays repeated twice to ensure same pattern was obtained. Data presented represents only one of these assays due to the variable nature of M-ASM

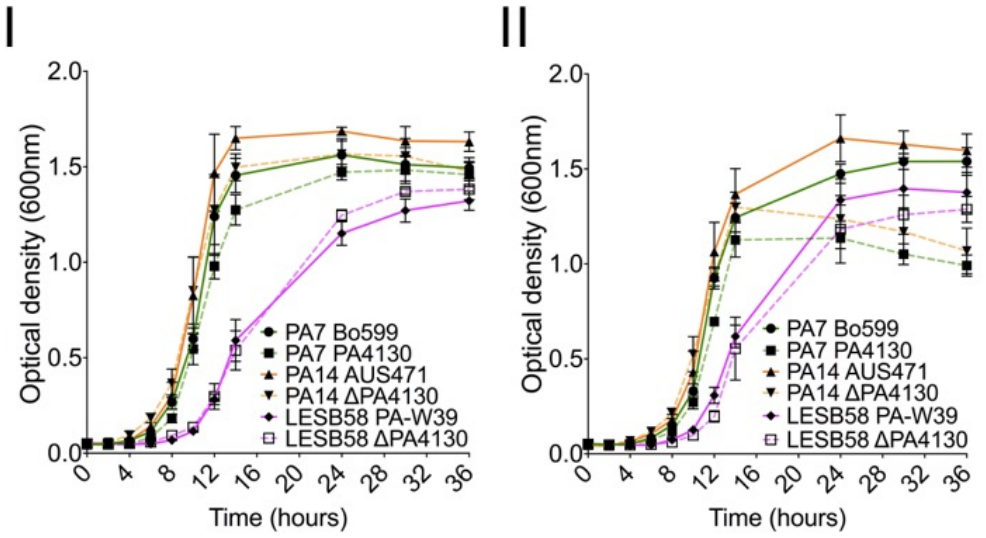

Figure 3.14 – Growth kinetics of PA4130 orthologue mutants in M-ASM with and without supplemented nitrate and sulphate under micro-aerobic conditions. (**I**) M-ASM without nitrate, (**II**) M-ASM without sulphate. Assays repeated twice to ensure same pattern was obtained. Data presented represents only one of these assays due to the variable nature of M-ASM.

3.3.3.6 Attachment and biofilm formation

3.3.3.6.1 Abiotic surface attachment

It was observed that deletion of PA4130 in PAO1-L resulted in increased attachment under oxygen limiting conditions. This phenotype was enhanced in the presence of nitrate, with addition to aerobic cultures also resulting in increased abiotic attachment. To determine if this is a conserved trait, the PA4130 orthologue mutants in PA7, PA14 and LESB58 were subjected to the same assays.

Under both aerobic and micro-aerobic conditions, no effect is seen on attachment in LB and MOPS-succinate-NH_4Cl (Figure 3.15). This differs to strains PAJD21 and PAJD25, where a moderate increase in attachment was observed under these conditions (Figure 3.9). Upon addition of nitrite and nitrate, attachment is observed in all PA4130 orthologue mutants in both LB and MOPS-succinate-minimal media (Fig 3.15). This phenotype is again enhanced under micro-aerobic conditions in the clinical strains (Figure 3.15). The increased attachment of all PA4130 mutant strains in response to nitrate

and nitrite indicates the function of PA4130 upon this phenotype is conserved amongst phylogenetically distinct strains.

3.3.3.6.2 Nitrate-dependent increased abiotic attachment does not occur at physiologically relevant concentrations of nitrate.

The conserved increase in abiotic attachment of PA4130 mutants in response to nitrate addition could be problematic for future therapeutic development. *P. aeruginosa* can colonise medical devices such as catheters and implants forming extensive biofilms. This increased abiotic attachment may indicate that inhibition of PA4130 would render *P. aeruginosa* more adept at colonising medical device surfaces impairing the use of any future inhibitor.

In the previous experimental design, 10mM of KNO_3 was supplemented into the relevant media. Whilst this was effective for inferring the biological function of PA4130, it does not reflect *in vivo* concentrations of NO_3^-. Therefore, all PA4130 mutants and their respective wild-type strains were subjected to the previously used abiotic attachment assay but this time only 500μM of KNO_3 was added. This is in line with concentrations found in the CF lung as determined by Palmer *et al* (209). Supplementation with 1mM KNO_3 under aerobic and micro-aerobic conditions did not significantly affect abiotic attachment of the PA4130 orthologue mutant strains (Figure 3.16). The same oxygen-dependent enhancement under micro-aerobic conditions was seen for PAJD25, but oxygenation had no effect on attachment for PA7, PA14 and LESB58 PA4130 mutants (Figure 3.16). The lack of nitrate dependent phenotypes observed at these lower concentrations indicates that physiologically relevant concentrations of nitrate do not affect PA4130 mutant attachment. As a result, inhibition of this potential target may still be effective for the treatment of patients with *P. aeruginosa* infections of medical devices.

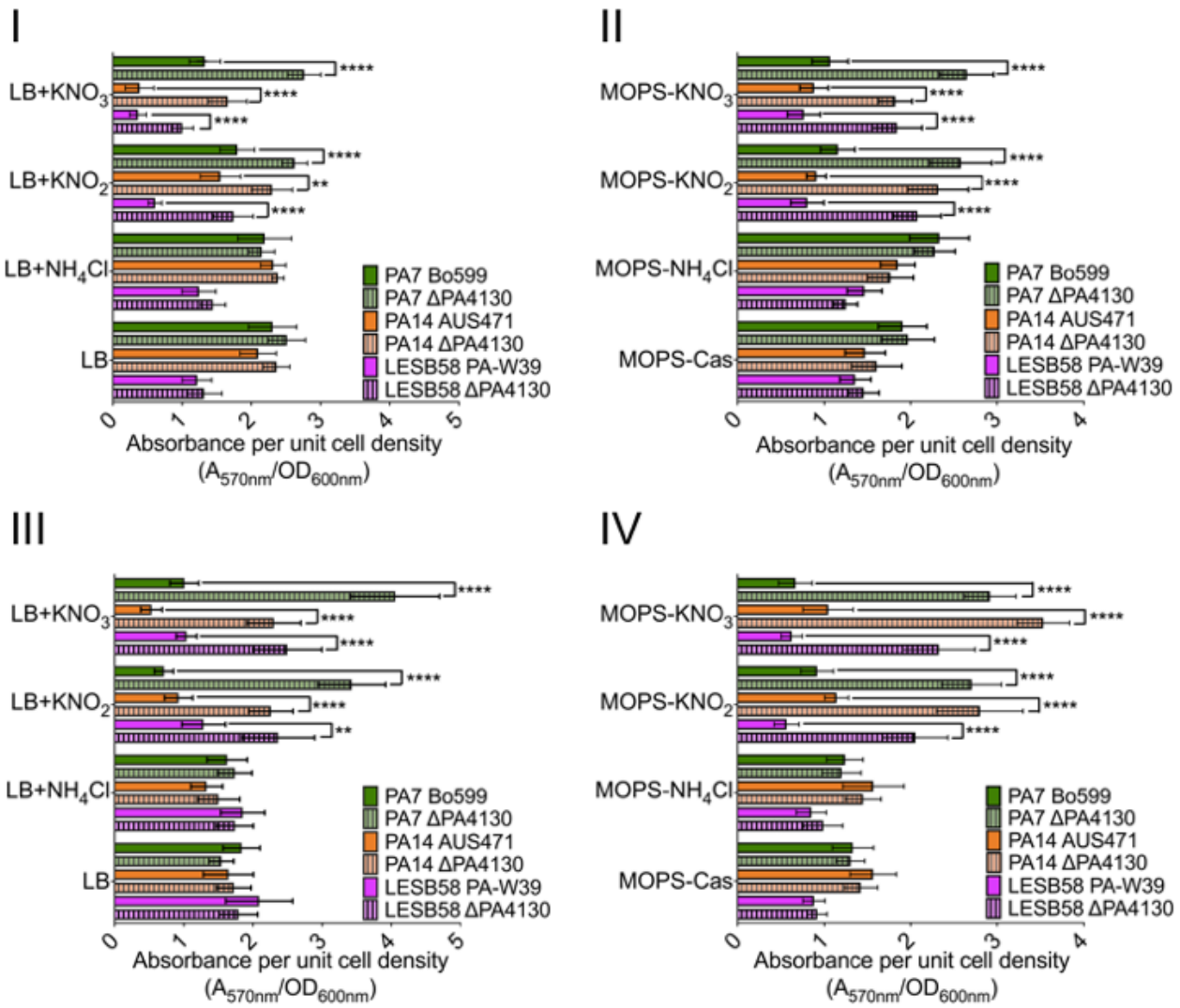

Figure 3.15 - Assessment of bacterial attachment to 48-well polypropylene plates in LB and MOPS-succinate minimal media supplemented with 10mM NH_4Cl, KNO_2, KNO_3. (**I)** LB with additional nitrogen sources under aerobic conditions. (**II)** MOPS-succinate minimal media with single nitrogen sources under aerobic conditions. (**III)** LB with additional nitrogen sources under micro-aerobic conditions. (**IV)** MOPS-succinate minimal media with single nitrogen sources under micro-aerobic conditions. Data collated from 2 independent experiments with 4-5 replicates and compared to isogenic wild-type strain. **P <0.0021, ****P <0.0001, Holm-Sidak t-test.

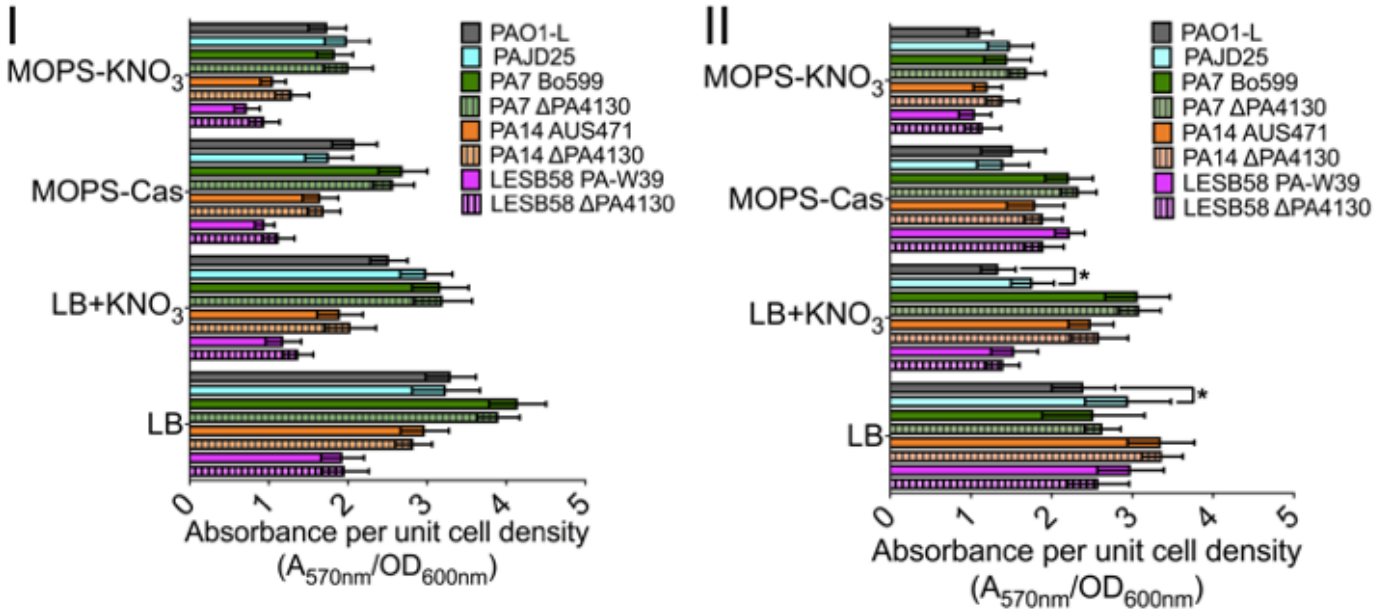

Figure 3.16 - Assessment of the attachment of PA4130 orthologue mutants in 48-well polypropylene plates in LB and MOPS-succinate minimal media supplemented with and without 1Mm KNO_3. (**I**) Aerobic attachment, (**II**) micro-aerobic attachment. Data collated from 2 independent experiments with at least 6 replicates. PA4130 deleted strains were compared to the relevant isogenic wild-type strain. *P <0.05, Holm-Sidak t-test.

3.3.3.6.3 Impact of nitrate on biofilm formation in PA4130 orthologue mutants

Further effects of nitrate were seen in the colony biofilm model with deletion mutants of PA4130 orthologues in PA7, PA14 and LESB58, in agreement with the results obtained for PAO1-L. In this instance, the effect was only screened micro-aerobically as this is when the phenotype was most pronounced in PAO1-L. No effect was seen at 0 or 0.1mM nitrate for any of the strains tested. At 1mM nitrate the PA7 and PA14 PA4130 orthologue mutants showed ~1-log CFU reductions whilst LESB58 was unaffected (Figure 3.17). However, all PA4130 orthologue mutants revealed drastically reduced CFUs at 10mM nitrate (1.5 to 2-log) in comparison to the wild-type strains (Figure 3.17).

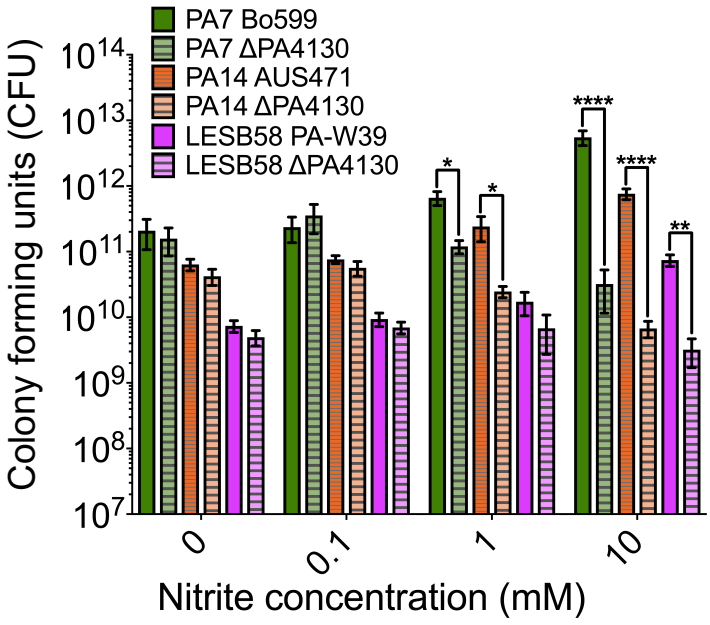

Figure 3.17 – CFU recovery of clinical *P. aeruginosa* strains with PA4130 orthologue mutations compared to their wild-types using a micro-aerobic colony biofilm model. Data collated from 3 independent experiments with 3 replicates. *P <0.05, **P <0.0021 and ****P <0.0001, Bonferroni's multiple comparisons test.

3.3.4 PA4130 contributes to virulence in phylogenetically diverse in vivo *models.*

Following *in vitro* virulence factor production assessment, a cascade of diverse *in vivo* and tissue culture models were used to study the impact of the PAO1-L PA4130 isogenic mutant (PAJD25) in virulence factor production (Figure 3.1).

3.3.4.1 Disclaimer

A large amount of the work presented is section **3.3.5** was performed in collaboration with the groups of Professor Alessandra Bragonzi (San Raffaelle Scientific Institute), Professor Leo Eberl (University of Zürich) and the late Professor Gerd Döring (University of Tübingen) as part of the NABATIVI project prior to the start of this PhD. Where appropriate, the correct lab and members who performed the experiments will be acknowledged in the figure legends. This is to ensure no information is overlooked in the development of the story surrounding PA4130. I wholeheartedly thank all those members involved, without whom, a project of this scope with multiple virulence models could not be completed. This work has recently been published in mBio PMID: 33879591.

3.3.4.2 Invertebrate infection models

The first set of *in vivo* models used to screen PAJD21 virulence were the nematode *C. elegans* and the fruit fly *D. melanogaster*. These models have been favoured as they are inexpensive in comparison to animal models and enable high-throughput assessment of mutant impact on virulence. Both of these models have been used extensively to understand *P. aeruginosa*, both in high-throughput screening and as validation for understanding gene function (169, 182, 187, 197, 201).

Using the *D. melanogaster* disease model, it was found that PAJD21 shows a reduction in virulence, with 30% less killing at 18H when compared to wild-type PAO1-L (Table 3.1). Assessment of PAJD25 virulence in *D. melanogaster* displayed a similar result, with 42% decreased killing compared to PAO1-L at

18H. However, by 22H complete killing of *D. melanogaster* was exhibited by both PAO1-L and PAJD25 (Figure 3.18 I). This information was missed in the initial assessment of the Tn5 mutant as a single time-point was selected to allow screening of multiple virulence targets simultaneously during the NABATIVI screen (149). Despite this, a temporal delay in virulence still confirmed that PA4130 plays a role in pathogenicity in the *D. melanogaster* disease model, validating the results previously obtained with PAJD21.

In the initial Tn5 transposon mutant screen, it was found that infection with PAJD21 decreased killing in *C. elegans* by 50% when compared to PAO1-L at 48H (Table 3.1). Similar results were obtained when *C. elegans* was challenged by PAJD25 and PAO1-L, with a 30%, 39% and 55% increase in PAJD25 survival at 24, 48 and 72H respectively (Figure 3.18 II). This clearly demonstrates that PA4130 plays a key role in disease of *C. elegans*, confirming the results obtained for PAJD21 are specific to this gene. Unlike in *D. melanogaster*, this attenuation does not appear to be delayed in *C. elegans* as the majority of nematodes survive past 72H (Figure 3.18 II). This highlights the differences in virulence requirement between these invertebrate models, backing the observations by Dubern and colleagues (149) that *P. aeruginosa* virulence factor requirement varies between disease models.

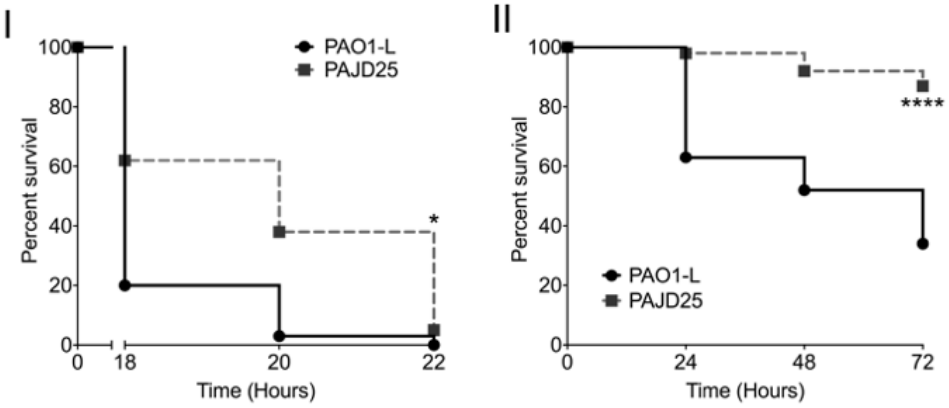

Figure 3.18 – Survival curves of (I) *D. melanogaster* and (II) *C. elegans* comparing infection of PAJD25 (PA4130) to the isogenic wild-type strain PAO1-L. The results presented display the mean values from three independent experiments. *P <0.032, ****P <0.0001 Log rank Mantel-Cox test. Experiments performed by Mario Juhas and Stephan Schwager in the lab of Professor Eberl.

3.3.4.3 A549 epithelial tissue culture assays

To understand the impact of the PA4130 mutation on eukaryotic cells, A549 epithelial cell tissue culture assays were used to assess cytotoxicity, IL-8 production and *P. aeruginosa* invasion of this mutant. PAJD21 showed reduced cytotoxicity and IL-8 production during the initial transposon screen, whilst invasion appeared to be unaffected. These hallmarks of *P. aeruginosa* infection were reassessed using PAJD25 and the wild-type strain PAO1-L. This confirmed the results previously seen in the transposon screen with cytotoxicity and IL-8 production drastically reduced in comparison to PAO1-L (Figure 3.19 I-II). However, the results obtained for PAJD21 and PAJD25 differ in A549 epithelial cell invation, with PAJD25 exhibiting a reduction using a polymyxin B exclusion assay (Figure 3.19 III). The reason for this difference is unclear with PAJD21 and PAJD25 exhibiting complete phenotypic overlap until this point. Regardless, these results confirm that interruption of PA4130 strongly attenuated the capacity of *P. aeruginosa* to kill, invade and trigger an immune response in eukaryotic cell lines.

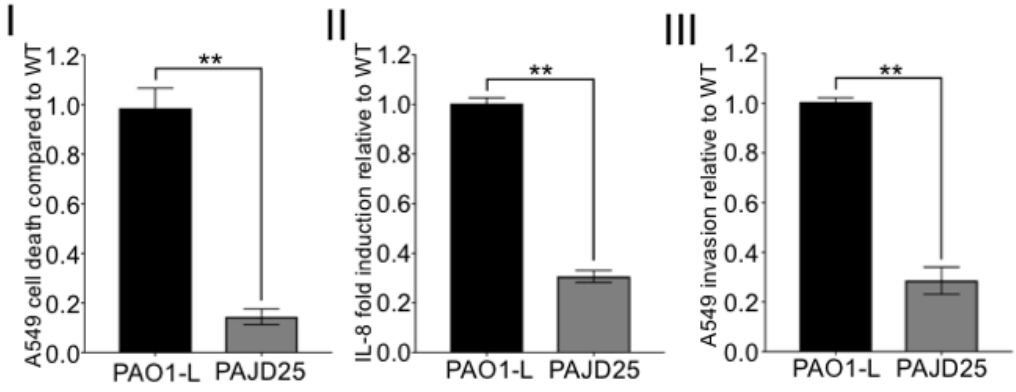

Figure 3.19 - Cytotoxicity, IL-8 release and invasion of A549 cells following infection with either PAO1-L or PAJD25. (**I**) Cytotoxicity assayed with Syto13/PI viability staining. (**II**) IL-8 released quantified by ELISA following infection. (**III**) Invasion quantified using an antibiotic (polymyxin B) exclusion assay. Data, from three independent experiments, expressed as mean (+/-) standard error of mean (SEM). **P <0.01, Student's t-test. Experiments performed in the labs of Professor Döring and Professor Bragonzi.

3.3.4.4 Murine infection models

The PAJD25 mutant strain was subjected to an acute murine lung infection model, to determine if the previously observed virulence attenuation translates into mammals. At 36H, a survival rate of 90% was exhibited by PAJD25 challenged mice, whilst no PAO1-L infected mice survive (Figure 3.20). The drastic reduction in mortality for PAJD25 confirms the important role PA4130 plays during acute murine lung infection. Attempts to understand the impact of PA4130 on chronic infection failed. Use of a murine agar-bead lung infection model displayed characteristics more consistent with acute infection with all PAO1-L infected mice lost inside 36H (Figure 3.21). This inability to establish a chronic infection is hypothesized to be due to the genetic background of the wild-type strain selected for transposon screen. PAO1-L is one of the most virulent PAO1 strains, essentially killing the mice during the acute infection phase before chronic infection can be establish. Despite this failure, the data generated from the agar-bead infection model served as a secondary acute murine lung infection model. This confirmed the results seen with the original acute murine lung infection model with PAJD25 demonstrating an 80% increase in survival when compared to PAO1-L infected mice at 36H (Figure 3.21 I). *P. aeruginosa* recovery from infected mice organs confirms this reduction in virulence with a 3-log decrease in colony forming units (CFUs) obtained from site of infection in the lung. Screening of the liver and spleen demonstrated that PAJD25 lacks the ability to spread systemically in mice, with all but 1 spleen sample clear of the mutant strain (Figure 3.21 II-IV).

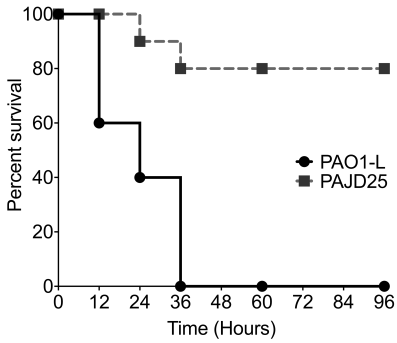

Figure 3.20 – Survival curve of C57BL/6NCrlBR mice infected with PAO1-L and PAJD25 in an acute lung infection model. At 36 hours PAJD25 exhibits a 90% increase in survival when compared to PAO1-L, with 80% of PAJD25 infected mice surviving past 96 hours. ****P<0.0001, Log rank Mantel-Cox test. Experiments performed by Dr. Cigana and Dr. De Simone in the lab of Professor Bragonzi.

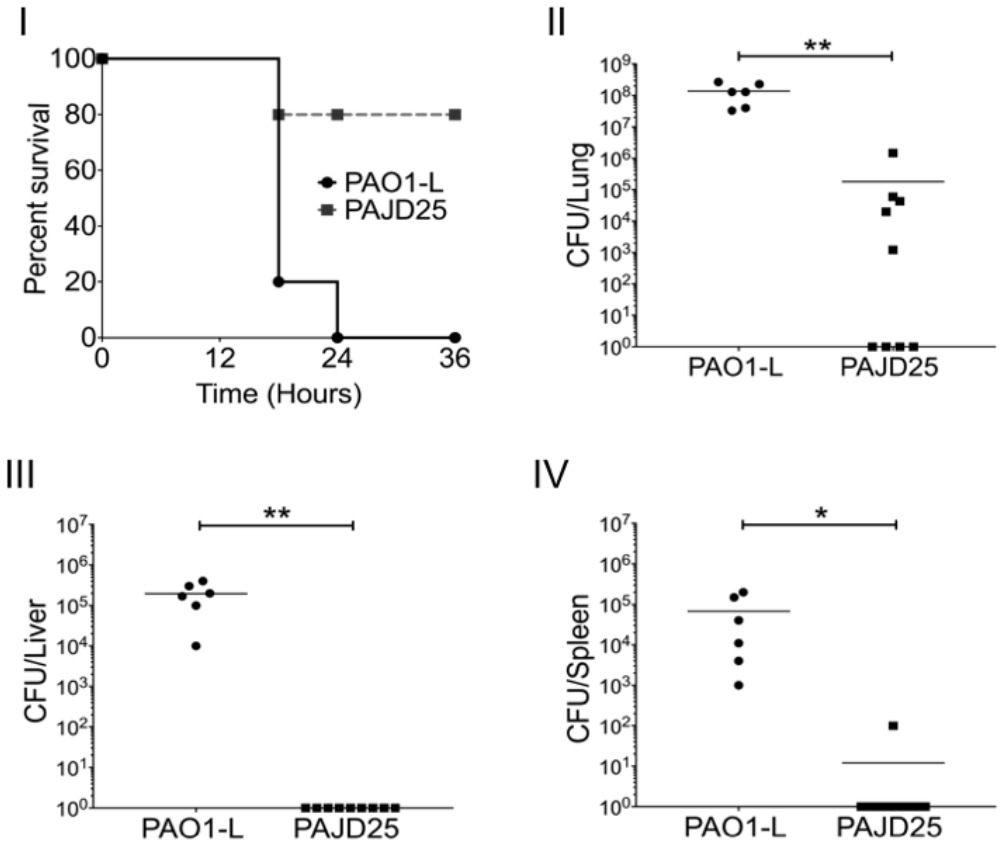

Figure 3.21 – Virulence of PAO1-L and PAJD25 in an agar bead murine lung infection model of colonisation in C57BL/6NCrlBR mice. (**I**) Survival curve, (**II**) CFU recovery from lung, (**III**) CFU recovery from the liver and (**IV**) CFU recovery from the spleen at 36h post infection. PAJD25 exhibits a significant increase in survival at 36h post inoculation with a CFU recovery 3-log lower than PAO1-L in the lungs. PAO1-L infection progresses to the liver and spleen within 36h whilst PAJD25 infection does not proceed to the liver and spleen as indicated by the absence of CFU recovery in all but one sample. ****P <0.0001 Log rank Mantel-Cox test for survival curve. *P <0.05, **P < 0.01 Student's t-test for CFU recovery. Experiments performed in the lab of Professor Döring.

3.4 Conclusions

The work presented in this chapter supports the observations of the previously conducted NABATIVI screen, with PA4130 demonstrated to play a key role in multiple *in vitro* and *in vivo* virulence models. Caveats to the whole genome screening methodology are also addressed, with PA4130-dependent virulence factor production restored through complementation, and the conserved role of PA4130 orthologues revealed through use of multiple clinical strains representing the phylogenetic structure of *P. aeruginosa*. The exact mechanism of this virulence attenuation is unknown. However, amino acid sequence analysis and the nitrate responsive nature of PA4130 mutants suggests it likely acts as a nitrite reductase in the nitrate reduction pathway. Given the pleiotropic impact of mutation, PA4130 was further investigated with a view to developing this hypothetical protein as a novel anti-virulence target.

Chapter 4

Overexpression and purification of PA4130

4.1 Introduction

One of the main bottlenecks in development of anti-virulence drugs is the functional and structural characterisation of potential targets (180). In structure-based drug design four main methods are used: X-ray crystallography, nuclear magnetic resonance (NMR), cryo-electron microscopy or homology modelling. In the case of X-ray crystallography, NMR and cryo-electron microscopy target purification is required, usually performed in a heterologous host such as *E. coli*. This can be extremely time consuming and is difficult to adapt for high throughput screening, accounting for the imbalance between the number of virulence targets identified versus characterised. Homology modelling utilises previously characterised homologous proteins as a template to model the 3D structure of a given target. However, significant amino acid sequence homology is required for this method to work reliably (216). With many of the virulence genes identified in *P. aeruginosa* encoding for hypothetical proteins of unknown function, homology models are not likely to be available making experimental structural determination essential.

In the case of PA4130, structural characterisation methods are limited. Generally, NMR is limited to small proteins <30kDa (217) whilst Cryo-EM struggles at <100kDa . Whilst recent advances in Cryo-EM have allowed structural determination of proteins below 100kDa to be achieved, these are often at much lower resolutions than those obtained with NMR or X-ray crystallography (218). With PA4130 predicted to be 62.2kDa, the analytical options lie between the conventional limits of NMR and Cryo-EM, leaving X-ray crystallography as the only viable physical method of PA4130 structural determination. Nitrite or sulphite reductases similar to PA4130 have been structurally determined in the past, potentially acting as a homology model. This is advantageous for structural prediction using both X-ray crystallography and *in silico* structural modelling. However, the low amino acid homology exhibited by these homologues may limit application of purely *in silico* methods (2).

Based on these observations, X-ray crystallography was chosen as the best approach to solve the structure of PA4130 to use as a basis for inhibitor screening. Crystallography can often require screening of thousands of

potential conditions using high concentrations of homogenous protein or enzyme and hence the purification of vast amounts of protein. Therefore key to the success of crystallisation and downstream functional characterisation is purification of both homogenous and high-yielding PA4130.

4.2 Aims of this chapter

The work presented in this chapter explores the overexpression and purification of the potential anti-virulence target PA4130. Optimisation of PA4130 purification, whilst laborious in the short-term, is beneficial long-term with production of homogenous PA4130 required for:

1. Functional characterisation
2. Structural determination
3. Inhibitor screening and identification

This is an essential step in understanding the role PA4130 plays during virulence and the impact inhibition would have using an anti-virulence strategy.

4.3 Results

4.3.1 Purification of PA4130 – method development

Bacterial protein overexpression experiments are usually performed in a well characterised heterologous host. If a target protein is overproduced in the native host, endogenous proteases can breakdown the excessively produced protein to protect the cell. *E. coli BL21* (DE3) derived strains are commonly used to overcome this problem as both Lon and OmpT proteases are genetically inactivated (154). The integration of the lysogen λDE3, encoding T7 RNA polymerase, also enables the utilisation of protein expression systems relying on the T7 promoter (154). *E. coli BL21* (DE3) and derived strains were used in expression of PA4130 to take advantage of the limited protease activity and the extensive range of T7 promoter based protein overexpression vectors available.

Heterologous gene expression can be troublesome due to differences in codon usages between the target encoding DNA and expression host. This causes ribosomal stalling when a codon specific tRNA is limiting in the overexpression host, preventing efficient translation of the target protein (219). Ideally target DNA should have similar codon usage, with codon optimisation or genetic addition of tRNAs with rare codons commonly used to overcome any differences in codon usage (220). To ensure *E. coli* BL21 (DE3) is a suitable overexpression host, the PA4130 nucleotide sequence was screened for rare codons with the graphical codon usage analyser developed by Fuhrmann and colleagues (178). This revealed that PA4130 expression to have an average relative codon adaptiveness of 74 when compared to *E. coli* codon usage. Relative codon adaptiveness is the ratio of codon usage compared to the most abundant codon used by an organism for each amino acid. Therefor a relative adaptiveness of 0.74:1 represents a good match between PA4130 and *E. coli* codon usage. It was found that 14 PA4130 codons were deemed to be rare with a relative adaptiveness of below 0.2 (Figure 4.1 and Table 4.1). Of the rare codons identified, 13 out of 14 encode CGG for arginine (Table 4.1). Arginine codon usage is a common problem for heterologous *E. coli* expression (221). This can be resolved by increasing the copy number or rare codon tRNA's through supplementation with an additional vector such as pRare vector series used to create *E. coli* ROSETTA strains (220). With the high codon usage match between *E. coli* and *P. aeruginosa*, we proceeded ahead with expression using the native PA4130 DNA sequence.

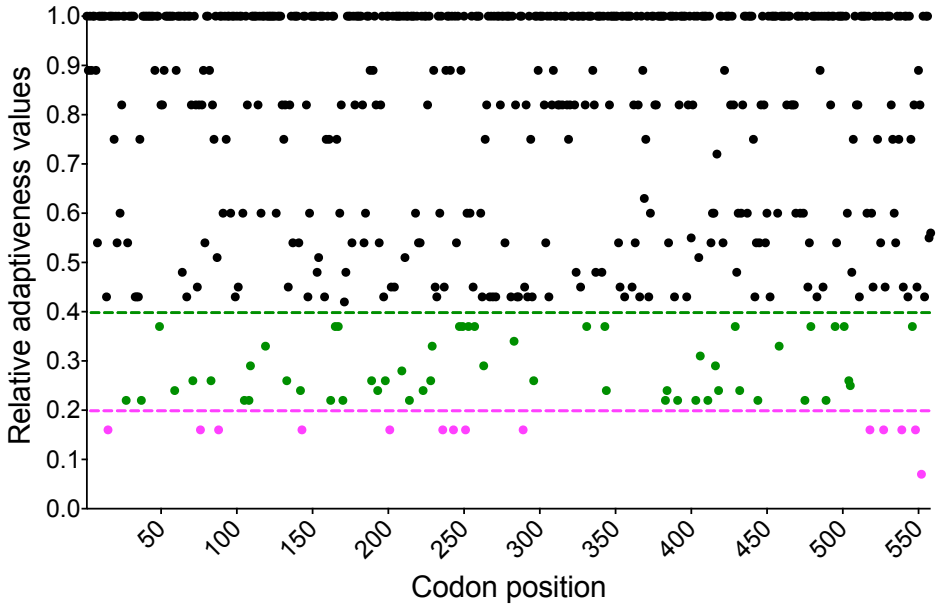

Figure 4.1 – **Relative codon adaptiveness values for PA4130 per amino acid position.** Points at <0.2 are considered rare, <0.4 less common and >0.4 common.

Table 4.1 – **Position and identity of rare codons found in PA4130 when compared to the tRNA usage of *E. coli* BL21 (DE3).** Rare codons found in PA4130 are primarily alanine, a common problem with expression of heterologous proteins in *E. coli*.

Codon position	Sequence	Codon adaptiveness value	Amino acid
15	CGG	0.16	Arginine
27	CTC	0.19	Leucine
76	CGG	0.16	Arginine
88	CGG	0.16	Arginine
143	CGG	0.16	Arginine
201	CGG	0.16	Arginine
236	CGG	0.16	Arginine
243	CGG	0.16	Arginine
251	CGG	0.16	Arginine
518	CGG	0.16	Arginine
527	CGG	0.16	Arginine
539	CGG	0.16	Arginine
548	CGG	0.16	Arginine
552	AGG	0.07	Arginine

4.3.1.1 Overexpression vector selection and synthesis

To increase the likelihood of obtaining soluble PA4130 upon overexpression we used three expression vectors with different properties, pSK67, pColdI and pCold-GST. Vector pSK67 is a standard IPTG inducible vector with T7 dependant promoter expression under control of the *lac* system. Plasmid pColdI is again an IPTG-inducible vector with the same mechanism of control as pSK67. However, a secondary control system has been integrated to enable stable target protein expression at temperatures as low as 10-15^{O}C. This system uses the cold-shock protein A promoter to drive expression, with the 3' and 5' UTR providing target transcript stability at lower temperatures (222). Overexpression vector pCold-GST uses the exact same mechanism as pColdI with T7 and *cspA* promoters controlling expression of the target protein. However, the target protein is fused to a cleavable Glutathione S transferase protein (222). GST is highly soluble and has been shown to enhance solubility of proteins when fused to their N-terminus (223).

For pSK67, PA4130 was amplified with an N-terminal hexa-histidyl tag and SacI restriction site via PCR using primer NTH-30F1, with the reverse primer NTH-30R1 modified with EcoR1. The generated DNA fragment was inserted into pSK67 using the SacI and EcoR1 restriction sites, forming PSJF01 (Figure 4.2 I). In pColdI and pCold-GST, PA4130 was amplified by PCR using the primer pair Co30F1/R1 modified with SacI and EcoR1 restriction sites. The PA4130 fragment was ligated in-frame with the pColdI N-terminal hexa-histidyl tag and GST of pCold-GST using SacI and EcoR1, producing vectors PSJF02 and PSJF03 respectively (Figure 4.2 II-III). The vectors were subsequently transformed into *E. coli* BL21 (DE3) and screened for PA4130 overexpression capacity.

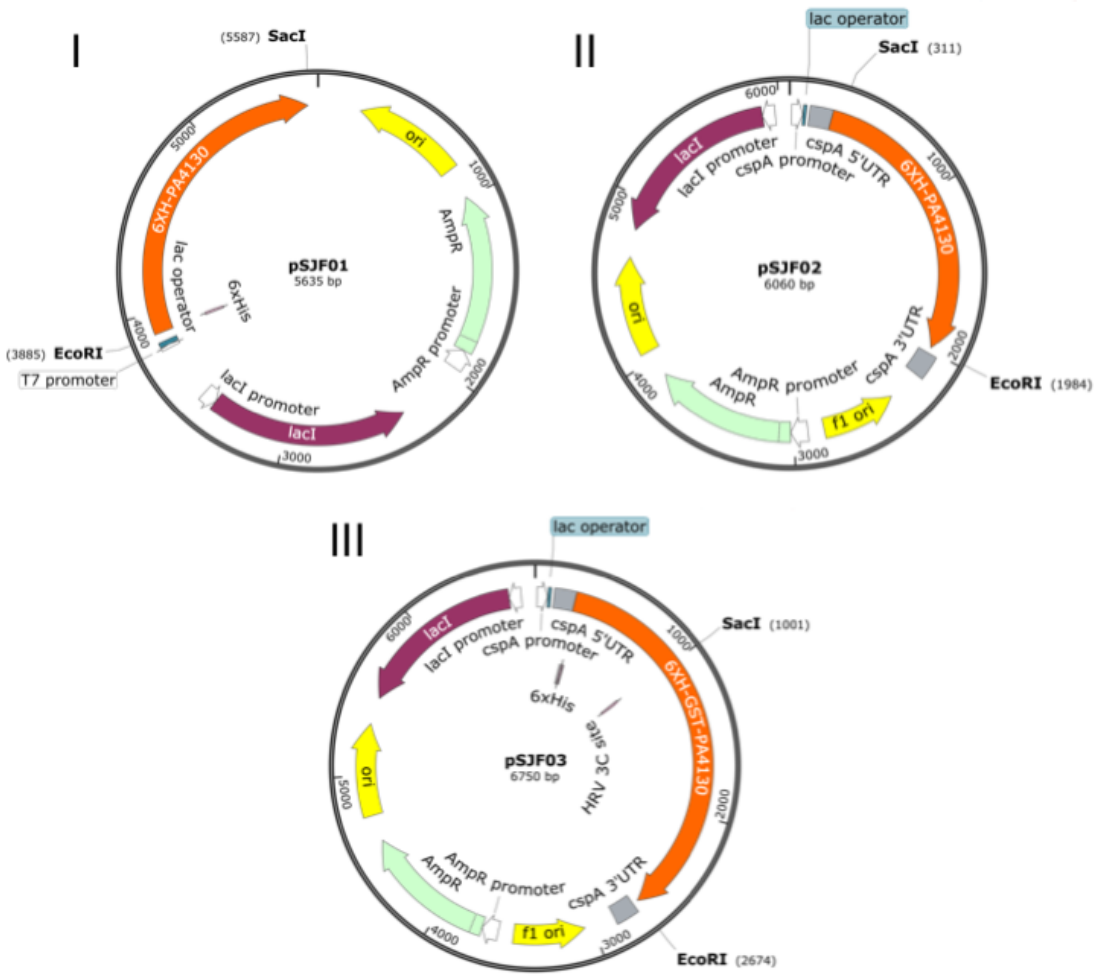

Figure 4.2 – **Diagram of PA4130 overexpression vectors**. (**I**) pSJF01, (**II**) pSJF02 and (**III**) pSJF03.

4.3.1.2 PA4130 induction and solubility trials

To maximise the production of soluble PA4130, an optimisation process of the conditions to use is critical. Multiple factors impact the overproduction of protein from a heterologous host with induction strength, temperature, length, strain and difference in target DNA codon usage all affecting the ability to successfully express and fold the protein. Defining and standardising protein overexpression conditions for a target protein early in the research process streamlines production of PA4130, minimising the required number of repeat purifications and ensuring comparability between different batches.

Vector pSJF01 was assayed at 4 and 18 hours post PA4130 induction across three different temperatures (20^{O}C, 25^{O}C and 30^{O}C) and IPTG concentrations

(0.1mM, 0.3mM and 0.5mM). Induction of PA4130 was clearly observed across all temperature and IPTG conditions, indicated through production of a ~60kDa protein (Figure 4.3). Minimal difference in PA4130 induction can be seen at 20^{O}C and 25^{O}C, irrespective of IPTG concentration. At 30^{O}C higher induction was seen at 4 hours with levels of PA4130 increasing step-wise alongside IPTG concentrations (Figure 4.3). Whilst quick induction of PA4130 is desirable, the key question is whether the enzyme is correctly folded and soluble. High-level heterologous protein overproduction often leads to production of inactive protein as the target is toxic or host-dependant factors are not present in the expression host (219). Solubility was determined through sonic disruption of cells harvested after 18 hours of induction at all temperatures and IPTG inductions previously assayed. This revealed that pSJF01 induction resulted in the production of insoluble PA4130 across all conditions tested (Figure 4.4).

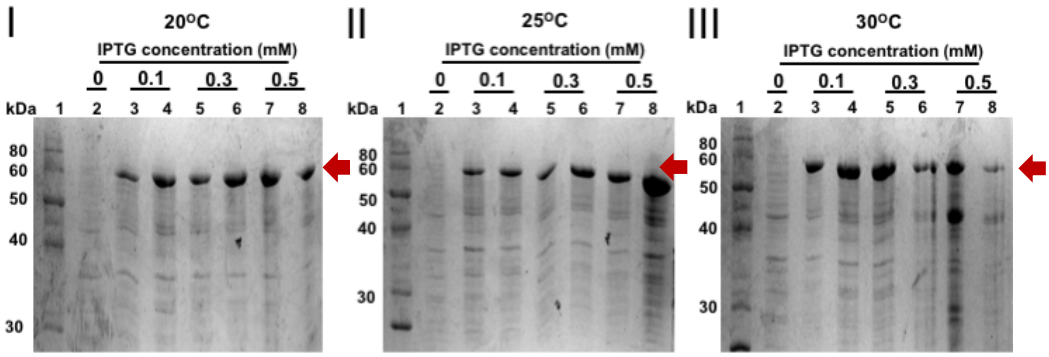

Figure 4.3 – **Whole cell PA4130 induction screening from plasmid pSJF01 using *E. coli* BL21 (DE3) as a host.** Protein overproduction was carried out at 20^{o}C, 25^{o}C and 30^{o}C and the IPTG concentrations used were 0mM (control), 0.1mM, 0.3mM and 0.5 mM as indicated. Lane 1 – broad-range MW ladder; Lanes 3, 5, 7 show 4 H post IPTG induction and Lanes 4, 6, 8 show 18H post IPTG induction. The red arrows indicate the 6His-PA4130.

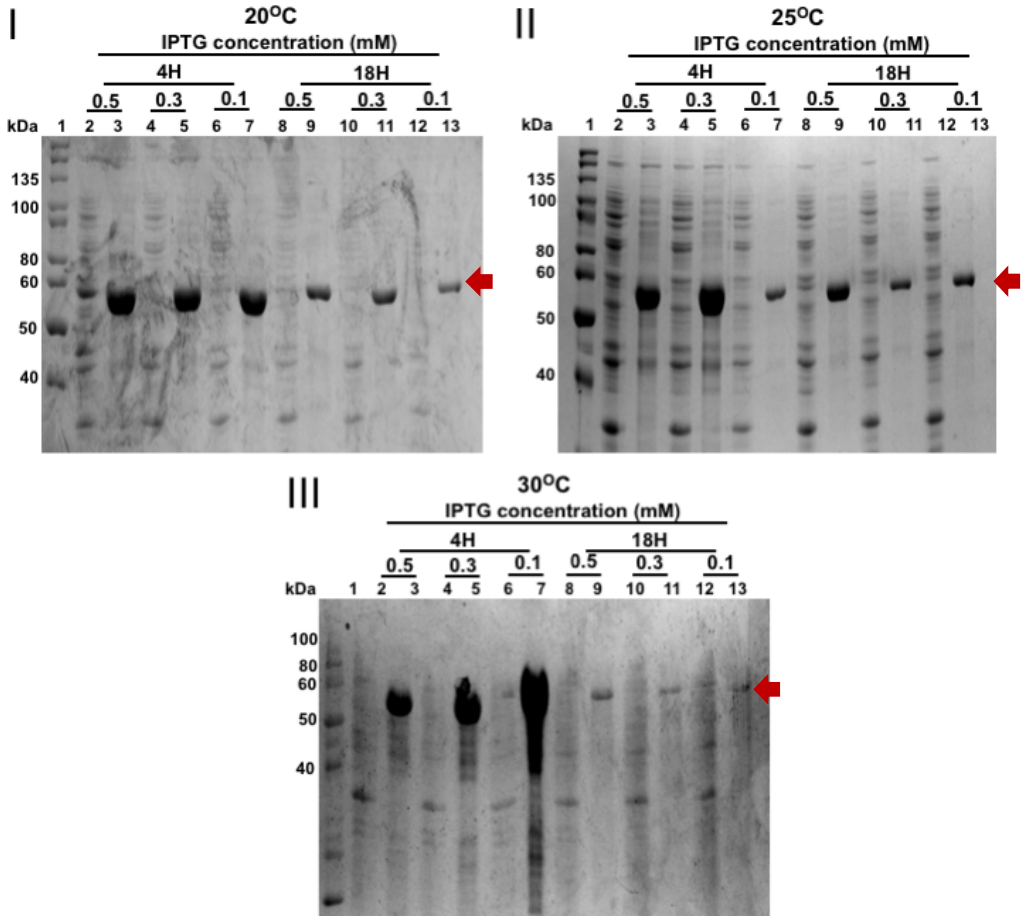

Figure 4.4 – Solubility assessment of PA4130 from plasmid pSJF01 using *E. coli* BL21 (DE3) as an expression host. Protein overproduction was carried out at 20°C, 25°C and 30°C for 4 and 18H at IPTG concentrations used were 0.1mM, 0.3mM and 0.5mM as indicated. Samples were lysed by sonication and pellet solubilised with 8M urea. Lane 1- broad-range molecular weight ladder; Lanes 2, 4, 6, 8, 10 and 12 show soluble fraction post IPTG induction; Lanes 3, 5, 7, 9, 11 and 13 shows insoluble fraction post IPTG induction. Red arrows indicate the 6His-PA4130.

Assessment of PA4130 induction and solubility using pCold-based vectors differs from pSK67 as there is less ability to optimise temperature. Protein expression from pCold vectors operates between 10-15°C under control of P_{cspA}, which inhibits transcription at temperatures higher than this. Optimisation of induction was not performed for these vectors as expression of PA4130 had been demonstrated to be successfully achieved at high-level in *E. coli* with pSJF01 (Figure 4.3). Assessment of solubility revealed the majority of PA4130 to be insoluble, irrespective of IPTG concentration using both pSJF02 and pSJF03 (Figure 4.5).

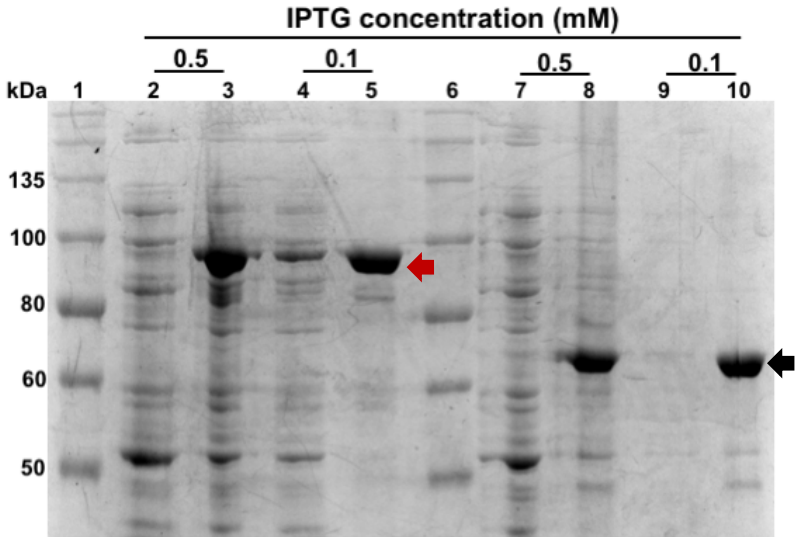

Figure 4.5 – Solubility assessment of PA4130 expressed from pSJF03 and pSJF02 using *E. coli* BL21 (DE3) as an expression host. Protein overproduction was carried out at 15^{O}C for 24H at IPTG concentrations of 0.1 and 0.5mM as indicated. . Samples were lysed by sonication and pellet solubilised with 8M urea. Lane 1- broad-range molecular weight ladder; Lanes 2, 4, 7 and 9 show soluble fractions post IPTG induction; Lanes 3, 5, 8 and 10 show insoluble fractions post IPTG induction. Red arrow indicates 6XH-GST-PA4130 whilst black arrows denotes 6XH-PA4130 produced using pSJF03 and pSJF02 respectively.

4.3.1.3 Identification of PA4130 siroheme and iron-sulphur cluster binding sites

The inability to produce soluble PA4130 was likely due to the heterologous expression in *E. coli* BL21 (DE3). Structurally determined models of PA4130 orthologues demonstrate the presence of 2 prosthetic groups essential for enzyme function. Both nitrite and sulphite reductases of this family require siroheme and an 4Fe-4S iron-sulphur cluster to form an electron transport chain resulting in the reduction of nitrite and sulphite to ammonium and hydrogen sulphide respectively. Amino acid sequence analysis of PA4130, compared to orthologues from both plants and bacteria, uncovered conserved residues indicative of the presence of siroheme and Iron-sulphur cluster binding sites (Figure 4.6). Analysis of structural orthologues revealed that both these prosthetic groups are centrally located in the active site. Siroheme has been demonstrated to interact with multiple residues close to the N and C terminus potentially playing a role in the correct folding of these enzymes. This led us to believe that the insolubility of PA4130 found upon expression from all

vectors may be due to prosthetic group limitation. Previous studies have demonstrated that siroheme-dependant enzymes require an excess of siroheme to retain both solubility and activity (179, 224).

4.3.1.4 Requirement of CysG for soluble PA4130 overproduction

To increase the levels of siroheme, an inducible copy of the siroheme synthase gene *cysG* must be co-express alongside PA4130. CysG is a multifunctional enzyme participating in the Cobalamin (vitamin B12) and siroheme synthase pathways (225). For the synthesis of siroheme, CysG is the only enzyme required, converting uroporphyrinogen-III to siroheme (225). The *cysG* gene was cloned from *E. coli* BL21 (DE3) and inserted into pCDF-DUET1 forming pSJF04. This vector was selected as the origin of replication is compatible with that of pSK67, pCold1 and pCold-GST. The pSJF04 plasmid was transformed into *E. coli* BL21 (DE3) with initial solubility trials revealing high-level overproduction of CysG at 0.1, 0.3 and 0.5mM IPTG (Figure 4.7).

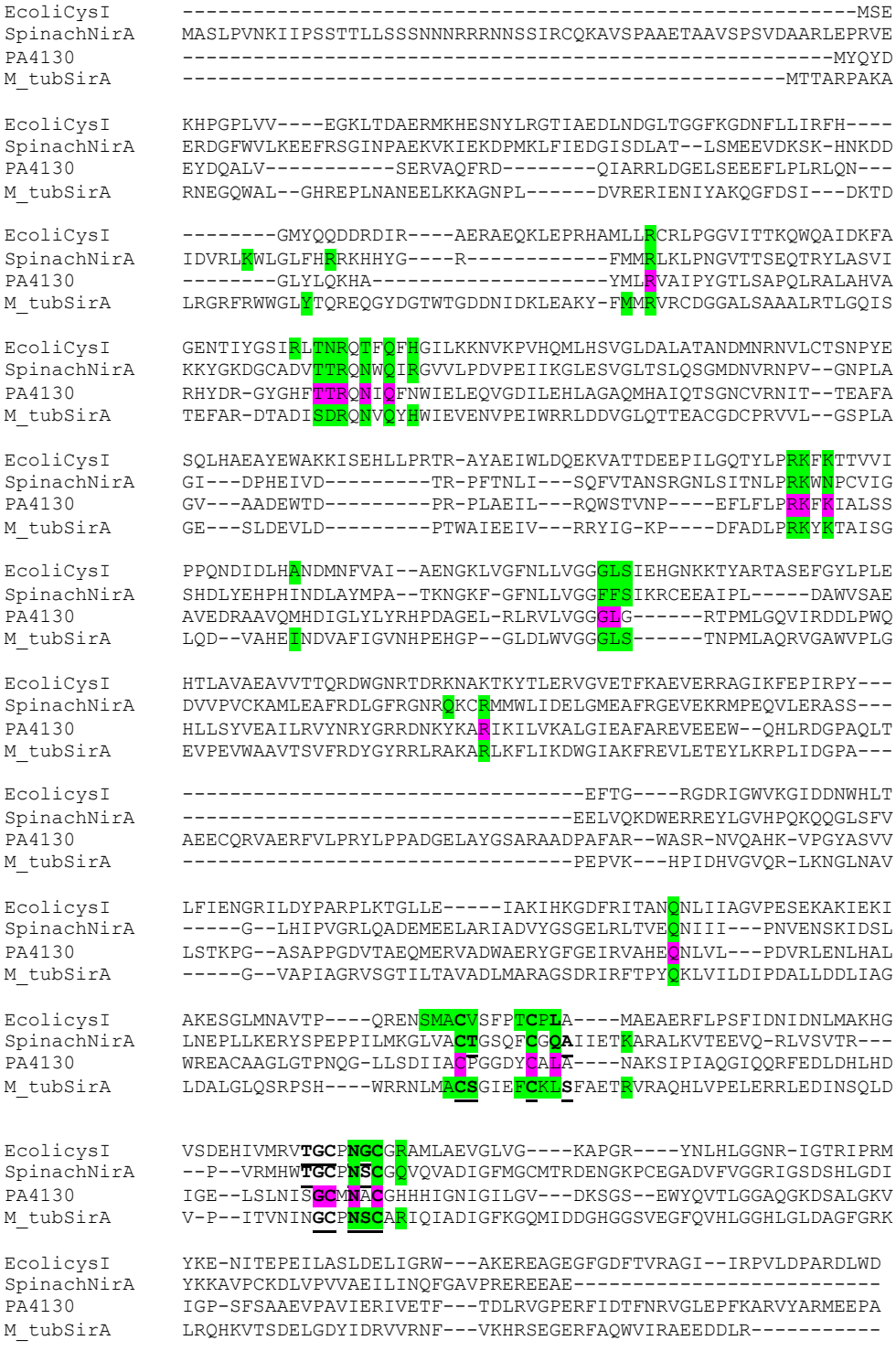

Figure 4.6 - Amino Acid alignment performed with ClustalW comparing PA4130 with homologous proteins CysI (*E. coli*), NirA (Spinach) and SirA (*M. tuberculosis*). Highlighted in green are Siroheme interacting residues observed in the crystal structures of CysI, NirA and SirA with conserved residues of PA4130 highlighted in pink. Conservation of these residues along with four essential cysteine residues required for iron-sulphur cluster insertion suggests that PA4130 requires Siroheme and 4Fe-4S for its functional activity.

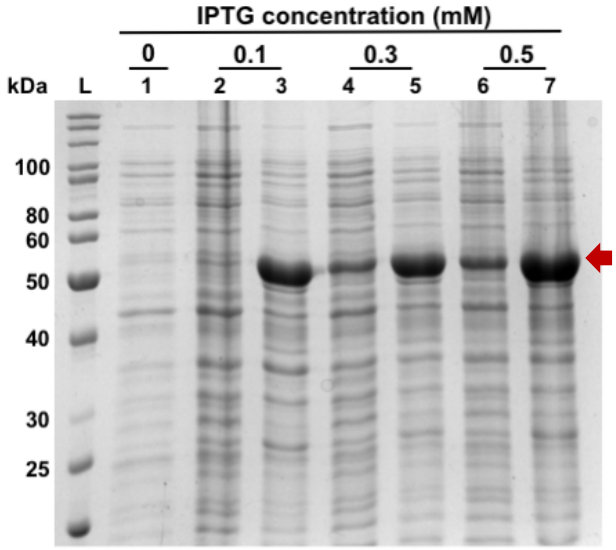

Figure 4.7 – Whole cell induction from plasmid pSJF04 using *E. coli* BL21 (DE3) as an expression host. Induction was performed at 20^{O}C with 0, 0.1, 0.3 and 0.5 IPTG as indicated. Lane L – Broad-range molecular weight protein ladder; lane 1 – no induction control; lanes 2, 4 and 6 show CysG whole cell induction 4H post IPTG addition; and lanes 3, 5 and 7 show CysG whole cell induction 16H post IPTG addition. Red arrow corresponds to CysG.

E. coli BL21 (DE3) PSJF04 competent cells were then transformed with pSJF01. Induction and solubility trials revealed high level soluble expression from pSJF01 in the presence of pSJF04, indicating that siroheme is required for correct folding of PA4130 (Figure 4.8). Solubility assessment of pSJF02 and PSJF03 in the presence of PSJF04 was not assessed due to the fact that the pSJF04 co-expression vector lacks both the 3' and 5' untranslated regions required for stabilisation of mRNA at low temperatures. With the pSJF01 and pSJF04 co-expression system demonstrated to work, pCold based PA4130 overexpression vectors were abandoned. The PSJF01 *PSJF04* dual vector system appeared to maximally express soluble PA4130 at the lower temperature of 20^{O}C with the strength of IPTG induction appearing to play very little role in PA4130 solubility levels at this temperature (Figure 4.8 I). Based on these observations, induction and overexpression of PA4130 was performed at 20^{o}C with 0.3mM IPTG induction for future PA4130 preparations.

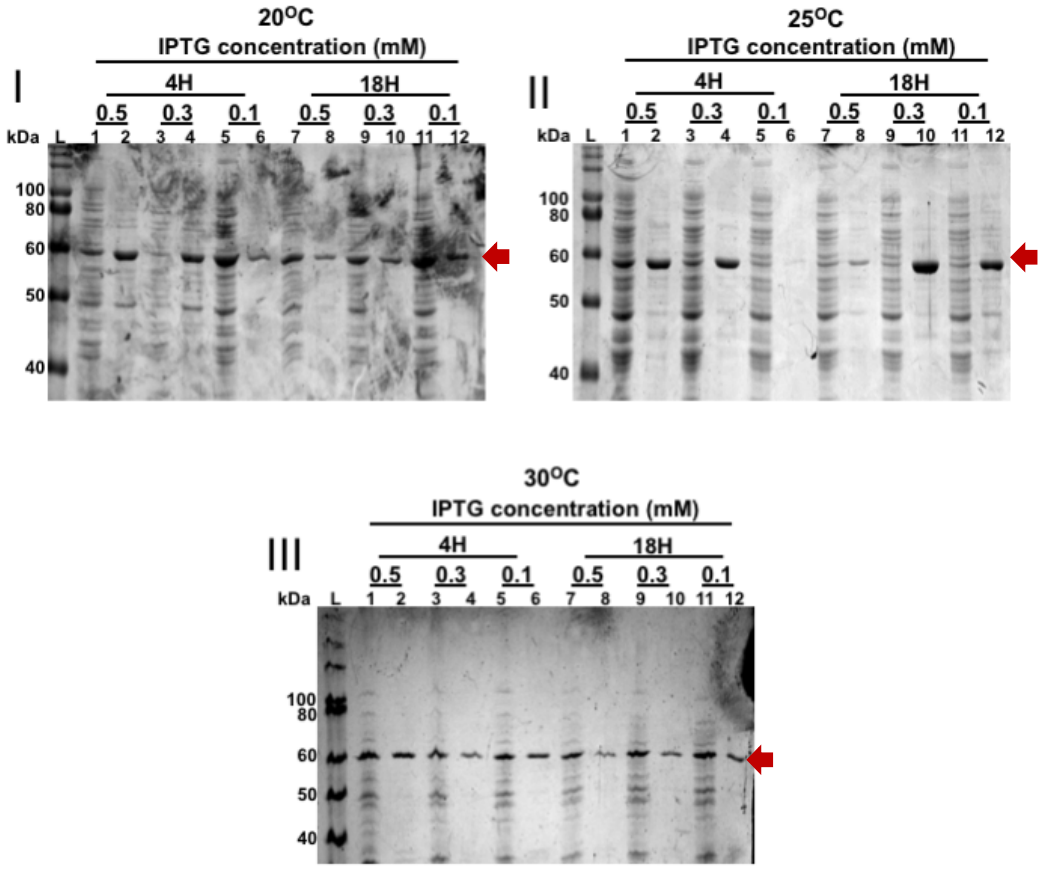

Figure 4.8 - Solubility assessment of PA4130 co-expressed from plasmid PSJF01 and PSJF04 using *E. coli* BL21 (DE3) as an expression host. Induction and overexpression performed at 20, 25 and 30°C with 0.1, 0.3 and 0.5mM IPTG as indicated. Lane 1 – Broad range molecular weight ladder; lanes 1, 3, 5, 7, 9 and 11 show soluble fractions post IPTG induction; lanes 2, 4, 6, 8, 10 and 12 show insoluble fractions post IPTG induction. Red arrows indicate bands corresponding to 6XH-PA4130.

4.3.1.5 Restoration of iron-sulphur cluster biogenesis does not affect PA4130 solubility

Iron-sulphur clusters are essential structures in all domains of life, allowing transduction of electrons and participating in multiple essential redox reactions. Many enzymes incorporate these molecules in their active site to facilitate catalytic activity. In the case of PA4130, this allows the 6-electron reduction of nitrite or sulphite. *E. coli* normally contains mechanisms of iron-sulphur cluster biogenesis, encoded by the *isc* and *suf* pathways (Figure 4.9). During the construction and mutagenesis of *E. coli* B-line cell types, the *suf* pathway was inactivated due to a 854 nucleotide deletion spanning *sufA* and *sufB* (Figure 4.10*)*. These strains remain viable due to the presence of the *isc* pathway however, the enzymatic pathway used to create iron-sulphur clusters are not

interchangeable, indicating that the structure or insertion mechanism of these iron-sulphur clusters are distinct (226). This has important implications for expression of iron-sulphur proteins in *E. coli* BL21 (DE3), and derived expression strains, as a defective *suf* pathway may prevent insertion of this prosthetic group, producing apo-forms of the target protein or enzyme (226).

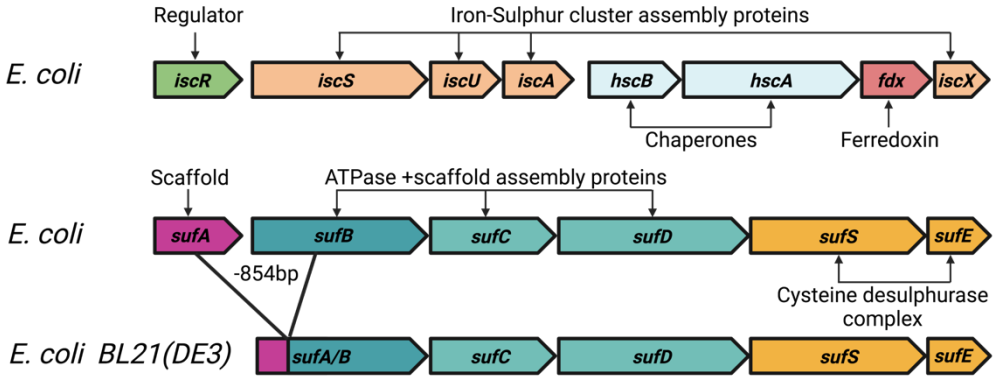

Figure 4.9 – Diagram of iron-sulphur cluster biogenesis pathways normally present in *E. coli* BL21 (DE3). An 854bp nucleotide deletion has resulted in fusion of *sufA* and *sufB* producing an inactive hybrid protein. This inactivates iron-sulphur cluster biogenesis through the *suf* pathway and may compromise assembly of proteins and enzymes containing these prosthetic groups. Adapted from Corless *et al* (226).

Corless and colleagues (226) engineered *E. coli* BL21 (DE3) SufFeScient (Suf^{++}) to overcome this problem of *suf* pathway inactivation. In this strain *sufAB* has been genetically restored with transcriptional repression by Fur removed through mutation of the binding site for this regulator (Fur box). This results in constitutive expression of the *suf* pathway, enhancing both yield and iron-sulphur cluster insertion into overproduced proteins. To assess the impact on PA4130 induction and solubility, *E. coli* Suf++ was transformed with pSJF01 and pSJF01/pSJF04. Solubility trials were then performed as previously, with PA4130 overproduced at 20, 25 and 30^{o}C at IPTG concentrations of 0.1, 0.3 and 0.5mM. Induction of PA4130 in *E. coli* Suf++ was unaltered, with high levels of PA4130 expression seen across all experimental conditions with both pSJF01 alone and pSJF01/pSJF04 (Figure 4.10). When transformed with pSJF01 alone, PA4130 solubility demonstrates no notable improvement at 25 and 30^{O}C with the majority remaining insoluble (Figure 4.10 II-III). However, at 20^{O}C with 0.1mM IPTG induction, PA4130 solubility appears to be enhanced (Figure 4.10 I). As previously seen in *E. coli* BL21 (DE3), co-overexpression with the siroheme synthase CysG results in a large increase in PA4130

solubility at lower expression temperatures (Figure 4.10 IV-VI). From this data, it was determined that optimal PA4130 solubility yield would be obtained with overexpression conducted at 20^{O}C for 16-18h. IPTG induction strength appears to have little effect on solubility of PA4130, therefore overexpression was induced with 0.1mM to account for the long expression duration. Exogenous Iron sulphate heptahydrate was added to a concentration of 0.2mM upon induction since PA4130 hypothetically requires 5Fe and 4S molecules. This supplementation was not formally assessed however and cultures reached higher optical densities with red/brown pellets indicating successful heme protein formation.

Taken together, this solubility assessment suggests that restoration of the *suf* pathway plays a small role in enhancing PA4130 solubility. However, increased siroheme availability is the primary requirement for correct PA4130 folding. This does not rule out a functional role for iron-sulphur cluster insertion as many iron-sulphur proteins remain soluble in their apo-forms. The impact of *suf* restoration was assessed later on to maximise production of active, soluble PA4130 for both functional and structural characterisation (Section 5.3.1.1).

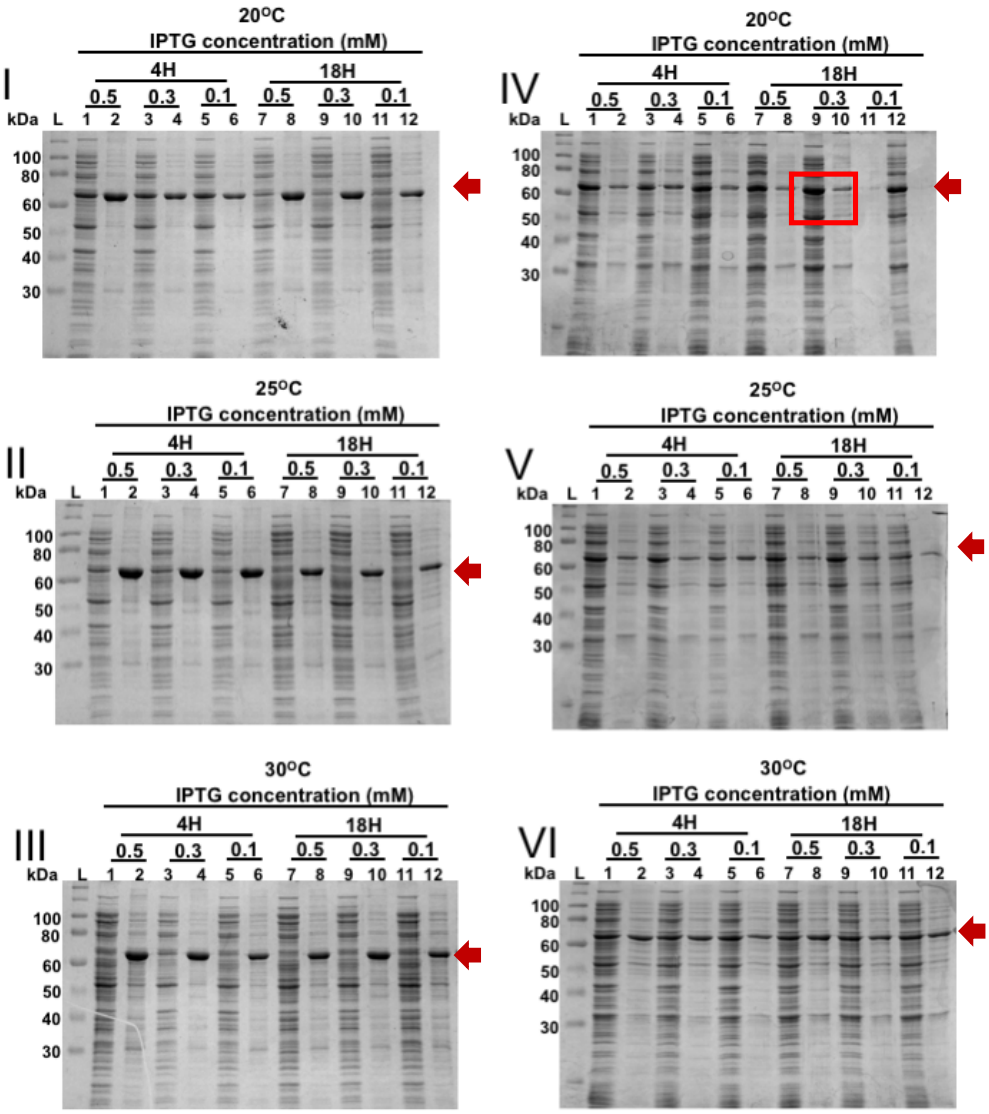

Figure 4.10 – Solubility assessment of PA4130 when produced in *E. coli* Suf++ (DE3) with pSJF01 in the presence and absence of pSJF04. Overexpression and induction performed at 20, 25 and 30^{O}C with 0.1, 0.3 and 0.5mM IPTG as indicated. Samples were lysed via sonication with cell pellet solubilised with 8M urea. Panels I,II and III represent soluble and insoluble fractions obtained without pSJF04, with panels IV,V and VI overproduced in presence of pSJF04. Lane L – broad range molecular weight ladder; lanes 1, 3, 5, 7, 9 and 11 represent soluble fractions; lanes 2, 4, 6, 8, 10 and 12 insoluble fractions. Red box highlights chosen conditions for future PA4130 overproduction. Red arrows indicate bands corresponding to 6XH-PA4130.

4.3.1.7 Optimisation of PA4130 purification

Purification of homogenous PA4130 is key to both structural and functional characterisation. In order to achieve this, methods of selective purification are required to enrich the target sample. Immobilised metal ion affinity chromatography (IMAC) was used as a first step to initially purify PA4130 from

E. coli Suf++ (DE3) when co-expressed with CysG. Using this method, a high quantity of PA4130 was selectively purified (Figure 4.11). However, the sample had 3 notable contaminants, suggesting the need for additional purification methods to produce homogenous PA4130 (Figure 4.11). The partially purified PA4130 sample was separated into 2 batches for use with two secondary purification methods, size exclusion chromatography (SEC) and ion exchange chromatography (IEC).

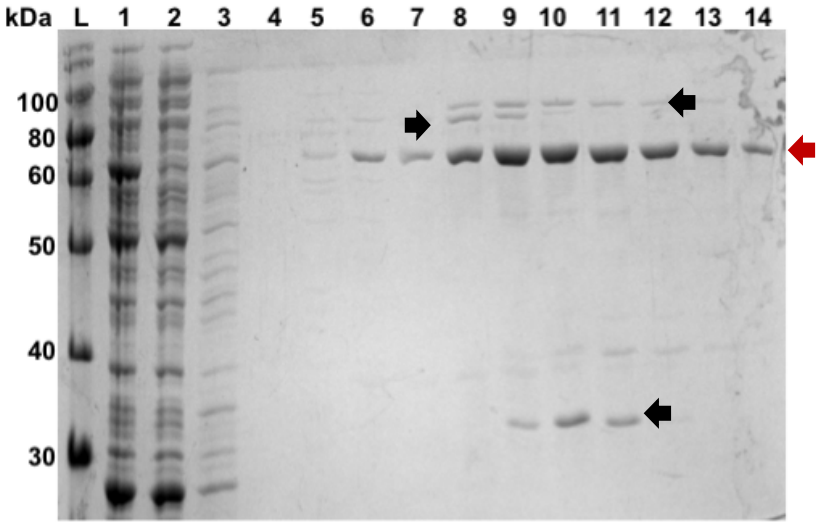

Figure 4.11 – IMAC purification of PA4130 overproduced in *E. coli* Suf++ (DE3) with pSJF01 and pSJF04. Cultures induced at 0.3mM IPTG for 18h. Selective purification of PA4130 results in contamination with multiple host proteins. Red arrow represents 6XH-PA4130, black arrows represent contaminating endogenous host proteins. Lane L – broad range molecular weight ladder; lane 1- whole cell lysate from *E. coli* Suf++ overproducing PA4130; lane 2 – sample flow-through post IMAC column; 3 – 20mM imidazole column wash; and lanes 4-14 represents 2.5ml elution fractions following application of a linear imidazole gradient from 20-400mM.

For the first batch, SEC was attempted to resolve these contaminants from PA4130 based on the hydrodynamic radius of each protein. This successfully removed the ~80kDa and ~25kDa contaminants however, this failed to resolve the ~70kDa protein from PA4130 due to the similar molecular weight or hydrodynamic radius of these proteins (Figure 4.12). SEC also revealed that the majority of PA4130 is found as a monomer in solution however, a small amount can be found in the void volume, indicating it may also be found in a higher oligomeric state.

For the second batch IEC was performed to resolve PA4130 from the contaminants based on charge. Predicted properties determined using

Protparam (ExPASY.com) estimated a predicted pI of 6.07 (Table 4.2). This suggested that anionic exchange chromatography (AEC) was more suitable for PA4130 to avoid potential inactivation at low pH. PA4130 was resolved using a linear gradient of NaCl (20mM to 1M) resulting in enrichment of PA4130. However, low level contamination of PA4130 is still exhibited when examined by SDS-PAGE combined with presumed sample breakdown (Figure 4.13). Whilst suitable for functional characterisation, structural determination via crystallography requires homogenous samples to encourage crystal nucleation and packing. A contaminant at this level will likely hinder crystallisation, therefore we sought to resolve this prior to crystallisation trials.

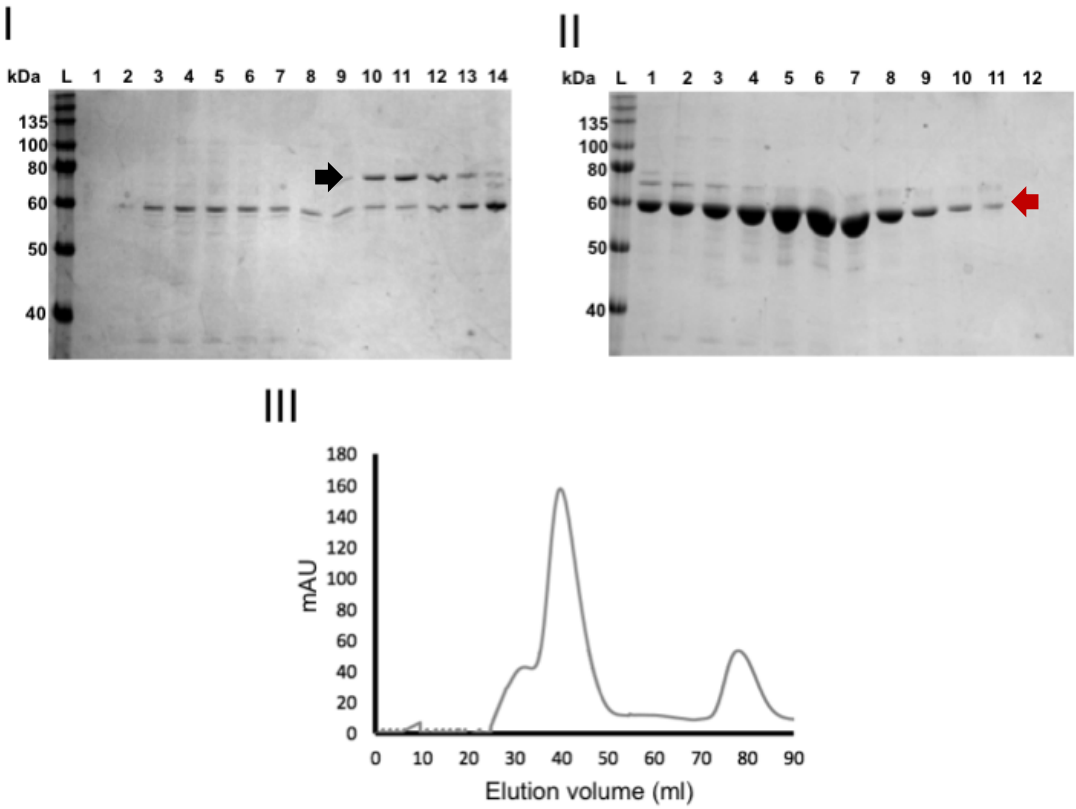

Figure 4.12 – SEC of contaminated PA4130 product obtained with IMAC. (I-II) SDS-PAGE gel of samples obtained based on 280nm peaks observed in SEC chromatogram (III). (I) Lanes 1-8 represent void volume samples; 9-14 correspond to peak 1. (II) Lanes 1-11 represent samples from PA4130 peak. Hydrodynamic focussing failed to resolve between PA4130 and ~70kDa contaminant. Red arrow indicates band corresponding to 6XH-PA4130, black arrows denotes ~70kDa E. coli contaminant co-purified with IMAC.

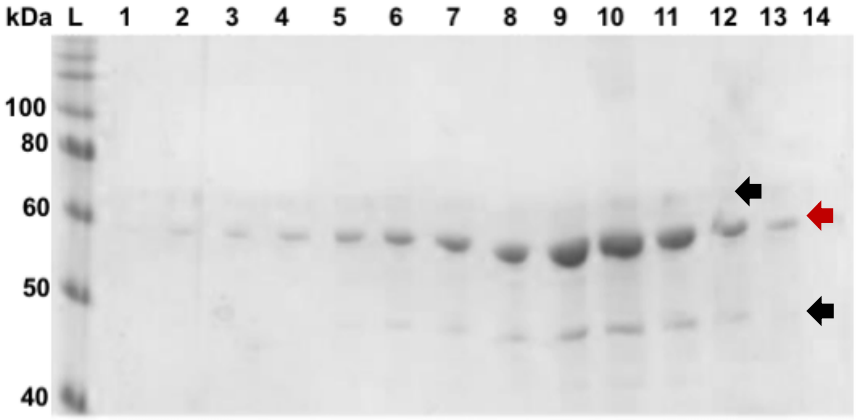

Figure 4.13 – SDS-PAGE of PA4130 samples obtained through AEC. Ionic exchange failed to purify homogenous PA4130 with low level contamination and sample breakdown observed. Red arrow represents bands corresponding to 6XH-PA4130 whilst contaminating proteins are indicated with black arrows.

Protein	Molecular weight (kDa)	Isoelectric point (pI)	Hydrophobicity
PA4130	62.2	6.02	-0.258
ArnA	74.28	6.39	-0.183
GlmS	65.89	5.89	-0.231
SlyD	20.85	4.86	-0.383

Table 4.2 – Predicted protein properties of 6XH-PA4130 and contaminating proteins using the ProtParam tool from expasy.com. Identities of PA4130 and IMAC contaminating protein confirmed with porcine trypsin digest followed by mass spectrometry at the University of York.

Contamination following SEC and AEC could be explained by two possibilities: i) PA4130 associates with an endogenous *E. coli* protein resulting in co-purification; or ii) the contaminating protein has both a similar hydrodynamic radius and isoelectric point (pI). To determine the identities of the proteins, the SDS-PAGE bands corresponding to PA4130 and the 3 contaminants were excised post-IMAC and sent for mass spectrometry. Mass spectrometry confirmed the identity of PA4130 and revealed the contaminants to be ArnA, GlmS and SlyD, endogenous *E. coli* proteins which commonly co-purify by IMAC (Table 4.2). These proteins have been demonstrated to contain surface-exposed histidine rich regions facilitating binding and purification during IMAC (227). ArnA and SlyD are easily removed with both SEC and AEC. However, GlmS is closely matched to PA4130 in both molecular weight, pI and hydrophobicity (Table 4.2). This complicates purification of homogenous

PA4130 by standard methods as a small amount of GlmS remains when using SEC and AEC.

Genetic manipulation of *E. coli* BL21 (DE3) has previously been used to avoid contamination of target protein when purified by IMAC. GlmS is an essential gene responsible for catalysis in the first step of hexoamine biosynthesis, forming the cell-wall precursor D-glucosamine 6-phosphate. Therefore, deletion of this gene from the *E. coli* BL21 (DE3) genome is not a viable strategy for avoiding contamination as growth is compromised unless supplemented with N-acetylglucosamine (228). In place of deletion mutants, some strains of *E. coli* BL21 (DE3) have previously been modified to reduce the binding affinity of contaminating proteins. Robichon and colleagues (155) developed a commercially available strain specifically designed to reduce contamination in IMAC. The strain *E. coli* NiCo21 (DE3) is a *E. coli* BL21 (DE3) derivative with three key differences. Both ArnA and SlyD have been fused in-frame with a chitin binding domain (CBD), enabling removal of these contaminants with chitin column chromatography (CCC). However, key to PA4130 purification is the site-directed mutagenesis of six surface exposed histidines to alanines in GlmS, reducing affinity of this contaminant to metal ions. Both the pSJF01 and pSJF04 vectors were transformed into *E. coli* NiCo21 (DE3) and overexpression of PA4130 induced. Subsequent purification using IMAC revealed that neither GlmS or SlyD-CBD were co-purified alongside PA4130 (Figure 4.14). ArnA-CBD was still co-purified however, this protein bound to chitin during CCC whilst PA4130 passed through the column in the flow-through (Figure 4.14). This enabled purification of homogenous PA4130 suitable for both functional and structural characterisation. The final yield varied with each preparation however, between 4-7mg of PA4130 was routinely obtained from 1L of terrific broth post purification.

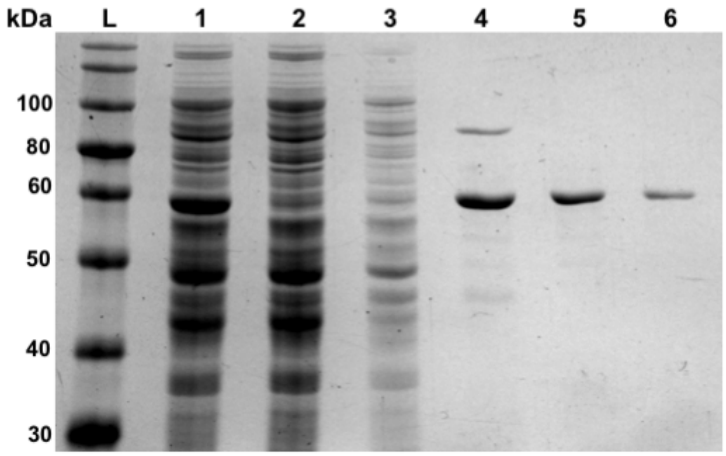

Figure 4.14 – Purification of homogenous PA4130 using a combination of IMAC, CCC and PD-10 column chromatography. Lane L – broad-range molecular weight ladder; 1 – Original lysate from *E. coli* NiCo21 (DE3) overexpressing PA4130 and CysG; 2 – Lysate flow-through post IMAC binding; 3 – 40mM Imidazole IMAC wash; 4- Concentrated PA4130 sample pooled from IMAC; 5 – PA4130 sample flow-through post CCC; 6 – PA4130 samples post PD-10 column desalting.

4.3.2 Spectral properties of PA4130

As discussed previously, PA4130 contains 2 prosthetic groups required to complete electron transport. The presence of the heme-like molecule siroheme and a 4Fe-4S iron-sulphur cluster means UV visible spectroscopy is a suitable tool to evaluate prosthetic group insertion into PA4130. This is especially pertinent to the PA4130 purification methodology described above, with capacity developed to enhance both siroheme and iron-sulphur cluster biogenesis through the use of different overexpression strains and vectors (226). Nitrite or sulphite reductases of this type typically display 3 characteristic peaks at 387-392 (Soret peak), 585-590 (α peak) and 709-714 (charge transfer peak) due to the presence of the ferri-siroheme complex (224, 229). The position or intensity of these bands can be altered depending the oxidation state of these groups. These spectral shifts also occur upon substrate or inhibitor binding, enabling rudimentary evaluation of interaction partners.

4.3.2.1 E. coli NiCo21 derived PA4130 does not display expected spectral properties of a nitrite/sulphite reductase

Fresh PA4130 samples purified by IMAC and CCC from *E. coli* NiCo21 (DE3) extracts were spin concentrated, desalted and buffer exchanged into 25mM

Tris, 50mM NaCl at pH 7.5. PA4130 samples were diluted to a concentration of 1mg/ml with 1ml of sample inserted into an Eppendorf UVette disposable UV/vis cuvette. The spectrum for NiCo21 derived PA4130, between 300-800nm, does not display the expected characteristics of a nitrite or sulphite reductase (Figure 4.15 I). Whilst a small Soret band is visible with a peak at 381nm, the characteristic α and charge transfer bands are not visible at this concentration of PA4130. When compared to spectrum generated for *Mycobacterium tuberculosis* derived PA4130 homologue SirA, it is clear that formation ferri-siroheme complex is limited (Figure 4.16 II) (179). Since overexpression of siroheme is required to obtain soluble PA4130, we assumed that siroheme had inserted correctly. Therefore, it was hypothesised that absence of the 4Fe-4s iron-cluster is responsible for the diminished NiCo21 derived PA4130 UV/vis spectrum.

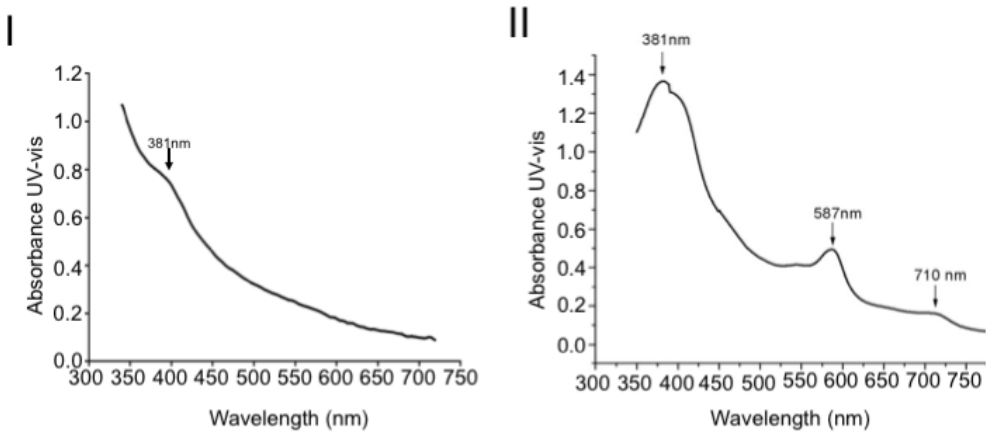

Figure 4.15 – Purified nitrite or sulphite reductase UV visible spectrum. (I) Spectrum obtained for PA4130 purified from *E. coli* NiCo21 (DE3); (II) spectrum reported for *Mycobacterium tuberculosis* SirA (179). PA4130 derived from *E. coli* NiCo21 (DE3) lacks the characteristic alpha and charge-transfer bands associated with nitrite or sulphite reductases of this family.

4.3.2.2 Overexpression of PA4130 in E. coli SuFEcient restores expected spectral properties

Overexpression of PA4130 in *E. coli* Suf++ demonstrated no notable effect on solubility. Obtaining soluble PA4130 appeared to be solely-dependent on

overexpression of the siroheme synthase CysG. However, many iron-sulphur proteins can be overproduced in an apo-form, devoid of an iron-sulphur cluster. Despite this absence, the protein remains soluble. To maximise the chance of 4Fe-4S iron-sulphur cluster insertion, pSJF01 and pSJF04 were transformed into *E. coli* Suf++ and overproduced as previously done for *E. coli* BL21 (DE3) and NiCo21 (DE3).

Previous IMAC purifications were significantly contaminated with ArnA, GlmS and SlyD. This was circumvented by use of *E. coli* NiCo21 (DE3) with the problematic GlmS surface exposed histidines mutated to alanine. *E. coli* Suf++ does not contain these mutations, suggesting that GlmS would again contaminate PA4130 preparations. However, now the identity of contaminating protein was known, a new purification strategy to eliminate the majority of GlmS at the IMAC step could be developed. It was shown by Bolanos-Garcia and Davies (227) that GlmS elutes at around 55-65mM imidazole. Previously PA4130 had been purified with a linear imidazole gradient. In an attempt to eliminate GlmS in non-mutated strains we used a step-wise gradient of imidazole with wash steps at 40 and 80mM. Whilst a significant amount of PA4130 was lost at the 80mM wash step, the PA4130 pooled from the elution fragments did not appear to possess GlmS (Figure 4.16). Low level contamination was still present but could be separated from PA4130 with SEC. This enabled purification of a homogenous sample of comparable standard to PA4130 produced in *E. coli* NiCo21 (DE3).

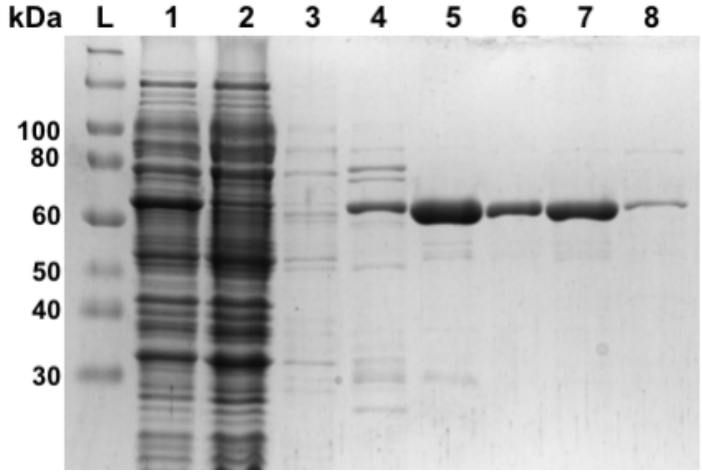

Figure 4.16 – IMAC purification of PA4130 expressed from PSJF01 and PSJF04 using *E. coli* Suf++ (DE3) as a host. Overexpression performed at 20^{O}C with 0.3mM IPTG for 18h. Lane L – broad-range molecular weight ladder; 1 - Original lysate from *E. coli* Suf++ (DE3) overexpressing PA4130 and CysG; 2 – Lysate flow-through post IMAC binding; 3 – 40mM imidazole wash; 4 – 80mM imidazole wash; 5 – 100mM imidazole elution; 6 - 150mM imidazole elution; 7 - 200mM imidazole elution; and 8 400mM imidazole elution.

UV-Vis spectral characterisation of newly purified PA4130 at a concentration of 1mg/ml revealed a pattern consistent with previously purified nitrite or sulphite reductases. PA4130 samples derived from *E. coli* Suf++ (DE3) demonstrate peaks at 389 (Soret peak), 569(α peak) and 712nm (charge transfer peak), characteristic of siroheme and iron-sulphur cluster insertion (Figure 4.15 II and 4.17 I). The samples with purified PA4130 were oxidised due to the presence of dissolved oxygen in all the buffers used during purification. Reduction of PA4130 using a 3-fold molar excess of sodium dithionite, with subsequent UV-Vis characterisation revealed spectral changes consistent with electron transfer to iron moieties of siroheme and the iron-sulphur cluster (Figure 4.17 II). The Soret band peak flattened and shifted slightly to 400nm whilst the charge transfer band (712nm) was no longer present. The Alpha band at 587nm was 'split', revealing 2 new broad peaks spanning ~480-535 and 560-635nm. These changes in spectral properties suggested that electron transfer was occurring between the ferri-siroheme complex, enabling reduction of either nitrite or sulphite when present (229).

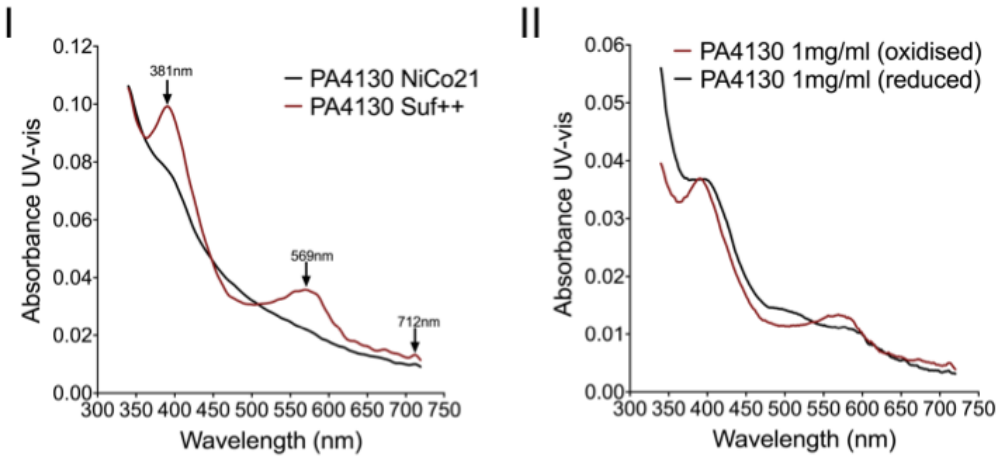

Figure 4.17 – UV-visible spectroscopy of PA4130. (**I**) Comparison of PA4130 spectrums obtained using *E. coli* NiCo21 (DE3) and *E. coli* Suf++ (DE3) as expression hosts. (**II**) Effect of sodium dithionite reduction on the spectrum of PA4130 purified from *E. coli* Suf++ (DE3).

To confirm that the altered spectral properties of PA4130 when produced in *E. coli* NiCo21 or Suf++ were due to prosthetic group insertion, acid labile sulphur and iron content of PA4130 were quantified. New samples of PA4130 from both NiCo21 and Suf++ were prepared simultaneously, to limit any sample degradation artefacts. A clear increase in labile sulphur and iron content was detected in PA4130 derived from Suf++ when compared to samples derived from NiCo21. When averaged from 4 independent purifications, PA4130 produced by Suf++ contained 3.1 and 3.3 moles of labile sulphur and iron per mole of PA4130, whilst samples derived from NiCo21 only contained 2.1 and 1.9 moles/mole of PA4130 respectively. (Table 4.3). PA4130 homologues contain a 4Fe-4S iron-sulphur cluster prosthetic group, suggesting that even expression in Suf++ does not allow for complete iron-sulphur cluster insertion. However, this system represents a significant improvement over PA4130 previously produced by NiCo21. This enhancement in iron-sulphur cluster insertion would indicate that PA4130 produced by *E. coli* Suf++ (DE3) is more active than that produced by *E. coli* NiCo21 (DE3) aiding functional studies. Correct prosthetic group insertion would also be beneficial for structural determination and future virulence inhibitor development as both siroheme and the iron-sulphur cluster interact with multiple residues in the catalytic site of these enzymes. Therefore, the absence of either prosthetic group would likely alter the structure of the active site, reducing the effectiveness of *in silico* docking experiments when attempting to identify inhibitors of PA4130.

	E. coli expression host	
Assay	**NiCo21 (DE3)**	**Suf++ (DE3)**
Labile Sulphur	2.1±0.23	3.1±0.35
Labile Iron	1.9±0.37	3.3±0.42

Table 4.3 – Comparison of acid labile sulphur and iron detected in PA4130 derived from *E. coli* NiCo21 (DE3) and Suf++ (DE3). PA4130 overproduced in Suf++ demonstrates higher levels of Fe and S incorporation, indicating enhanced insertion of the 4Fe-4S iron-sulphur cluster.

4.3.3 Attempted structural determination of PA4130

Protein crystallisation is a highly variable process relying upon numerous parameters. Successful crystal formation relies on optimising these parameters to obtain a solution which is super-satured. Supersaturation occurs when a macromolecule is beyond the solubility limit of the solution however, importantly this state does not alter its natural structure. This process aids the poorly understood process of nucleation and subsequent growth of diffraction quality crystals.

4.3.3.1 Pre-crystallisation assessment of PA4130

One of the major variables explored in crystallization trials is protein concentration. Samples precipitate out of solution as disordered aggregates if too highly concentrated. Conversely, at low concentrations the sample is too stable to promote crystal nucleation (230). To determine a good starting point, a simple pre-crystallisation test (Hampton) is used to determine solubility in commonly used crystallisation buffers and salts. Freshly purified PA4130 was subjected to assessment using concentrations ranging from 1-10mg/ml at room temperature (~25^{O}C). At PA4130 concentrations above 4mg/ml, all samples resulted in large amounts of amorphous precipitate, whilst samples below this threshold demonstrated light granular precipitate or clear drops (Table 4.4). From this it was determined that initial high-throughput crystallisation screens needed to be performed at 1, 2, 3 and 4mg/ml using multiple temperatures.

	PA4130 concentration (mg/ml)						
Solution	1	2	3	4	5	7.5	10
A1	LG	LG	LG	HA	HA	HA	HA
A2	C	C	LG	LG	HA	HA	HA
B1	LG	LG	LG	HA	HA	HA	HA
B2	LG	HA	HA	HA	HA	HA	HA

Table 4.4 – Summary of pre-crystallization test used to determine the correct concentration of PA4130 to use during screening. C – clear drop; LG – light granular precipitate; and HA – heavy amorphous precipitate.

4.3.3.2 Factorial and high-throughput crystal screening

Multiple PA4130 homologues have been crystallized and structures solved (179, 231-235). Investigation of the conditions required for crystallisation uncovered that enzymes of this type demonstrate remarkably consistent crystallisation conditions (Table 4.5). Predominantly crystallisation occurs at a slightly alkaline pH, using Tris.HCl as a buffer, $MgCl_2$ as a salt and polyethylene glycol 4000 (PEG) as a precipitation agent (Table 4.5). Usually in crystal formation trials, high-throughput screening kits are used covering a diverse range of conditions. From here crystal hits are optimised based on the parameters found in that well. However, in the case of PA4130 it was decided that a more specific factorial screen may be more advantageous, given the conserved crystallisation conditions exhibited by PA4130 homologues (Table 4.5).

A series of factorial screens were designed with Make-Tray (Hampton). This primarily focussed on varying pH and the concentration of PEG 4000. Despite monitoring samples for 6 months, no PA4130 crystals were observed at any concentration or temperature. PA4130 crystal trials were subsequently attempted using multiple commercially available kits at multiple concentrations and temperatures. To date, no crystals have been observed, with 75-90% of samples forming amorphous precipitate within 24 hours, irrespective of sample concentration. This may indicate that the PA4130 solutions used in these trials are too concentrated to achieve the desired supersaturation or that PA4130 degrades during the process of setting up trials.

Organism	Protein	AA Sequence identity (%)	Condition	Ref
Myocobacterium tuberculosis	SirA	28.23	0.1M Tris.HCl pH 8.2-8.7, 0.2M MgCl2, 30% PEG 4000.	(179)
Escherichia coli	CysI	21.36	0.065M KPO4 pH 8.0, 20% PEG 4000.	(231)
Desulfovibrio gigas	DsrI	20.74	0.1M Tris.HCl pH 8.5, 0.2M MgCl2, 12.5% PEG 4000.	(233)
Spinacia oleracea	NirA	26.05	0.05M Tris.HCl pH 8.5, 0.1M MgCl2, 15% PEG 4000.	(232)
Nicotiana tabacum	Nii3	26.99	0.1M Tris.HCl, pH 8.5, 0.2M MgCl2, 30% PEG 4000, 3% MPD.	(234)
Zea Mays	SirA	23.75	0.085M Tris- 0.17M NaOAc.3H2O pH 8.5, 25.5% PEG 4000, 15% glycerol	(235)

Table 4.5 – Summary of PA4130 homologue successful crystallization conditions from bacteria and plants. Despite being derived from diverse sources; enzymes of this type appear to crystallise under similar conditions with a particular focus on slightly alkaline conditions and PEG 4000 acting as a nucleation catalyst.

4.3.3.3 In silico *structural prediction of PA4130 reveals novel insertion*

With crystallisation of PA4130 failing, molecular modelling was next explored to assess whether a structural prediction of sufficient quality for inhibitor screening could be produced. Modelling was performed with SWISS-MODEL. The native PA4130 amino acid sequence was used to screen PDB for templates, with the 6 structures indicated in table 4.5 used for modelling. SWISS-MODEL employs 2 different internal assessments to determine the quality of a model. Global Model Quality Estimation (GMQE) assesses the expected accuracy of model taking into account the alignment and quality of the template, normalised by the coverage of the target sequence. QMEAN determines quality based on the 4 main geometric properties, torsion, solvation, all atoms and Cβ. This provides both global and local quality estimates enabling model quality to be explored at the residue level. All models constructed were assessed to be of poor quality by the internal quality control checks used by SWISS-MODEL. GMQE was determined to be below the 0.6

(60% structural similarity) threshold for all models, whilst QMEAN scores are all below -4.0, indicating a low-quality model (Table 4.6).

Organism	Protein	Swiss Model template ID	GMQE	QMEAN
Myocobacterium tuberculosis	SirA	1zj9.1	0.58	-5.64
Escherichia coli	CysI	6c3m.1	0.49	-5.98
Deinococcus vulgaris	DsrI	1aop.1	0.47	-5.76
Spinacia oleracea	NirA	2akj.1.A	0.52	-4.89
Nicotiana tabacum	Nii3	3b0g.1.A	0.55	-5.48
Zea Mays	SirA	5h8v.1.A	0.41	-6.14

Table 4.6 – Summary of PA4130 models rendered using the listed homologues as models. All models rendered were of poor quality when using GMQE or QMEAN for assessment. Predicted structures generated using SWISS-MODEL (216).

When analysing the quality of the models at the residue level, it was observed that the majority of residues are predicted to have a local similarity of between 0.6-0.8. However, there is a drastic drop predicted in quality at residues ~250-320 for all models (Figure 4.18). Amino acid sequence alignment with the PA4130 homologues listed in table 4.5, alongside those from the more closely related *P. aeruginosa* CysI, *Burkholderia cenocepacia* N/SirA and *Ralstonia solanacaerum* N/SirA, revealed a novel 29 amino acid insertion between R275 and D304 (Figure 4.19 I). Overlay of the previously constructed PA4130 models suggested that these residues are likely surface exposed however, the structure of this region could not be predicted (Figure 4.19 II). These differences in surface topology may explain the difficulty with PA4130 crystallisation in comparison to other nitrite or sulphite reductases. If this region is as unstable as portrayed in the models, crystal nucleation and lattice packing would be hindered.

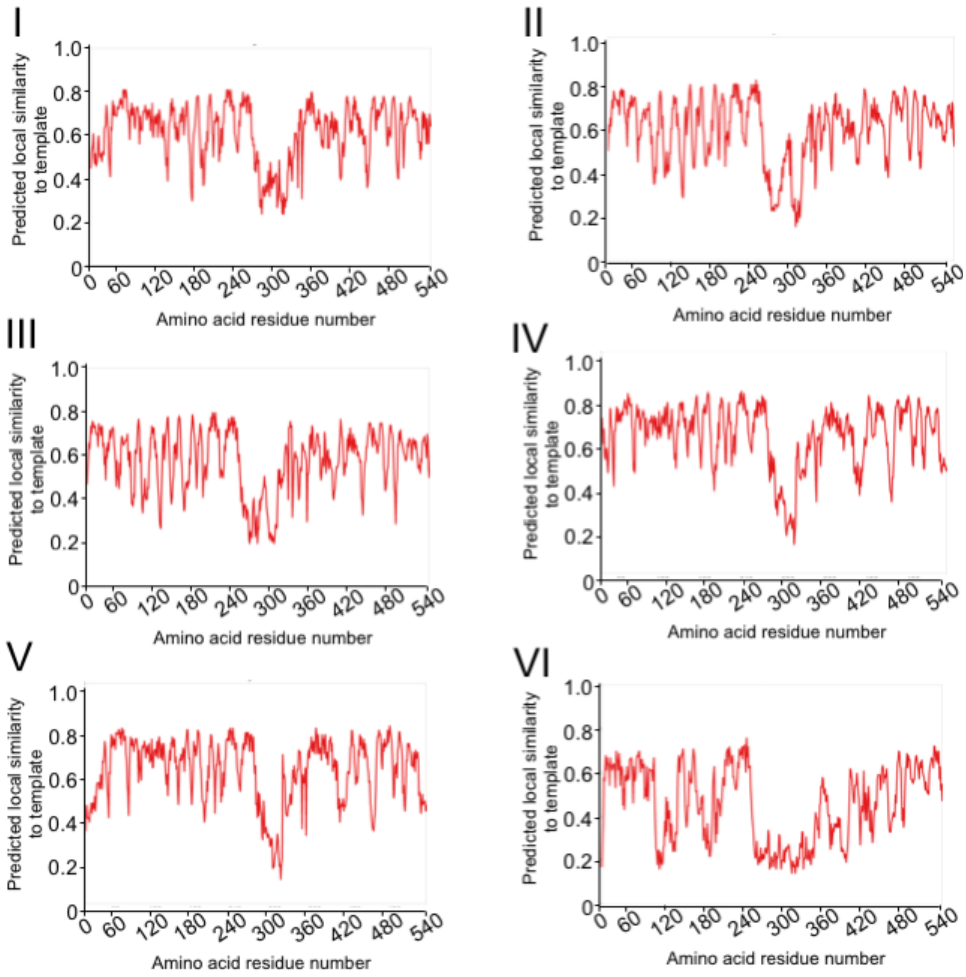

Figure 4.18 – Local quality assessment of PA4130 models produced using SWISS-MODEL. (I) Predicted PA4130 model quality at the residue quality level using *M. tuberculosis* SirA, (II) *E. coli* CysI, (III) *D. vulgaris* DsrI, (IV) *S. oleracea* NirA, (V) *N. tabacum* Nii3 and (VI) *Z. mays* SirA as templates.

I

```
Ps.a_PA4130      EAFAREVEEEWQHLRDGPAQLTAEECQRVAERFVLPRYLPPADGELAYGSARAADPAFAR
Ps.a_CysI        EVFAERVEAEWANLKDGPSTLTEAEVQRVAAHFVDPAYKALDDLDESLARLDAEHPGFAR
Ra.s_N/SiR       EEFARQVEEEWQHIKDGPSTITQAEFDRVAQYFAPPAYEKLADTDAGYEKALLENQAFAR
B.cc_N/SiR       AKFAQQVEEEWQHLKDGPSTLTQAEVDRVSQYFKPPVYEKLADTDASFEQHLLENKAFAR
E.co_CysI        ETFKAEVERRAGIK-----------------------------FEPIRPYEFTGRGDRIG
M.tb_SirA        AKFREVLETEYLKR-----------------------------PLIDGPAPEPVKHPIDHV
N.tb_NiR         EGFRAEVEKRMPQQ-----------------------------QLERASPEDLVQKQWER
Sp.o_NiR         EAFRGEVEKRMPEQ-----------------------------VLERASSEELVQKDWER
Z.ms_SiR         DRFRAEVEKYYGKK-----------------------------FESFRPLPEWQFNSYLG
```

II

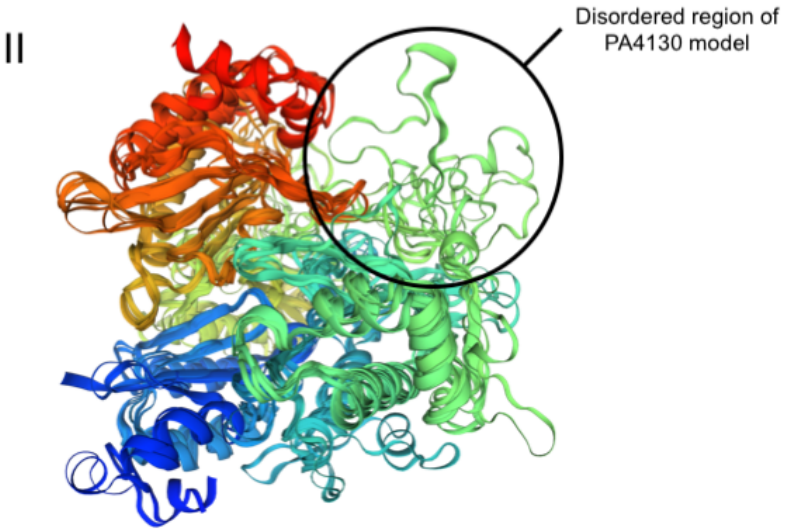

Figure 4.19 – Amino acid sequence alignment (I) and structural model (II) demonstrating the effect of R275-D304 insertion on PA4130 modelling. Structural model consists of 6 individual models overlaid using NGL 3D viewer. Majority of models exhibit good structural similarity. However, the R275-D304 insertion and local region is very disordered with minimal overlap seen between models.

4.4 Conclusions

Use of both siroheme overexpression and restoration of iron-sulphur cluster biogenesis was required to produce soluble PA4130 with the expected physical characteristics. This is important for functional characterisation of PA4130 (Chapter 5), and essential in future structural determination with crystallography, and *in vitro* inhibitor screens conducted downstream. Whilst structural characterisation remains elusive, the identification of a novel amino acid insertion provides crucial insight into the difficulty observed for PA4130 crystallisation and structural modelling. This provides a new avenue of investigation, with deletion or stabilisation of the insertion region possibly key to structural characterisation of PA4130.

For now, this work represents a crucial step in understanding the role PA4130 plays during *P. aeruginosa* infection. However, further work is required on the structural characterisation aspect of this project, with accurate model development essential to directed virulence inhibitor identification.

Chapter 5

Functional characterisation of PA4130

5.1 Introduction

The ability to purify the virulence target PA4130 opens up numerous avenues of research. Key to understanding the role PA4130 plays during *P. aeruginosa* infection, and the development of any inhibitors, is determining the molecular function of PA4130. As discussed in Chapter 3, the PA4130 amino acid sequence is homologous to nitrite and sulphite reductases. These enzymes have the capacity to reduce both nitrite and sulphite however, they often possess a pronounced preference for one (Figure 3.3). Nitrite or sulphite reductases have a wide variety of roles including redox balancing, biomolecule synthesis, energy conservation/generation and metabolite detoxification (236). All of which may contribute to *P. aeruginosa* survival and virulence in multiple ways. These reductases can be categorized based on molecular function and divided into sub-pathways within wider nitrate or sulphate metabolism, and further divided based on electron donor usage (Figure 5.1 and 5.2) (237, 238).

5.1.1 Nitrite or sulphite reductase metabolic pathways

Nitrite and sulphite reductases can be broadly classified as assimilatory or dissimilatory. In assimilatory reduction, nitrate and sulphate are reduced to ammonium and hydrogen sulphide respectively (237, 238). These compounds can subsequently serve as nitrogen or sulphur sources for synthesis of organic molecules, such as amino acids (Figure 5.1). Nitrite and sulphite are intermediates in this pathway, with PA4130 potentially reducing either of these toxic compounds to maintain nitrogen or sulphur. Dissimilatory nitrate or sulphate metabolism enables use of these molecules as terminal electron donors, facilitating anaerobic respiration (237, 239). However, based on the available literature, PA4130 is unlikely to contribute to anaerobic respiration in either of these pathways. Whilst the PA4130 amino acid sequence resembles dissimilatory sulphite reductase DsrA, the rest of the canonical pathway is absent from the *P. aeruginosa* genome (Figure 5.1) (240). Combined with the fact that *P. aeruginosa* has never been shown to utilise sulphate as a terminal electron acceptor to support anaerobic survival, it is unlikely that PA4130 participates in dissimilatory sulphate reduction. Dissimilatory nitrate metabolism utilises a specialised pathway termed denitrification. This reduces

nitrate to gaseous dinitrogen, with the nitrite intermediate reduced to nitrous oxide by another nitrite reductase NirS (Figure 5.1) (237, 241). NirS resembles *cbb*$_3$-cytochrome C oxidase catalytic sub-units, making it structurally distinct from PA4130 (241). As a result, PA4130 is unlikely to contribute to dissimilatory denitrification.

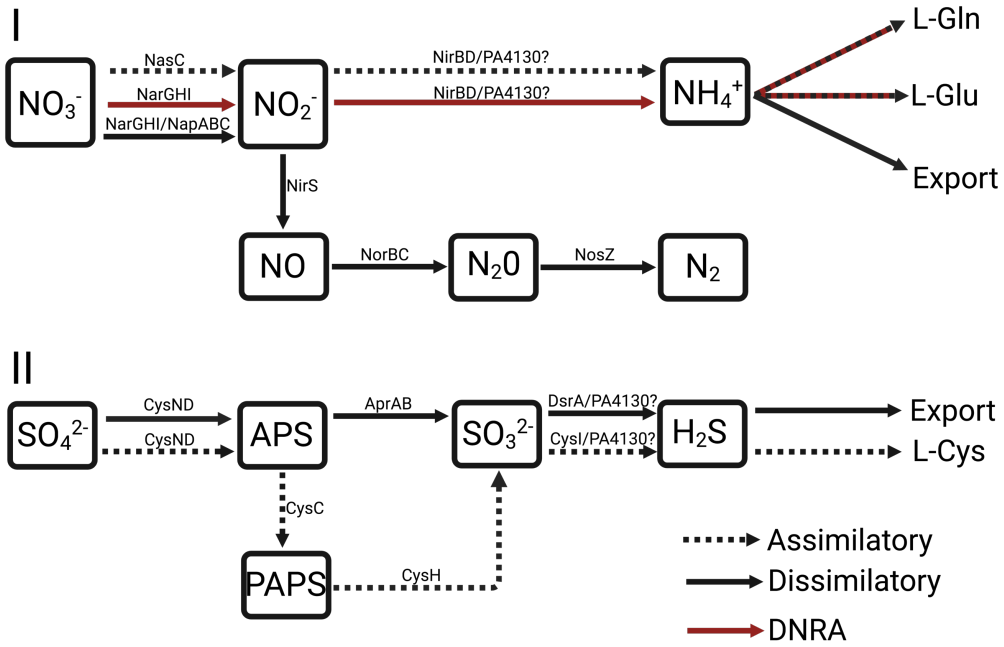

Figure 5.1 – Diagram of genetic pathway required for assimilatory or dissimilatory (A) nitrate and (B) sulphate reduction in bacteria. *P. aeruginosa* is reported to be capable of assimilatory nitrate and sulphate reduction, whilst only performing dissimilatory nitrate reduction for anaerobic respiration. This indicates that PA4130 may be a secondary assimilatory nitrite or sulphite reductase operating alongside NirBD or CysI.

In the case of nitrate metabolism another defined pathway exists which combines both assimilatory and dissimilatory denitrification termed dissimilatory nitrate reduction to ammonium (DNRA). Respiration occurs at the nitrate to nitrite and nitric oxide to nitrous oxide reduction steps through use of the membrane-bound nitrate reductase NarGHI, whilst N sources are maintained through use of an assimilatory nitrite reductase, converting nitrite to ammonium (Figure 5.1) (242, 243). A similar pathway does not exist within sulphate metabolism as energy generation occurs downstream of the sulphate to sulphite reduction. DNRA highlights the flexibility of nitrate reduction in *P. aeruginosa*, with PA4130 potentially participating in this aspect of metabolism.

5.1.2 Nitrite or sulphite reductase electron donor utilisation

Siroheme-dependent nitrite or sulphite reductases can be further subdivided based on electron donor requirement. These enzymes utilise 3 main electron donors, NADH, NADPH and reduced ferredoxin (Figure 5.2) (244-246). In the case of PA4130, NADH can be ruled out as an electron donor as NADH dependent nitrite or sulphite reductases are structurally distinct to the NADPH reductases, despite containing the same prosthetic groups (246). NADPH-dependent nitrite or sulphite reductases form heterogeneous oligomeric structures consisting of a hemoprotein subunit (PA4130) and a flavin-binding protein (247). Electrons are transferred to the flavin containing sub-unit, which are subsequently transduced to the [4Fe-4S] iron-sulphur cluster and siroheme of the hemoprotein sub-unit (Figure 5.2) (248, 249). This transfer of electrons to the nitrite or sulphite occurs at the same time, with the number of electron carrying centres possessed by this oligomeric structure facilitating a 6-electron transfer in a single step (232). Ferredoxin dependent nitrite or sulphite reductase are rare in bacteria and largely associated with plants. Ferredoxins are small acidic proteins harbouring a diverse range of iron-sulphur clusters through interaction with conserved cysteine containing motifs. These proteins can accept or donate electrons, participating in a wide variety of essential redox reactions throughout all domains of life (250). Ferredoxin-dependent nitrite or sulphite reductases utilise these mediators to deliver electrons from its contained iron-sulphur cluster, to the [4Fe-4S] cluster of the hemoprotein sub-unit (232, 244). However, reductases of this type are monomeric, requiring no flavin-binding component to transduce electrons. This means electrons are delivered one at a time, with oxidation of 6 reduced ferredoxins required to reduce nitrite or sulphite to ammonium or hydrogen sulphide respectively (232).

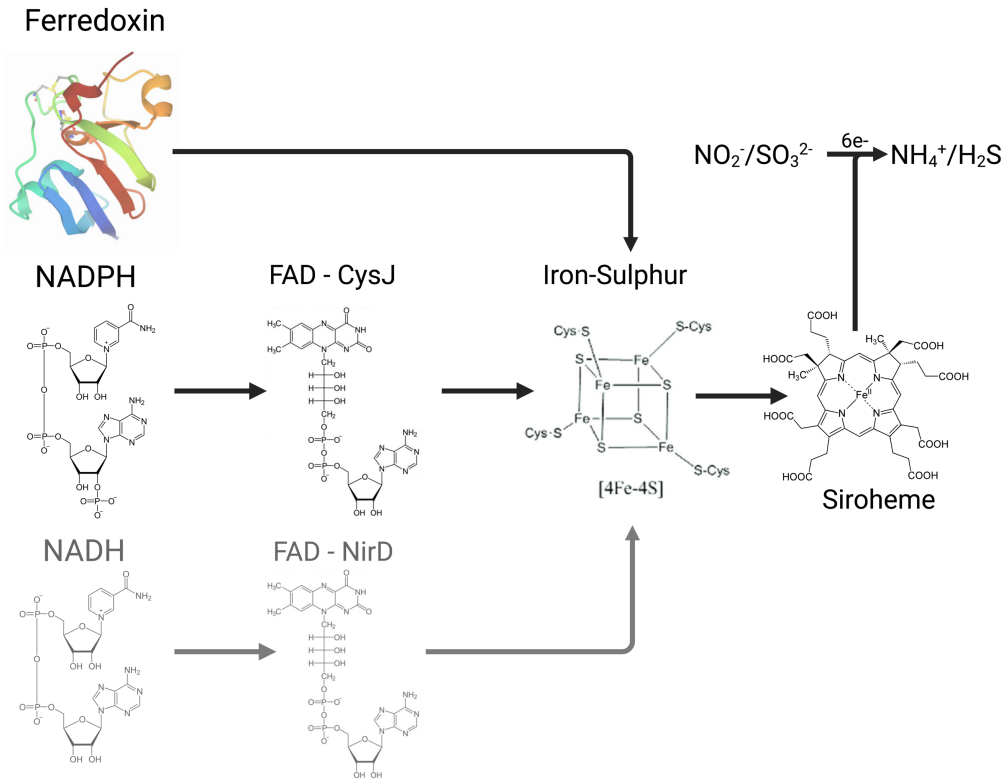

Figure 5.2 – Diagram of electron donors and transfer pathway utilised for reduction of nitrite or sulphite. Arrows indicate direction of electron transfer. PA4130 amino acid sequence resembles ferredoxin and NADPH dependent nitrite or sulphite reductases. NADH dependent reductases exclusively reduce nitrite, with the hemoprotein sub-unit of the complex structurally distinct to PA4130 homologues.

5.2 Aims of this chapter

In this chapter, the main aim was to determine the molecular function of PA4130 in an effort to understand how this enzyme impacts nitrate or sulphate reduction in the context of *P. aeruginosa* virulence. For this we needed to elucidate:

1. The native electron acceptor of PA4130
2. Preferred electron donor utilised by PA4130 for reduction.

This information would enable PA4130 to be assigned to a metabolic network and begin forming hypothesis for the role of this enzyme in virulence and approaches for the design of inhibitors which can ultimately be used for therapeutic intervention in the treatment of *P. aeruginosa* infections.

Determining the native electron donor would also be beneficial for future *in vitro* inhibitor screening, reducing reliance on artificial electron donors for the development of a system resembling the native reduction pathway.

5.3 Results

5.3.1 PA4130 is an ammonium forming nitrite reductase

Biochemical assessment of PA4130 function is required for 2 key reasons: (I) Determination of molecular function; and (II) *In vitro* assay development for downstream inhibitor screening. It was shown in Chapter 3 that the effect of PA4130 deletion mutants appear to be responsive to the presence of nitrate (Figures 3.7-3.9). With PA4130 predicted to encode a nitrite or sulphite reductase, it's reasonable to assume PA4130 encodes a nitrite reductase. However, since these enzymes can catalyse the reduction of both nitrite and sulphite, both electron acceptors need to be assessed to confirm PA4130 is nitrite specific.

5.3.1.1 PA4130 utilises nitrite as its native electron acceptor

In order to assess whether PA4130 utilises nitrite or sulphite as its native electron acceptor, a methyl-viologen (MV) oxidation assay was performed with both potential acceptors (247, 251). MV is a 4,4-viologen which, upon a one-electron reduction undergoes a colorimetric change to a deep blue. Oxidation back to its di-cationic form results in transition back to its original colourless appearance. This colorimetric redox reaction allows MV to act as an artificial electron donor for PA4130, with electron transfer only occurring in the presence of the correct electron acceptor. PA4130 prepared from *E. coli* Suf++ (DE3), was used in these initial experiments, owing to its enhanced UV-visible spectrophotometric properties when compared to NiCo21 (DE3).

PA4130 dependent oxidation of reduced MV only occurred in the presence of nitrite, with minimal oxidation observed with sulphite (Figure 5.3 I). Increasing the concentration of sulphite had no effect on the rate of MV re-oxidation,

demonstrating PA4130 mediated reduction is specific to nitrite. Enzymes of this type have been shown to catalyse the 6-electron reduction of nitrite to ammonium (232, 234). To confirm that PA4130 reduces nitrite and forms ammonium the same MV oxidation assay was performed. However, instead of tracking the colour change of MV, the disappearance of nitrite and subsequent ammonium production were directly assessed using Griess diazotization (Promega) and the o-phthalaldehyde method (Sigma). This enabled quantitative tracking of nitrite reduction and ammonium production by PA4130, confirming PA4130 is an ammonium-forming nitrite reductase, with reduction of nitrite accompanied by a concomitant increase in ammonium at a 1:1 ratio (Figure 5.3 II). Therefore, PA4130 was named NirA thereon to fit with current nomenclature for monomeric enzymes of this family (232, 234).

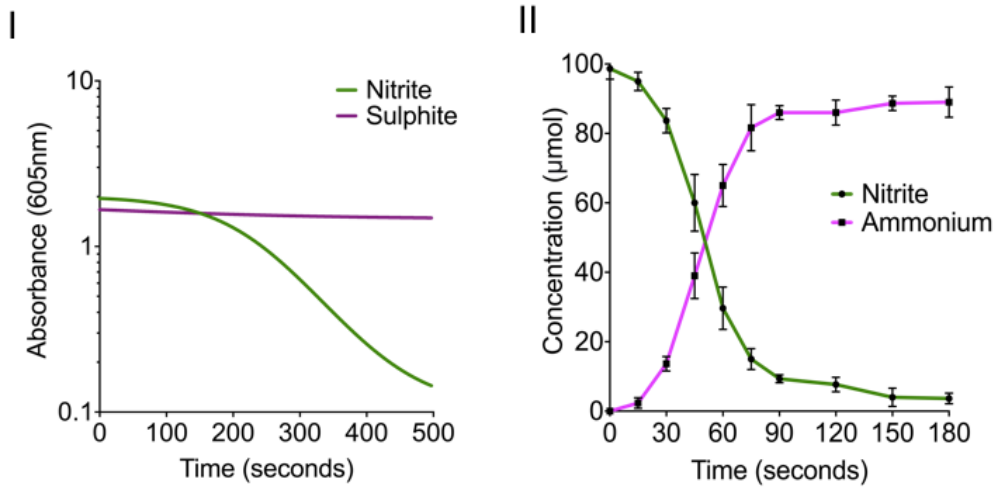

Figure 5.3 – MV oxidation assays to determine the native substrate (I) and end-product of PA4130-dependent reduction (II). MV oxidation only occurs in the presence of nitrite. Ammonium is produced as a result of nitrite reduction at a 1:1 ratio using MV as an artificial electron donor. Assays performed with 2µm NirA with 5 replicates from 2 separate enzyme preparations. I) Performed under anaerobic conditions at room temperature, II) carried out under aerobic conditions at 37^{O}C.

During NirA purification optimisation it was shown that overexpression in an *E. coli* background with *sufAB* restored, increased the amount of labile sulphur and iron present (Table 4.3). This is associated with increased insertion of the 4Fe-4S iron-sulphur cluster prosthetic group. To confirm this increased prosthetic group insertion enhanced nitrite reductase activity, NirA prepared from *E. coli* Suf^{++} and NiCo21 were subjected to MV oxidation assays. NirA produced by Suf^{++} demonstrated enhanced nitrite reduction when compared to

NiCo21 NirA (Figure 5.4). Following this experiment, NirA preparations from *E. coli Suf*++ (DE3) were used exclusively.

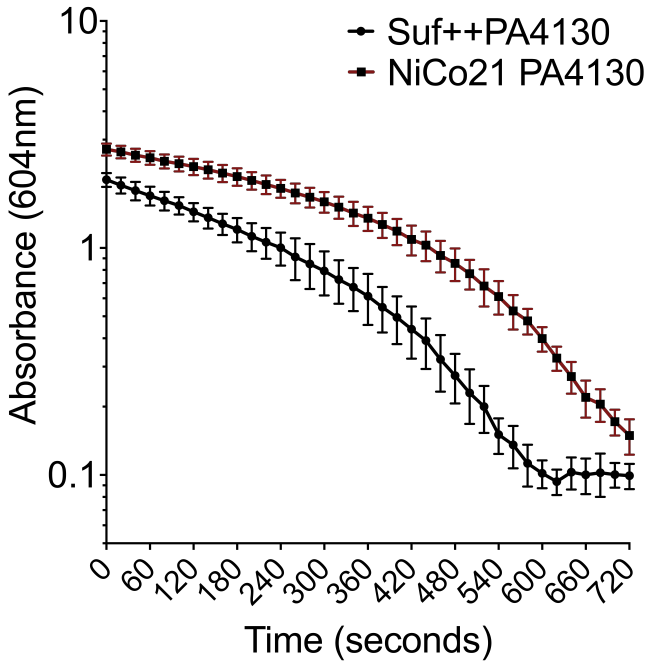

Figure 5.4 – MV oxidation assay comparing activity of NirA derived from *E. coli* Suf++ (DE3) and NiCo21 (DE3). NirA overproduced in *E. coli* Suf++ (DE3) allows for quicker oxidation of MV when compared to NirA overproduced in *E. coli* NiCo21 (DE3). Assays performed at 1um NirA with 5 replicates from 2 separate preparations. MV oxidation assay carried out under anaerobic conditions at room temperature. Error bars represent standard deviation.

5.3.1.2 NirA is a ferredoxin dependent nitrite reductase

Alongside an electron acceptor, nitrite reductases require electron donors to act as a source of electrons. Numerous donors have been demonstrated to operate with nitrite reductases with c-type cytochromes, NADH, NADPH and ferredoxins possible sources of electrons (244, 246, 247, 252). Both c-type cytochromes and NADH were eliminated as possible electron donors as these electron donors operate exclusively with the structurally distinct NirS and NirB-like nitrite reductases (246, 252). NirA homologues have been shown to use either NADPH or ferredoxin as electron donors, irrespective of the native electron acceptor (179, 232, 234, 249).

It was suspected that NirA is a ferredoxin dependent nitrite reductase. Based on the SEC data, NirA is found as a monomer in solution which is indicative of a ferredoxin-dependent nitrite reductase (Figure 4.12 III) (179, 232, 234, 244). NADPH dependant nitrite reductases form hetero-oligomeric complexes with a flavin-binding protein. The hemoprotein and flavin binding protein components are usually in an operon in bacteria for example *cysIJ* in *E. coli* and *Salmonella* (224). Whilst *nirA* is in an operon with PA4129, this sequence bears no resemblance to CysJ and is not reported to bind flavin. *P. aeruginosa* does not encode a *cysJ* homologue, indicating the function of NirA is independent of the traditional Flavin-binding protein. This prevents use of NADPH as an electron donor since the first electron transfer step in this chain is from NADPH to FAD (248, 249). To confirm this suspicion, NirA was subjected to reactions similar to the previously used MV oxidation assay however, MV was substituted with both reduced spinach ferredoxin and NADPH (with FAD and FMN). Under these conditions it was shown NirA nitrite reduction only occurs with MV and reduced ferredoxin, revealing NirA is a ferredoxin dependent nitrite reductase (Figure 5.5). Spinach ferredoxin acted as a slightly more efficient electron donor than MV, with a maximal reaction rate of 21.7µmol/min/µmol (µmol of nitrite consumed per minute per µmol of NirA) compared to 18.05 µmol/min/µmol. (Figure 5.5). These figures are lower than previously reported for NirA homologues with spinach NirA reducing 23.1 µmol/min/µmol of nitrite using MV as an electron donor (253).

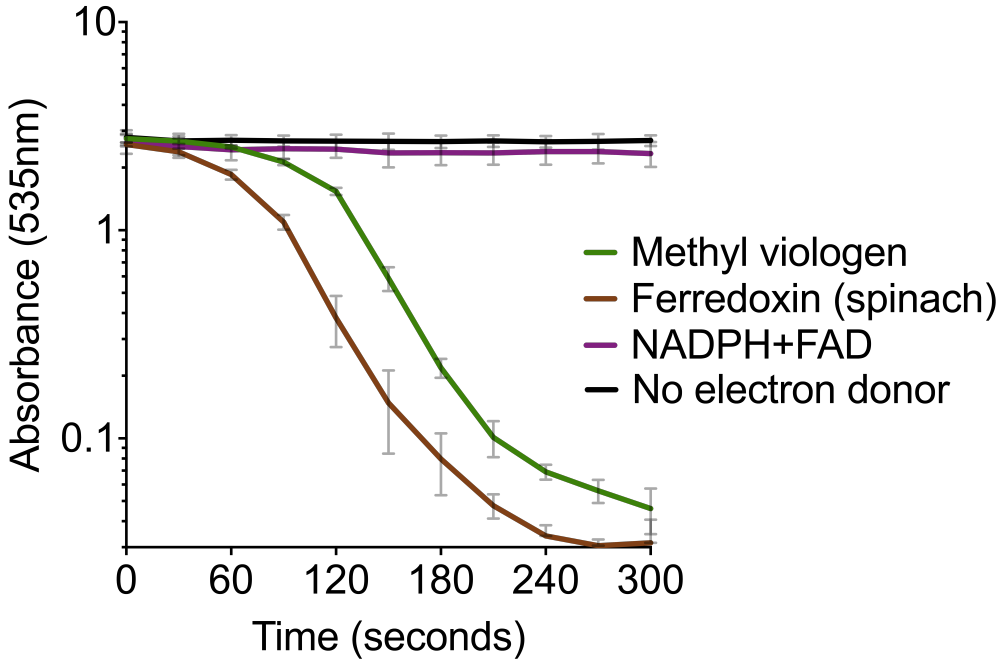

Figure 5.5 – Comparison of nitrite reduction rates using alternative electron donors for NirA-dependent reduction. Remaining nitrite proportional to azo-dye produced in Griess diazotization reaction. Spinach ferredoxin acts as an efficient electron donor for NirA with NADPH unable to facilitate nitrite reduction. Assays performed at 5µm NirA with 8 replicates per time-point using 2 separate preparations. Reactions performed under anaerobic conditions at 37^{O}C. Error bars represent standard deviation.

5.3.1.3 NirA exhibits activity over a broad pH range

With a potential role in redox balancing and thus pH maintenance, NirA was next screened to determine activity at a range of pH values. The same reaction system described above was used with the exception that the Tris.HCl buffer component was varied from pH 6.0-9.0 in increments of 0.5. This demonstrated that NirA has a broad-active pH range, with nitrite reductase activity detected across all conditions, using both MV and reduced spinach ferredoxin as an electron donor (Figure 5.6). NirA activity peaked at pH 7.5, fitting with the prediction that this enzyme is cytoplasmic, with pH maintenance mechanisms ensuring the intracellular environment remains in this range (Figure 5.6).

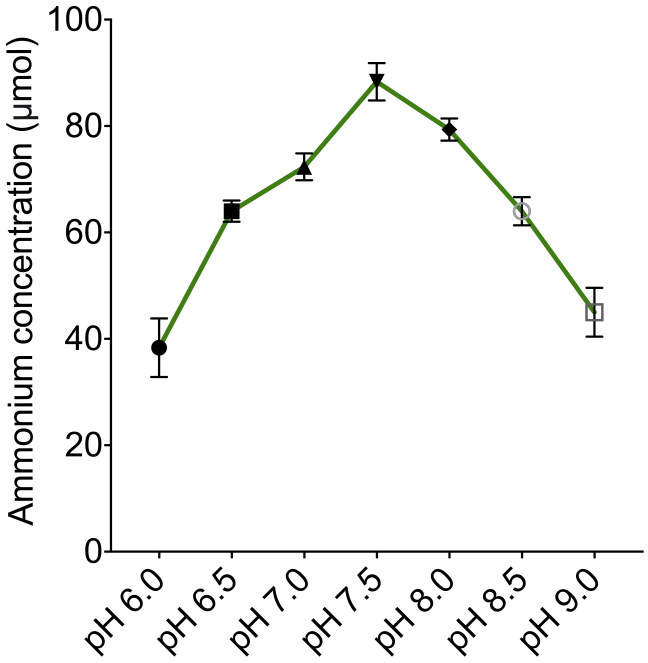

Figure 5.6 – Assessment of ammonium production by NirA at different pH. NirA exhibits maximal activity at physiological pH. Activity exhibited at all pHs tested with a 58% reduction in activity at pH 6.0 and 52% at pH 9.0. Assays performed with 5 replicates and repeated from 2 separate preparations. Error represents standard deviation.

5.3.1.5 High salinity impedes ferredoxin-dependent NirA activity

Ferredoxin interaction with NirA is reported to be stabilised through ionic interactions between a series of acidic residues harboured by the ferredoxin, and basic residues contained by NirA-like enzymes (253). This reaction is transient, allowing delivery of a single electron from the iron-sulphur cluster of the ferredoxin. To confirm these previous observations, nitrite reductase assays were monitored with Griess diazotization in the presence of increasing salinity. As NaCl concentrations increase above 200mM, there is a concomitant drop in nitrite reduction when using reduced ferredoxin as an electron donor (Figure 5.7 I). This coincides with the intracellular Na^+ ion concentration of the bacterial cytoplasm reported to fall in 120-280mM range, although this is heavily dependent on the external environment (254). The presence of Na^+ above these values inhibits formation of the ferredoxin-NirA complex as the NirA interaction sites would be occluded. NirA activity is not affected by salinity

when using MV as an electron donor since this molecule does not rely upon ionic interactions for electron delivery (Figure 5.7 II).

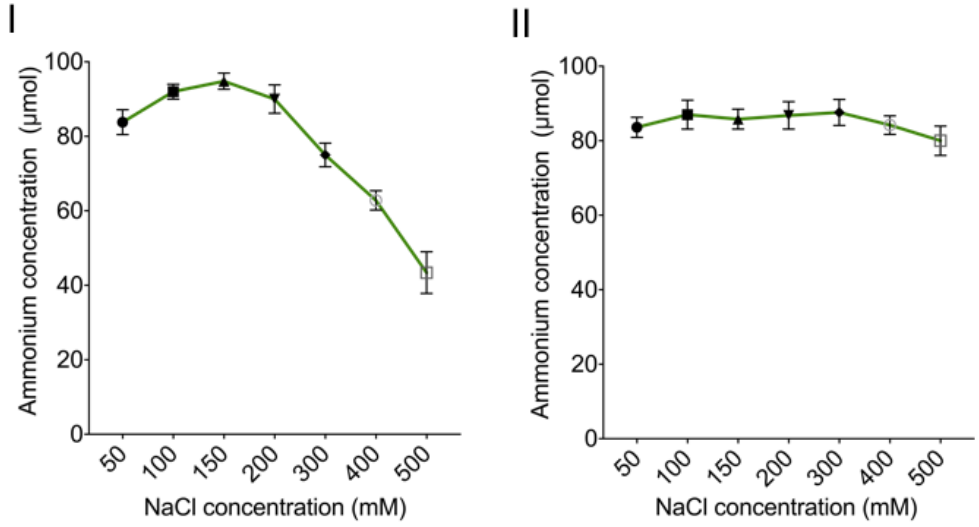

Figure 5.7 – The impact of salinity of ferredoxin-linked and MV-linked nitrite reduction with NirA. I) Ferredoxin-linked nitrite reduction assessed through ammonium production. **II)** MV-linked nitrite reduction assessed through ammonium production. Assays performed with 5 replicates using 2 separate NirA preparations. Error bars represent standard deviation.

5.3.2 NirA utilises 2Fe-2S ferredoxins as electron donors

Ferredoxins are small, usually acidic, proteins harbouring a wide range of iron-sulphur clusters through interaction with cysteine containing motifs. These proteins can accept or discharge electrons, participating in a wide variety of essential redox reactions throughout all domains of life (255). Previous categorisation of these proteins as plant-type 2Fe-2S and bacterial-type 4Fe-4S ferredoxins has been shown to be outdated since multiple bacteria possess a wide-range of ferredoxins, including plant-type 2Fe-2S type (256). Ferredoxins are usually classified depending on both sequence similarity, the nature of the iron-sulphur clusters and how many it harbours. This allows separation into 4 main categories, the [2Fe-2S], [4Fe-4S], 7Fe and 2[4Fe-4S] dicluster-type ferredoxins (255).

5.3.2.1 P. aeruginosa *contains multiple ferredoxins*

Whilst use of spinach ferredoxin demonstrates that NirA requires these proteins for electron transfer, the native interaction partners of many of these ferredoxins is unknown. Spinach ferredoxin is a 2Fe-2S-type however, it is possible that NirA utilises a wide range of these protein *in situ*. Purified spinach ferredoxin is also extremely expensive. Therefore, in order to use a ferredoxin-linked nitrite reduction assay as a screen for NirA inhibitors, determination and purification of the native ferredoxin required would be advantageous to keep costs down for high-throughput screening.

Screening of pseudomonas.com for ferredoxins revealed a total of 12 annotated ferredoxins (Table 5.1) (257). In some instances, these are not true ferredoxins. Some larger proteins and enzymes contain ferredoxin-like domains with iron-sulphur clusters inserting as prosthetic groups in multiple enzymes, including NirA (255). After eliminating such targets, *P. aeruginosa* still contains 9 proteins annotated as ferredoxins, serving as potential NirA electron donors. Since over-expression, purification and assessment of this number of proteins is unfeasible during the time constraints of a UK based PhD, a member of each ferredoxin family from the *P. aeruginosa* genome was selected for purification. Fdx1, Fdx2, FdxA, NapF and HcnA were targeted based on similarity of expression profiles using the work of Ortega and colleagues (258). These ferredoxins have been demonstrated to be upregulated in response to oxygen limitation or play a role in nitrate metabolism, thus are likely to be upregulated under similar conditions to *nirA* (258, 259). The ferredoxins selected for purification represent major families of ferredoxin. Fdx1 is a short 2[4Fe-4S]; Fdx2 a [2Fe-2S]; FdxA a 7Fe; HcnA a [2Fe-2S]; and NapF a long 2[4Fe-4S] di-cluster ferredoxin. Whilst HcnA is also a [2Fe-2S] ferredoxin, this target was selected as cyanogenesis has been shown to upregulate NirA.

Gene name	PAO1 designation	Length (bp)	Associated role
fdx1	**PA0362**	252	Short 4Fe-4S dicluster ferredoxin. Function undefined but essential for *P. aeruginosa* under lab conditions
napF	**PA1179**	492	Long 4Fe-4S dicluster ferredoxin. Functions in periplasmic nitrate reduction with *nap* system.
-	PA1551	1416	Iron-sulphur protein with ferredoxin-like domain. Cytochrome-c-oxidase accessory component of unknown function.
-	PA1931	513	2Fe-2S cluster ferredoxin associated with uncharacterised aldehyde oxidase.
hcnA	**PA2193**	315	2Fe-2S cluster ferredoxin. Part of HCN synthesis operon with HcnBC. Deletion inhibits HCN production.
-	PA2297		4Fe-4S dicluster ferredoxin in operon with an uncharacterised fumarate reductase/ succinate dehydrogenase.
-	PA2715	339	7Fe centre ferredoxin upregulated alongside molybdopterin binding oxidoreductase of unknown function
-	PA3490	567	4Fe-4S dicluster ferredoxin for the NADH:ubiquinone respiratory chain complex involved with reduction of SoxR
bfd	PA3530	222	2Fe-2S cluster ferredoxin associated with bacterioferritin. Facilitates release of Fe2+ from ferritin as needed.
fdxA	**PA3621**	324	7Fe cluster ferredoxin. Function is poorly defined although appears to be important during denitrification.
fdx2	**PA3809**	339	2Fe-2S cluster ferredoxin upregulated alongside the isc iron-sulphur cluster biogenesis pathway. Non-essential under lab conditions
-	PA4772	2817	FAD-linked oxidoreductase of unknown function harbouring a ferredoxin-like domain.

Table 5.1 – Identification of genes annotated as ferredoxins using PAO1 as the reference genome on pseudomonas.com.

5.3.2.2 Construction of ferredoxin overexpression vectors

Vector pSK67 was selected as an over-expression vector for the ferredoxins. A N-terminal hexa-histidyl tag was added to each ferredoxin DNA sequence using PCR with primer pairs Hfdx1F1/R1, Hfdx2F1/R, HfdxAF1/R1, HnapFF1/R1 and HhcnAF1/R1. The newly synthesized fragments were then inserted into pSK67 by restriction digest using EcoR1 and SacI, with the exception of *fdxA* which used NcoI and XhoI. This resulted in formation of pSJF05 (pSK67::6XH-*fdx1*), pSJF06 (pSK67::6XH-*fdx2*), pSJF07 (pSK67::6XH-*fdxA*), pSJF08 (pSK67::6XH-*napF*) and pSJF09 (pSK67::6XH-*hcnA*).

5.3.2.3 Overexpression and purification of Fdx1, Fdx2, FdxA, HcnA and NapF ferredoxins

To ensure the ferredoxin over-expression vectors are functional, all were transformed into *E. coli* Suf++ (DE3). Initial induction trials with 1mM IPTG revealed successful expression of Fdx2, FdxA, NapF and HcnA when visualised using a 16% Tricine gel (Figure 5.8 I). Fdx1 expression was not detected however, this was assumed to be due to either low expression or a lack of resolution with the gel used. Fdx1 has a predicted molecular weight of 8.2kDa. Whilst Tricine gels are used to resolve proteins as low as 4 kDa, detection becomes difficult below 10kDa. Despite not being able to visualise the Fdx1 band via Tricine SDS-PAGE from whole cell lysate, it was presumed to be successfully expressed due to the red/brown colouration of the pellets following induction.

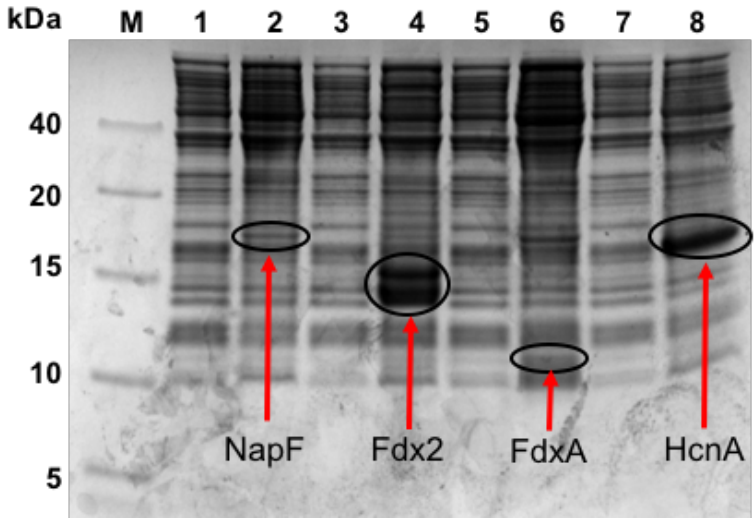

Figure 5.8 – Whole cell ferredoxin induction from PSJF07, PSJF08 and PSJF09 using *E. coli* Suf++ (DE3) as an expression host. Strains cultured in terrific broth supplemented with 0.5mM $FeS_O4.6H_20$ and induced with 1mM IPTG for 4 hours at 30^OC. Lane M – Spectra low-range molecular weight ladder; lanes 1, 3, 5 and 7 show samples pre-IPTG addition; lanes 2, 4, 6 and 8 show 4h post IPTG induction. Red arrows indicate bands corresponding to *P. aeruginosa* ferredoxins with.

For initial assessment of electron donor activity with NirA only small amounts of ferredoxin will be required. This renders the laborious and time-consuming procedure of optimising ferredoxin overexpression at this stage obsolete. Once the NirA interaction partner has been identified, optimisation of target

ferredoxin overexpression can begin to enable large quantities to be produced for inhibitor screening assays. For initial purifications *E. coli* Suf++ (DE3) harbouring each of the overexpression vectors were cultured to an OD_{600nm} of 0.8 in 1L of Terrific broth supplemented with 0.5mM of iron sulphate heptahydrate. Samples were then induced with 0.5mM IPTG and harvested after 4 hours. Attempted IMAC purification of these ferredoxins demonstrated variable results. Fdx1, Fdx2 and HcnA were selectively purified to a high level at 3mg/L, 32mg/L and 4.2mg/L respectively (data not shown). The 7Fe ferredoxin FdxA was purified however, only with an extremely low yield of 0.25mg/L of culture All samples were contaminated and require further purification methods downstream before use in inhibitor identification. Purification of NapF proved unsuccessful with all of the overproduced ferredoxin found in the insoluble fraction. Whilst this is usually due to translational defects, the red/brown coloration demonstrated by induced *E. coli* Suf++ (DE3) pSJF08 pellets indicates successful translation of NapF. Homologues of this ferredoxin have been shown to be membrane associated proteins appearing as part of the insoluble fraction whilst *P. aeruginosa* NapF potentially remains associated with the *E. coli* membrane. Attempts to liberate NapF with mild detergents such as CHAPS and Triton X-100 during lysis and IMAC purification were unsuccessful. Due to time constraints following the SARS-COV2 pandemic, purification of NapF was abandoned as Fdx1 is also a 2[4Fe-4S] ferredoxin.

5.3.2.4 Spectral properties of purified ferredoxins

As seen with NirA, the presence of prosthetic groups such as siroheme and iron-sulphur clusters can be detected by UV-visible spectroscopy. *E. coli* Suf++ (DE3) has been shown to enhance iron-sulphur cluster formation and insertion (226). To ensure the ferredoxins purified contain these elements all samples, were desalted and buffer exchanged into 25mM Tris.HCl pH 7.4 with 50mM NaCl and concentrated to 1mg/ml. UV-visible spectroscopy of Fdx1 demonstrated a shoulder at 320nm with a broad peak at 405nm, consistent with previously purified Fdx1 homologues from other bacteria and archaea (Figure 5.10 I) (260). Both Fdx2 and HcnA possess spectral patterns in line with spinach [2Fe-2S]-type ferredoxin, with a shoulder at 320nm and peaks at 415nm and 460nm (Figure 5.10 II). The 7Fe ferredoxin FdxA possesses a

similar spectral profile to Fdx1 with a broad peak at 407nm however, the 320nm peak appears to be split between 315-330nm (Figure 5.10 I) (261). This asymmetry could perhaps indicate that this ferredoxin is found in both an oxidised and reduced form. These profiles are similar to previously published UV-visible spectrum obtained for 2Fe-2S, 4Fe-4S dicluster and 7Fe ferredoxins and was used as confirmation of protein identity.

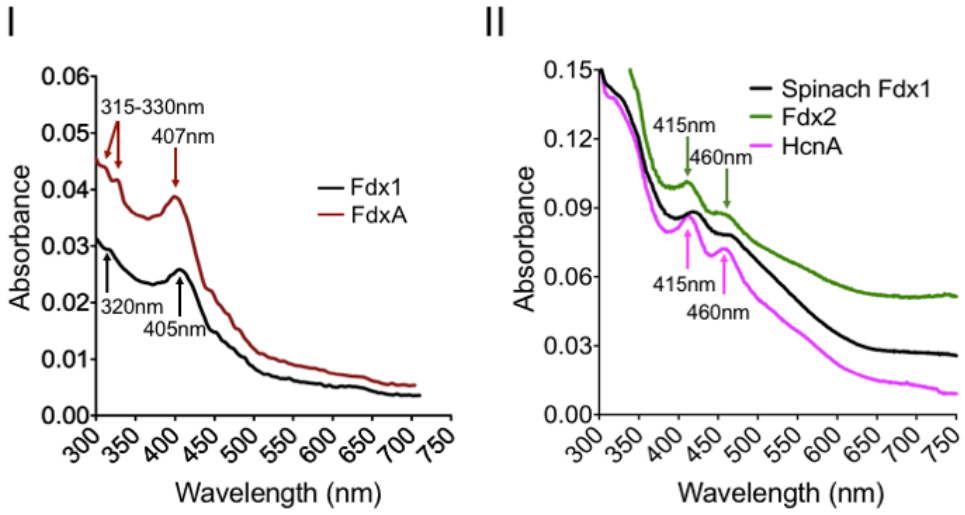

Figure 5.10 – UV-visible spectrum of purified *P. aeruginosa* ferredoxins. I) Similar profiles were generated for Fdx1 and FdxA with both ferredoxins containing 2 separate iron-sulphur clusters. **II**) Spectrums generated for the 2Fe-2S type ferredoxins, Fdx2, HcnA and spinach Fdx1.

5.3.2.5 NirA nitrite reduction is dependent on [2Fe-2S] ferredoxins

To determine which type of ferredoxin NirA utilises, the previously conducted nitrite reductase assay was repeated with the newly purified electron donors. Same-day ferredoxin preparations were used for these assays to minimise any degradation artefacts, as it had been observed that the UV-visible spectrum of Fdx1 degrades after O/N storage at 4^{O}C. Tracking of nitrite consumption revealed that NirA can only use [2Fe-2S] ferredoxins as electron donors with spinach ferredoxin and *P. aeruginosa* Fdx2 allowing the efficient reduction of nitrite (Figure 5.11). Fdx1 and FdxA did not enable nitrite reduction thus ferredoxins of this type are unlikely to act as electron donors for NirA (Figure 5.11). It is possible that these ferredoxins iron-sulphur clusters are oxygen sensitive with the presence of oxygen during purification inactivating these proteins. Purification of Fdx1 and FdxA needs to be performed under anaerobic

conditions and reassessed with NirA to rule out these ferredoxins at electron donor. With NirA utilising Fdx2 as an electron donor, further optimisation of purification will not be needed as 1L of terrific broth yields 36mg of Fdx2. The ease of purification makes it ideal for use as an electron donor in future high-throughput NirA inhibitor screens, where large amounts of Fdx2 will be required.

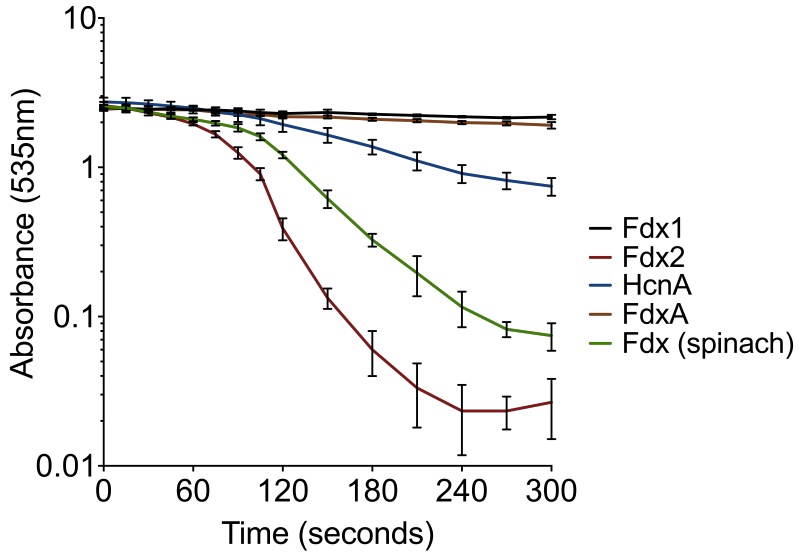

Figure 5.11 – NirA nitrite reductase assays using various *P. aeruginosa* ferredoxins as electron donors. Only 2Fe-2S type ferredoxins act as NirA electron donors. Fdx2 facilitates reduction of nitrite at a rate of 23.65µmol/min/µmol (µmol of nitrite consumed per min per µmol of NirA), compared to spinach ferredoxin (16.5µM/min/µM) and HcnA (7.2µM/min/µM). Assays performed with 6 replicates at each time point under anaerobic conditions at 30^{O}C. Each individual assay contained 2µm NirA and 60µm of ferredoxin. Error bars represent standard deviation.

Interestingly, the [2Fe-2S] ferredoxin HcnA was also able to act as an electron donor. However, it facilitated nitrite reduction at a rate of only 7.2 µM/min/µM (µmol of nitrite consumed per minute per µmol of NirA) compared to spinach ferredoxin and Fdx2 at 23.65µM/min/µM and 16.5 µM/min/µM respectively (Figure 5.11). The reason for this discrepancy was not explored further, although it is likely to be due to the fact HcnA is not an acidic ferredoxin. HcnA predicted pI is 8.22 compared to the spinach ferredoxin and Fdx2 with a reported pI's of ~4. This underpins its function in HCN biosynthesis where it has a poorly characterised role in the oxidation of glycine to HCN (262). It is hypothesised that HcnA acts as an electron acceptor in this reaction and thus may not be an efficient electron donor at physiological pH.

5.4 Conclusions

The previously hypothetical protein PA4130 has been demonstrated to encode a ferredoxin-nitrite reductase and was renamed NirA. 2Fe-2S type ferredoxins are the preferred electron donor however, commercial purified ferredoxin (spinach) is an expensive resource, complicating development of a cost effective high throughput screening assay for inhibitor screening. The discovery that *P. aeruginosa* Fdx2 is an efficient redox partner alleviates this potential financial issue whilst also representing a more realistic reaction model for inhibitor identification. One key principle in virulence inhibitor identification is that the target must be highly specific to the organism. *P. aeruginosa* NirA-type are broadly conserved in bacteria. However, most are multimeric NADPH-dependent nitrite reductases. Whilst the active sites of ferredoxin and NADPH-dependent nitrite reductases are conserved, the electron donor binding sites are variable. This means targeting of NirA-ferredoxin binding may enable discovery of a more selective virulence inhibitor. How NirA contributes to *P. aeruginosa* is currently unknown. Various aspects of nitrate metabolism have been demonstrated to contribute to virulence and virulence factor production. The role NirA plays alongside these other nitrite reductases will be explored in Chapter 6.

Chapter 6

Interplay between the ammonium-forming nitrite reductases and cyanogenesis.

6.1 Introduction

P. aeruginosa is a metabolically flexible organism capable of using a wide array of carbon and nitrogen sources. The control of carbon and nitrogen source use is predominantly mediated by the two-component regulatory systems CbrAB and NtrBC respectively (263). Deletion of either of these regulators compromises the use of a large subset of C and N sources, with loss of *ntrBC* abolishing or retarding the use of multiple compounds as single N sources including, nitrate, nitrite, L-tryptophan, L-tyrosine and uridine (263, 264). Utilisation of these carbon and nitrogen sources has been demonstrated to play a key role in survival in diverse environments. This includes *in vivo,* with *cbrAB* and *ntrBC* required for colonisation and virulence in murine lung infections models (264-266). Interestingly succinate, L-glutamine, L-glutamate, L-aspartate, glycerol, fumarate, α-ketoglutarate and L-asparagine were not subject to control by CbrAB or NtrBC (263). Whilst these compounds can still be used as N sources, the lack of carbon catabolite repression suggests they are the preferred carbon sources for *P. aeruginosa*.

6.1.1 Loss of nitrate reduction attenuates P. aeruginosa virulence

The attenuated virulence shown by both *cbrAB* and *ntrBC* mutants demonstrates that these preferred carbon and nitrogen sources are not enough to support infection *in vivo*. Secondary sources such as host derived amino acids, nitrite and nitrate are also important for *P. aeruginosa* colonisation and infection (264, 267). Deletion of *nirA* has been shown to compromise *P. aeruginosa* virulence in multiple *in vivo* models suggesting this aspect of nitrite reduction is important for disease progression (Figures 3.17-20). This is not limited to NirA, various components of the nitrate reduction pathways have been demonstrated to influence virulence factor production and compromise *in vivo* virulence. Deletions in *narGH* and *nirS* of the denitrification pathway resulted in decreased swarming motility, reduced cytotoxicity in a THP-1 phagocyte model of infection and compromised virulence in *C. elegans* (268, 269). The role these reductases play in virulence are usually linked to their role in anaerobic respiration, with physiological concentrations of nitrate shown to support anaerobic and micro-aerobic growth *in vitro* (270). Interestingly the

virulence phenotypes described for a *nirS* mutant are very similar to *nirA* interrupted strains, and these phenotypes are observed under aerobic conditions in the absence of nitrate (269). The reduced virulence of both *narGH* and *nirS* mutants has been linked to downregulation of T3SS expression however, this was shown to be dependent on nitric and nitrous oxide production (268, 269). This would suggest that NirA does not employ the same mechanism to regulate virulence in *P. aeruginosa* as the end product of reduction is ammonium, although like NirS, there is an unexplored aerobic regulatory role.

The role of ammonium-forming nitrite reductases in disease has remained unexplored in *P. aeruginosa*. Limited studies in *M. tuberculosis* suggest enzymes of this type are important for protection in oxygen-limited environments during dormancy (271, 272). With maximal expression of NirA presumed to be under micro-aerobic conditions, it may suggest this enzyme plays a similar role, protecting *P. aeruginosa* during periods of reduced oxygenation. However, the function of NirBD with regards to virulence factor production and virulence has never been explored. To elucidate if the virulence phenotypes observed in a *nirA* mutant are specific to this protein function or the wider nitrate reduction pathway, the function of this nitrite reductase must be compared to that of NirBD and NirS. This will allow a virulence mechanism to be defined and inform proper use of any future anti-virulence compounds potentially targeting NirA.

6.1.2 P. aeruginosa *nitrite reductases are differentially regulated*

With the discovery that PA4130 encodes a nitrite reductase, *P. aeruginosa* has now been demonstrated to express three structurally distinct nitrite reductases, NirS, NirBD and NirA. NirS participates in the denitrification nitrite reduction pathway, facilitating detoxification of nitrite to gaseous dinitrogen and enabling anaerobic respiration with nitrate as a terminal electron acceptor (Figure 6.1) (273). NirA and NirBD are ammonium-forming nitrite reductases catalysing the reduction of nitrite to ammonium. Whilst NirA and NirBD are structurally distinct they both rely upon the same prosthetic groups, siroheme and a 4Fe-4S iron-sulphur cluster. All of these nitrite reductases exhibit distinct regulatory mechanisms ensuring expression under the correct environmental conditions. This is especially important for distinguishing the roles of NirA and NirBD, with

both reductases performing the same molecular function, albeit with different electron donors.

6.1.2.1 Regulation of nirS *and denitrification*

NirS is a dimeric periplasmic nitrite reductase requiring cytochrome C and *d1* haem to facilitate electron transfer (274). These enzymes are structurally similar to cytochrome C oxidase sub-unit III, which facilitate the use of oxygen for respiration. Regulation of *nirS* is well characterised with the FNR-type regulators DNR and ANR controlling expression of the *nirSMCF*-PA0515-*nirLGHJEN* operon (275). ANR and DNR regulation is hierarchal, with ANR required for *dnr* expression (Figure 6.1) (276). These regulators bind to the same recognition sequences however; they respond to different regulatory signals with divergent mechanisms resulting is governance of overlapping, but distinct, regulons (277).

ANR is responsive to the presence of oxygen through the use of a surface exposed iron-sulphur cluster. In the absence of oxygen, ANR contains a reduced $[4Fe\text{-}4S]^{2+}$ cluster required for dimerization and thus binding to the *dnr* promoter. When oxygen is present this iron-sulphur cluster is oxidised and degrades to a $[2Fe\text{-}4S]^{+}$, with prolonged incubation destroying this prosthetic group and inhibiting dimerization (278). DNR is responsive to the presence of nitric oxide and also contains this surface exposed iron-sulphur cluster which may also be sensitive to oxygen. However, since ANR governs expression of this regulator it will only be expressed under oxygen limiting conditions. NO sensing is mediated by the ability of DNR to bind ferrous haem, with NO binding to the haem prosthetic group triggering a conformational change which enables upregulation of *nirS* and *norBC* nitrite and nitric oxide reductases (Figure 6.1) (279, 280). ANR has also been shown to directly activate the NirS promoter at a low level, accounting for the production of NO required to trigger DNR mediated expression of *nirS* (275).

Whilst the ANR-DNR system for *nirS* regulation is the most comprehensibly studied, it is by no means the only regulatory system shown to influence *nirS*. Quorum sensing systems have been shown to influence *nirS* expression, with the las, *rhl* and *pqs* systems all repressing denitrification (281, 282). However,

without any recognised LasR, RhlR and PqsR binding sites, the mechanism behind this regulation has yet to be determined. Carbon source metabolism also influences expression of denitrification apparatus with growth on acetate positively regulating all components of this system. This is mediated through higher levels of *narXL* and *dnr* expression, although these results are surprising since growth was performed under aerobic conditions, perhaps suggesting DNR is not inactivated by the presence of oxygen like other members of the FNR-family (283).

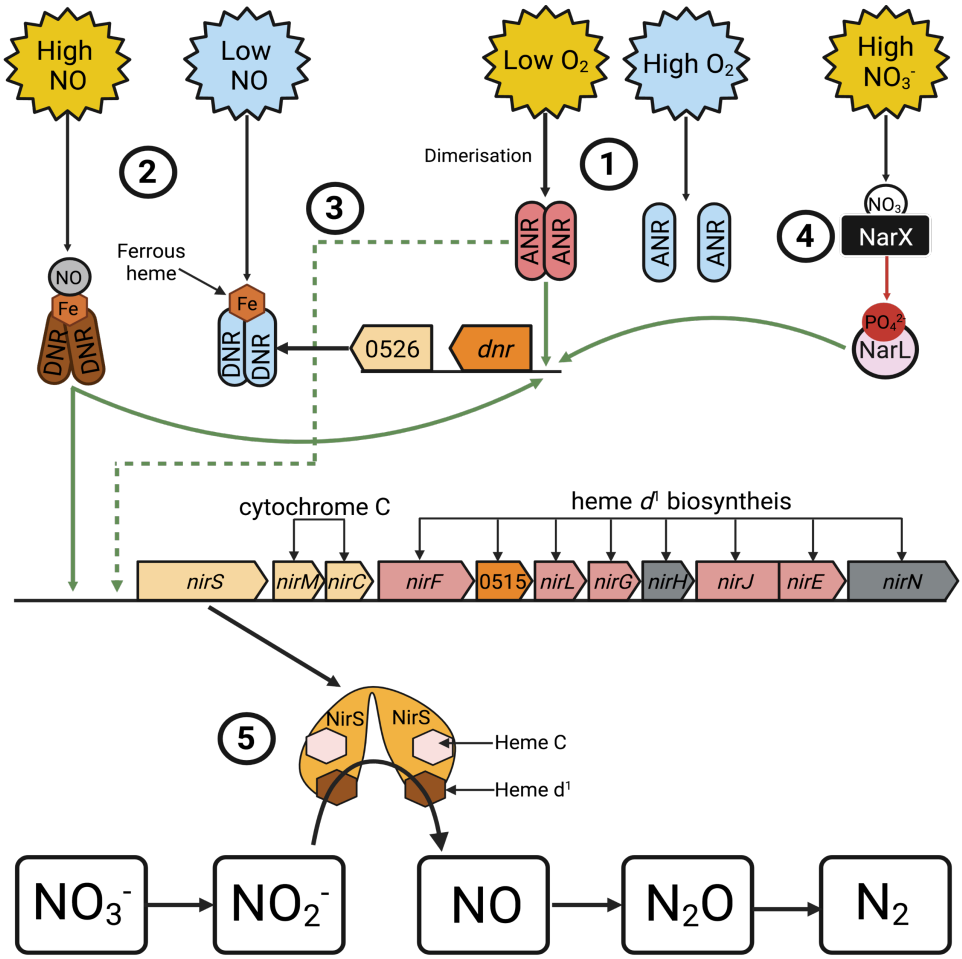

6.1 – Regulation and function of *P. aeruginosa* Nitric oxide-forming nitrite reductase NirS. 1) Under low oxygen conditions the oxygen labile iron-sulphur cluster of ANR is reduced, allowing formation of the active dimeric regulator. **2)** Dimeric ANR activates low-level expression of *nirS*, enabling production of NO when nitrite is present. **3)** ANR also upregulates DNR, a specialised FNR-type regulator which binds ferrous heme. This heme group binds NO produced through ANR dependent NirS expression. NO-binding triggers a conformational change in the DNR, allowing transcriptional upregulation of itself and *nirS*. **4)** In the presence of nitrate, NarX phosphorylates the response regulator NarL, enhancing *dnr* transcription. **5)** NirS utilises heme C and the specialised heme d1 to form an electron transport change, facilitating the reduction of nitrite to nitric oxide.

6.1.2.2 Regulation of ammonium-forming nitrite reductases

Ammonium-forming nitrite reductases are usually associated with anaerobic metabolism, largely due to work on the prototype Enterobacteriaceae *E. coli*. Like *P. aeruginosa*, *E. coli* encodes two ammonium-forming nitrite reductases, the *nirBD* and *nrfABCDEFGH* system. The *nirBD* system is conserved amongst bacteria, with a siroheme-containing subunit (NirB) and flavin-binding sub-unit (NirD) facilitating the 6-electron reduction from nitrite to ammonium using NADH as an electron donor. NrfA is a membrane associated respiratory cytochrome C552 nitrite reductase conserved in Enterobacteriaceae. This enzyme forms a redox loop with formate dehydrogenase whereby reduction of nitrite is coupled to formate oxidation allowing generation of membrane potential for energy generation. In *E. coli* both systems are upregulated by FNR in response to low-oxygenation, with high levels of nitrate maximising *nirBD* expression, and lower levels of nitrate enhancing *nrfABCDEFGH* transcription. This fits with the physiological roles of these nitrite reductases, whereby by *nirBD* expression is only triggered when nitrate or nitrite concentrations are beyond the ability of *E. coli* to process and detoxify. Whilst *nrfABCDEFGH* is induced when oxygen and nutrients are limiting enabling generation of energy and maintenance of N sources through dissimilatory nitrate reduction to ammonium (DNRA).

The genetic components constituting nitrate or nitrite reduction differ in *P. aeruginosa*, with the order Pseudomonales not encoding NrfA-type respiratory nitrite reductases. Until the discover of NirA, NirBD was assumed to be the only ammonium-forming nitrite reductase, performing the assimilatory, DNRA and detoxification roles accounted for by NirBD and NrfA in *E. coli*. In *P. aeruginosa*, there is no oxygen-dependent regulation of *nirBD*. Expression of the *nirBD-PA1779-cobA* operon is dependent on three regulators; the sigma factor RpoN, NtrBC and the NasST system (284). NtrBC responds to low N source availability, with the membrane bound histidine kinase NtrBC phosphorylating NtrC, enabling binding to a NtrC box located in the *nirBD* promoter (Figure 6.2). NasST responds to the presence of nitrate and nitrite using a transcriptional anti-termination mechanism. Preceding the *nirBD-PA1779-cobA* operon is the non-coding RNA *nalA* responsible for terminating transcription by RNA polymerase through formation of a stem-loop. When Nitrate or nitrite are not

present, NasT remains bound to NasS however, in the presence of either substrate, NasT is displaced and binds to the *nalA* region. This inhibits formation of the stem-loop responsible for transcriptional termination (284) (Figure 6.2). Both the NtrBC and NasST systems operate to ensure NirBD is only expressed under conditions of low N source availability in the presence of nitrate (Figure 6.2). In the absence of the *nalA-nirBD-PA1779-cobA* system, *P. aeruginosa* loses the ability to grow using nitrate as a single N source confirming that this operon is responsible for assimilatory nitrate reduction (284).

Prior to this study it was not known that NirA was a nitrite reductase, therefore the effect of nitrate or nitrite on *nirA* regulation has never been explored. Understanding if a relationship exists between substrate availability and *nirA* induction will be key to determining the role this enzyme plays in nitrate reduction and virulence. The *nirA*-PA4129 operon is upregulated in response to HCN in the absence of nitrate or nitrite, with quorum-sensing and ANR maximising production of this secondary metabolite (199, 208) (Figure 6.2). As a result, NirA is maximally expressed at high cell-densities and low oxygenation (199). Upregulation of *nirA* by cyanide is peculiar since HCN has been demonstrated to be a potent inhibitor of both cytochrome c and heme containing enzymes (205, 274, 285). With NirA containing siroheme as a prosthetic group, it appears this enzyme is upregulated by its own inhibitor.

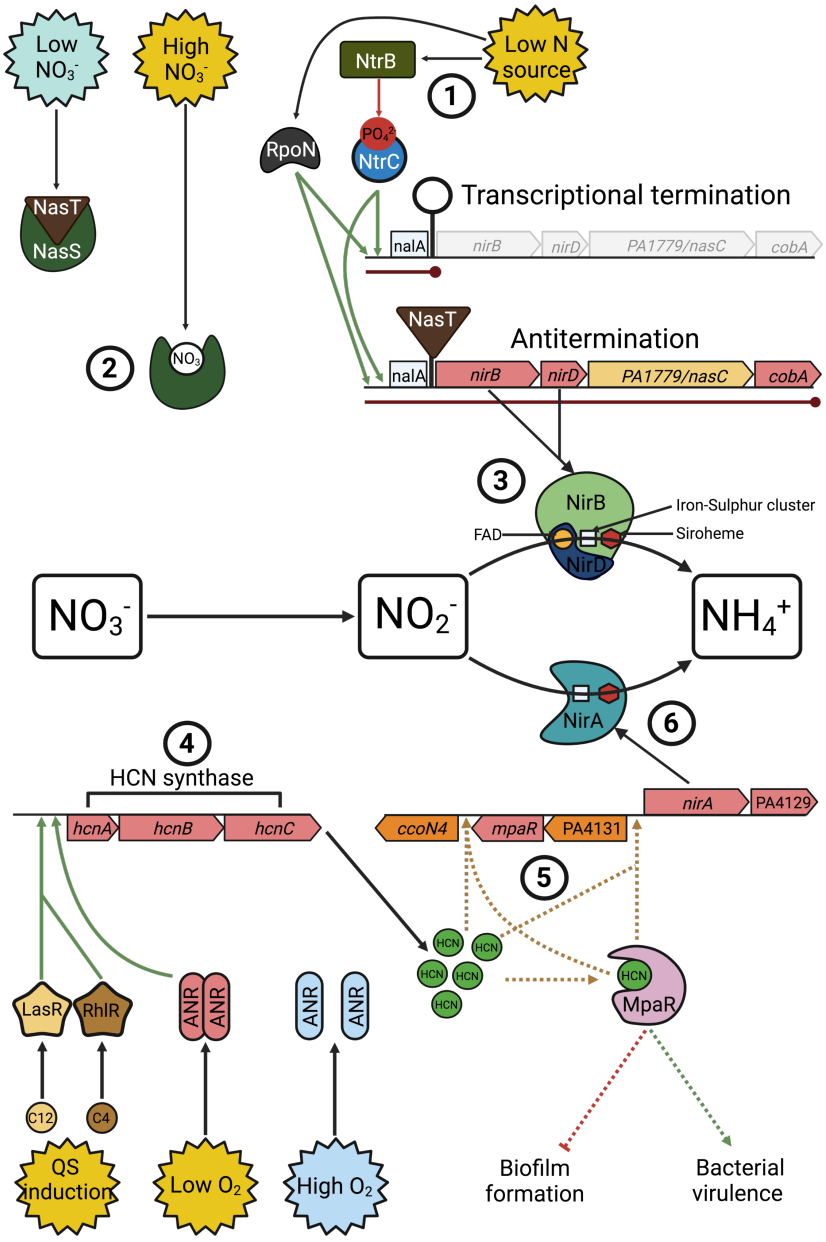

Figure 6.2 – Regulation and function of *P. aeruginosa* ammonium-forming nitrite reductases NirA and NirBD. 1) Low level of nitrogen sources such as L-glutamate activates sigma factor RpoN and triggers NtrB to phosphorylate NtrC, activating the *nalA-nirBD*-PA1779-*cobA* promoter. **2)** In the presence of nitrate, the anti-termination protein NasT is displaced from NasS and subsequently binds to the hairpin loop formed in the ncRNA nalA, enabling transcription of *nirBD* and the remainder of the operon. **3)** Functional nitrite reductase consists of the heme containing sub-unit NirB and Flavin-binding protein NirD. Electrons derived from NADH delivered to Flavin of NirD, and subsequently shuttled from the iron-sulphur cluster and siroheme of NirB reducing nitrite to ammonium. **4)** Transcription of *nirA* is induced by production of cyanide, which itself is under the control of multiple transcriptional and post-transcriptional regulators. Key environmental stimuli for maximal HCN production are high cell density and low oxygen tensions, mediated by the las/rhl QS circuit and dimerised ANR. **5)** Transcriptional activation of the PA4129-34 region is induced by cyanide with an unconfirmed mechanism. Likely that MpaR recognises HCN and binds to promoters upstream of *nirA*, *mpaR* and *ccoN4*, although direct transcriptional activation by HCN cannot be ruled out**. 6)** Functional NirA derives electrons from reduced ferredoxin. Electrons delivered to iron-sulphur cluster of NirA and passed onto siroheme catalysing the reduction of nitrite to ammonium.

6.2 Aims of this chapter

The attenuation in multiple *in vivo* models exhibited by a *nirA* mutant, combined with the previously observed reduction in virulence with other components of the nitrate reductase pathway, suggests that the targeting of nitrate reduction is a viable anti-virulence strategy. However, numerous questions surround the function of NirA, and how it fits into the nitrate reduction and wider virulence of *P. aeruginosa*. Hence, to begin to elucidate the complexities of the three nitrite reductase systems and how they overlap, this chapter aims to:

1. Explore the overlap and differences in NirA, NirBD and NirS function.
2. Determine whether NirA participates in assimilatory or the DNRA nitrate reduction pathway.
3. Understand how cyanide influences NirA from both a regulatory and functional standpoint.

6.3 Results

6.3.1 NirA is not an assimilatory nitrite reductase

6.3.1.1 NirB and NirAB mutant construction

In order to understand how NirB impacts virulence factor production and functionally overlaps with NirA and NirS, a clean in-frame *nirB* deletion was constructed in PAO1-L and PAJD25. To construct the *nirB* deletion suicide vector the upstream 762bp and downstream 795bp regions of this gene were amplified and fused together with overlap extension PCR. The upstream fragment was amplified using primer nirBF1, modified with an EcoRI restriction site and nirBR1, containing the first 18 nucleotides of *nirB* with an overhanging end containing the last 15 nucleotides of the *nirB* ORF. The downstream fragment was amplified with nirBF2, containing the first and last 15 nucleotides of *nirB* and nirBR2, modified with a HindIII restriction site. These 2 fragments were linearized using the engineered homologous overlap regions and served as a template for overlap PCR with nirBF1/nirBR2. The final PCR product was

cloned into pME3087 using the EcoR1 and HindIII restriction sites, forming suicide-vector pME*nirB*. This vector was mobilised into PAO1-L and PAJD25 with conjugation, and an in-frame deletion mutants generated by allelic exchange forming strains PASF10 (*ΔnirB*) and PASF11 (*ΔnirAB*). Construction of a *nirS* deletion vector was interrupted by the SARS-Cov-2 pandemic and was not completed in time for submission of this thesis.

6.3.1.2 NirA is not required for growth during N source limitation

To understand the intricacies in NirA and NirB nitrogen source utilisation for *P. aeruginosa*, strains PAO1-L, PAJD25, PASF10 and PASF11 were grown in MOPS-succinate minimal media with individual nitrogen sources under aerobic conditions. Cultures were inoculated to an OD_{600nm} of 0.05 and grown at 37^{O}C with aeration at 200rpm. When ammonium chloride was supplemented as a nitrogen source all strains reached an OD_{600nm} of ~1.2, with no difference in growth kinetics exhibited (Figure 6.3 I). In the presence of both potassium nitrate and nitrite, all strains harbouring a *nirB* deletion (PASF10 and PASF11) were unable to grow, whilst PAJD25 demonstrated wild-type growth (Figure 6.3 II-III). When grown in LB supplemented with 10mM nitrate and nitrite, all mutants harbouring a *nirA* mutation (PAJD25 and PASF11) demonstrated a reduction in OD_{600nm} upon entry into stationary phase as seen with addition of nitrate to ASM (Figures 3.6 and 3.7). PASF10 was unaffected by addition of all nitrate and nitrite in LB, reflecting the availability of alternative nitrogen sources in this rich media (Figure 6.4). The lack of growth in *nirB* deletion mutants on nitrate and nitrite as a single source confirms that this enzyme functions as an assimilatory nitrite reductase and that NirB alone was required for assimilation. NirA was unable to functionally compensate for the absence of NirB under these conditions, thus NirA is unlikely to be an assimilatory nitrite reductase.

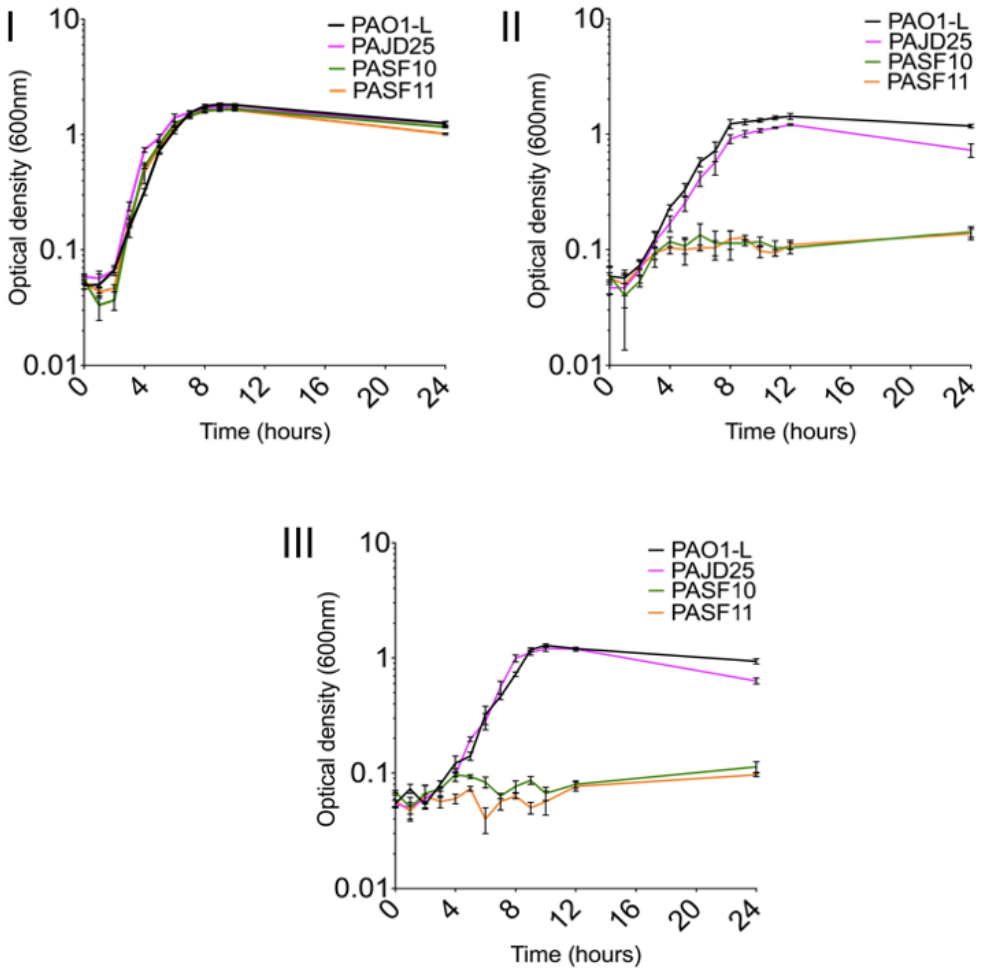

Figure 6.3 - Growth kinetics of *P. aeruginosa* nitrite reductase mutants in MOPS-succinate-minimal media under aerobic conditions. Cultured with 10mM ammonium (**I**), 10mM nitrite (**II**) and 10mM nitrate (**III**) as a single nitrogen source. Growth assessed using 5 biological replicates with 2 independent experiments. Error represents standard deviation.

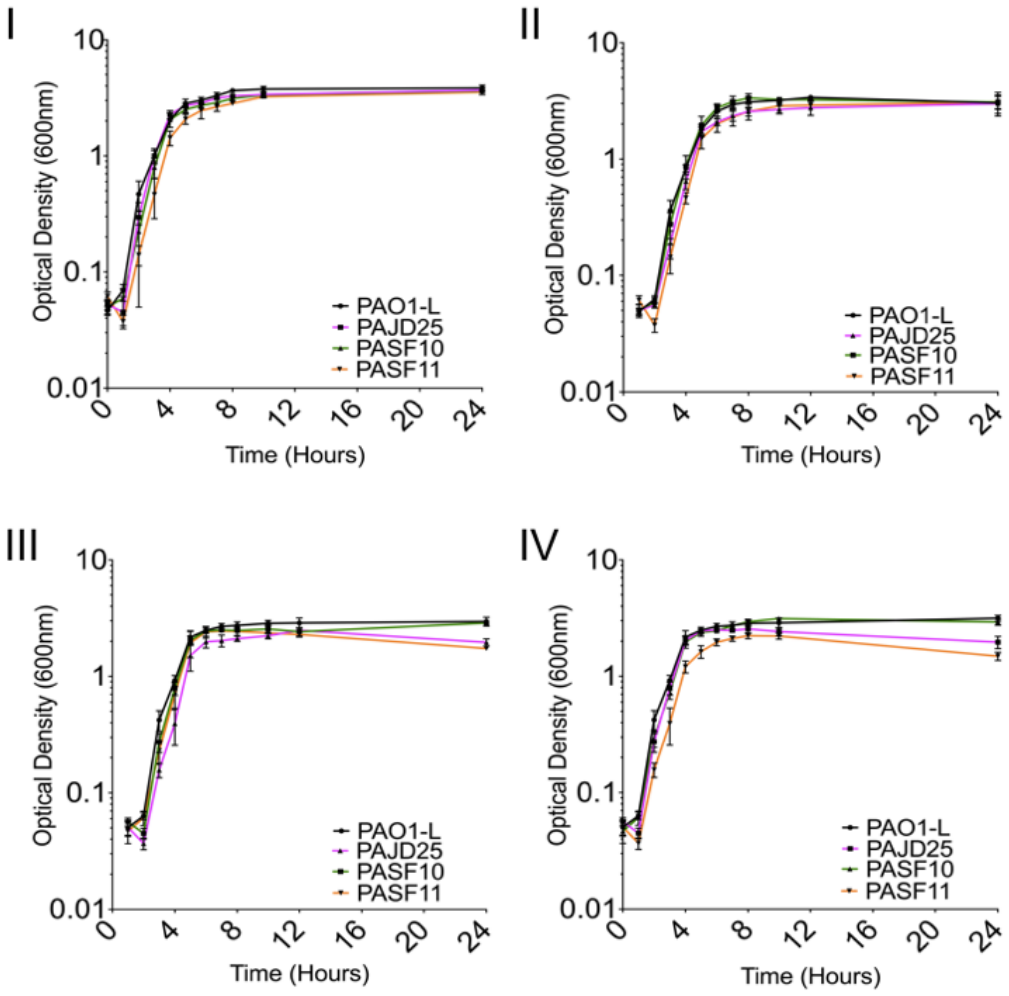

Figure 6.4 – Growth kinetics of *P. aeruginosa* nitrite reductase mutants in LB under aerobic condition, supplemented with additional nitrogen sources. Cultured in LB only **(I),** 10mM ammonium, **(II)** 10mM nitrite and **(III)** 10mM nitrate. Growth assessed using 5 biological replicates with 2 independent experiments. Error bars represent standard deviation.

6.3.1.3 *Can* NirA function as an assimilatory nitrite reductase at high cell densities?

The inability of NirA to compensate for the absence of NirB as an assimilatory nitrite reductase was likely due to the differential regulation demonstrated by these enzymes in *P. aeruginosa*. With *nirB* under the control of RpoN, NtrBC and NasST, successful expression is dependent on low nitrogen source availability and the presence of nitrate or nitrite (Figure 6.2). Since *nirA* is upregulated by cyanogenesis, which is under the control of the las/rhl quorum sensing (QS) circuit, *nirA* transcription would only be induced at high-cell

density (Figure 6.2). This explains why NirA and NirB do not exhibit functional redundancy when grown on single nitrogen sources under the previously assessed conditions, as the initial inoculum was not sufficient to induce *nirA* via QS activation of cyanogenesis. As a result, NirB deficient strains are unable to utilise nitrate or nitrite as a single N source.

6.3.1.2.1 Construction of nirA and hcnA translational reporters

Since NirA and NirB both reduce nitrite to ammonium, NirA should be able to functionally compensate for the absence of NirB when exposed to the right environmental conditions. Confirming this would require exposing the nitrite reductase mutant strains to nitrate and nitrite as a single nitrogen source once QS has been activated. To determine the correct time to expose the strains to nitrate or nitrite in minimal media LacZ translational reporters were constructed using the pUC118-Tn7-Gm-LacZ vector. LacZ was selected as a reporter due to the variable oxygen concentration to be used in future experiments. To construct the *nirA* and *hcnA* translational reporters, the *nirA* and *hcnA* promoter regions were amplified with primer pairs PnirAF1/R1 and PhcnAF1/R1 and modified with restriction sites NsiI/KpnI. The synthesized DNA fragments, spanning +6bp to -499bp and +6bp to -500bp relative to the *nirA and hcnA* transcriptional start sites respectively, were cloned into pUC118-Tn7-Gm-LacZ using NsiI and KpnI restriction sites, forming vectors pSJF10 (P*nirA*) and pSJF11 (P*hcnA*). These vectors were electroporated into PAO1-L alongside the transposase containing vector pSTNK, and integration confirmed using the procedure detailed in 2.8.3.

6.3.1.2.2 NirA functions as an assimilatory nitrite reductase at high cell density

Using the generated PAO1-L P*nirA*-lacZ and P*hcnA*-lacZ strains, *nirA* transcriptional activity was monitored in MOPS-succinate minimal media, supplemented with 10mM ammonium chloride. Promoter activity of *nirA* shadowed that of *hcnA*, confirming the previously reported relationship between cyanogenesis and *nirA* transcription (199) (Figure 6.5). Maximal *nirA* transcriptional induction was observed between 10-14 hours, correlating with the reported optimal production of HCN upon entry into stationary phase (199,

208) . Since *nirA* and *hcnA* induction begins at 4 hours, this time-point was selected for the previously discussed nitrate/nitrite exposure experiment. (Figure 6.5).

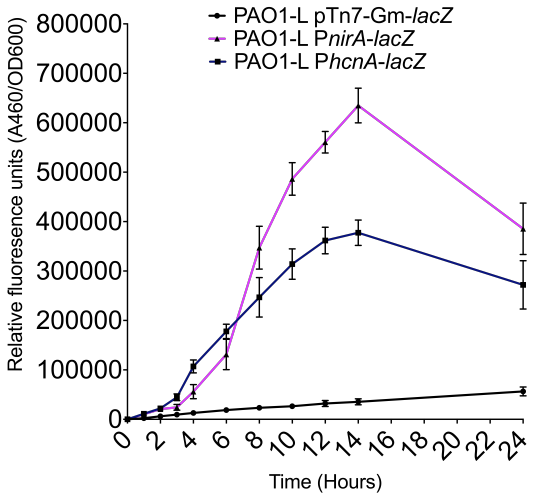

Figure 6.5 – Transcriptional activity of *nirA* and *hcnA* promoters monitored through production of LacZ. LacZ monitored through degradation of the fluorogenic substrate 3-carboxy-umbelliferyl β-D-galactopyranoside (CUG) normalised against OD_{600nm}. Each time point represents 6 biological replicates, with each biological replicate the average of 4 technical replicates. Inter-experimental variability in fluorescence prevents amalgamation of multiple independent experiments. However, 3 technical repeats were performed to ensure consistency in result patterns. Error bars represent standard deviation.

Strains PAO1-L, PAJD25, PASF10 and PASF11 were inoculated into MOPS-succinate-NH_4Cl minimal media and cultured for 4h. The cells were pelleted, washed and re-suspended in fresh MOPS-succinate-minimal media containing ammonium, nitrite or nitrate. To ensure the cultured bacteria are viable post-transfer to nitrite or nitrate, colony forming units (CFU) were tracked as the presence of dead cells can contribute to optical density. Previously at low-cell densities, PASF10 and PASF11 were unable to grow on nitrate or nitrite as a single nitrogen source (Figure 6.3 II-III). However, when exposed to nitrate or nitrite at a higher cell density, PASF10 was capable of using both as nitrogen sources, whilst PASF11 fails to grow (Figure 6.6 II-III). This suggests that in PASF10, *nirA* functionally compensates for the absence of *nirB* as an assimilatory nitrite reductase whilst PASF11 possesses no ammonium-forming nitrite reductase, rendering it unable to assimilate nitrate or nitrite. When transferred to nitrite, single nitrite reductase mutants were initially capable of a 1-log increase in growth however, 4h post nitrite exposure all nitrite reductase mutants demonstrate a loss in viability as determined by CFU's, whilst PAO1-L enters stationary phase 6h post exposure (Figure 6.6 II). This CFU reduction

was not seen in the ammonium transfer whilst when transferred to nitrate, the *nirAB* double mutant has a 1-log reduction in viable count (Figure 6.6 I and III). The loss in viability exhibited may suggest detoxification issues with basal NirS expression levels and a single nitrite reductase unable to reduce the high concentrations of nitrite used in this experiment. When exposed to nitrate, the concentration of nitrite would not exceed the capacity of a single ammonium-forming nitrite reductase to detoxify, potentially explaining why only the double mutant was affected by nitrate shock.

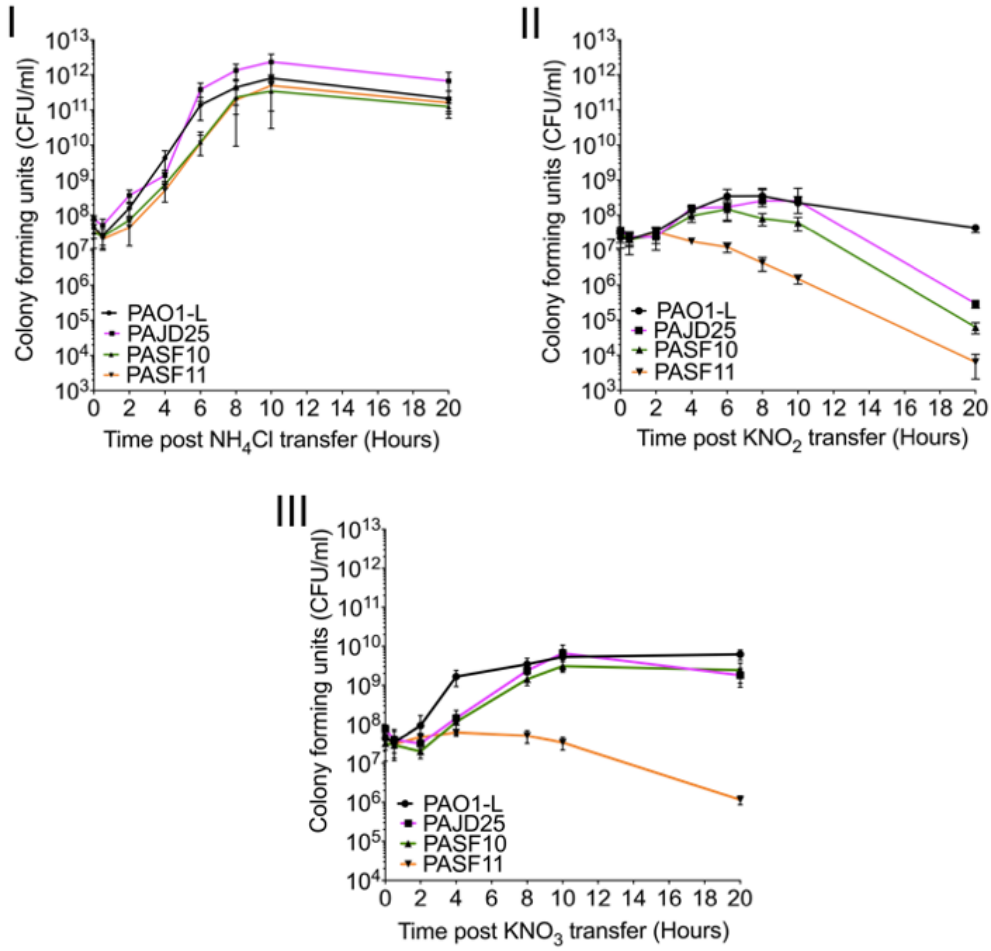

Figure 6.6 – Response of nitrite reductase mutants transferred to MOPS-succinate-minimal media with single nitrogen sources upon induction of P*hcnA*. (**I**) ammonium to ammonium transfer; (**II**) ammonium to nitrite; (**III**) ammonium to nitrate. Each time point consists of 3 biological replicates with 3 technical replicates. Assays repeated on 2 separate occasions to ensure consistency in results. Error bars represent standard error of mean.

6.3.1.3 NirA is not responsive to the presence of nitrate or nitrite

Whilst NirA can function as an assimilatory nitrite reductase, this is unlikely to be its primary function. Assimilatory nitrate and nitrite reductases are required to respond to substrate availability to perform their function effectively (237, 284). The expression of *nirA* has not been shown to be responsive to nitrite or nitrate, whilst that of *nirB* requires both low N source availability and high concentrations of nitrate to be present (284). To serve as a control, a *nirB* transcriptional reporter was constructed in pUC118-Tn7-Gm-*lacZ*. Primer pair PnirbF1/R1 were modified with restriction sites NsiI/KpnI and used to amplify the *nirB* promoter region, corresponding to between +6 and -490bp relative to the annotated transcriptional start site. The fragment was then cloned into pUC118-Tn7-Gm-*lacZ* using restriction sites NsiI and KpnI, forming pSJF12. This vector was subsequently integrated into PAO1-L via electroporation and the plasmid backbone removed using the procedure described in 2.8.3, leaving *lacZ* under the control of P*nirB*.

Initially, strains PAO1-L P*nirA*-*lacZ*, P*hcnA*-*lacZ* and P*nirB*-*lacZ* were cultured in MOPS-succinate-NH_4Cl to an OD_{600nm} of ~0.4, and subsequently transferred into MOPS-succinate minimal media with ammonium, nitrite or nitrate. This demonstrated that the *nirB* transcriptional reporter functioned as expected. No *nirB* induction was seen when exposed to ammonium however, high level LacZ expression was detected when transferred to nitrate (Figure 6.7 I and II). The same effect was observed when PAO1-L P*nirB*-*lacZ* was transferred to nitrite although the level of induction decreased when compared to nitrate (Figure 6.7 III), consistent with the substrate recognition regulation mechanism governed by NasST having a higher affinity for nitrate. Transcription of *nirA* does not appear to be influenced by the presence of high nitrate or nitrite levels, following a similar trend whereby it mirrors *hcnA* induction. However, regulation by cyanogenesis may mask any contribution nitrate or nitrite plays in inducing or enhancing transcription of *nirA*.

To remove the contribution of HCN upon *nirA* regulation, the previously published HCN null mutant PAO6344 deleted in *hcnB,* was transformed with the pSJF1*0 (nirA)*, pSJF11 *(hcnA)* and pSJF12 *(nirB)* transcriptional reporter vectors and the backbones removed as performed in PAO1-L. These reporter strains were then subjected to the same nitrate transfer experiment as

performed above. The *nirB* and *hcnA* transcriptional reporters functioned in the same manner as seen previously for wild-type PAO1-L (Figure 6.5 and 6.7). However, activation of the *nirA* promoter was non-existent, with removal of HCN synthesis abolishing *nirA* transcription (Figure 6.7 IV). Subsequent addition of 20μM KCN at the point of media transfer resulted in up-regulation of *nirA*, although not to the same extent as wild-type PAO1-L (Figure 6.7 IV). This dependence on cyanide for *nirA* expression confirms the results obtained by Frangipani and colleagues, with this work demonstrating that high substrate availability does not regulate *nirA*, suggesting its prime function is not as an assimilatory nitrite reductase. The influence of lower nitrite or nitrate levels or rich media could not be assessed due to interruption by the SARS-COV2 pandemic. It would be interesting to observe if lower levels of nitrite or nitrate maximise expression in a manner similar to *nrfA* from *E. coli*, reducing nitrite produced as a consequence of respiratory nitrate reduction under low oxygen conditions through the DNRA pathway.

6.3.2 Impact of oxygenation on NirA function

Oxygenation is likely to play a key role in regulation of *nirA*. With the PA4129-34 genomic region induced by cyanogenesis, maximal expression will occur at low oxygen tension with ANR contributing to HCN synthase (*hcnABC*) transcriptional activation. Therefor NirA is likely to be relevant under these environmental conditions. Various studies have begun to show that *P. aeruginosa* encounters low oxygen environments during various aspects of infection. This may suggest that the role NirA plays a critical role in virulence in virulence under oxygen limitation.

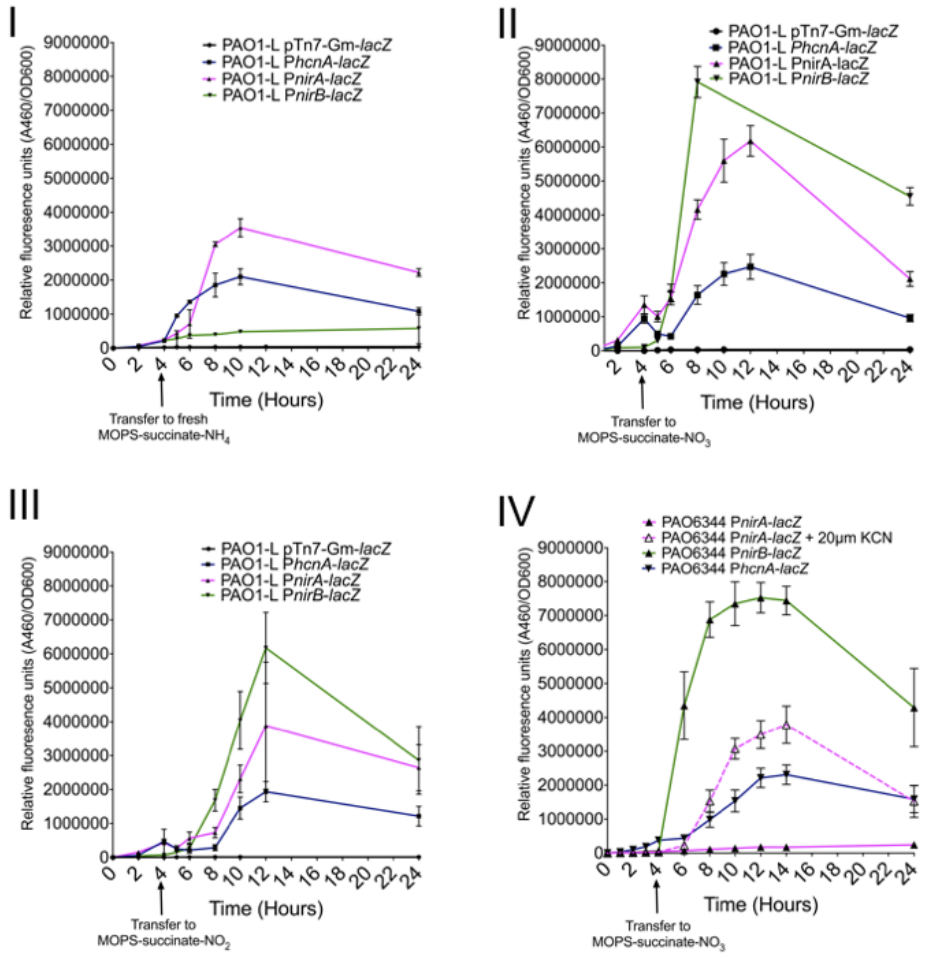

Figure 6.7- Transcriptional activity of *nirA*, *hcnA* and *nirB* promoters in response to single nitrogen source. Activation monitored through production of LacZ and degradation of the fluorogenic substrate CUG. **(I)** Activation after transfer into fresh MOPS-succinate-NH_4Cl in PAO1-L; **(II)** transfer into MOPS-succinate-KNO_3 in PAO1-L; **(III)** transfer into MOPS-succinate-KNO_2 in PAO1-L; **(IV)** transfer into MOPS-succinate-KNO_3 with 20um KCN using PAO6344 (*ΔhcnB*). Time points represent 3 biological replicates, each with 3 technical replicates. Error bars display standard deviation.

6.3.2.1 NirA is upregulated at low oxygenation

To confirm the assumption that *nirA* is indirectly regulated through oxygenation via HCN and ANR, PAO1-L P*nirA-lacZ* and P*hcnA-lacZ* were grown in MOPS-succinate-NH_4Cl and M-ASM under aerobic and micro-aerobic conditions (5%O_2). Samples were taken throughout growth and assessed for LacZ production at 4, 8, 12 and 24h. Minimal LacZ was detected at 4h when expression was driven by P*hcnA* and P*nirA* (Figure 6.8). This is consistent with the *las* and *rhl* QS systems being the prime transcriptional regulators of HCN biosynthesis, indirectly driving *nirA* expression. The P*hcnA* promoter activity

peaked at 12h in both MOPS-succinate-NH_4Cl and M-ASM, with maximal induction seen under micro-aerobic conditions (Figure 6.8). Activation of P*nirA* shadows that of P*hcnA*, with a 2.5 and 1.9-fold upregulation seen in MOPS-succinate-NH_4Cl and M-ASM at 12h respectively, as compared to the corresponding aerobic samples (Figure 6.8). This demonstrates that oxygenation does regulate *nirA*, likely through enhanced ANR-dependent P*hcnA* activation and subsequent HCN production.

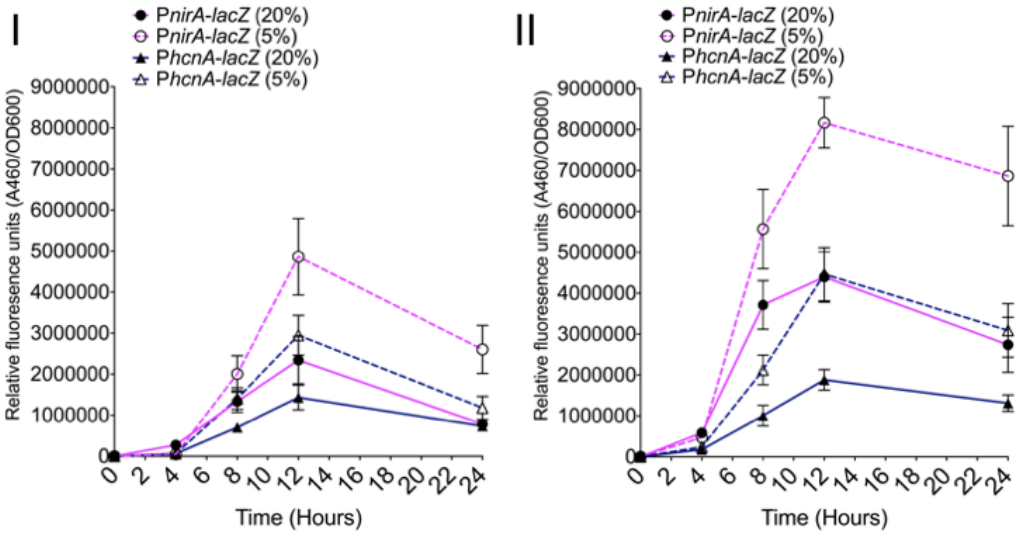

Figure 6.8 – Transcriptional activation of *nirA* and *hcnA* promoters in PAO1-L under aerobic and micro-aerobic conditions. I) LacZ induction in MOPS-succinate-NH_4Cl minimal media. **II)** LacZ induction in M-ASM. Time points represent 5 biological replicates, each with 3 technical replicates. Inter-experimental variability in fluorescence prevents amalgamation of multiple independent experiments. However, 2 technical repeats performed to ensure consistency in result pattern. Error bars represent standard deviation.

6.3.2.2 NirA is required for P. aeruginosa *growth under low oxygen in the presence of nitrate and nitrite.*

With *nirA* induced maximally at lower oxygenation, assessment of growth on single nitrogen sources was repeated under micro-aerobic conditions (5% oxygen) with strains PAO1-L, PAJD25, PASF10 and PASF11. When grown using MOPS-succinate minimal media with single nitrogen sources, the PAO1-L wild-type strain was able to reach on OD_{600nm} of 1-2, depending on the N source, with all nitrite reductase mutant strains able to grow unhindered in MOPS-succinate-NH_4Cl (Figure 6.9 I). As shown under aerobic conditions, strains PASF10 and PASF11 harbouring a *nirB* deletion, were unable to grow

using nitrite or nitrate as single nitrogen sources at 5% O_2 (Figure 6.3). However, the single *nirA* deletion mutant PAJD25 also struggled to grow under these conditions (Figure 6.9 II-III). Unlike *nirB* mutants, PAJD25 demonstrated initial growth to an OD600nm of ~0.2-0.3 using both nitrite and nitrate as single N sources although this initial growth declined from 12 hours onwards (Figure 6.9 II-III). Since PAJD25 only encodes *nirB* as an assimilatory nitrite reductase, it suggests that NirB was only essential to growth in the very initial stages under micro-aerobic conditions, whilst NirA takes over at higher cell densities. The initial growth and decline of PAJD25 under micro-aerobic conditions suggests an unknown variable is preventing NirB from functioning correctly. This may be an inhibitor produced under these conditions, or a lack of NADH compromising the ability of NirB to reduce nitrite.

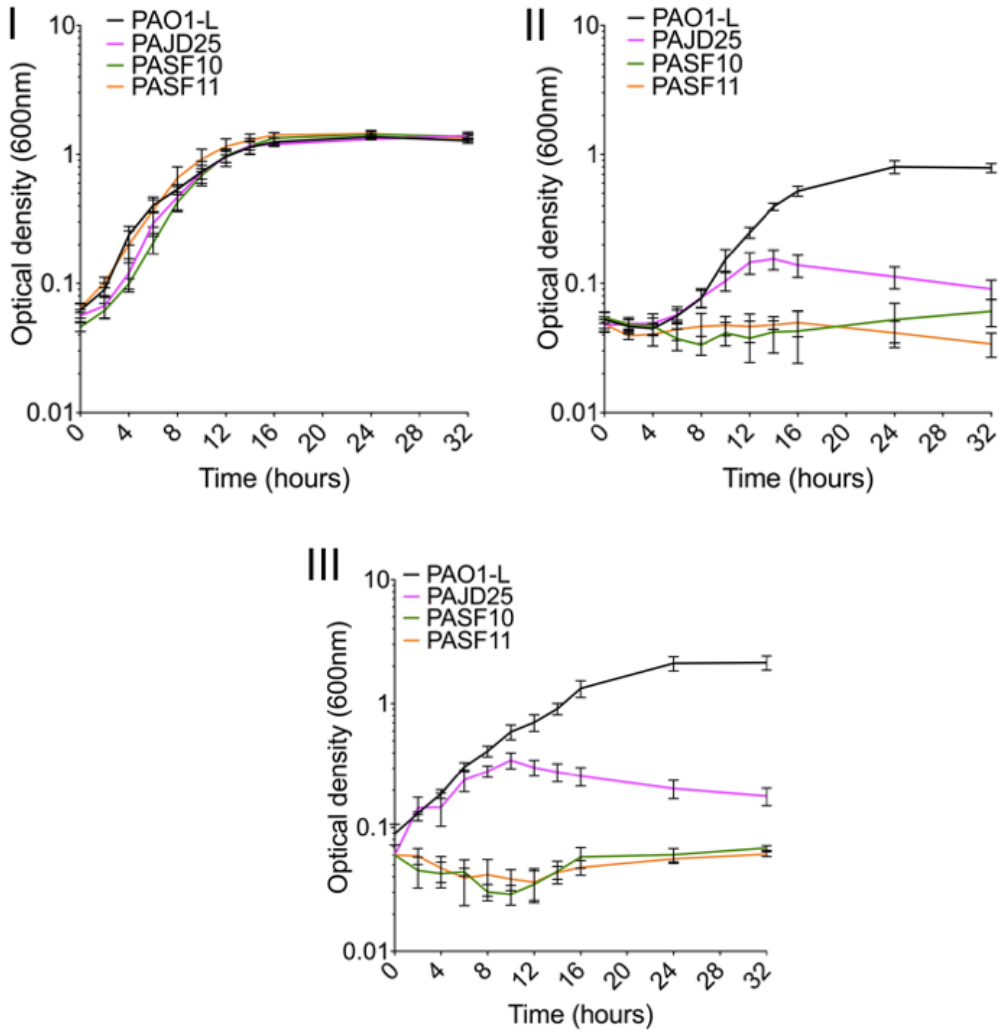

Figure 6.9 – Growth kinetics of PAO1-L nitrite reductase mutants in MOPS-succinate minimal media with single nitrogen sources under micro-aerobic conditions (5%O_2). (I) MOPS-succinate-NH_4Cl; **(II)** MOPS-succinate-KNO_2; and **(III)** MOPS-succinate-KNO_3. Experiments repeated 2 times with 3 biological replicates per attempt. Error bars represent standard deviation.

6.3.2.2 NirA encodes a cyanide-resistant nitrite reductase

One inhibitor known to interfere with the function of heme-containing enzymes is HCN. Cyanide has been shown to reduce activity of NirA and NirB homologues in *E. coli*, *M. tuberculosis* and *S. oleracea* by binding at the siroheme prosthetic group, inhibiting electron transfer (274, 285, 286). This makes upregulation of *nirA* by HCN in *P. aeruginosa* unusual, since it is assumed to inhibit NirA function. Alongside *nirA*, HCN upregulates expression of PA4129-34 with MpaR (PA4132) presumed to recognise the presence of cyanide based on RNA sequencing data generated by Wang and colleagues (200). PA4133-34 have been shown to encode a cyanide-resistant cbb_3-cytochome oxidase catalytic sub-unit and accessory protein, allowing respiration of oxygen in the presence of HCN (199, 205). How this occurs at a mechanistic level is unclear however, PA4129-34 has also been shown to provide *P. aeruginosa* cyanide resistance alongside the cyanide insensitive terminal oxidase *cioAB* (199). This led us to hypothesize that *nirA* may be linked to this cyanide tolerance, potentially encoding a cyanide-resistant nitrite reductase.

6.3.2.2.1 CysI overexpression and purification

The impact of cyanide addition was initially assessed *in vitro*. As a control, the NirA homologue CysI (*E. coli*) was selected for purification as it had previously been shown to be inhibited by cyanide addition, although the exact concentration inhibition occurred was not investigated (285). The *cysI* ORF was amplified with PCR from *E. coli* MG1655 using cysIF1, modified with a N-terminal hexa-histidyl tag and SacI restriction site, and reverse primer cysIR1 modified with an EcoR1 restriction site. The newly generated fragment was then inserted into pSK67 using the SacI and EcoR1 restriction sites, forming pSJF13. In a manner similar to NirA, pSJF13 was transformed into *E. coli* Suf++ (DE3) alongside pSJF004 (pCDF-DUET1-*cysG*) for overexpression.
CysI was overproduced using the conditions optimised for NirA (Chapter 4.3.1.4). Since CysI was not required for structural assessment, purification optimisation was not performed. CysI was purified by IMAC to a sufficient quality for cyanide sensitivity assays alongside NirA (Figure 6.10).

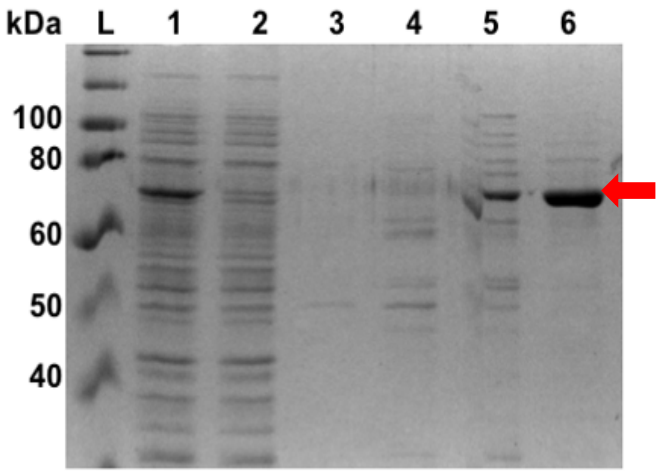

Figure 6.10 – IMAC purification of *E. coli* MG1655 CysI from overexpression vector pSJF13 using *E. coli* Suf+ (DE3) as a host. Overexpression performed at 20^{O}C for 18h with 0.3mM IPTG. Lane L - broad-range molecular weight ladder; 2 - Original lysate from *E. coli* Suf++ (DE3) overexpressing CysI and CysG; 2 – Lysate flow-through post IMAC binding; 3 – 10mM imidazole wash; 4 – 20mM imidazole wash; 5 – 40mM imidazole wash; 6 - 200mM imidazole elution. Red arrow indicates target protein CysI

6.3.2.2.2 NirA demonstrates cyanide tolerance in vitro

The functionality of the purified CysI was confirmed using the artificial electron donor methyl-viologen, with reduced methyl-viologen only oxidised in the presence of sulphite (data not shown). To assess cyanide sensitivity of CysI and NirA, newly purified batches of enzyme were prepared via IMAC. Samples were then spin concentrated and de-salted into 20mM Tris, 50mM NaCl, pH 7.5. Activity of both enzymes was then assessed simultaneously at varying potassium cyanide (KCN) concentrations under anaerobic conditions. To ensure KCN does not alter non-enzymatic methyl-viologen reduction and oxidation process with nitrite and sulphite, controls were set up at 0, 100 and 800µM KCN. This confirmed that KCN does not cause auto-oxidation of reduced methyl-viologen in the absence of NirA and CysI, allowing this assay to be used for the assessment of KCN sensitivity (Figure 6.11 I). CysI demonstrated a 61% inhibition as low as 25µM KCN after 300s, with activity completely abolished at 100µM KCN (Figure 6.11 II). NirA dependent methyl-viologen oxidation was not significantly altered at 100µM, with activity detected at 600µM KCN (Figure 6.11 III-IV). At concentratios higher than 200µM KCN, NirA activity was reduced in a step-wise manner suggesting cyanide still acts as an inhibitor, albeit with a lower affinity for NirA compared to CysI (Figure

6.11 IV). With *P. aeruginosa* NirS and NirB homologues demonstrated to be inhibited by cyanide, this may leave NirA as the only functional nitrite reductase during cyanogenesis. Attempts to validate this *in vitro* and purify the secondary ammonium-forming nitrite reductase NirB failed due to problems with expression in a heterologous *E. coli* host (data not shown), whilst overexpression of NirS was not completed due to time constraints imparted during the SARS-COV2 pandemic.

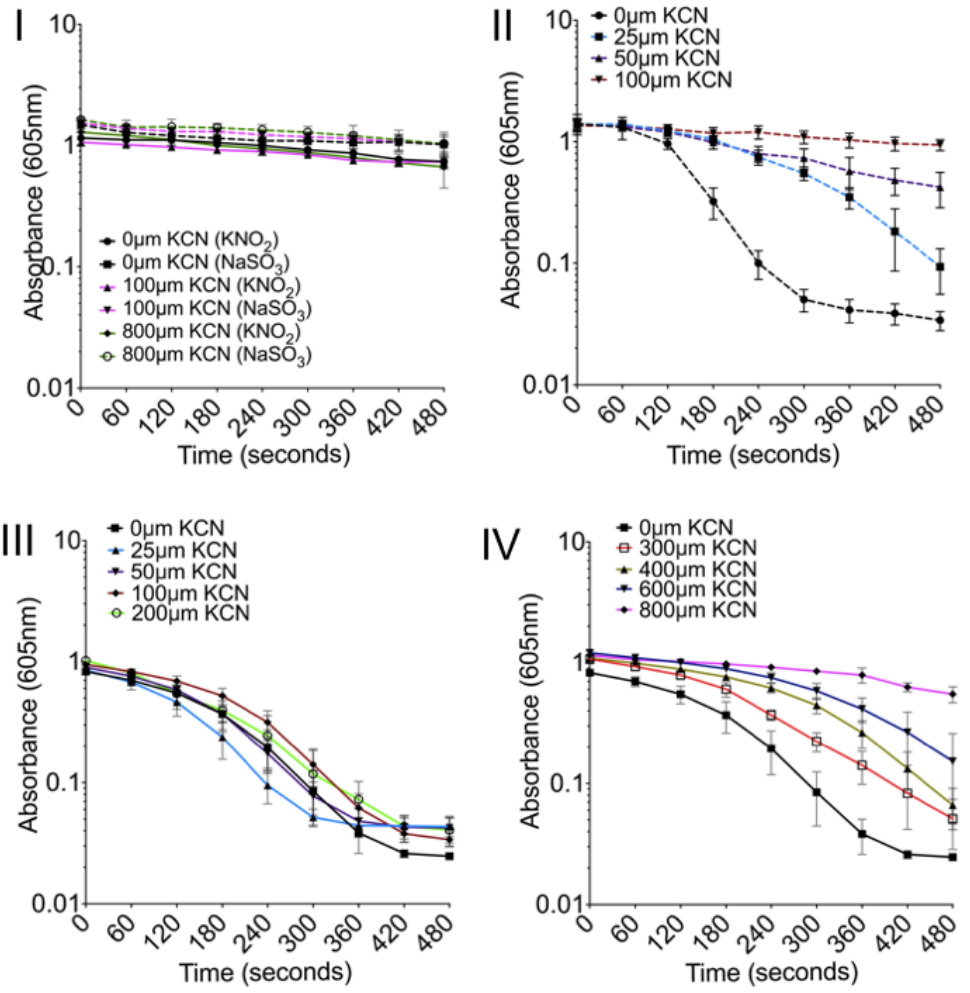

Figure 6.11 – *In vitro* assessment of *P. aeruginosa* NirA and *E. coli* CysI cyanide sensitivity using methyl-viologen oxidation assays. (I) Control reactions without NirA and CysI enzymes. **(II)** Effect of cyanide on CysI. **(III and IV)** Effect of cyanide on NirA. Each time-point represents at least 8 independent reaction, with error bars displaying standard deviation. Inter-experimental variability in initial methyl-viologen reduction prevents amalgamation of multiple independent experiments. However, 3 repeats were performed to ensure consistency in result pattern.

As an alternative to purification and *in vitro* assessment of cyanide tolerance for NirB, growth of the previously constructed nitrite reductase mutants was again assessed aerobically in the presence of ammonium and nitrate as a single N sources however, 100μM KCN was also added to the medium. As seen previously (Figure 6.12 I), all strains grew with wild-type kinetics in MOPS-succinate-NH_4Cl, whilst strains harbouring a *nirB* deletion (PASF10 and PASF11) failed to grow on nitrate (Figure 6.12 I). However, in the presence of cyanide, PAJD25 struggles to grow on nitrate when compared to the wild-type PAO1-L strain (Figure 6.12 II), producing a similar curve to that exhibited under reduced oxygen conditions (Figure 6.9). This suggests that in the absence of NirA, assimilatory nitrate reduction was inhibited by the presence of cyanide under aerobic conditions with NirBD a possible target of inhibition. Addition of high KCN levels also delayed PAO1-L growth in minimal media. This was likely due to the fact that endogenous HCN production is primarily produced under low oxygen conditions (208). Since this experiment was performed aerobically, the intrinsic defence mechanisms, such as the PA4129-34 genomic region, which prevent *P. aeruginosa* HCN self-intoxication would not be expressed as freely (199).

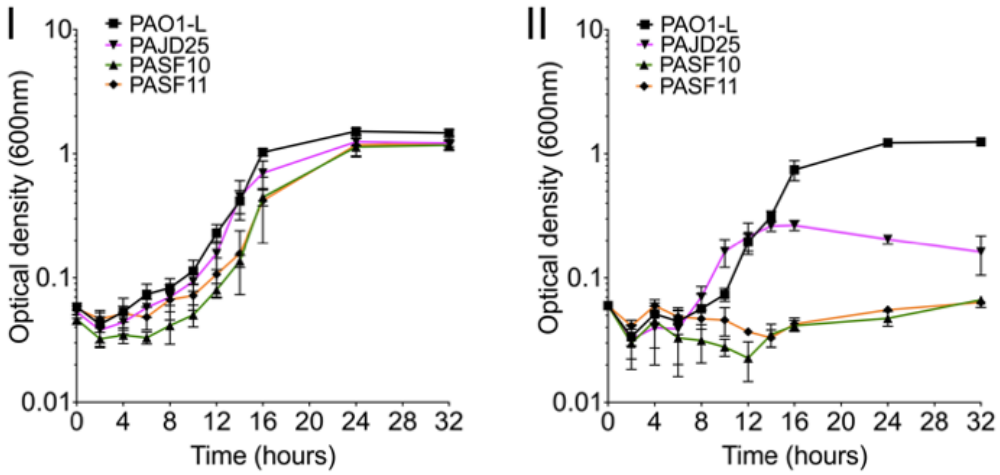

Figure 6.12 – Growth kinetics of PAO1-L nitrite reductase mutants in MOPS-succinate-minimal media alongside 100um KCN. (I) Growth with NH_4Cl; **(II)** and KNO_3 as single nitrogen sources. Experiments repeated 2 times with 3 biological replicates per attempt. Error bars represent standard deviation.

6.4 Conclusions

The work presented in this chapter attempts to determine the overlapping roles of the ammonium-forming nitrite reductase NirA and NirB. As previously shown by Romeo and colleagues, the *nalA-nirBD-PA1779-cobA* operon is required for assimilatory nitrate reduction. In this chapter, we show that *nirBD* alone is essential for nitrate assimilation under all conditions tested, acting as an assimilatory nitrite reductase. Under aerobic conditions at low cell density, the secondary ammonium-forming nitrite reductase NirA plays no discernible role in assimilation. However, NirA appears to act as an assimilatory nitrite reductase at high cell densities; under reduced oxygen conditions; and in the presence of cyanide. In order to be classified as part of an efficient assimilatory pathway, biosynthetic enzymes should be substrate (nitrite or nitrate) responsive in order to enable efficient utilisation. Expression of *nirA* was confirmed to be dependent on cyanide, in agreement with Frangipani and colleagues (199) however, no transcriptional activation was observed upon addition of nitrite or nitrate. This suggests NirA is not strictly an assimilatory nitrite reductase with the previous seen virulence phenotypes attributed to another aspect of *P. aeruginosa* nitrate reduction. Since NirA cannot be considered an assimilatory reductase, nor participate in denitrification, it seems likely that the main function of NirA would be in DNRA, detoxifying nitrite under conditions that NirS and NirBD are not active or expressed.

The observation that purified NirA can function at higher concentrations of cyanide than expected may point towards an avenue of exploration in defining a virulence mechanism. Aerobic growth of a *nirA* mutant with cyanide results in a remarkably similar growth attenuation as seen under micro-aerobic conditions. This suggests that the impact under reduced oxygenation in the presence of nitrate may be due to cyanide intoxication, when HCN production is maximal. Frangipani and colleagues alluded to this when they demonstrated that the PA4129-34 genomic region, alongside CioAB, enables *P. aeruginosa* to survive and grow in the presence of cyanide. This was presumed to be due to the PA4129-34 region encoding a cyanide resistant cbb_3-type cytochrome oxidase catalytic sub-unit, however this work suggests that NirA also contributes to this cyanide resistance mechanism. The work presented here was performed under highly defined conditions and does not

reflect the complexities of the *in vivo* environment. Further work is required to understand this relationship between the nitrite reductases and cyanide production using conditions more pertinent to infection.

Chapter 7

Discussion

7.1 Does NirA represent a viable anti-virulence target

At the outset of this project the main aim was to identify candidate virulence factors with potential for therapeutic development and identify inhibitors using a structurally-directed design strategy. For use of anti-virulence as an effective strategy, targets should aim to satisfy 3 main parameters: I) impact multiple virulence pathways; II) are specific to *P. aeruginosa*; and III) do not directly impact microbial growth.

7.1.1 Is in vitro *virulence factor production dependent on nitrate?*

Whilst satisfying these parameters is advantageous, it is not an essential requirement. In the absence of the newly identified nitrite reductase NirA, phylogenetically conserved reduction in pyocyanin production and swarming motility indicates that multiple virulence pathways are compromised, satisfying parameter I (Figures 3.4-3.5 and 3.10-11). This is backed up by the *in vivo* virulence data where deletion of *nirA* resulted in attenuated virulence in all models tested (Figures 3.17-20). *P. aeruginosa* virulence is specific to the disease model used, suggesting that interruption of *nirA* does impact multiple pathways as each model is dependent on expression of different virulence factors (149). With *nirA* encoding a nitrite reductase, it seems likely that these phenotypes are regulated at a metabolic level however, pyocyanin and swarming motility reductions are observed in rich media without additional nitrate under aerobic conditions.

In the case of pyocyanin production, the NirA-dependent attenuation is enhanced in M-ASM, which contains 500μm KNO_3 (Figure 3.5 and 3.10). It has also been shown that rich media contains trace amounts of nitrate, with LB containing 20-40μm, potentially explaining the phenotypes seen despite the lack of exogenous nitrate addition. The link between phenazine production and nitrate reduction has already been established in *Pseudomonas.* Denitrification components are upregulated in phenazine-null *P. aeruginosa* colony biofilms indicating the presence of phenazines negatively impacts denitrification (210). Both are used to balance the intracellular redox state by oxidising NADH in *P. aeruginos*a, with oxidised phenazines also shuttling electrons to oxygen

depleted regions, facilitating redox balancing of NAD+/NADH and enabling aerobic respiration apparatus to function (140, 287). How NirA causes a reduction in pyocyanin production is currently unclear however, with redox the common denominator between these two systems, it seems likely that this reduction is metabolically mediated as opposed to NirA acting as a direct regulator. This effect was not explored further in the context of this PhD as attenuation in pyocyanin production was used as a screening method to indicate potential attenuation in *vivo*. Further characterisation of NirA-dependent phenazine production is required under relevant conditions (microaerobic and in the presence of HCN), to determine whether this reduction in pyocyanin is pertinent *in vivo* and how this occurs at a mechanistic level.

Similarly, for swarming motility, the attenuation exhibited may be due to the presence of nitrate. Swarming is an extremely complex community behaviour which is strongly influenced by N source and C source availability (288). Disruption in N sources or how they are synthesized can lead to reduced or enhanced swarming, depending on what nitrogen source is impacted. Nitrate, L-glutamate, L-aspartate and L-histidine have all been shown to enhance swarming, whilst various L-amino acids repress swarming alongside the presence of ammonium (268, 288). With NirA participating in nitrate metabolism it likely participates in the regulation of N source availability. How the reduction in swarming motility occurs mechanistically is still unclear. Further experimentation in defined swarming media such as BM2 is require to fully elucidate whether this inhibition is dependent on the presence of nitrate, or via an undefined mechanism.

Whether the attenuation of these virulence traits is responsible for the reduction in virulence is unclear. Reductions in phenazine production has been demonstrated to reduce virulence in *C. elegans*, *D. melanogaster* and murine lung infection models (289-291), matching the results obtained when NirA is deleted. This suggests that NirA-dependent reduction in pyocyanin may play a role in the virulence attenuation exhibited by mutants of this nitrite reductase. Since NirA is expressed under oxygen limitation, any pyocyanin-dependent loss in virulence would likely be due to its role in redox cycling alongside its cytotoxic effects. In the absence of NirA and wild-type pyocyanin production, the redox state of the cell would be altered under conditions of oxygen limitation with the concentrations of nitrate *in vivo* unlikely to allow full NADH oxidation.

Whilst pyocyanin production was screened aerobically, the use of LB and M-ASM to support high level *P. aeruginosa* growth likely results in formation of an oxygen limited environment due to the biological oxygen demand of the culture. This potentially explains the aerobic impact of NirA deletion on both pyocyanin production and swarming motility, with the latter potentially generating an oxygen gradient due to the thickness of the swarming colonies.

7.1.2 Failure to determine the structure of NirA

In this project, a rational approach to inhibitor identification and development was attempted to target NirA. Unfortunately, structural determination failed despite extensive crystallisation trials, hindering identification and development of NirA inhibitors. However, this target should not be abandoned as a virulence target based on this difficulty. The conserved *in vivo* virulence across phylogenetically distinct disease models exhibited by a NirA mutant suggests that this target is universally required for virulence, including in humans (Figures 3.18-3.21). This may prove extremely valuable as a target since humans do not possess a nitrate reduction pathway, limiting any possible NirA inhibitor cross-reactivity with host proteins and processes. Whilst enzymes of this structure are widespread throughout bacteria, use of ferredoxin as an electron donor is less common. Most bacterial nitrite and sulphite reductases utilise NADH or NADPH as electron donor, with enzymes of this type associating with a flavin binding protein to facilitate electron transfer (224, 237). Ferredoxin is more commonly used as an electron donor in photosynthetic organisms such as plants and cyanobacteria (237). The active site of these enzymes is highly conserved, with any inhibitor developed against this structure likely to have off-site effects on the host microbiota. Use of ferredoxin by NirA may allow this specificity problem to be circumvented, by targeting the ferredoxin-NirA interaction. Since using reduced ferredoxin as an electron donor for nitrite reduction is less common in bacteria, it should enable development of an inhibitor with minimal impact on both host and the host microbiota. As such NirA satisfies parameter II for potential anti-virulence targets, with potential for development of highly specific inhibitors.

Of course, exploiting this target still relies upon obtaining a structure for this enzyme. From the structure the ferredoxin-NirA interaction can be modelled

and co-crystallisation attempted. NirA orthologues appear to crystallise under similar, standard conditions (Table 4.5). With sample purity and stability not an issue, the likely root of the failure to obtain crystals may lies with NirA itself. Sequence analysis revealed a 29-amino acid insertion, which modelling predicted is surface exposed and impacts a >100 amino acid region (Figure 4.19). Whilst the models could not agree on a consistent structure in this region, the surface exposed nature may inhibit crystal nucleation and thus crystallisation when compared to similar enzymes of this structure. Since this region is removed from the active site of NirA, it is unlikely to play a role in nitrite reduction to ammonium or modulate ferredoxin binding (Figure 4.19). However, a functional role for this region cannot be excluded with NirA demonstrating cyanide resistance when compared to purified *E. coli* CysI. To assess this cyanide-resistance property and enhance crystallisation efforts, genetic deletion of the NirA 29-amino acid region should next be performed.

7.1.3 Impact of NirA on growth and biofilm formation under micro-aerobic conditions

Parameter III of anti-virulence target identification and development states that standard microbial growth pathways should not be affected. Depending on the environmental conditions, deletion of NirA can interfere with *P. aeruginosa* growth. However, these conditions are unlikely to be encountered *in vivo*. A strong growth defect is only observed when grown under micro-aerobic conditions or in the presence of potassium cyanide, when nitrate is the only available nitrogen source (Figures 6.9 and 6.12). This is not reflective of the human environment where a wide array of amino acids are found as both carbon and nitrogen sources. For example, in the cystic fibrosis lung, amino acids can be found at between 5-25mM, supporting high density growth (209, 292).

More pertinent to the effect of NirA is the impact observed when grown in more complex media such as LB and M-ASM, as this more accurately represents the nitrogen source profile available during infection. In the absence of nitrate, NirA mutant growth is indistinguishable from the wild-type PAO1-L on either LB or M-ASM under normoxic and microoxic conditions (Figures 3.6 and 6.3-4). When nitrate is added to these medias, a loss in OD_{600nm} is observed upon

entry into stationary phase (Figures 3.8 and 3.14). The lack of impact on active growth and division indicates that microbial growth pathways are not affected, satisfying parameter III of anti-virulence target identification. However, the loss in *P. aeruginosa* viability when exposed to nitrate or nitrite during stationary phase may indicate that detoxification of these molecules and intermediates is compromised. The NADH-dependent nitrite reductase NirB will not be expressed under these conditions due to high N source availability, whilst *nirS* transcription is under control of the ANR-DNR system, requiring anaerobic conditions and nitric oxide production (273, 284). As a result, NirA may be the primary nitrite reductase upregulated at stationary phase, with removal compromising reduction of nitrate or nitrite. The impact of these nitrogen sources is magnified under reduced-oxygen conditions when assessing growth kinetics and the effect on colony biofilm CFU's (Figures 3.7 and 3.9). This coincides with maximal upregulation of this enzyme under cyanogenic conditions, which is optimally produced under low oxygen tensions (199, 208). Stationary phase culture are also oxygen-limited due to the biological oxygen demand of a high-cell density *P. aeruginosa* culture. The inability to reduce nitrite under these conditions may affect survival directly though nitrite accumulation, inhibiting respiration, or through altering the intracellular redox state and energy balance (205, 293). Tracking of nitrate reduction intermediates such as nitrite or nitric oxide, combined with monitoring intracellular redox (NAD+:NADH ratio) or ATP availability throughout growth, may allow elucidation of the mechanism responsible for this loss in *P. aeruginosa* viability.

7.2 Hypothetical role of NirA in *P. aeruginosa* virulence.

7.2.1 Reduced oxygenation and nitrate availability in vivo.

The effect of *nirA* deletion under reduced oxygenation is extremely interesting in the context of infection. *P. aeruginosa* encounters highly variable oxygen concentrations *in vivo*, with microenvironments forming as a consequence of *P. aeruginosa* infection(258, 294, 295). Proliferation of *P. aeruginosa* at the site of infection utilises local dissolved oxygen, reducing that available to itself and competing bacteria. Establishment of robust biofilms and aggregates during

chronic infection form a physical barrier, leading to formation of oxygen and nutrient gradients. Indeed, encountering reduced oxygen and nutrient concentrations is a key mechanism in development of *P. aeruginosa* biofilm antimicrobial tolerance, promoting reduced metabolic activity and establishment of a persistor cell population (296, 297). Inflammation caused by migration of immune cells to the site of infection also results in production of a reduced oxygen microenvironments. Production of reactive oxygen species (ROS) by polymorphnuclear leukocytes (PMN's) and infected tissues, utilises local available oxygen, reducing availability for bacterial respiration, and inhibiting localised phagocytosis due to oxygen starvation (298, 299). When phagocytosed, bacteria are exposed to a respiratory burst, with drastically elevated levels of ROS produced to kill the pathogen (Figure 7.1 I). In the case of *P. aeruginosa*, production of ROS leads to activation or pel, psl and alginate production, stimulating biofilm formation. This is especially pertinent in chronic infection when large bacterial aggregates develop, with the secretions of exopolysaccharide and eDNA inhibiting phagocytosis (298, 299). As a result, sustained inflammation is encountered, with recruitment of PMN's and continuous activation of ROS production utilising locally available oxygen (299). It is hypothesized that *P. aeruginosa* actively promotes the establishment of hypoxic or microoxic conditions *in vivo*, until reduced ROS stress is encountered due to the lack of available oxygen for superoxide synthesis, driving persistence during infection (299, 300). Reduced ROS would prove advantageous to any other competing bacteria in the local microenvironment. However, the diverse respiratory chain of *P. aeruginosa* combined with upregulation of virulence factors such as HCN, elastase and pyocyanin, ensures this pathogen dominates under reduced oxygen tensions (205, 300).

With *nirA* encoding a nitrite reductase, any effect seen under reduced oxygen conditions would only be relevant in the presence of nitrate or nitrite. Whilst humans cannot reduce or utilise nitrate, it is naturally found in the body through dietary consumption and oxidation of host-derived nitric oxide produced as part of the endocrine system, or in response to infection (301). Nitric oxide production is induced in PMN's through a combination of cytokines (IL-1β, IFN-γ and TNFα), which are activated in response to bacterial LPS and pyocyanin production (134) (Figure 7.1). Humans encode 3 nitric oxide synthases (NOS)

which allow production of nitric oxide from arginine and oxygen (301). The majority of this is produced by inducible NOS (iNOS2) in response to bacterial infection, with nitric oxide used to produce various radical and non-radical reactive nitrogen species (RNS) (134). Nitric oxide and superoxide (O_2^-) also undergo spontaneous conversion to peroxynitrite (ONO_2^-), an unstable isomer of nitrate (302). Together, ROS and RNS target broadly similar pathways, with lipids, proteins and DNA/RNA damaged by these highly reactive compounds. These molecules also react with iron-sulphur clusters, compromising the majority of respiratory chains which rely on iron (134, 303) (Figure 7.1). Many pathogens have evolved sophisticated ROS and RNS detoxification mechanisms such as superoxide dismutase, catalase, flavohemoprotein and denitrification (134, 298, 299). Disruption of these processes compromises virulence in an array of pathogens, highlighting the importance of resistance ROS and RNS stress *in vivo*.

Depending on the redox environment, nitric oxide can be auto-oxidised to nitrite or nitrate, as well as forming RNS (Figure 7.1). *P. aeruginosa* is also capable of detoxifying nitric oxide through 2 main pathways, denitrification under anaerobic conditions, or via flavohemaglobin (Fhp) under aerobic or micro-aerobic conditions (205, 237, 303) (Figure 7.1). Fhp demonstrates nitric oxide dioxygenase activity, oxidising nitric oxide to nitrate in the presence of oxygen, and is responsible for the majority of bacterial nitric oxide turnover in the presence of oxygen (303). This not only detoxifies increasing levels of nitric oxide and subsequent production of reactive nitrogen species (RNS), but provides a substrate for dissimilatory nitrate reduction, which supports *P. aeruginosa* growth under hypoxic or microoxic conditions (237, 258). This is especially important during sustained production of ROS and RNS, with both processes requiring high use of locally dissolved oxygen, resulting in production of a microoxic or hypoxic local environment (295, 298, 299). Conversion of nitric oxide to nitrate essentially flips the innate immune response, aiding survival of *P. aeruginosa* infection and supporting respiration. Production of nitric oxide and oxidation to nitrate under these reduced oxygen conditions may explain why *nirA* is pertinent for human infection, with reduction of nitrate leading to sustained build-up of toxic nitrite in the local micro-environment. Nitrite acts as an inhibitor of respiration and damages many metal-containing proteins, disrupting normal cellular redox and function. This may suggest that the role of NirA is in adaptation to the host environment as

opposed to being a true virulence factor, reducing nitrite to ammonium under conditions relevant to infection across disease models.

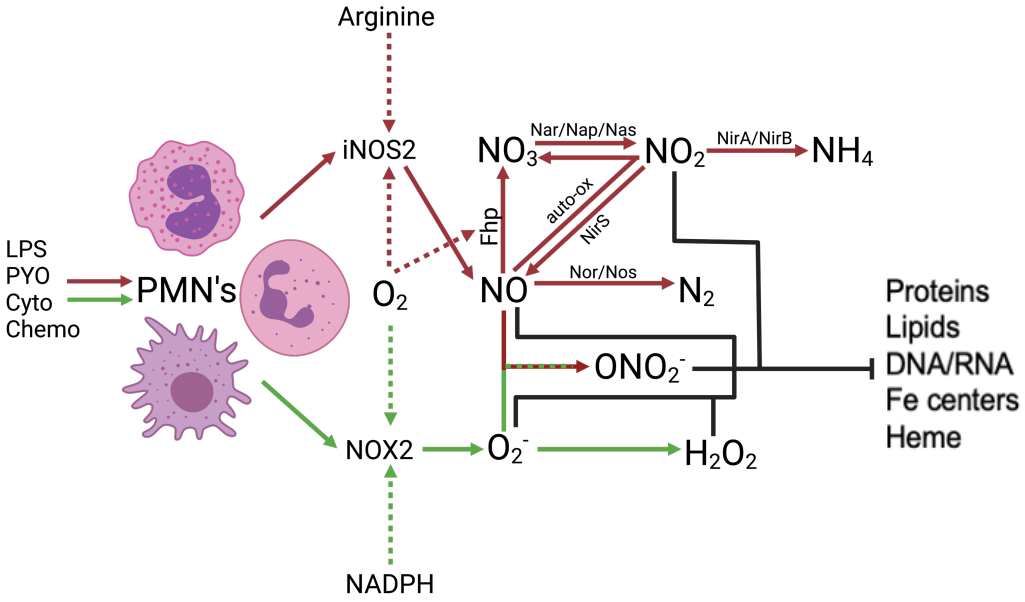

Figure 7.1 – Diagram depicting the interplay between host synthesis of RNS and ROS in the context of *P. aeruginosa* nitrate reduction. 1) *P. aeruginosa* products such as LPS and pyocyanin are recognised by Pattern recognition receptors (PRR) induce production of multiple cytokines and chemokines. **2a)** A combination of IL-1β, IFN-γ and TNFα trigger expression of the inducible nitric oxide synthase (iNOS2) in PMN's such as macrophages, neutrophils and eosinophils. This gene utilises arginine and O_2 to release citrulline and NO. **2b)** *P. aeruginosa* utilises Fhp in the presence of O_2 to detoxify NO, forming NO_3. **2c)** Alternatively, NO can be auto-oxidised to NO_2 or NO_3, depending on the micro-environmental redox conditions. **2d)** If NO is not oxidised, it can be detoxified by *P. aeruginosa* denitrification, with the *nor* and *nos* systems catalysing formation of N_2. **2e)** If oxidised to NO_3 or NO_2 respiratory nitrate reduction can occur, allowing production of ATP, or detoxification of NO_2 to ammonium can be catalysed by assimilatory or DNRA *P. aeruginosa* pathways. **3a)** PRR's alongside TNFα and IL-8 trigger expression of the NADPH oxidase NOX2. **3b)** NOX2 utilises O_2 and NADPH to synthesis superoxide (O_2^-). **3c)** Highly reactive $O2^-$ can be used to produce H_2O_2, either spontaneously or through dismutation. **4)** The products of INOS2 (NO) and NOX2 (O_2^-) can further react to form peroxynitrate (ONO_2^-). **5)** NO, NO_2, ONO_2^-, H_2O_2, O_2^- and numerous other RNS or ROS species derived from these molecules, have a broadly similar effect aiding control of bacterial infections. Proteins, lipids and DNA/RNA are modified and inactivated by redox reactions. Fe centres and heme are bound and inactivated, inhibiting electron transport activity in respiration, largely an Fe-dependent process. Generation of these RNS and ROS compounds results in high use of locally dissolved O_2, with sustained activation triggering production of a microoxic or hypoxic local micro-environment.

7.2.2 Impact of cyanide on P. aeruginosa *respiration*

The ability of *P. aeruginosa* to survive across a variety of oxygenations conditions is underpinned by the highly branched respiratory chain of *P. aeruginosa*. A total of 17 respiratory dehydrogenases, 7 aerobic respiratory chains, respiratory nitrate reduction and fermentation of arginine or pyruvate, combine to enable *P. aeruginosa* to adapt to all oxygen concentrations from normoxic to anaerobic (205, 304-307). Production of cyanide has a profound effect on both aerobic respiration and nitrate reduction. These systems are reliant on either quinol, cytochrome c, cytochrome bc_1 complex and heme as both a source of electrons or to facilitate electron transfer. However, cyanide is a potent inhibitor of cytochrome C, cytochrome bc_1 and heme, resulting in a drastically altered respiratory pathway with CcoN1, CcoN2, CcoN3, Cox, NirS, NorBC And NosZ likely inhibited by cyanide production (205, 307) (Figure 7.2). This is the reason for stringent control of HCN production, with minimal production observed under strictly aerobic or anaerobic conditions (208). However, the impact of cyanide production on the *P. aeruginosa* aerobic respiratory chain is mitigated through use of 3 remaining alternate respiratory complexes. In the presence of cyanide, aerobic respiration can be performed by the bo_3-quinol oxidase and CioAB, which derives electrons from the membrane ubiquinone pool. Whilst the novel cbb_3-type cytochrome c oxidase catalytic sub-unit CcoN4 (PA4133) is more tolerant of cyanide despite being dependent on cytochrome c, allowing aerobic respiration to proceed (304, 306) (Figure 7.2).

Remodelling of *P. aeruginosa* nitrate reduction has not been explored in the context of cyanide production. It is theorized that respiratory nitrate reduction supplements aerobic respiration under reduced oxygen condition (258, 295). However, this is when *P. aeruginosa* HCN production is maximal. With NirS, NorBC and NosZ all dependent on cytochrome c as an electron donor, the presence of cyanide would likley prevent denitrification from being completed. However, with the respiratory nitrate reductases (NarGHI) deriving electrons from the ubiquinone pool, nitrate reduction would still occur at physiologically relevant concentrations of cyanide (205, 308) (Figure 7.2). This would result in accumulation of nitrite if no mechanism of detoxification existed. Under conditions of nitrogen source limitation NirBD can perform this role, reducing nitrite to ammonium which can be used for biosynthesis of amino acids. *In vivo*,

nitrogen and carbon sources are widely available to infecting bacteria with *P. aeruginosa* evolving in chronic infections to more efficiently utilise the compounds on offer (209, 292). This inhibits transcriptional activation of NirBD as alternative nitrogen sources are available, such as host-derived amino acids (284). Potentially leaving NirA as the only nitrite reductase capable of detoxifying nitrite under conditions of reduced oxygenation.

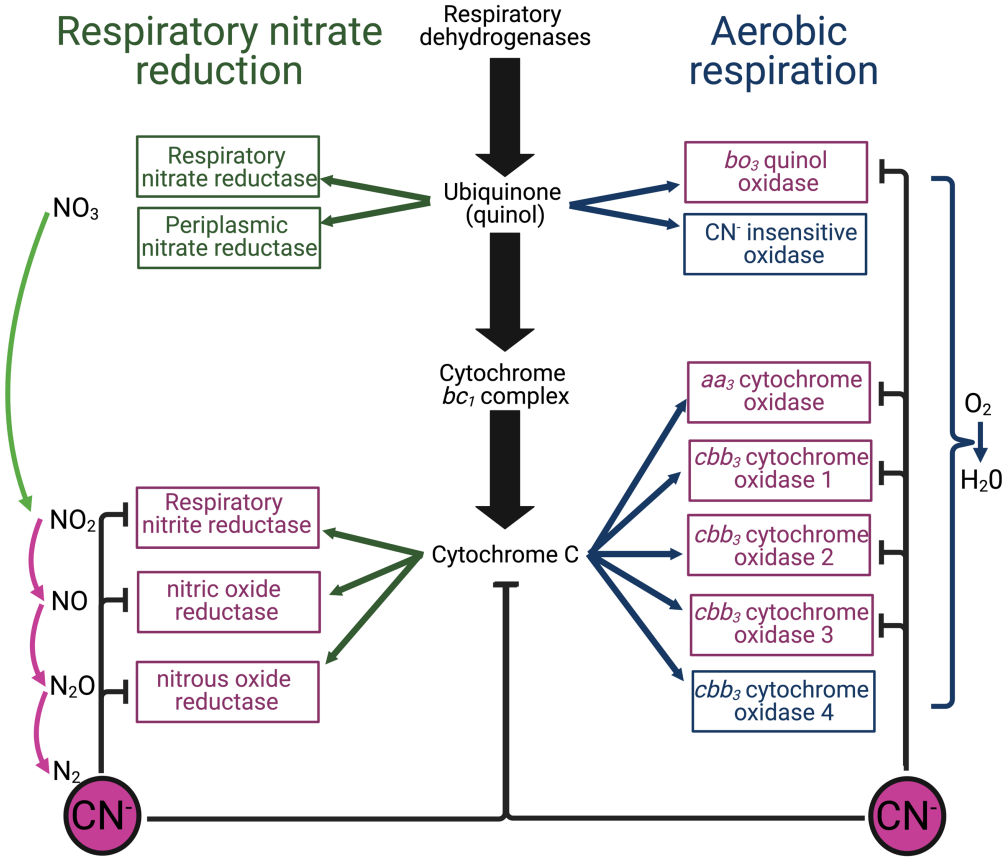

Figure 7.2 – Remodelling of aerobic respiration and denitrification in *P. aeruginosa* under cyanogenic conditions. Arrows denote flow of electrons. Lines at end of arrows denote inhibition. In general, cytochrome c dependent enzymes are inhibited by cyanide, with binding preventing electron transport. For aerobic respiration, aa_3 cytochrome oxidase (CoxAB), bo_3 quinol oxidase (CyoABCDE) and cbb_3-type cytochrome oxidases (CcoN1O1P1Q1, CcoN2O2P2Q2 and CcoN3Q3) are inhibited by cyanide at sub micro-molar concentrations through heme-group binding. Aerobic respiration can proceed in the presence of cyanide by utilising the cyanide insensitive oxidase (CioAB), which use ubiquinone or ubiquinol as an electron donor. The orphan cbb_3 cytochrome oxidase 4 (CcoN4Q4), demonstrates cyanide resistance an order of magnitude higher than other cbb_3-type isoforms, supporting aerobic respiration under low oxygen conditions when HCN production is maximal. Based on the dependence of NirS (nitrite reductase), NorBC (nitric oxide reductase) and NosZ (nitrous oxide reductase) on cytochrome C, these components of denitrification would be inhibited by cyanogenesis. Respiratory (NarGHI) and periplasmic nitrate reduction (NapABC is able to proceed at physiologically relevant concentrations of cyanide, as it is dependent on ubiquinone or ubiquinol as an electron donor. Figure adapted (205).

7.2.3 Cyanide, host-derived nitrate and NirA

Data produced during this thesis, combined with the growing body of work exploring *P. aeruginosa* virulence in relation to reduced oxygen conditions, allows a hypothetical role for NirA-dependent virulence inhibition to be developed. The first observation is the conserved nature of attenuation across disease models exhibited by *nirA* mutants suggests that large aspects of virulence occur under reduced oxygen conditions, regardless of the model. NirA is maximally upregulated by HCN at low-oxygen tension with any virulence attenuation likely to occur under these conditions, indicating development of these environments is a common consequence of *P. aeruginosa* infection.

The significance of NirA under these conditions is backed up by the reduced growth and loss of viability of *nirA* mutants at 5% oxygen (Figures 6.9), or in the presence of cyanide (Figure 6.12). Depletion of micro-environmental oxygen is likely to occur in all models utilised in Chapter 4, with production of ROS and nitric oxide phylogenetically conserved by both cell lines and the innate immune systems. Formation of reduced oxygen conditions by PMN activation and active growth of *P. aeruginosa* would trigger maximal HCN and NirA production, whilst sustained induction of iNOS in response in *P. aeruginosa* infection results in increased availability of nitrate (Figure 7.1 and 7.3). With NarGHI utilising the membrane ubiquinone pool as an electron donor, cyanide has less of an effect on reduction of NO_3 (Figure 7.2). This allows respiratory nitrate to nitrite reduction to occur under low oxygen conditions to support *P. aeruginosa* growth. However, cyanide inhibits cytochrome c and cytochrome bc_1 dependent enzymes, including denitrification components NirS, NorBC and NosZ, preventing detoxification of nitrite to gaseous dinitrogen (Figure 7.2). The *in vivo* environment contains an array of bioavailable nitrogen source, inhibiting induction of *nirBD*, as NtrC is not phosphorylated, with cyanide also potentially inhibiting this nitrite reductase (Figure 6.2). As a result, the cyanide-resistant nitrite reductase NirA, is the only reductase capable of functioning in the presence of cyanide, induced by low oxygenation. As a consequence, ATP synthesis via respiratory nitrate reduction can proceed without the build-up in nitrite as a toxic intermediate (Figure 7.3)

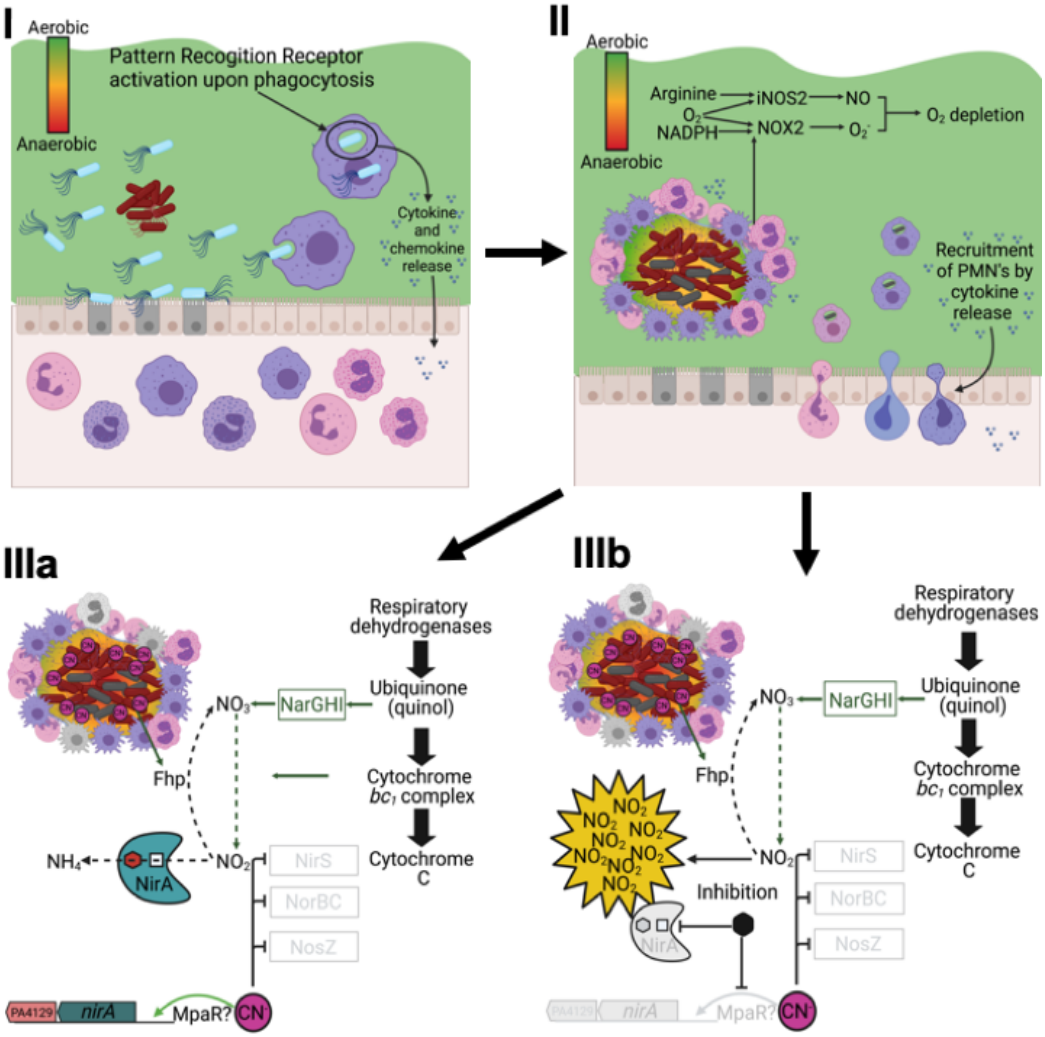

Figure 7.3 – Hypothetical model of virulence attenuation when *P. aeruginosa nirA* is deleted or inhibited. I) Upon infection, *P. aeruginosa* causes local cellular damage through release of numerous virulence factors. PMN's phagocytose *P. aeruginosa* and PRR's detect bacterial components such as LPS, triggering release of pro-inflammatory cytokines and chemokines. **II)** Release of cytokines and chemokines recruits more PMN's such as neutrophils, macrophages and granulocytes to the site of *P. aeruginosa* infection. These cytokines and chemokines trigger up-regulation of iNOS2 and NOX2 as part of the host innate immune response. Planktonic *P. aeruginosa* are phagocytosed or neutralised effectively. However, aggregation or micro-colony formation characterised by EPS and eDNA production prevents efficient clearance, with a sustained inflammation response occurring. This leads to O_2 depletion in the local micro-environment of infection, as O_2 is required to synthesize RNS and ROS. **IIIa)** Production of a reduced O_2 environment triggers *P. aeruginosa* to produce HCN, inhibiting cytochrome c dependent respiratory activities. This includes denitrification components NirS, NorBC and NosZ. Instead NO is detoxified by Fhp which oxidises NO to NO_3, further contributing to generation of a reduced oxygen environment. NarGHI derives electrons from the ubiquinone pool enabling respiratory NO_3 reduction to occur in the presence of CN^-. The presence of CN^- inhibits NirS however, transcriptional activation of *nirA* by cyanogenesis enables reduction of toxic NO_2 to NH_4, completing the DNRA pathway**. IIIb)** Inactivation of NirA would result in build-up of NO_2 in the local micro-environment. As a result, energy generation via the remaining cyanide-tolerant aerobic respiratory chains and respiratory nitrate reduction would be inhibited due to the interaction of NO_2 with metal ions and the metal centres which underpin electron transfer, and thus respiration.

7.3 Future perspectives

This model presented in this thesis is hypothetical, with numerous aspects of this pathway yet to be characterised. Many assumptions are made in regards to production of cyanide, availability of nitrate or nitrite and the interaction with the host immune system. Substantial amounts of work remain to validate this model, with this preliminary work pointing towards modified redox as a mechanism of virulence inhibition.

The growth defect exhibited by *nirA* mutants in response to reduced oxygenation and nitrate is suggested to be due to cyanide production and accumulation of nitrite (Figures 3.7, 6.9 and 6.12). However, neither cyanide or nitrite were directly quantified in the supernatant of *P. aeruginosa* cultures. Production of cyanide has been documented in LB and M-ASM however not in MOPS-succinate minimal media (309, 310). This experiment was planned, alongside monitoring ATP production and the NAD+:NADH ratio. However, problems with safety approval of new procedures in the wake of SARS-COV2 prevented the correct permissions from being obtained for direct cyanide quantification. The aim would be to monitor any build-up of denitrification intermediates in conjunction with production of cyanide, ATP and redox, monitored through NAD+/NADH. This would allow us to determine if cyanide toxicity is causing the theorised build-up in nitrite in *nirA* mutants through inhibition of enzymes downstream of NirS due to reliance on cytochrome c or cytochrome bc_1. Does this impact the ability of *P. aeruginosa* to produce ATP or oxidise and reduce NAD+/NADH in the context of the host environment? Further work is now planned to perform these experiments in *P. aeruginosa* mutants deleted for *nirA*, *nirB* and *nirS* alongside relevant double and triple mutants.

Another key question that requires answering is how would deletion of *nirA* impact biofilm formation or survival in mixed species communities. Mutants in *nirA* displayed reduced survival in a micro-aerobic colony biofilm model when grown in the presence of nitrate, with a mild effect also observed under aerobic conditions (Figures 3.9 and 3.17). Whilst oxygen gradients establish during biofilm formation, metabolites are also shared (311). For example, if nitrite accumulation does occur due to inhibition of NirA in a region of the biofilm where HCN production is maximal, these molecules can theoretically diffuse to

regions of the biofilm where denitrification is still active, although HCN likely spreads at a similar rate. The same can be said if other bacteria or fungi are present, could they detoxify any nitrate reduction intermediates in the absence of *P. aeruginosa* NirA? Whilst inhibition of metabolic pathways looks to be an attractive target for anti-virulence development, they must be assessed in the context of a community and the metabolites they produce and utilise (311). Many bacteria and fungi contain nitrate and nitrite reductases, therefore assessing the impact of NirA in a community will be essential before any future inhibitor development.

References

1. Abraham EP, Chain E. An enzyme from bacteria able to destroy penicillin. 1940. Rev Infect Dis. 1988;10(4):677-8.
2. Lobanovska M, Pilla G. Penicillin's Discovery and Antibiotic Resistance: Lessons for the Future? Yale J Biol Med. 2017;90(1):135-45.
3. Sengupta S, Chattopadhyay MK, Grossart HP. The multifaceted roles of antibiotics and antibiotic resistance in nature. Front Microbiol. 2013;4:47.
4. Resistance TRoA. Antimicroobial Resistance: Tackling a crisis for the health and wealth of nations Online: Wellcome Trust; 2014 [Available from: https://amr-review.org/home.html.
5. Stover CK, Pham XQ, Erwin AL, Mizoguchi SD, Warrener P, Hickey MJ, et al. Complete genome sequence of *Pseudomonas aeruginosa* PAO1, an opportunistic pathogen. Nature. 2000;406(6799):959-64.
6. Lyczak JB, Cannon CL, Pier GB. Establishment of *Pseudomonas aeruginosa* infection: lessons from a versatile opportunist. Microbes Infect. 2000;2(9):1051-60.
7. Högberg L D, K. W, C. S, J. G, D. M, O H. Annual epidemiological report - Antimicrobial resistance and healthcare-associated infections. European Centre for Disease Prevention and Control. 2014.
8. Juan C, Pena C, Oliver A. Host and Pathogen Biomarkers for Severe *Pseudomonas aeruginosa* Infections. J Infect Dis. 2017;215(suppl_1):S44-S51.
9. Rice LB. Federal funding for the study of antimicrobial resistance in nosocomial pathogens: no ESKAPE. J Infect Dis. 2008;197(8):1079-81.
10. Hsueh PR, Tseng SP, Teng LJ, Ho SW. Pan-drug-resistant *Pseudomonas aeruginosa* causing nosocomial infection at a university hospital in Taiwan. Clin Microbiol Infect. 2005;11(8):670-3.
11. Yakupogullari Y, Otlu B, Dogukan M, Gursoy C, Korkmaz E, Kizirgil A, et al. Investigation of a nosocomial outbreak by alginate-producing pan-antibiotic-resistant *Pseudomonas aeruginosa*. Am J Infect Control. 2008;36(10):e13-8.
12. Fernandes M, Vira D, Medikonda R, Kumar N. Extensively and pan-drug resistant *Pseudomonas aeruginosa* keratitis: clinical features, risk factors, and outcome. Graefes Arch Clin Exp Ophthalmol. 2016;254(2):315-22.
13. Control ECfDPa. Antimicrobial resistance in EU/EEA (EARS-Net). Stockholm; 2019.
14. Organization WH. WHO publishes list of bacteria for which new antibiotics are urgently needed Online2017 [News Release]. Available from: http://www.who.int/mediacentre/news/releases/2017/bacteria-antibiotics-needed/en/.
15. D. H. Tracking the Pipeline of Antibiotics in Development Pewtrusts.org2021 [cited 2021 12/10/21]. Available from: https://www.pewtrusts.org/en/research-and-

analysis/articles/2016/12/tracking-the-pipeline-of-antibiotics-in-development.
16. Ciofu O, Tolker-Nielsen T. Tolerance and Resistance of *Pseudomonas aeruginosa* Biofilms to Antimicrobial Agents-How P. aeruginosa Can Escape Antibiotics. Front Microbiol. 2019;10:913.
17. Moradali MF, Ghods S, Rehm BH. *Pseudomonas aeruginosa* Lifestyle: A Paradigm for Adaptation, Survival, and Persistence. Front Cell Infect Microbiol. 2017;7:39.
18. Valentini M, Gonzalez D, Mavridou DA, Filloux A. Lifestyle transitions and adaptive pathogenesis of *Pseudomonas aeruginosa*. Curr Opin Microbiol. 2018;41:15-20.
19. Chang CY. Surface Sensing for Biofilm Formation in *Pseudomonas aeruginosa.* Front Microbiol. 2017;8:2671.
20. Pamp SJ, Gjermansen M, Tolker-Nielsen T. The biofilm mode of life. Mechanisms and adaptations. Horizon Bioscience. 2007;16:37-69.
21. Rada B. Interactions between Neutrophils and *Pseudomonas aeruginosa* in Cystic Fibrosis. Pathogens. 2017;6(1).
22. Hunt BE, Weber A, Berger A, Ramsey B, Smith AL. Macromolecular mechanisms of sputum inhibition of tobramycin activity. Antimicrob Agents Chemother. 1995;39(1):34-9.
23. Tseng BS, Zhang W, Harrison JJ, Quach TP, Song JL, Penterman J, et al. The extracellular matrix protects *Pseudomonas aeruginosa* biofilms by limiting the penetration of tobramycin. Environ Microbiol. 2013;15(10):2865-78.
24. Pamp SJ, Gjermansen M, Johansen HK, Tolker-Nielsen T. Tolerance to the antimicrobial peptide colistin in *Pseudomonas aeruginosa* biofilms is linked to metabolically active cells, and depends on the pmr and *mexAB-oprM* genes. Mol Microbiol. 2008;68(1):223-40.
25. Chiang WC, Nilsson M, Jensen PO, Hoiby N, Nielsen TE, Givskov M, et al. Extracellular DNA shields against aminoglycosides in *Pseudomonas aeruginosa* biofilms. Antimicrob Agents Chemother. 2013;57(5):2352-61.
26. Nickel JC, Ruseska I, Wright JB, Costerton JW. Tobramycin resistance of *Pseudomonas aeruginosa* cells growing as a biofilm on urinary catheter material. Antimicrob Agents Chemother. 1985;27(4):619-24.
27. Hall CW, Mah TF. Molecular mechanisms of biofilm-based antibiotic resistance and tolerance in pathogenic bacteria. FEMS Microbiol Rev. 2017;41(3):276-301.
28. Xu KD, Stewart PS, Xia F, Huang CT, McFeters GA. Spatial physiological heterogeneity in *Pseudomonas aeruginosa* biofilm is determined by oxygen availability. Appl Environ Microbiol. 1998;64(10):4035-9.
29. Walters MC, 3rd, Roe F, Bugnicourt A, Franklin MJ, Stewart PS. Contributions of antibiotic penetration, oxygen limitation, and low metabolic activity to tolerance of *Pseudomonas aeruginosa* biofilms to ciprofloxacin and tobramycin. Antimicrob Agents Chemother. 2003;47(1):317-23.
30. Stewart PS, Zhang T, Xu R, Pitts B, Walters MC, Roe F, et al. Reaction-diffusion theory explains hypoxia and heterogeneous growth

within microbial biofilms associated with chronic infections. NPJ Biofilms Microbiomes. 2016;2:16012.
31. Grassi L, Di Luca M, Maisetta G, Rinaldi AC, Esin S, Trampuz A, et al. Generation of Persister Cells of *Pseudomonas aeruginosa* and Staphylococcus aureus by Chemical Treatment and Evaluation of Their Susceptibility to Membrane-Targeting Agents. Front Microbiol. 2017;8:1917.
32. Pang Z, Raudonis R, Glick BR, Lin TJ, Cheng Z. Antibiotic resistance in *Pseudomonas aeruginosa*: mechanisms and alternative therapeutic strategies. Biotechnol Adv. 2019;37(1):177-92.
33. Lewis K. Multidrug tolerance of biofilms and persister cells. Curr Top Microbiol Immunol. 2008;322:107-31.
34. Dorr T, Lewis K, Vulic M. SOS response induces persistence to fluoroquinolones in *Escherichia coli*. PLoS Genet. 2009;5(12):e1000760.
35. Wang T, El Meouche I, Dunlop MJ. Bacterial persistence induced by salicylate via reactive oxygen species. Sci Rep. 2017;7:43839.
36. Sugawara E, Nestorovich EM, Bezrukov SM, Nikaido H. *Pseudomonas aeruginosa* porin OprF exists in two different conformations. J Biol Chem. 2006;281(24):16220-9.
37. Bellido F, Martin NL, Siehnel RJ, Hancock RE. Reevaluation, using intact cells, of the exclusion limit and role of porin OprF in *Pseudomonas aeruginosa* outer membrane permeability. J Bacteriol. 1992;174(16):5196-203.
38. Hancock RE, Brinkman FS. Function of *Pseudomonas* porins in uptake and efflux. Annu Rev Microbiol. 2002;56:17-38.
39. Nikaido H, Takatsuka Y. Mechanisms of RND multidrug efflux pumps. Biochim Biophys Acta. 2009;1794(5):769-81.
40. Dreier J, Ruggerone P. Interaction of antibacterial compounds with RND efflux pumps in *Pseudomonas aeruginosa*. Front Microbiol. 2015;6:660.
41. Alcalde-Rico M, Olivares-Pacheco J, Alvarez-Ortega C, Camara M, Martinez JL. Role of the Multidrug Resistance Efflux Pump MexCD-OprJ in the *Pseudomonas aeruginosa* Quorum Sensing Response. Front Microbiol. 2018;9:2752.
42. Evans K, Passador L, Srikumar R, Tsang E, Nezezon J, Poole K. Influence of the MexAB-OprM multidrug efflux system on quorum sensing in *Pseudomonas aeruginosa*. J Bacteriol. 1998;180(20):5443-7.
43. Lamarche MG, Deziel E. MexEF-OprN efflux pump exports the *Pseudomonas* quinolone signal (PQS) precursor HHQ (4-hydroxy-2-heptylquinoline). PLoS One. 2011;6(9):e24310.
44. Torrens G, Hernandez SB, Ayala JA, Moya B, Juan C, Cava F, et al. Regulation of AmpC-Driven beta-Lactam Resistance in *Pseudomonas aeruginosa*: Different Pathways, Different Signaling. mSystems. 2019;4(6).
45. Jacobs C, Frere JM, Normark S. Cytosolic intermediates for cell wall biosynthesis and degradation control inducible beta-lactam resistance in gram-negative bacteria. Cell. 1997;88(6):823-32.
46. Poole K, Tetro K, Zhao Q, Neshat S, Heinrichs DE, Bianco N. Expression of the multidrug resistance operon *mexA-mexB-oprM* in

Pseudomonas aeruginosa: *mexR* encodes a regulator of operon expression. Antimicrob Agents Chemother. 1996;40(9):2021-8.
47. Sobel ML, Hocquet D, Cao L, Plesiat P, Poole K. Mutations in PA3574 (nalD) lead to increased MexAB-OprM expression and multidrug resistance in laboratory and clinical isolates of *Pseudomonas aeruginosa*. Antimicrob Agents Chemother. 2005;49(5):1782-6.
48. Daigle DM, Cao L, Fraud S, Wilke MS, Pacey A, Klinoski R, et al. Protein modulator of multidrug efflux gene expression in *Pseudomonas aeruginosa*. J Bacteriol. 2007;189(15):5441-51.
49. Kiser TH, Obritsch MD, Jung R, MacLaren R, Fish DN. Efflux pump contribution to multidrug resistance in clinical isolates of *Pseudomonas aeruginosa*. Pharmacotherapy. 2010;30(7):632-8.
50. Jorth P, McLean K, Ratjen A, Secor PR, Bautista GE, Ravishankar S, et al. Evolved Aztreonam Resistance Is Multifactorial and Can Produce Hypervirulence in *Pseudomonas aeruginosa*. mBio. 2017;8(5).
51. Poole K, Gotoh N, Tsujimoto H, Zhao Q, Wada A, Yamasaki T, et al. Overexpression of the *mexC-mexD-oprJ* efflux operon in nfxB-type multidrug-resistant strains of *Pseudomonas aeruginosa*. Mol Microbiol. 1996;21(4):713-24.
52. Aires JR, Kohler T, Nikaido H, Plesiat P. Involvement of an active efflux system in the natural resistance of *Pseudomonas aeruginosa* to aminoglycosides. Antimicrob Agents Chemother. 1999;43(11):2624-8.
53. Fetar H, Gilmour C, Klinoski R, Daigle DM, Dean CR, Poole K. *mexEF-oprN* multidrug efflux operon of *Pseudomonas aeruginosa*: regulation by the MexT activator in response to nitrosative stress and chloramphenicol. Antimicrob Agents Chemother. 2011;55(2):508-14.
54. Arber W. Horizontal Gene Transfer among Bacteria and Its Role in Biological Evolution. Life (Basel). 2014;4(2):217-24.
55. Carattoli A. Importance of integrons in the diffusion of resistance. Vet Res. 2001;32(3-4):243-59.
56. Poirel L, Lambert T, Turkoglu S, Ronco E, Gaillard J, Nordmann P. Characterization of Class 1 integrons from *Pseudomonas aeruginosa* that contain the bla(VIM-2) carbapenem-hydrolyzing beta-lactamase gene and of two novel aminoglycoside resistance gene cassettes. Antimicrob Agents Chemother. 2001;45(2):546-52.
57. Partridge SR, Kwong SM, Firth N, Jensen SO. Mobile Genetic Elements Associated with Antimicrobial Resistance. Clin Microbiol Rev. 2018;31(4).
58. Cazares A, Moore MP, Hall JPJ, Wright LL, Grimes M, Emond-Rheault JG, et al. A megaplasmid family driving dissemination of multidrug resistance in *Pseudomonas*. Nat Commun. 2020;11(1):1370.
59. Lin DM, Koskella B, Lin HC. Phage therapy: An alternative to antibiotics in the age of multi-drug resistance. World J Gastrointest Pharmacol Ther. 2017;8(3):162-73.
60. Hyman P, Abedon ST. Bacteriophage host range and bacterial resistance. Adv Appl Microbiol. 2010;70:217-48.
61. Jamal M, Bukhari S, Andleeb S, Ali M, Raza S, Nawaz MA, et al. Bacteriophages: an overview of the control strategies against multiple

bacterial infections in different fields. J Basic Microbiol. 2019;59(2):123-33.
62. Jault P, Leclerc T, Jennes S, Pirnay JP, Que YA, Resch G, et al. Efficacy and tolerability of a cocktail of bacteriophages to treat burn wounds infected by *Pseudomonas aeruginosa* (PhagoBurn): a randomised, controlled, double-blind phase 1/2 trial. Lancet Infect Dis. 2019;19(1):35-45.
63. Aslam S, Courtwright AM, Koval C, Lehman SM, Morales S, Furr CL, et al. Early clinical experience of bacteriophage therapy in 3 lung transplant recipients. Am J Transplant. 2019;19(9):2631-9.
64. Law N, Logan C, Yung G, Furr CL, Lehman SM, Morales S, et al. Successful adjunctive use of bacteriophage therapy for treatment of multidrug-resistant *Pseudomonas aeruginosa* infection in a cystic fibrosis patient. Infection. 2019;47(4):665-8.
65. Dedrick RM, Guerrero-Bustamante CA, Garlena RA, Russell DA, Ford K, Harris K, et al. Engineered bacteriophages for treatment of a patient with a disseminated drug-resistant *Mycobacterium abscessus*. Nat Med. 2019;25(5):730-3.
66. Nale JY, Vinner GK, Lopez VC, Thanki AM, Phothaworn P, Thiennimitr P, et al. An Optimized Bacteriophage Cocktail Can Effectively Control Salmonella in vitro and in Galleria mellonella. Front Microbiol. 2020;11:609955.
67. Hargreaves KR, Clokie MR. Clostridium difficile phages: still difficult? Front Microbiol. 2014;5:184.
68. Poolman JT. Expanding the role of bacterial vaccines into life-course vaccination strategies and prevention of antimicrobial-resistant infections. NPJ Vaccines. 2020;5(1):84.
69. Gruver AL, Hudson LL, Sempowski GD. Immunosenescence of ageing. J Pathol. 2007;211(2):144-56.
70. Cunningham AL, Lal H, Kovac M, Chlibek R, Hwang SJ, Diez-Domingo J, et al. Efficacy of the Herpes Zoster Subunit Vaccine in Adults 70 Years of Age or Older. N Engl J Med. 2016;375(11):1019-32.
71. Aabenhus R, Hansen MP, Siersma V, Bjerrum L. Clinical indications for antibiotic use in Danish general practice: results from a nationwide electronic prescription database. Scand J Prim Health Care. 2017;35(2):162-9.
72. Priebe GP, Goldberg JB. Vaccines for Pseudomonas aeruginosa: a long and winding road. Expert Rev Vaccines. 2014;13(4):507-19.
73. Solanki V, Tiwari M, Tiwari V. Prioritization of potential vaccine targets using comparative proteomics and designing of the chimeric multi-epitope vaccine against *Pseudomonas aeruginosa*. Sci Rep. 2019;9(1):5240.
74. Bianconi I, Alcala-Franco B, Scarselli M, Dalsass M, Buccato S, Colaprico A, et al. Genome-Based Approach Delivers Vaccine Candidates Against *Pseudomonas aeruginosa*. Front Immunol. 2018;9:3021.
75. Graham BS, Ambrosino DM. History of passive antibody administration for prevention and treatment of infectious diseases. Curr Opin HIV AIDS. 2015;10(3):129-34.

76. Andersen KK, Strokappe NM, Hultberg A, Truusalu K, Smidt I, Mikelsaar RH, et al. Neutralization of *Clostridium difficile* Toxin B Mediated by Engineered Lactobacilli That Produce Single-Domain Antibodies. Infect Immun. 2016;84(2):395-406.
77. Long SS. Infant botulism and treatment with BIG-IV (BabyBIG). Pediatr Infect Dis J. 2007;26(3):261-2.
78. Kummerfeldt CE. Raxibacumab: potential role in the treatment of inhalational anthrax. Infect Drug Resist. 2014;7:101-9.
79. Tabor DE, Yu L, Mok H, Tkaczyk C, Sellman BR, Wu Y, et al. Staphylococcus aureus Alpha-Toxin Is Conserved among Diverse Hospital Respiratory Isolates Collected from a Global Surveillance Study and Is Neutralized by Monoclonal Antibody MEDI4893. Antimicrob Agents Chemother. 2016;60(9):5312-21.
80. Mejias MP, Hiriart Y, Lauche C, Fernandez-Brando RJ, Pardo R, Bruballa A, et al. Development of camelid single chain antibodies against Shiga toxin type 2 (Stx2) with therapeutic potential against Hemolytic Uremic Syndrome (HUS). Sci Rep. 2016;6:24913.
81. Hall G, Kurosawa S, Stearns-Kurosawa DJ. Shiga Toxin Therapeutics: Beyond Neutralization. Toxins (Basel). 2017;9(9).
82. Santajit S, Seesuay W, Mahasongkram K, Sookrung N, Ampawong S, Reamtong O, et al. Human single-chain antibodies that neutralize *Pseudomonas aeruginosa*-exotoxin A-mediated cellular apoptosis. Sci Rep. 2019;9(1):14928.
83. Shadman Z, Farajnia S, Pazhang M, Tohidkia M, Rahbarnia L, Najavand S, et al. Isolation and characterizations of a novel recombinant scFv antibody against exotoxin A of *Pseudomonas aeruginosa*. BMC Infect Dis. 2021;21(1):300.
84. Santajit S, Kong-Ngoen T, Chongsa-Nguan M, Boonyuen U, Pumirat P, Sookrung N, et al. Human Single-Chain Antibodies That Neutralize Elastolytic Activity of *Pseudomonas aeruginosa* LasB. Pathogens. 2021;10(6).
85. Crousilles A, Maunders E, Bartlett S, Fan C, Ukor EF, Abdelhamid Y, et al. Which microbial factors really are important in *Pseudomonas aeruginosa* infections? Future Microbiol. 2015;10(11):1825-36.
86. Depluverez S, Devos S, Devreese B. The Role of Bacterial Secretion Systems in the Virulence of Gram-Negative Airway Pathogens Associated with Cystic Fibrosis. Front Microbiol. 2016;7:1336.
87. Hauser AR. The type III secretion system of *Pseudomonas aeruginosa*: infection by injection. Nat Rev Microbiol. 2009;7(9):654-65.
88. Fasciano AC, Shaban L, Mecsas J. Promises and Challenges of the Type Three Secretion System Injectisome as an Antivirulence Target. EcoSal Plus. 2019;8(2).
89. Milla CE, Chmiel JF, Accurso FJ, VanDevanter DR, Konstan MW, Yarranton G, et al. Anti-PcrV antibody in cystic fibrosis: a novel approach targeting *Pseudomonas aeruginosa* airway infection. Pediatr Pulmonol. 2014;49(7):650-8.
90. DiGiandomenico A, Keller AE, Gao C, Rainey GJ, Warrener P, Camara MM, et al. A multifunctional bispecific antibody protects against *Pseudomonas aeruginosa*. Sci Transl Med. 2014;6(262):262ra155.

91. Jain R, Beckett VV, Konstan MW, Accurso FJ, Burns JL, Mayer-Hamblett N, et al. KB001-A, a novel anti-inflammatory, found to be safe and well-tolerated in cystic fibrosis patients infected with *Pseudomonas aeruginosa*. J Cyst Fibros. 2018;17(4):484-91.
92. Ali SO, Yu XQ, Robbie GJ, Wu Y, Shoemaker K, Yu L, et al. Phase 1 study of MEDI3902, an investigational anti-*Pseudomonas aeruginosa* PcrV and Psl bispecific human monoclonal antibody, in healthy adults. Clin Microbiol Infect. 2019;25(5):629 e1- e6.
93. Feng C, Huang Y, He W, Cheng X, Liu H, Huang Y, et al. Tanshinones: First-in-Class Inhibitors of the Biogenesis of the Type 3 Secretion System Needle of *Pseudomonas aeruginosa* for Antibiotic Therapy. ACS Cent Sci. 2019;5(7):1278-88.
94. Marsden AE, King JM, Spies MA, Kim OK, Yahr TL. Inhibition of *Pseudomonas aeruginosa* ExsA DNA-Binding Activity by N-Hydroxybenzimidazoles. Antimicrob Agents Chemother. 2016;60(2):766-76.
95. Berube BJ, Murphy KR, Torhan MC, Bowlin NO, Williams JD, Bowlin TL, et al. Impact of Type III Secretion Effectors and of Phenoxyacetamide Inhibitors of Type III Secretion on Abscess Formation in a Mouse Model of *Pseudomonas aeruginosa* Infection. Antimicrob Agents Chemother. 2017;61(11).
96. Wang C, Liu X, Wang J, Zhou J, Cui Z, Zhang LH. Design and characterization of a polyamine derivative inhibiting the expression of type III secretion system in *Pseudomonas aeruginosa*. Sci Rep. 2016;6:30949.
97. Wang J, Wang J, Zhang LH. Immunological blocking of spermidine-mediated host-pathogen communication provides effective control against *Pseudomonas aeruginosa* infection. Microb Biotechnol. 2020;13(1):87-96.
98. Anantharajah A, Buyck JM, Sundin C, Tulkens PM, Mingeot-Leclercq MP, Van Bambeke F. Salicylidene Acylhydrazides and Hydroxyquinolines Act as Inhibitors of Type Three Secretion Systems in *Pseudomonas aeruginosa* by Distinct Mechanisms. Antimicrob Agents Chemother. 2017;61(6).
99. Massai F, Saleeb M, Doruk T, Elofsson M, Forsberg A. Development, Optimization, and Validation of a High Throughput Screening Assay for Identification of Tat and Type II Secretion Inhibitors of *Pseudomonas aeruginosa*. Front Cell Infect Microbiol. 2019;9:250.
100. Moir DT, Di M, Wong E, Moore RA, Schweizer HP, Woods DE, et al. Development and application of a cellular, gain-of-signal, bioluminescent reporter screen for inhibitors of type II secretion in *Pseudomonas aeruginosa* and *Burkholderia pseudomallei*. J Biomol Screen. 2011;16(7):694-705.
101. Fuqua C, Winans SC, Greenberg EP. Census and consensus in bacterial ecosystems: the LuxR-LuxI family of quorum-sensing transcriptional regulators. Annu Rev Microbiol. 1996;50:727-51.
102. Williams P, Camara M. Quorum sensing and environmental adaptation in *Pseudomonas aeruginosa*: a tale of regulatory networks and multifunctional signal molecules. Curr Opin Microbiol. 2009;12(2):182-91.

103. Ji C, Sharma I, Pratihar D, Hudson LL, Maura D, Guney T, et al. Designed Small-Molecule Inhibitors of the Anthranilyl-CoA Synthetase PqsA Block Quinolone Biosynthesis in *Pseudomonas aeruginosa*. ACS Chem Biol. 2016;11(11):3061-7.
104. Smith KM, Bu Y, Suga H. Induction and inhibition of *Pseudomonas aeruginosa* quorum sensing by synthetic autoinducer analogs. Chem Biol. 2003;10(1):81-9.
105. Ishida T, Ikeda T, Takiguchi N, Kuroda A, Ohtake H, Kato J. Inhibition of quorum sensing in *Pseudomonas aeruginosa* by N-acyl cyclopentylamides. Appl Environ Microbiol. 2007;73(10):3183-8.
106. Persson T, Hansen TH, Rasmussen TB, Skinderso ME, Givskov M, Nielsen J. Rational design and synthesis of new quorum-sensing inhibitors derived from acylated homoserine lactones and natural products from garlic. Org Biomol Chem. 2005;3(2):253-62.
107. O'Loughlin CT, Miller LC, Siryaporn A, Drescher K, Semmelhack MF, Bassler BL. A quorum-sensing inhibitor blocks *Pseudomonas aeruginosa* virulence and biofilm formation. Proc Natl Acad Sci U S A. 2013;110(44):17981-6.
108. Grossman S, Soukarieh F, Richardson W, Liu R, Mashabi A, Emsley J, et al. Novel quinazolinone inhibitors of the *Pseudomonas aeruginosa* quorum sensing transcriptional regulator PqsR. Eur J Med Chem. 2020;208:112778.
109. Fleitas Martinez O, Cardoso MH, Ribeiro SM, Franco OL. Recent Advances in Anti-virulence Therapeutic Strategies With a Focus on Dismantling Bacterial Membrane Microdomains, Toxin Neutralization, Quorum-Sensing Interference and Biofilm Inhibition. Front Cell Infect Microbiol. 2019;9:74.
110. Fetzner S. Quorum quenching enzymes. J Biotechnol. 2015;201:2-14.
111. Dong YH, Xu JL, Li XZ, Zhang LH. AiiA, an enzyme that inactivates the acylhomoserine lactone quorum-sensing signal and attenuates the virulence of *Erwinia carotovora*. Proc Natl Acad Sci U S A. 2000;97(7):3526-31.
112. Birmes FS, Wolf T, Kohl TA, Ruger K, Bange F, Kalinowski J, et al. Mycobacterium abscessus subsp. abscessus Is Capable of Degrading *Pseudomonas aeruginosa* Quinolone Signals. Front Microbiol. 2017;8:339.
113. Hraiech S, Hiblot J, Lafleur J, Lepidi H, Papazian L, Rolain JM, et al. Inhaled lactonase reduces *Pseudomonas aeruginosa* quorum sensing and mortality in rat pneumonia. PLoS One. 2014;9(10):e107125.
114. Migiyama Y, Kaneko Y, Yanagihara K, Morohoshi T, Morinaga Y, Nakamura S, et al. Efficacy of AiiM, an N-acylhomoserine lactonase, against *Pseudomonas aeruginosa* in a mouse model of acute pneumonia. Antimicrob Agents Chemother. 2013;57(8):3653-8.
115. Thomann A, de Mello Martins AG, Brengel C, Empting M, Hartmann RW. Application of Dual Inhibition Concept within Looped Autoregulatory Systems toward Antivirulence Agents against *Pseudomonas aeruginosa* Infections. ACS Chem Biol. 2016;11(5):1279-86.

116. Lidor O, Al-Quntar A, Pesci EC, Steinberg D. Mechanistic analysis of a synthetic inhibitor of the *Pseudomonas aeruginosa* LasI quorum-sensing signal synthase. Sci Rep. 2015;5:16569.
117. Kumar L, Chhibber S, Kumar R, Kumar M, Harjai K. Zingerone silences quorum sensing and attenuates virulence of *Pseudomonas aeruginosa*. Fitoterapia. 2015;102:84-95.
118. Kutty SK, Barraud N, Ho KK, Iskander GM, Griffith R, Rice SA, et al. Hybrids of acylated homoserine lactone and nitric oxide donors as inhibitors of quorum sensing and virulence factors in *Pseudomonas aeruginosa*. Org Biomol Chem. 2015;13(38):9850-61.
119. Kalia M, Yadav VK, Singh PK, Sharma D, Narvi SS, Agarwal V. Exploring the impact of parthenolide as anti-quorum sensing and anti-biofilm agent against *Pseudomonas aeruginosa*. Life Sci. 2018;199:96-103.
120. Kalaiarasan E, Thirumalaswamy K, Harish BN, Gnanasambandam V, Sali VK, John J. Inhibition of quorum sensing-controlled biofilm formation in *Pseudomonas aeruginosa* by quorum-sensing inhibitors. Microb Pathog. 2017;111:99-107.
121. Park S, Kim HS, Ok K, Kim Y, Park HD, Byun Y. Design, synthesis and biological evaluation of 4-(alkyloxy)-6-methyl-2H-pyran-2-one derivatives as quorum sensing inhibitors. Bioorg Med Chem Lett. 2015;25(15):2913-7.
122. Heidari A, Noshiranzadeh N, Haghi F, Bikas R. Inhibition of quorum sensing related virulence factors of *Pseudomonas aeruginosa* by pyridoxal lactohydrazone. Microb Pathog. 2017;112:103-10.
123. Amara N, Gregor R, Rayo J, Dandela R, Daniel E, Liubin N, et al. Fine-Tuning Covalent Inhibition of Bacterial Quorum Sensing. Chembiochem. 2016;17(9):825-35.
124. Gokalsin B, Aksoydan B, Erman B, Sesal NC. Reducing Virulence and Biofilm of *Pseudomonas aeruginosa* by Potential Quorum Sensing Inhibitor Carotenoid: Zeaxanthin. Microb Ecol. 2017;74(2):466-73.
125. Chatterjee M, D'Morris S, Paul V, Warrier S, Vasudevan AK, Vanuopadath M, et al. Mechanistic understanding of Phenyllactic acid mediated inhibition of quorum sensing and biofilm development in *Pseudomonas aeruginosa*. Appl Microbiol Biotechnol. 2017;101(22):8223-36.
126. Abbas HA, Elsherbini AM, Shaldam MA. Repurposing metformin as a quorum sensing inhibitor in *Pseudomonas aeruginosa*. Afr Health Sci. 2017;17(3):808-19.
127. Abbas HA, Shaldam MA. Glyceryl trinitrate is a novel inhibitor of quorum sensing in *Pseudomonas aeruginosa*. Afr Health Sci. 2016;16(4):1109-17.
128. Soukarieh F, Vico Oton E, Dubern JF, Gomes J, Halliday N, de Pilar Crespo M, et al. *In Silico* and *in Vitro*-Guided Identification of Inhibitors of Alkylquinolone-Dependent Quorum Sensing in *Pseudomonas aeruginosa*. Molecules. 2018;23(2).
129. Zhang Y, Sass A, Van Acker H, Wille J, Verhasselt B, Van Nieuwerburgh F, et al. Coumarin Reduces Virulence and Biofilm Formation in *Pseudomonas aeruginosa* by Affecting Quorum Sensing, Type III Secretion and C-di-GMP Levels. Front Microbiol. 2018;9:1952.

130. D'Angelo F, Baldelli V, Halliday N, Pantalone P, Polticelli F, Fiscarelli E, et al. Identification of FDA-Approved Drugs as Antivirulence Agents Targeting the pqs Quorum-Sensing System of *Pseudomonas aeruginosa*. Antimicrob Agents Chemother. 2018;62(11).
131. Birmes FS, Saring R, Hauke MC, Ritzmann NH, Drees SL, Daniel J, et al. Interference with *Pseudomonas aeruginosa* Quorum Sensing and Virulence by the Mycobacterial *Pseudomonas* Quinolone Signal Dioxygenase AqdC in Combination with the N-Acylhomoserine Lactone Lactonase QsdA. Infect Immun. 2019;87(10).
132. Qvortrup K, Hultqvist LD, Nilsson M, Jakobsen TH, Jansen CU, Uhd J, et al. Small Molecule Anti-biofilm Agents Developed on the Basis of Mechanistic Understanding of Biofilm Formation. Front Chem. 2019;7:742.
133. Opoku-Temeng C, Sintim HO. Targeting c-di-GMP Signaling, Biofilm Formation, and Bacterial Motility with Small Molecules. Methods Mol Biol. 2017;1657:419-30.
134. Svensson L, Poljakovic M, Demirel I, Sahlberg C, Persson K. Chapter One - Host-Derived Nitric Oxide and Its Antibacterial Effects in the Urinary Tract. Poole RK, editor: Academic Press; 2018.
135. Barraud N, Schleheck D, Klebensberger J, Webb JS, Hassett DJ, Rice SA, et al. Nitric oxide signaling in *Pseudomonas aeruginosa* biofilms mediates phosphodiesterase activity, decreased cyclic di-GMP levels, and enhanced dispersal. J Bacteriol. 2009;191(23):7333-42.
136. Sambanthamoorthy K, Luo C, Pattabiraman N, Feng X, Koestler B, Waters CM, et al. Identification of small molecules inhibiting diguanylate cyclases to control bacterial biofilm development. Biofouling. 2014;30(1):17-28.
137. Brown HL, Hanman K, Reuter M, Betts RP, van Vliet AH. *Campylobacter jejuni* biofilms contain extracellular DNA and are sensitive to DNase I treatment. Front Microbiol. 2015;6:699.
138. DiGiandomenico A, Warrener P, Hamilton M, Guillard S, Ravn P, Minter R, et al. Identification of broadly protective human antibodies to *Pseudomonas aeruginosa* exopolysaccharide Psl by phenotypic screening. J Exp Med. 2012;209(7):1273-87.
139. Price-Whelan A, Dietrich LE, Newman DK. Rethinking 'secondary' metabolism: physiological roles for phenazine antibiotics. Nat Chem Biol. 2006;2(2):71-8.
140. Jo J, Cortez KL, Cornell WC, Price-Whelan A, Dietrich LE. An orphan *cbb3*-type cytochrome oxidase subunit supports *Pseudomonas aeruginosa* biofilm growth and virulence. Elife. 2017;6.
141. Das T, Kutty SK, Tavallaie R, Ibugo AI, Panchompoo J, Sehar S, et al. Phenazine virulence factor binding to extracellular DNA is important for *Pseudomonas aeruginosa* biofilm formation. Sci Rep. 2015;5:8398.
142. Allesen-Holm M, Barken KB, Yang L, Klausen M, Webb JS, Kjelleberg S, et al. A characterization of DNA release in *Pseudomonas aeruginosa* cultures and biofilms. Mol Microbiol. 2006;59(4):1114-28.
143. Nakamura S, Higashiyama Y, Izumikawa K, Seki M, Kakeya H, Yamamoto Y, et al. The roles of the quorum-sensing system in the release of extracellular DNA, lipopolysaccharide, and membrane

vesicles from *Pseudomonas aeruginosa*. Jpn J Infect Dis. 2008;61(5):375-8.
144. Wang J, Yu B, Tian D, Ni M. Rhamnolipid but not motility is associated with the initiation of biofilm seeding dispersal of *Pseudomonas aeruginosa* strain PA17. J Biosci. 2013;38(1):149-56.
145. Pamp SJ, Tolker-Nielsen T. Multiple roles of biosurfactants in structural biofilm development by *Pseudomonas aeruginosa*. J Bacteriol. 2007;189(6):2531-9.
146. Sakuragi Y, Kolter R. Quorum-sensing regulation of the biofilm matrix genes (pel) of *Pseudomonas aeruginosa*. J Bacteriol. 2007;189(14):5383-6.
147. Ueda A, Wood TK. Connecting quorum sensing, c-di-GMP, pel polysaccharide, and biofilm formation in *Pseudomonas aeruginosa* through tyrosine phosphatase TpbA (PA3885). PLoS Pathog. 2009;5(6):e1000483.
148. Solano C, Echeverz M, Lasa I. Biofilm dispersion and quorum sensing. Curr Opin Microbiol. 2014;18:96-104.
149. Dubern JF, Cigana C, De Simone M, Lazenby J, Juhas M, Schwager S, et al. Integrated whole-genome screening for *Pseudomonas aeruginosa* virulence genes using multiple disease models reveals that pathogenicity is host specific. Environ Microbiol. 2015;17(11):4379-93.
150. Lyon BR, Skurray R. Antimicrobial resistance of *Staphylococcus aureus:* genetic basis. Microbiol Rev. 1987;51(1):88-134.
151. Heurlier K, Denervaud V, Pessi G, Reimmann C, Haas D. Negative control of quorum sensing by RpoN (sigma54) in *Pseudomonas aeruginosa* PAO1. J Bacteriol. 2003;185(7):2227-35.
152. Freschi L, Jeukens J, Kukavica-Ibrulj I, Boyle B, Dupont MJ, Laroche J, et al. Clinical utilization of genomics data produced by the international *Pseudomonas aeruginosa* consortium. Front Microbiol. 2015;6:1036.
153. Metcalf WW, Jiang W, Wanner BL. Use of the rep technique for allele replacement to construct new *Escherichia coli* hosts for maintenance of R6K gamma origin plasmids at different copy numbers. Gene. 1994;138(1-2):1-7.
154. Studier FW, Moffatt BA. Use of bacteriophage T7 RNA polymerase to direct selective high-level expression of cloned genes. J Mol Biol. 1986;189(1):113-30.
155. Robichon C, Luo J, Causey TB, Benner JS, Samuelson JC. Engineering *Escherichia coli* BL21(DE3) derivative strains to minimize *E. coli* protein contamination after purification by immobilized metal affinity chromatography. Appl Environ Microbiol. 2011;77(13):4634-46.
156. Voisard C, Bull CT, Keel C, Laville J, Maurhofer M, Schnider U, et al. Biocontrol of root diseases by *Pseudomonas fluorescens* CHA0: current concepts and experimental approaches. Molecular ecology of rhizosphere microorganisms. 1994;73:2504-14.
157. Hoang TT, Kutchma AJ, Becher A, Schweizer HP. Integration-proficient plasmids for *Pseudomonas aeruginosa:* site-specific integration and use for engineering of reporter and expression strains. Plasmid. 2000;43(1):59-72.

158. Choi KH, Gaynor JB, White KG, Lopez C, Bosio CM, Karkhoff-Schweizer RR, et al. A Tn7-based broad-range bacterial cloning and expression system. Nat Methods. 2005;2(6):443-8.
159. Crepin S, Harel J, Dozois CM. Chromosomal complementation using Tn7 transposon vectors in Enterobacteriaceae. Appl Environ Microbiol. 2012;78(17):6001-8.
160. Kirchner S, Fothergill JL, Wright EA, James CE, Mowat E, Winstanley C. Use of artificial sputum medium to test antibiotic efficacy against *Pseudomonas aeruginosa* in conditions more relevant to the cystic fibrosis lung. J Vis Exp. 2012(64):e3857.
161. LaBauve AE, Wargo MJ. Growth and laboratory maintenance of *Pseudomonas aeruginosa*. Curr Protoc Microbiol. 2012;Chapter 6:Unit 6E 1.
162. Sambrook JF, Russell SA. Molecular cloning: A Labaratory Manual. 3rd edition ed. NY: Cold Spring Harbour Laboratory Press: Cold Spring Harbour 2001.
163. Winsor GL, Griffiths EJ, Lo R, Dhillon BK, Shay JA, Brinkman FS. Enhanced annotations and features for comparing thousands of *Pseudomonas* genomes in the Pseudomonas genome database. Nucleic Acids Res. 2016;44(D1):D646-53.
164. Rice P, Longden I, Bleasby A. EMBOSS: the European Molecular Biology Open Software Suite. Trends Genet. 2000;16(6):276-7.
165. Choi KH, Kumar A, Schweizer HP. A 10-min method for preparation of highly electrocompetent *Pseudomonas aeruginosa* cells: application for DNA fragment transfer between chromosomes and plasmid transformation. J Microbiol Methods. 2006;64(3):391-7.
166. Sacherer P, Defago G, Haas D. Extracellular protease and phospholipase C are controlled by the global regulatory gene gacA in the biocontrol strain *Pseudomonas fluorescens* CHA0. FEMS Microbiol Lett. 1994;116(2):155-60.
167. Essar DW, Eberly L, Hadero A, Crawford IP. Identification and characterization of genes for a second anthranilate synthase in *Pseudomonas aeruginosa*: interchangeability of the two anthranilate synthases and evolutionary implications. J Bacteriol. 1990;172(2):884-900.
168. Sokol PA, Ohman DE, Iglewski BH. A more sensitive plate assay for detection of protease production by *Pseudomanas aeruginosa*. J Clin Microbiol. 1979;9(4):538-40.
169. Apidianakis Y, Rahme LG. Drosophila melanogaster as a model host for studying *Pseudomonas aeruginosa* infection. Nat Protoc. 2009;4(9):1285-94.
170. Lore NI, Cigana C, De Fino I, Riva C, Juhas M, Schwager S, et al. Cystic fibrosis-niche adaptation of *Pseudomonas aeruginosa* reduces virulence in multiple infection hosts. PLoS One. 2012;7(4):e35648.
171. Ulrich M, Beer I, Braitmaier P, Dierkes M, Kummer F, Krismer B, et al. Relative contribution of *Prevotella intermedia* and *Pseudomonas aeruginosa* to lung pathology in airways of patients with cystic fibrosis. Thorax. 2010;65(11):978-84.
172. Bianconi I, Milani A, Cigana C, Paroni M, Levesque RC, Bertoni G, et al. Positive signature-tagged mutagenesis in *Pseudomonas*

aeruginosa: tracking patho-adaptive mutations promoting airways chronic infection. PLoS Pathog. 2011;7(2):e1001270.
173. Pirone L, Bragonzi A, Farcomeni A, Paroni M, Auriche C, Conese M, et al. *Burkholderia cenocepacia* strains isolated from cystic fibrosis patients are apparently more invasive and more virulent than rhizosphere strains. Environ Microbiol. 2008;10(10):2773-84.
174. Hoffmann N, Rasmussen TB, Jensen PO, Stub C, Hentzer M, Molin S, et al. Novel mouse model of chronic *Pseudomonas aeruginosa* lung infection mimicking cystic fibrosis. Infect Immun. 2005;73(4):2504-14.
175. Bragonzi A, Worlitzsch D, Pier GB, Timpert P, Ulrich M, Hentzer M, et al. Nonmucoid *Pseudomonas aeruginosa* expresses alginate in the lungs of patients with cystic fibrosis and in a mouse model. J Infect Dis. 2005;192(3):410-9.
176. Laemmli UK. Cleavage of structural proteins during the assembly of the head of bacteriophage T4. Nature. 1970;227(5259):680-5.
177. Schagger H. Tricine-SDS-PAGE. Nat Protoc. 2006;1(1):16-22.
178. Fuhrmann M, Hausherr A, Ferbitz L, Schodl T, Heitzer M, Hegemann P. Monitoring dynamic expression of nuclear genes in *Chlamydomonas reinhardtii* by using a synthetic luciferase reporter gene. Plant Mol Biol. 2004;55(6):869-81.
179. Schnell R, Sandalova T, Hellman U, Lindqvist Y, Schneider G. Siroheme- and [Fe4-S4]-dependent NirA from *Mycobacterium tuberculosis* is a sulfite reductase with a covalent Cys-Tyr bond in the active site. J Biol Chem. 2005;280(29):27319-28.
180. Maura D, Ballok AE, Rahme LG. Considerations and caveats in anti-virulence drug development. Curr Opin Microbiol. 2016;33:41-6.
181. Fernebro J. Fighting bacterial infections-future treatment options. Drug Resist Updat. 2011;14(2):125-39.
182. Kim SH, Park SY, Heo YJ, Cho YH. *Drosophila melanogaste*r-based screening for multihost virulence factors of *Pseudomonas aeruginosa* PA14 and identification of a virulence-attenuating factor, HudA. Infect Immun. 2008;76(9):4152-62.
183. Feinbaum RL, Urbach JM, Liberati NT, Djonovic S, Adonizio A, Carvunis AR, et al. Genome-wide identification of *Pseudomonas aeruginosa* virulence-related genes using a *Caenorhabditis elegans* infection model. PLoS Pathog. 2012;8(7):e1002813.
184. Potvin E, Lehoux DE, Kukavica-Ibrulj I, Richard KL, Sanschagrin F, Lau GW, et al. *In vivo* functional genomics of *Pseudomonas aeruginosa* for high-throughput screening of new virulence factors and antibacterial targets. Environ Microbiol. 2003;5(12):1294-308.
185. Winstanley C, Langille MG, Fothergill JL, Kukavica-Ibrulj I, Paradis-Bleau C, Sanschagrin F, et al. Newly introduced genomic prophage islands are critical determinants of in vivo competitiveness in the Liverpool Epidemic Strain of *Pseudomonas aeruginosa*. Genome Res. 2009;19(1):12-23.
186. Rahme LG, Stevens EJ, Wolfort SF, Shao J, Tompkins RG, Ausubel FM. Common virulence factors for bacterial pathogenicity in plants and animals. Science. 1995;268(5219):1899-902.

187. Tan MW, Mahajan-Miklos S, Ausubel FM. Killing of Caenorhabditis elegans by *Pseudomonas aeruginosa* used to model mammalian bacterial pathogenesis. Proc Natl Acad Sci U S A. 1999;96(2):715-20.
188. Chieda Y, Iiyama K, Yasunaga-Aoki C, Lee JM, Kusakabe T, Shimizu S. Pathogenicity of *gacA* mutant of *Pseudomonas aeruginosa* PA01 in the silkworm, Bombyx mori. FEMS Microbiol Lett. 2005;244(1):181-6.
189. Jander G, Rahme LG, Ausubel FM. Positive correlation between virulence of *Pseudomonas aeruginosa* mutants in mice and insects. J Bacteriol. 2000;182(13):3843-5.
190. Clatworthy AE, Lee JS, Leibman M, Kostun Z, Davidson AJ, Hung DT. *Pseudomonas aeruginosa* infection of zebrafish involves both host and pathogen determinants. Infect Immun. 2009;77(4):1293-303.
191. Harrison F, Diggle SP. An ex vivo lung model to study bronchioles infected with *Pseudomonas aeruginosa* biofilms. Microbiology (Reading). 2016;162(10):1755-60.
192. van Heeckeren AM, Schluchter MD. Murine models of chronic *Pseudomonas aeruginosa* lung infection. Lab Anim. 2002;36(3):291-312.
193. Bayes HK, Ritchie N, Irvine S, Evans TJ. A murine model of early *Pseudomonas aeruginosa* lung disease with transition to chronic infection. Sci Rep. 2016;6:35838.
194. Stieritz DD, Holder IA. Experimental studies of the pathogenesis of infections due to *Pseudomonas aeruginosa*: description of a burned mouse model. J Infect Dis. 1975;131(6):688-91.
195. Brandenburg KS, Weaver AJ, Jr., Qian L, You T, Chen P, Karna SLR, et al. Development of *Pseudomonas aeruginosa* Biofilms in Partial-Thickness Burn Wounds Using a Sprague-Dawley Rat Model. J Burn Care Res. 2019;40(1):44-57.
196. Koch G, Nadal-Jimenez P, Cool RH, Quax WJ. Assessing *Pseudomonas* virulence with nonmammalian host: *Galleria mellonella*. Methods Mol Biol. 2014;1149:681-8.
197. Gallagher LA, Manoil C. *Pseudomonas aeruginosa* PAO1 kills *Caenorhabditis elegans* by cyanide poisoning. J Bacteriol. 2001;183(21):6207-14.
198. Stroupe E, Getzoff E. The Role of Siroheme in Sulfite and Nitrite Reductases: Springer, New York, NY.; 2009.
199. Frangipani E, Perez-Martinez I, Williams HD, Cherbuin G, Haas D. A novel cyanide-inducible gene cluster helps protect *Pseudomonas aeruginosa* from cyanide. Environ Microbiol Rep. 2014;6(1):28-34.
200. Wang T, Qi Y, Wang Z, Zhao J, Ji L, Li J, et al. Coordinated regulation of anthranilate metabolism and bacterial virulence by the GntR family regulator MpaR in *Pseudomonas aeruginosa*. Mol Microbiol. 2020;114(5):857-69.
201. Broderick KE, Chan A, Balasubramanian M, Feala J, Reed SL, Panda M, et al. Cyanide produced by human isolates of *Pseudomonas aeruginosa* contributes to lethality in *Drosophila melanogaster*. J Infect Dis. 2008;197(3):457-64.

202. Carroll W, Lenney W, Wang T, Spanel P, Alcock A, Smith D. Detection of volatile compounds emitted by *Pseudomonas aeruginosa* using selected ion flow tube mass spectrometry. Pediatr Pulmonol. 2005;39(5):452-6.
203. Ryall B, Davies JC, Wilson R, Shoemark A, Williams HD. *Pseudomonas aeruginosa*, cyanide accumulation and lung function in CF and non-CF bronchiectasis patients. Eur Respir J. 2008;32(3):740-7.
204. Way JL. Cyanide intoxication and its mechanism of antagonism. Annu Rev Pharmacol Toxicol. 1984;24:451-81.
205. Hirai T, Osamura T, Ishii M, Arai H. Expression of multiple *cbb3* cytochrome c oxidase isoforms by combinations of multiple isosubunits in *Pseudomonas aeruginosa*. Proc Natl Acad Sci U S A. 2016;113(45):12815-9.
206. Lee DG, Urbach JM, Wu G, Liberati NT, Feinbaum RL, Miyata S, et al. Genomic analysis reveals that *Pseudomonas aeruginosa* virulence is combinatorial. Genome Biol. 2006;7(10):R90.
207. Frangipani E, Slaveykova VI, Reimmann C, Haas D. Adaptation of aerobically growing *Pseudomonas aeruginosa* to copper starvation. J Bacteriol. 2008;190(20):6706-17.
208. Pessi G, Haas D. Transcriptional control of the hydrogen cyanide biosynthetic genes *hcnABC* by the anaerobic regulator ANR and the quorum-sensing regulators LasR and RhlR in *Pseudomonas aeruginosa*. J Bacteriol. 2000;182(24):6940-9.
209. Palmer KL, Aye LM, Whiteley M. Nutritional cues control *Pseudomonas aeruginosa* multicellular behavior in cystic fibrosis sputum. J Bacteriol. 2007;189(22):8079-87.
210. Lin YC, Sekedat MD, Cornell WC, Silva GM, Okegbe C, Price-Whelan A, et al. Phenazines Regulate Nap-Dependent Denitrification in *Pseudomonas aeruginosa* Biofilms. J Bacteriol. 2018;200(9).
211. Price MN, Wetmore KM, Waters RJ, Callaghan M, Ray J, Liu H, et al. Mutant phenotypes for thousands of bacterial genes of unknown function. Nature. 2018;557(7706):503-9.
212. Freschi L, Bertelli C, Jeukens J, Moore MP, Kukavica-Ibrulj I, Emond-Rheault JG, et al. Genomic characterisation of an international *Pseudomonas aeruginosa* reference panel indicates that the two major groups draw upon distinct mobile gene pools. FEMS Microbiol Lett. 2018;365(14).
213. Cunliffe HE, Merriman TR, Lamont IL. Cloning and characterization of pvdS, a gene required for pyoverdine synthesis in *Pseudomonas aeruginosa:* PvdS is probably an alternative sigma factor. J Bacteriol. 1995;177(10):2744-50.
214. Frangipani E, Visaggio D, Heeb S, Kaever V, Camara M, Visca P, et al. The Gac/Rsm and cyclic-di-GMP signalling networks coordinately regulate iron uptake in *Pseudomonas aeruginosa*. Environ Microbiol. 2014;16(3):676-88.
215. Little AS, Okkotsu Y, Reinhart AA, Damron FH, Barbier M, Barrett B, et al. *Pseudomonas aeruginosa* AlgR Phosphorylation Status Differentially Regulates Pyocyanin and Pyoverdine Production. mBio. 2018;9(1).

216. Waterhouse A, Bertoni M, Bienert S, Studer G, Tauriello G, Gumienny R, et al. SWISS-MODEL: homology modelling of protein structures and complexes. Nucleic Acids Res. 2018;46(W1):W296-W303.
217. Sugiki T, Kobayashi N, Fujiwara T. Modern Technologies of Solution Nuclear Magnetic Resonance Spectroscopy for Three-dimensional Structure Determination of Proteins Open Avenues for Life Scientists. Comput Struct Biotechnol J. 2017;15:328-39.
218. Wu M, Lander GC. How low can we go? Structure determination of small biological complexes using single-particle cryo-EM. Curr Opin Struct Biol. 2020;64:9-16.
219. Smith DW. Problems of translating heterologous genes in expression systems: the role of tRNA. Biotechnol Prog. 1996;12(4):417-22.
220. Fu W, Lin J, Cen P. 5-Aminolevulinate production with recombinant *Escherichia coli* using a rare codon optimizer host strain. Appl Microbiol Biotechnol. 2007;75(4):777-82.
221. McNulty DE, Claffee BA, Huddleston MJ, Porter ML, Cavnar KM, Kane JF. Mistranslational errors associated with the rare arginine codon CGG in *Escherichia coli*. Protein Expr Purif. 2003;27(2):365-74.
222. Qing G, Ma LC, Khorchid A, Swapna GV, Mal TK, Takayama MM, et al. Cold-shock induced high-yield protein production in *Escherichia coli*. Nat Biotechnol. 2004;22(7):877-82.
223. Zhou P, Wagner G. Overcoming the solubility limit with solubility-enhancement tags: successful applications in biomolecular NMR studies. J Biomol NMR. 2010;46(1):23-31.
224. Wu JY, Siegel LM, Kredich NM. High-level expression of *Escherichia coli* NADPH-sulfite reductase: requirement for a cloned *cysG* plasmid to overcome limiting siroheme cofactor. J Bacteriol. 1991;173(1):325-33.
225. Spencer JB, Stolowich NJ, Roessner CA, Scott AI. The *Escherichia coli cysG* gene encodes the multifunctional protein, siroheme synthase. FEBS Lett. 1993;335(1):57-60.
226. Corless EI, Mettert EL, Kiley PJ, Antony E. Elevated Expression of a Functional Suf Pathway in *Escherichia coli* BL21(DE3) Enhances Recombinant Production of an Iron-Sulfur Cluster-Containing Protein. J Bacteriol. 2020;202(3).
227. Bolanos-Garcia VM, Davies OR. Structural analysis and classification of native proteins from *E. coli* commonly co-purified by immobilised metal affinity chromatography. Biochim Biophys Acta. 2006;1760(9):1304-13.
228. Plumbridge J, Vimr E. Convergent pathways for utilization of the amino sugars N-acetylglucosamine, N-acetylmannosamine, and N-acetylneuraminic acid by *Escherichia coli*. J Bacteriol. 1999;181(1):47-54.
229. Walters KA, Golbeck JH. Expression, purification and characterization of an active C491G variant of ferredoxin sulfite reductase from *Synechococcus elongatus* PCC 7942. Biochim Biophys Acta Bioenerg. 2018;1859(10):1096-107.

230. McPherson A, Gavira JA. Introduction to protein crystallization. Acta Crystallogr F Struct Biol Commun. 2014;70(Pt 1):2-20.
231. Crane BR, Siegel LM, Getzoff ED. Sulfite reductase structure at 1.6 A: evolution and catalysis for reduction of inorganic anions. Science. 1995;270(5233):59-67.
232. Swamy U, Wang M, Tripathy JN, Kim SK, Hirasawa M, Knaff DB, et al. Structure of spinach nitrite reductase: implications for multi-electron reactions by the iron-sulfur:siroheme cofactor. Biochemistry. 2005;44(49):16054-63.
233. YC H, Liu M, VC W, YL C, EH L, WG W, et al. Structure insights into the enzyme catalysis from comparison of three forms of dissimilatory sulfite reductase from *Desulfovibrio gigas*. Protein Data Bank2010.
234. Nakano S, Takahashi M, Sakamoto A, Morikawa H, Katayanagi K. Structure-function relationship of assimilatory nitrite reductases from the leaf and root of tobacco based on high-resolution structures. Protein Sci. 2012;21(3):383-95.
235. Kim JY, Nakayama M, Toyota H, Kurisu G, Hase T. Structural and mutational studies of an electron transfer complex of maize sulfite reductase and ferredoxin. J Biochem. 2016;160(2):101-9.
236. Crane BR, Getzoff ED. The relationship between structure and function for the sulfite reductases. Curr Opin Struct Biol. 1996;6(6):744-56.
237. Moreno-Vivian C, Cabello P, Martinez-Luque M, Blasco R, Castillo F. Prokaryotic nitrate reduction: molecular properties and functional distinction among bacterial nitrate reductases. J Bacteriol. 1999;181(21):6573-84.
238. Romeo A, Sonnleitner E, Sorger-Domenigg T, Nakano M, Eisenhaber B, Blasi U. Transcriptional regulation of nitrate assimilation in *Pseudomonas aeruginosa* occurs via transcriptional antitermination within the *nirBD-PA1779-cobA* operon. Microbiology. 2012;158(Pt 6):1543-52.
239. Stewart V. Regulation of nitrate and nitrite reductase synthesis in enterobacteria. Antonie Van Leeuwenhoek. 1994;66(1-3):37-45.
240. Muller AL, Kjeldsen KU, Rattei T, Pester M, Loy A. Phylogenetic and environmental diversity of DsrAB-type dissimilatory (bi)sulfite reductases. ISME J. 2015;9(5):1152-65.
241. Nurizzo D, Cutruzzola F, Arese M, Bourgeois D, Brunori M, Cambillau C, et al. Conformational changes occurring upon reduction and NO binding in nitrite reductase from *Pseudomonas aeruginosa*. Biochemistry. 1998;37(40):13987-96.
242. Su W, Zhang L, Li D, Zhan G, Qian J, Tao Y. Dissimilatory nitrate reduction by *Pseudomonas alcaliphila* with an electrode as the sole electron donor. Biotechnol Bioeng. 2012;109(11):2904-10.
243. Huang X, Weisener CG, Ni J, He B, Xie D, Li Z. Nitrate assimilation, dissimilatory nitrate reduction to ammonium, and denitrification coexist in *Pseudomonas putida* Y-9 under aerobic conditions. Bioresour Technol. 2020;312:123597.
244. Joy KW, Hageman RH. The purification and properties of nitrite reductase from higher plants, and its dependence on ferredoxin. Biochem J. 1966;100(1):263-73.

245. Stroupe E, Getzoff E. The Role of Siroheme in Sulfite and Nitrite Reductases. Tetrapyrroles. Molecular Biology Intelligence Unit: Springer, New York, NY.; 2009.
246. Jackson RH, Cornish-Bowden A, Cole JA. Prosthetic groups of the NADH-dependent nitrite reductase from *Escherichia coli* K12. Biochem J. 1981;193(3):861-7.
247. Murphy MJ, Siegel LM, Kamin H. Reduced nicotinamide adenine dinucleotide phosphate-sulfite reductase of enterobacteria. VI. The reaction of carbon monoxide with the *Escherichia coli* holoenzyme, the hemoprotein, and free siroheme. J Biol Chem. 1974;249(5):1610-4.
248. Coves J, Zeghouf M, Macherel D, Guigliarelli B, Asso M, Fontecave M. Flavin mononucleotide-binding domain of the flavoprotein component of the sulfite reductase from *Escherichia coli*. Biochemistry. 1997;36(19):5921-8.
249. Zeghouf M, Fontecave M, Macherel D, Coves J. The flavoprotein component of the *Escherichia coli* sulfite reductase: expression, purification, and spectral and catalytic properties of a monomeric form containing both the flavin adenine dinucleotide and the flavin mononucleotide cofactors. Biochemistry. 1998;37(17):6114-23.
250. Beinert H, Holm RH, Munck E. Iron-sulfur clusters: nature's modular, multipurpose structures. Science. 1997;277(5326):653-9.
251. Murphy MJ, Siegel LM, Tove SR, Kamin H. Siroheme: a new prosthetic group participating in six-electron reduction reactions catalyzed by both sulfite and nitrite reductases. Proc Natl Acad Sci U S A. 1974;71(3):612-6.
252. Hasegawa N, Arai H, Igarashi Y. Two c-type cytochromes, NirM and NirC, encoded in the nir gene cluster of *Pseudomonas aeruginosa* act as electron donors for nitrite reductase. Biochem Biophys Res Commun. 2001;288(5):1223-30.
253. Hirasawa M, Tripathy JN, Somasundaram R, Johnson MK, Bhalla M, Allen JP, et al. The interaction of spinach nitrite reductase with ferredoxin: a site-directed mutation study. Mol Plant. 2009;2(3):407-15.
254. Szatmari D, Sarkany P, Kocsis B, Nagy T, Miseta A, Barko S, et al. Intracellular ion concentrations and cation-dependent remodelling of bacterial MreB assemblies. Sci Rep. 2020;10(1):12002.
255. Meyer J. Iron-sulfur protein folds, iron-sulfur chemistry, and evolution. Journal of Biological Inorganic Chemistry. 2008;13:157-70.
256. Bruschi M, Guerlesquin F. Structure, function and evolution of bacterial ferredoxins. FEMS Microbiol Rev. 1988;4(2):155-75.
257. Winsor GL, Griffiths EJ, Lo R, Dhillon BK, Shay JA, Brinkman FS. Enhanced annotations and features for comparing thousand of Pseudomonas genomes in teh *Pseudomonas* genome database. Nucleic Acids Research. 2016;4(44):646-53.
258. Alvarez-Ortega C, Harwood CS. Responses of *Pseudomonas aeruginosa* to low oxygen indicate that growth in the cystic fibrosis lung is by aerobic respiration. Mol Microbiol. 2007;65(1):153-65.
259. Nilavongse A, Brondijk THC, Overton TW, Richardson DJ, Leach ER, Cole JA. The NapF protein of the *Escherichia coli* periplasmic nitrate reductase system: demonstration of a cytoplasmic location and

interaction with the catalytic subunit, NapA. Microbiology (Reading). 2006;152(Pt 11):3227-37.
260. Yan Z, Wang M, Ferry JG. A Ferredoxin- and F420H2-Dependent, Electron-Bifurcating, Heterodisulfide Reductase with Homologs in the Domains Bacteria and Archaea. mBio. 2017;8(1).
261. Gomes GM, Faria A, Carita CC, Mendes J, Regalla M, Chicau P, et al. Di-cluster, seven-iron ferredoxins from hyperthermophilic Sulfolobales. European Journal of Biochemistry. 1998;3(5):499-507.
262. Wissing F. Cyanide Formation from Oxidation of Glycine by a *Pseudomonas* Species. Journal of Bacteriology. 1973;117(3):1289-94.
263. Li W, Lu CD. Regulation of carbon and nitrogen utilization by CbrAB and NtrBC two-component systems in *Pseudomonas aeruginosa*. J Bacteriol. 2007;189(15):5413-20.
264. Alford MA, Baghela A, Yeung ATY, Pletzer D, Hancock REW. NtrBC Regulates Invasiveness and Virulence of *Pseudomonas aeruginosa* During High-Density Infection. Front Microbiol. 2020;11:773.
265. Yeung AT, Bains M, Hancock RE. The sensor kinase CbrA is a global regulator that modulates metabolism, virulence, and antibiotic resistance in *Pseudomonas aeruginosa*. J Bacteriol. 2011;193(4):918-31.
266. Yeung AT, Janot L, Pena OM, Neidig A, Kukavica-Ibrulj I, Hilchie A, et al. Requirement of the *Pseudomonas aeruginosa* CbrA sensor kinase for full virulence in a murine acute lung infection model. Infect Immun. 2014;82(3):1256-67.
267. La Rosa R, Johansen HK, Molin S. Adapting to the Airways: Metabolic Requirements of *Pseudomonas aeruginosa* during the Infection of Cystic Fibrosis Patients. Metabolites. 2019;9(10).
268. Van Alst NE, Picardo KF, Iglewski BH, Haidaris CG. Nitrate sensing and metabolism modulate motility, biofilm formation, and virulence in *Pseudomonas aeruginosa.* Infect Immun. 2007;75(8):3780-90.
269. Van Alst NE, Wellington M, Clark VL, Haidaris CG, Iglewski BH. Nitrite reductase NirS is required for type III secretion system expression and virulence in the human monocyte cell line THP-1 by *Pseudomonas aeruginosa.* Infect Immun. 2009;77(10):4446-54.
270. Line L, Alhede M, Kolpen M, Kuhl M, Ciofu O, Bjarnsholt T, et al. Physiological levels of nitrate support anoxic growth by denitrification of *Pseudomonas aeruginosa* at growth rates reported in cystic fibrosis lungs and sputum. Front Microbiol. 2014;5:554.
271. Hampshire T, Soneji S, Bacon J, James BW, Hinds J, Laing K, et al. Stationary phase gene expression of *Mycobacterium tuberculosis* following a progressive nutrient depletion: a model for persistent organisms? Tuberculosis (Edinb). 2004;84(3-4):228-38.
272. Akhtar S, Khan A, Sohaskey CD, Jagannath C, Sarkar D. Nitrite reductase NirBD is induced and plays an important role during in vitro dormancy of *Mycobacterium tuberculosis*. J Bacteriol. 2013;195(20):4592-9.
273. Arai H, Igarashi Y, Kodama T. Structure and ANR-dependent transcription of the nir genes for denitrification from *Pseudomonas aeruginosa.* Biosci Biotechnol Biochem. 1994;58(7):1286-91.

274. Cutruzzola F, Brown K, Wilson EK, Bellelli A, Arese M, Tegoni M, et al. The nitrite reductase from *Pseudomonas aeruginosa*: essential role of two active-site histidines in the catalytic and structural properties. Proc Natl Acad Sci U S A. 2001;98(5):2232-7.
275. Kuroki M, Igarashi Y, Ishii M, Arai H. Fine-tuned regulation of the dissimilatory nitrite reductase gene by oxygen and nitric oxide in *Pseudomonas aeruginosa*. Environ Microbiol Rep. 2014;6(6):792-801.
276. Arai H, Kodama T, Igarashi Y. Cascade regulation of the two CRP/FNR-related transcriptional regulators (ANR and DNR) and the denitrification enzymes in *Pseudomonas aeruginosa.* Mol Microbiol. 1997;25(6):1141-8.
277. Trunk K, Benkert B, Quack N, Munch R, Scheer M, Garbe J, et al. Anaerobic adaptation in *Pseudomonas aeruginosa*: definition of the Anr and Dnr regulons. Environ Microbiol. 2010;12(6):1719-33.
278. Yoon SS, Karabulut AC, Lipscomb JD, Hennigan RF, Lymar SV, Groce SL, et al. Two-pronged survival strategy for the major cystic fibrosis pathogen, *Pseudomonas aeruginosa*, lacking the capacity to degrade nitric oxide during anaerobic respiration. EMBO J. 2007;26(15):3662-72.
279. Giardina G, Rinaldo S, Johnson KA, Di Matteo A, Brunori M, Cutruzzola F. NO sensing in *Pseudomonas aeruginosa:* structure of the transcriptional regulator DNR. J Mol Biol. 2008;378(5):1002-15.
280. Lobato L, Bouzhir-Sima L, Yamashita T, Wilson MT, Vos MH, Liebl U. Dynamics of the heme-binding bacterial gas-sensing dissimilative nitrate respiration regulator (DNR) and activation barriers for ligand binding and escape. J Biol Chem. 2014;289(38):26514-24.
281. Toyofuku M, Nomura N, Fujii T, Takaya N, Maseda H, Sawada I, et al. Quorum sensing regulates denitrification in *Pseudomonas aeruginosa* PAO1. J Bacteriol. 2007;189(13):4969-72.
282. Toyofuku M, Nomura N, Kuno E, Tashiro Y, Nakajima T, Uchiyama H. Influence of the Pseudomonas quinolone signal on denitrification in Pseudomonas aeruginosa. J Bacteriol. 2008;190(24):7947-56.
283. Dolan SK, Kohlstedt M, Trigg S, Vallejo Ramirez P, Kaminski CF, Wittmann C, et al. Contextual Flexibility in Pseudomonas aeruginosa Central Carbon Metabolism during Growth in Single Carbon Sources. mBio. 2020;11(2).
284. Romeo A, Sonnleitner E, Sorger-Domenigg T, Nakano M, Eisenhaber B, Blasi U. Transcriptional regulation of nitrate assimilation in *Pseudomonas aeruginosa* occurs via transcriptional antitermination within the *nirBD-PA1779-cobA* operon. Microbiology (Reading). 2012;158(Pt 6):1543-52.
285. Crane BR, Siegel LM, Getzoff ED. Probing the catalytic mechanism of sulfite reductase by X-ray crystallography: structures of the *Escherichia coli* hemoprotein in complex with substrates, inhibitors, intermediates, and products. Biochemistry. 1997;36(40):12120-37.
286. Song Q, Wang B, Zhao F, Han Y, Zhao Z. Expression, characterisation and molecular docking of the assimilatory NaDH-nitrite reductase from *Acidovorax wautersi*i QZ-4. Biochemical Engineering Journal. 2020;159:107589.

287. Price-Whelan A, Dietrich LE, Newman DK. Pyocyanin alters redox homeostasis and carbon flux through central metabolic pathways in *Pseudomonas aeruginosa* PA14. J Bacteriol. 2007;189(17):6372-81.
288. Kohler T, Curty LK, Barja F, van Delden C, Pechere JC. Swarming of *Pseudomonas aeruginosa* is dependent on cell-to-cell signaling and requires flagella and pili. J Bacteriol. 2000;182(21):5990-6.
289. Mahajan-Miklos S, Tan MW, Rahme LG, Ausubel FM. Molecular mechanisms of bacterial virulence elucidated using a *Pseudomonas aeruginosa-Caenorhabditis elegans* pathogenesis model. Cell. 1999;96(1):47-56.
290. Lau GW, Goumnerov BC, Walendziewicz CL, Hewitson J, Xiao W, Mahajan-Miklos S, et al. The *Drosophila melanogaster* toll pathway participates in resistance to infection by the Gram-negative human pathogen *Pseudomonas aeruginosa*. Infect Immun. 2003;71(7):4059-66.
291. Lau GW, Ran H, Kong F, Hassett DJ, Mavrodi D. *Pseudomonas aeruginosa* pyocyanin is critical for lung infection in mice. Infect Immun. 2004;72(7):4275-8.
292. Palmer KL, Mashburn LM, Singh PK, Whiteley M. Cystic fibrosis sputum supports growth and cues key aspects of *Pseudomonas aeruginosa* physiology. J Bacteriol. 2005;187(15):5267-77.
293. Cole J. Nitrate reduction to ammonia by enteric bacteria: redundancy, or a strategy for survival during oxygen starvation? FEMS Microbiol Lett. 1996;136(1):1-11.
294. Worlitzsch D, Tarran R, Ulrich M, Schwab U, Cekici A, Meyer KC, et al. Effects of reduced mucus oxygen concentration in airway *Pseudomonas* infections of cystic fibrosis patients. J Clin Invest. 2002;109(3):317-25.
295. Kamath KS, Krisp C, Chick J, Pascovici D, Gygi SP, Molloy MP. *Pseudomonas aeruginosa* Proteome under Hypoxic Stress Conditions Mimicking the Cystic Fibrosis Lung. J Proteome Res. 2017;16(10):3917-28.
296. Borriello G, Werner E, Roe F, Kim AM, Ehrlich GD, Stewart PS. Oxygen limitation contributes to antibiotic tolerance of *Pseudomonas aeruginosa* in biofilms. Antimicrob Agents Chemother. 2004;48(7):2659-64.
297. Wessel AK, Arshad TA, Fitzpatrick M, Connell JL, Bonnecaze RT, Shear JB, et al. Oxygen limitation within a bacterial aggregate. mBio. 2014;5(2):e00992.
298. Paiva CN, Bozza MT. Are reactive oxygen species always detrimental to pathogens? Antioxid Redox Signal. 2014;20(6):1000-37.
299. Mauch RM, Jensen PO, Moser C, Levy CE, Hoiby N. Mechanisms of humoral immune response against *Pseudomonas aeruginosa* biofilm infection in cystic fibrosis. J Cyst Fibros. 2018;17(2):143-52.
300. Riquelme SA, Wong Fok Lung T, Prince A. Pulmonary Pathogens Adapt to Immune Signaling Metabolites in the Airway. Front Immunol. 2020;11:385.

301. Forstermann U, Closs EI, Pollock JS, Nakane M, Schwarz P, Gath I, et al. Nitric oxide synthase isozymes. Characterization, purification, molecular cloning, and functions. Hypertension. 1994;23(6 Pt 2):1121-31.
302. Martinez MC, Andriantsitohaina R. Reactive nitrogen species: molecular mechanisms and potential significance in health and disease. Antioxid Redox Signal. 2009;11(3):669-702.
303. Robinson JL, Brynildsen MP. A kinetic platform to determine the fate of nitric oxide in *Escherichia coli*. PLoS Comput Biol. 2013;9(5):e1003049.
304. Cunningham L, Pitt M, Williams HD. The *cioAB* genes from *Pseudomonas aeruginosa* code for a novel cyanide-insensitive terminal oxidase related to the cytochrome bd quinol oxidases. Mol Microbiol. 1997;24(3):579-91.
305. Comolli JC, Donohue TJ. Differences in two *Pseudomonas aeruginosa cbb3* cytochrome oxidases. Mol Microbiol. 2004;51(4):1193-203.
306. Williams HD, Zlosnik JE, Ryall B. Oxygen, cyanide and energy generation in the cystic fibrosis pathogen *Pseudomonas aeruginosa*. Adv Microb Physiol. 2007;52:1-71.
307. Arai H. Regulation and Function of Versatile Aerobic and Anaerobic Respiratory Metabolism in *Pseudomonas aeruginosa*. Front Microbiol. 2011;2:103.
308. Adams MW, Mortenson LE. The effect of cyanide and ferricyanide on the activity of the dissimilatory nitrate reductase of *Escherichia coli*. J Biol Chem. 1982;257(4):1791-9.
309. Carterson AJ, Morici LA, Jackson DW, Frisk A, Lizewski SE, Jupiter R, et al. The transcriptional regulator AlgR controls cyanide production in Pseudomonas aeruginosa. J Bacteriol. 2004;186(20):6837-44.
310. Blier AS, Vieillard J, Gerault E, Dagorn A, Varacavoudin T, Le Derf F, et al. Quantification of *Pseudomonas aeruginosa* hydrogen cyanide production by a polarographic approach. J Microbiol Methods. 2012;90(1):20-4.
311. D'Souza G, Shitut S, Preussger D, Yousif G, Waschina S, Kost C. Ecology and evolution of metabolic cross-feeding interactions in bacteria. Nat Prod Rep. 2018;35(5):455-88.